Macro Synthetic Fiber Reinforcement for Improved Structural Performance of Concrete Bridge Girders

Final Report **September 2019**

Principal investigators:
H. R. Hamilton

Research assistants:
Glenda Diaz Acosta

Department of Civil and Coastal Engineering
University of Florida
P.O. Box 116580
Gainesville, Florida 32611

Sponsor:
Florida Department of Transportation (FDOT)
Project Manager:
William Potter

Contract:
UF Project No. 00122739 & 00122740
FDOT Contract No. BDV31-977-41

University of Florida
Engineering School of Sustainable Infrastructure and Environment
Department of Civil and Coastal Engineering
University of Florida
P.O. Box 116580
Gainesville, Florida 32611

Disclaimer

The opinions, findings, and conclusions expressed in this publication are those of the authors and not necessarily those of the State of Florida Department of Transportation

Unit of Measurement Conversions

SI* (MODERN METRIC) CONVERSION FACTORS

*APPROXIMATE CONVERSIONS **TO** SI UNITS*

SYMBOL	WHEN YOU KNOW	MULTIPLY BY	TO FIND	SYMBOL
LENGTH				
in	inches	25.4	millimeters	mm
ft	feet	0.305	meters	m
yd	yards	0.914	meters	m
mi	miles	1.61	kilometers	km
AREA				
in^2	square inches	645.2	square millimeters	mm^2
ft^2	square feet	0.093	square meters	m^2
yd^2	square yard	0.836	square meters	m^2
ac	acres	0.405	hectares	ha
mi^2	square miles	2.59	square kilometers	km^2
VOLUME				
fl oz	fluid ounces	29.57	milliliters	mL
gal	gallons	3.785	liters	L
ft^3	cubic feet	0.028	cubic meters	m^3
yd^3	cubic yards	0.765	cubic meters	m^3
NOTE: volumes greater than 1000 L shall be shown in m^3				
MASS				
oz	ounces	28.35	grams	g
lb	pounds	0.454	kilograms	kg
T	short tons (2000 lb)	0.907	megagrams	Mg (or "t")
TEMPERATURE (exact degrees)				
°F	Fahrenheit	5(F-32)/9 or (F-32)/1.8	Celsius	°C
ILLUMINATION				
fc	foot-candles	10.76	lux	lx
fl	foot-Lamberts	3.426	candela/m^2	cd/m^2
FORCE and PRESSURE or STRESS				
kip	1000 pound force	4.45	kilonewtons	kN
lbf	pound force	4.45	newtons	N
lbf/in^2	pound force per square inch	6.89	kilopascals	kPa

*SI is the symbol for the International System of Units. Appropriate rounding should be made to comply with Section 4 of ASTM E380.

SI* (MODERN METRIC) CONVERSION FACTORS

*APPROXIMATE CONVERSIONS **FROM** SI UNITS*

SYMBOL	WHEN YOU KNOW	MULTIPLY BY	TO FIND	SYMBOL
LENGTH				
mm	millimeters	0.039	inches	in
m	meters	3.28	feet	ft
m	meters	1.09	yards	yd
km	kilometers	0.621	miles	mi
AREA				
mm^2	square millimeters	0.0016	square inches	in^2
m^2	square meters	10.764	square feet	ft^2
m^2	square meters	1.195	square yards	yd^2
ha	hectares	2.47	acres	ac
km^2	square kilometers	0.386	square miles	mi^2
VOLUME				
mL	milliliters	0.034	fluid ounces	fl oz
L	liters	0.264	gallons	gal
m^3	cubic meters	35.314	cubic feet	ft^3
m^3	cubic meters	1.307	cubic yards	yd^3
MASS				
g	grams	0.035	ounces	oz
kg	kilograms	2.202	pounds	lb
Mg (or "t")	megagrams (or "metric ton")	1.103	short tons (2000 lb)	T
TEMPERATURE (exact degrees)				
°C	Celsius	1.8C+32	Fahrenheit	°F
ILLUMINATION				
lx	lux	0.0929	foot-candles	fc
cd/m^2	candela/m^2	0.2919	foot-Lamberts	fl
FORCE and PRESSURE or STRESS				
kN	kilonewtons	0.225	1000 pound force	kip
N	newtons	0.225	pound force	lbf
kPa	kilopascals	0.145	pound force per square inch	lbf/in^2

*SI is the symbol for the International System of Units. Appropriate rounding should be made to comply with Section 4 of ASTM E380.

Technical Report Documentation Page

1. Report No.	2. Government Accession No.	3. Recipient's Catalog No.
4. Title and Subtitle Macro Synthetic Fiber Reinforcement for Improved Structural Performance of Concrete Bridge Girders		5. Report Date 6. Performing Organization Code
7. Author(s) Diaz Acosta, G. and Hamilton, H. R.		8. Performing Organization Report No.
9. Performing Organization Name and Address University of Florida Department of Civil & Coastal Engineering P.O. Box 116580 Gainesville, FL 32611-6580		10. Work Unit No. (TRAIS) 11. Contract or Grant No. BDV31-977-41
12. Sponsoring Agency Name and Address Florida Department of Transportation 605 Suwannee Street, MS 30 Tallahassee, FL 32399		13. Type of Report and Period Covered Final Report 14. Sponsoring Agency Code
15. Supplementary Notes		

16. Abstract

In prestressed bridge girders, end region reinforcement is used to control cracking caused by high tensile stresses that occur due to prestress transfer. Partial strand debonding and additional mild steel reinforcement are commonly used to control end region cracking. In some cases, these measures do not effectively control cracking, resulting in construction delays, potential repairs, additional costs, and potential compromise of long-term durability. Fiber-reinforced concrete (FRC) provides a possible solution to end region cracking. Since end region cracking is a serviceability state, not an ultimate strength state, crack control using fibers may provide better results than conventional end region detailing. To evaluate the effectiveness of FRC, experimental and analytical work were conducted.

The experimental program covered the evaluation of the effectiveness of steel and macrosynthetic fibers to control end region cracking. Five precast prestressed Florida I-beams were constructed using fiber volume ratios of 0.3%, 0.5%, and 0.7%. Hooked-end steel fibers at a volume of 0.3% and 0.7%, crimped steel fibers at volume of 0.7% and macrosynthetic fiber at a volume of 0.5% were used in the investigation. Concrete and mild steel reinforcement strain were collected during prestressed transfer, and end region cracks were monitored immediately following prestress transfer and for a period of 148 days. The experimental results indicated that the use of FRC can reduce end region crack widths. In addition, the use of steel fibers at a volume fraction of 0.7% combined with reduced end region reinforcement was more effective than the FDOT typical end region reinforcement at maintaining crack widths smaller than 0.006 in. A comparison of crack repair that would be required for the test specimens is presented to provide a practical comparison of FRC performance in this testing.

The analytical program was conducted in two phases. The first phase consisted of calibrating a material model that represents the post-cracking behavior of FRC. The second phase consisted of modeling of the FIB-78 girders during prestress transfer. The results from the experimental program were used to validate the analytical model. Good agreement was found between the experimental and analytical results of end region cracking immediately following prestress transfer. The results from the analytical work confirm that FRC can effectively be used to reduce end region cracks.

Prestressed concrete, End Region, Fiber-reinforced concrete, Florida I-Beam	18. Distribution Statement No restrictions

19. Security Classif. (of this report)	20. Security Classif. (of this page)	21. No. of Pages	22. Price
Unclassified	Unclassified	290	

Form DOT F 1700.7 (8-72) Reproduction of completed page authorized

Acknowledgments

The authors would like to gratefully acknowledge and thank the Florida Department of Transportation (FDOT) for the financial support of this research project. The project was managed by William Potter, and the authors thank him for his technical input and support throughout the project. The authors would like to thank the FDOT State Materials Office and Structures Research Center for their assistance with experimental testing. In particular, the authors would like to acknowledge Patrick Carlton, Nelson Diaz, Stephen Eudy, Christina Freeman, Steven Nolan, Justin Robertson, Juan Sanchez, and Paul Tighe.

The authors would like to thank Dura-Stress and its personnel for their support and contributions during mixture development and construction of test girders, especially, Dr. Miles Zeman, Dr. Audi Sriboonlue, and Mr. John Jarrett. The authors would also like to thank those manufactures who donated cement and fiber materials for this project. Additionally, the authors would like to thank the many graduate students that contributed to the project, including Felix Garcia, Carson Gonzalez, Shanyue Guan, Jeffrey Honig, Satyajeet Patil, and Eduardo Torres for assistance with experimental testing and data collection, as well as Dr. Gary Consolazio for his assistance during development and validation of the analytical work.

Executive Summary

In prestressed bridge girders, end region reinforcement is used to control cracking caused by high tensile stresses that occur due to prestress transfer. Partial strand debonding and additional mild steel reinforcement are commonly used to control end region cracking. In some cases, these measures do not effectively control cracking, resulting in construction delays, potential repairs, additional costs, and potential compromise of long-term durability. Fiber-reinforced concrete (FRC) provides a possible solution to end region cracking. Since end region cracking is a serviceability state, not an ultimate strength state, crack control using fibers may provide better results than conventional end region detailing.

The research conducted to evaluate the effectiveness of FRC at controlling end region cracks included both experimental and analytical work. Because self-consolidating concrete (SCC) is typically used to produce precast girders in Florida, it was necessary to integrate the fibers into an SCC mixture while still maintaining the flowability and passing ability properties of SCC. The experimental program was divided into two phases: mixture development and full-scale testing of FIB-78 girder segments. The analytical program was also divided into two phases. The first phase consisted of calibrating a material model that represented the post-cracking behavior of FRC. The second phase consisted of modeling of the FIB-78 girders during prestress transfer.

The first phase of the experimental program focused on development of SCC mixtures with fiber reinforcement. Macrosynthetic, basalt, and steel fibers at volume fractions ranging from 0.1% to 0.7% was evaluated. The effect of including fibers on concrete workability and residual strength were considered when selecting the mixtures to use in the full-scale girder production. In general, higher fiber volumes and the use of stiffer fibers led to a higher residual strength. When used at the same volume fraction, steel fibers provided residual strengths that were 60% higher than that of the macrosynthetic fibers and 90% higher than that of the basalt fibers. Mixtures with macrosynthetic fibers had higher residual strength than basalt fibers. Reduced workability was observed, however, in mixtures with dosages of macrosynthetic fibers greater than 0.5%. Based on results from workability and residual strength, mixtures with hooked end steel fibers at 0.3% and 0.7%, crimped steel fibers at 0.7%, and macrosynthetic fiber at 0.5% were selected for full-scale testing.

In the second phase of the experimental program, five precast prestressed FIB-78 specimens were constructed to evaluate the effectiveness of FRC at controlling end region cracking. Each girder end was designed with different end region detailing to evaluate the effectiveness of FRC in combination with conventional FDOT end region detailing versus significantly reduced end region reinforcement. The strain in concrete and mild steel reinforcement was measured during prestressed transfer, and end region cracks were monitored immediately following prestress transfer and for a period of 150 days. The data collected were utilized to quantify the effectiveness of FRC to control end region cracking. The experimental results indicated that the use of FRC can reduce end region crack widths. In addition, the use of steel fibers at a volume fraction of 0.7% combined with reduced end region reinforcement was found to be more effective than FDOT typical end region reinforcement at maintaining crack widths smaller than 0.006 in.

The first phase of the experimental program focused on the calibration of a material model that could predict the post-cracking behavior of FRC. To accomplish this, FRC was represented analytically using a smeared reinforcement approach, where the fibers are defined as a fraction of the solid concrete element. Experimental results from laboratory testing of FRC

mixtures was used for material calibration. The simulation showed that a smeared reinforcement approach can be used to accurately represent the post-cracking response of FRC.

Using the calibrated material model, the second phase of the analytical model included simulation of prestressed FIB-78 girders. Concrete and mild steel reinforcement, along with end region crack data recorded experimentally, were used to validate the analytical model. Good agreement was found between the experimental and analytical results of end region cracking immediately following prestress transfer.

Test specimens were evaluated using crack treatment requirements from current FDOT specifications.

Table of Contents

List of Figures

List of Tables

1 Introduction

U.S. precast bridge girders are typically produced in a fixed-location facility with long-line beds in which girders are fabricated end-to-end using bonded pretensioned prestressing strands. Girders with lengths in excess of 200 ft. (60 m) are produced in these facilities. The large eccentricity and magnitude of the prestressing forces necessary to reach such lengths can result in significant tensile stresses and cracking in the concrete in the end region of the girders (Figure 1-1(a)). This cracking often initiates during or right after prestress transfer and can continue to grow for up to three months. End region cracking is more common when using deeper and slender cross-sections, and higher amounts of prestressing. In general, partial strand debonding and added mild steel reinforcement are utilized to control the resulting cracking (Figure 1-1(b)). At times, however, this approach does not effectively control cracking, resulting in construction delays, potential repairs, additional costs, and potential compromise of long-term durability.

(a) (b)

Figure 1-1 End region cracking (a) (highlighted in blue) (Hamilton et al. 2013) and conventional end region reinforcement (b)

One possible solution to end region cracking is the use of fiber-reinforced concrete. Because end region cracking is a serviceability state and not an ultimate strength state, crack control using fibers may provide better results than conventional reinforcement. Historically, the use of fibers has been limited to control of temperature and shrinkage cracking. However, newly developed fibers with higher modulus and tensile strength become an alternative for structural applications.

This report presents the results from experimental and analytical investigations conducted to evaluate the effectiveness of steel and synthetic fibers at controlling end region cracking in prestressed girders.

Experimental work included the laboratory testing of synthetic, steel, and basalt fibers to evaluate their effect on fresh properties and residual strength. These results were used to develop final mixture proportions to be used in the testing of five (5) prestressed, precast I-girders. Testing included monitoring strain in concrete and mild steel reinforcement during prestress transfer, and end region crack monitoring from prestress transfer to an age of 148 days.

This report presents the results of research conducted on FRC used to control end-region cracking in precast, prestressed bridge girders. The literature review in Chapter 2 provides background current knowledge of end region cracking and FRC. FRC background includes coverage of fiber types and properties; effects of fibers on fresh concrete properties and mechanical properties; use of fibers in self-consolidating concrete; and standard test methods for FRC. Chapters 3 covers the mixture development that was be used to construct the mockup specimens. Chapter 4 describes tests conducted on full-scale FIB girder segments using FRC. Chapter 5 describes FEA simulation work that was conducted in support of the experimental testing.

1.1 Research objectives

Both experimental and analytical work were conducted to achieve the following objectives:

- Develop self-consolidating concrete mixtures including fiber reinforcement
- Test mixtures fresh and hardened properties to assess effect of including fiber reinforcement on mixture workability and residual strength
- Evaluate the effectiveness of fiber-reinforced concrete at controlling end region cracking
- Evaluate the efficiency of current design practices of end region detailing
- Develop recommendations for including fiber-reinforced concrete contribution in end region detailing design

1.2 Research approach

The efforts conducted to accomplish the research objective can be divided into three (3) major components:

- Experimental investigation within a laboratory setting focused on developing FRC mixtures that comply with workability and strength requirements.
- Full-scale experimental investigation focused in evaluating effectiveness of FRC at controlling end region cracking, and characterizing end region crack growth over time.
- Analytical investigation focused on evaluating the efficiency of current design methods at controlling end region cracking.

2 Literature review

2.1 End region

Fabrication of precast prestressed elements is performed in stages. Prior to concrete casting, the prestressing tendons are stressed. Once concrete has reached its specified strength, the tendons are released, causing a sudden application of force at the end of the member. This force is introduced into the concrete over the transfer length of the prestressing strands. Intense and highly variable tensile stresses are generated in the end region of the girder from this prestressing force (Figure 2-1

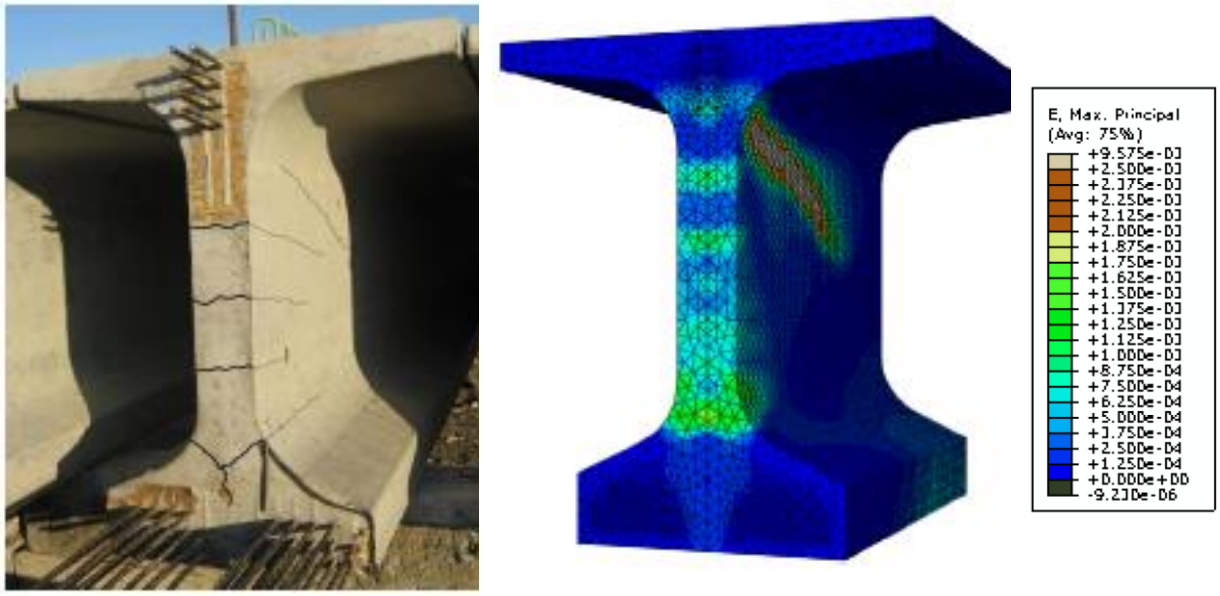

Figure 2-1 End zone cracks and maximum tensile strains (Oliva and Okumus 2011)

Figure 2-2 shows an idealized prestressing force load path within the end region, along with a strut and tie model of the end region of prestressed girder as developed by Schlaich et al. 1987. Away from the end region a linear distribution of longitudinal stresses exist, where because of the prestressing force the bottom of the girder is under compression and the top of the girder is in tension. These stresses can be divided into four components, by equilibrium C1+ C2 equals the magnitude of the prestressing force (F). The two remaining forces, T3 and C4, have equal magnitude and opposite direction, U-turn forces that enter the structure and leave it. When stresses generated are greater than tensile capacity of the concrete, cracking in the end zone occurs. Cracks are longitudinal, occurring in the web or at the intersection between web and bottom flange (Figure 2-3). Since concrete tensile strength is relatively low these cracks are very common on prestress elements. In a survey of 900 I-girders, the Missouri Department of

Transportation observed that more than 100 showed end zone cracking (Earney 2002). .

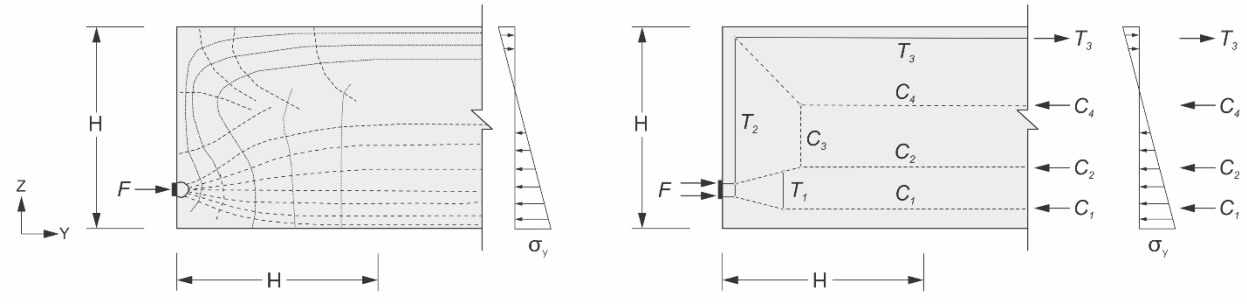

Figure 2-2 End region (a) elastic stress distribution and (b) strut-and-tie model (Schlaich et al 1987)

NCHRP 654 identifies several factors, in addition to the prestress transfer, that can affect the formation of end region cracks, including

- method of detensioning (hydraulic release provides a more uniform transfer of forces, and gives time for the girder to accommodate the forces, thus decreasing the formation of end zone cracks),
- order of strand release,
- strand distribution,
- friction with prestressing bed,
- design of end zone reinforcement,
- concrete properties,
- and Hoyer effect.

Cracks can expose reinforcement to extreme environmental conditions, resulting in corrosion of the strands or bars, and compromising the strength and durability of the structure. In addition, cracks running parallel and intersecting the pretensioning strands can cause debonding, which can result in decreased shear and flexural strength of the element. To control the width and propagation of cracks caused by tensile stresses, transverse reinforcement is typically provided.

Installation of end region reinforcement can lengthen construction duration, increase project cost, and has proven marginally effective at controlling end-region cracking. Other methods used to address durability concerns with cracks include (but are not limited to):

- debonding of strands at the end,
- crack injection,
- controlling prestress levels,
- and coating the ends of the member.

In some cases, methods for repair may not be sufficient to restore the integrity of the element and rejection is necessary.

Figure 2-3 End zone cracks, marked in blue (Hamilton et al. 2013)

2.1.1 Reported deficiencies

Tadros et al. (2010) performed testing on two 42-ft span, 60-in. deep inverted-tee girders using 0.6-in. diameter low-relaxation strands. The girders were constructed in accordance with provisions from American Association of State Highway and Transportation Officials (AASHTO) Load Resistance Factor Design (LRFD) Bridge Design Specifications (AASHTO 2017) and FDOT end region detailing practices. After prestressing release, end zone cracks were identified and measured. They were found to vary in width from 0.004 to 0.006 in. with lengths less than 3 ft. Girders in four different states were also constructed following provisions from their respective states (Table 2-1). Specimens were loaded to determine whether structural integrity of the elements was compromised by end region cracking. All specimens tested had capacities at or higher than the expected capacity (determined based on measured and specified material properties). Results from the load testing indicated that end region cracking is a service issue and did not compromise the structural capacity of the prestressed girders.

Table 2-1 End region crack width and length for various girder types (Tadros et al. 2010)

State	Girder Type	Crack width (in.)	Crack length
Tennessee	Type III AASHTO beam	none	none
Washington	WF58G	Not reported	Not reported
Virginia	PCEF45	0.004-0.010	Less than 3 ft.
Florida	60-in. inverted-T beam	0.004-0.006	Less than 3 ft.

Tadros et al. (2010) also conducted field inspections on highway bridges in Nebraska and Virginia. The Platte River Bridge in Nebraska had end zone crack widths between 0.004 in. and

0.008 in. with lengths of 2 to 6 ft. The Platte River Bridge was constructed using 79-in. deep NU-I girders with spans of approximately 160 ft. At the time of the inspection, the girders were a few years old and displayed no visible sign of corrosion.

Inspection of three Virginia bridges revealed end region cracking and some corrosion. In one bridge, inspection showed end zone cracks of 0.008 to 0.010 in. wide with some moderate corrosion stains. Similar crack widths and patterns were observed in the other two bridges, but no sign of corrosion was observed.

Hamilton et al. (2013) performed research to develop improved detailing practices to control end region cracking. Experimental work was performed on FIB 63 specimens with a 50 ft. length. Crack width data were collected during construction and in the weeks and months following release of prestressing strands. Control specimens were prepared following detailing for end reinforcement required by FDOT. Specimens showed average crack widths on the web of 0.0046 in. with a maximum of 0.008 in.

2.1.2 Crack width limits and treatment

Specifications or recommendations regarding acceptable crack widths and treatment of cracks are discussed in this section. Specifications from FDOT were used as thresholds in this investigation to evaluate the effectiveness of FRC at controlling end region cracking.

Tadros et al. 2010 conducted field inspections, durability and load testing of full-scale prestressed girders. The work focused on evaluation of the effect of end region cracking on structural integrity and long term durability of full-scale prestressed girder. Based on the work conducted, guidelines were developed for acceptance and repair methods of end region cracking. Table 2-2 shows acceptance and treatment recommendations for end region cracks.

Table 2-2 End zone cracks treatment recommendations (Tadros et al. 2010)

Width (in.)	Treatment
<0.012	None
0.012-0.025	Fill with cementitious material, end 4 ft of the girder should be coated with a sealant
0.025-0.05	Fill with epoxy or cementitious patching material, and coated with a sealant
>0.05	Rejection, or further engineering analysis

FDOT specifications are more conservative in nature than recommendations made by Tadros et al. 2010. Florida Department of Transportation (FDOT) Standard Specifications for Road and Bridge Construction (FDOT 2018) section 450-12.5 provides compliance criteria for precast elements. Crack treatment is determined based on the crack width, location, and environmental exposure to which the element will be subjected. The crack location is classified as either critical or non-critical. Non-critical locations are defined by the position and crack orientation; for all types of simple span pretensioned precast girders the non-critical location is defined by criteria presented in Table 2-3. A critical location is defined as a location where a crack will open when the element is subjected to service-level stress. Critically located cracks may reduce ultimate capacity, or fatigue resistance of the element. Critical locations are also those not encompassed by the non-critical locations as specified in Table 2-3.

In cases where the total length of all cracks located in the end zones of an element exceeds one quarter of the total element length, an engineering evaluation is required, regardless

of the crack width. Based on reported deficiencies in available literature, for the majority of cases it can be expected that end region cracks fall under the non-critical classification.

Table 2-3 Non-critical locations per Standard Specifications for Road and Bridge Construction (FDOT 2018)

Crack direction	Location	Location within cross-section	Length
Horizontal	End zone (3×depth)	Top flange and web	From end for length less than depth
Horizontal	Any location	Interface of web and top flange	From end for length less than depth
Diagonal	End zone (3×depth)	Top flange and web	From end for length less than depth
Vertical	End zone (3×depth)	Extending through top flange	Less than one-half the depth after detensioning
Vertical	Midspan (between end zones)	Extending through top flange and web	-

Table 2-4 Crack treatment per Standard Specifications for Road and Bridge Construction (FDOT 2018)

Classification	Width (in.)	Location	Environment	Treatment
Cosmetic Crack	$w \leq 0.006$ in	Non-critical	Slight or moderate	Do not treat
			Extreme	Penetrant sealer
Minor Crack	$0.006 \leq w \leq 0.012$	Non-critical	Slight	Do not treat
			Moderate	Do not treat (elevation of more than 12 ft.) or penetrant sealer
			Extreme	Penetrant sealer (elevation of more than 12 ft.) or inject epoxy
Major Crack	$w > 0.012$	Non-critical	-	Engineering evaluation
	Any	Critical	-	Engineering evaluation

2.1.3 End region design

AASHTO LRFD Bridge Design Specifications (hereafter referred as "AASHTO LRFD") section 5.9.4.4.1 (2017) states that sufficient reinforcement to resist 4% of the maximum prestressing force from fully bonded strands be provided from the girder end to a distance of h/4. In addition, the stress in the steel reinforcement during prestress transfer is limited to 20ksi to control cracking within the end region.

FDOT Structures Design Guidelines (FDOT 2016) section 4.3.1.D has adopted provisions following AASHTO LRFD with some modifications. This document specifies that enough vertical reinforcement should be provided to carry 3% of the maximum prestressing force from fully bonded strands (Pu) for a distance of h/8, 5% of Pu for a distance of h/4 and 6% for a distance of 3h/8 from the girder end.

2.2 Effect of fiber addition on end region crack control

Dhonde et al. 2005 performed work to determine the effect of fibers on end region cracking; his work covered both SCC and conventional concrete. Work was performed using steel fibers of 1.2- and 2-in. (30- and 50-mm) length at volumes ranging from 0.5% to 1%. In mixtures prepared with conventional concrete, no end region cracking was observed. In specimens prepared using SCC, control specimens showed maximum crack width of 0.005 in, while FRSCC specimens showed a reduction in end zone crack width of less than 0.001 in. Strain data were collected on steel reinforcement in all specimens during curing and prestress release. Tensile strains were significantly reduced when using steel fiber reinforcement, indicating that fibers were effective at redistributing tensile stresses developed in concrete during early ages. Maximum tensile strain during prestress release were more than 50% lower for specimens cast using SCC when compared to samples cast with conventional concrete (selected specimens are shown in Table 2-5).

Haroon et al. 2004 evaluated the effectiveness of FRC to reduce or eliminate secondary reinforcement in anchorage zones in post-tensioned elements. AASHTO cyclic loading tests were performed on control and steel fiber (deformed 1.5 in. (38 mm), hooked end 1.2 in. (30 mm) fibers) reinforced samples (Figure 2-4 and Table 2-6). Maximum crack width was reduced by 70-100% using FRC, even when using reduced secondary reinforcement. For 4.4 ksi concrete, using 1% hooked end 1.2 in. (30 mm) fibers, crack width was reduced from 0.006-0.007 in. to 0.002 in., it was determined that steel fibers could potentially reduce the quantity of secondary reinforcement by up to 79%.

Table 2-5 Tensile strain measured on reinforcement during prestress transfer (Dhonde et al. 2005)

	Fibers volume (%)	Fiber length (in.)	Fiber length (mm)	Max. tensile strain (10^{-2} in/in)
Conventional	0	-	-	1.8
	1	1.2	30	1.9
	0.5	2.4	60	1.3
SCC	0.5	2.4	60	0.4
	1	1.2	30	0.8

Blanco 2013 performed third point load testing on samples prepared with 1.4 in. (35 mm) and 2.4 in. (60 mm) hooked end steel fibers. Data collected shows that as aspect ratio and fiber volume are increased a better control of crack width is observed (Figure 2-5).

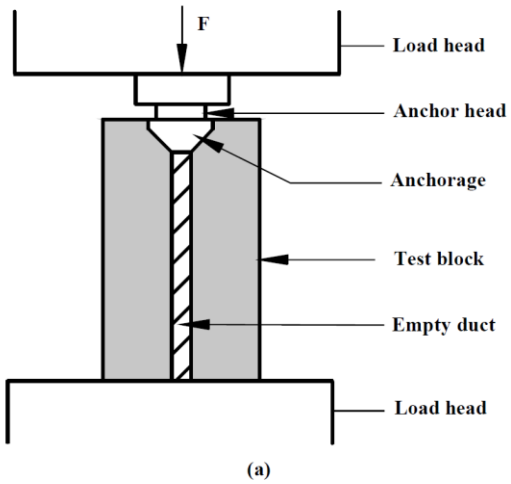

Figure 2-4 Test setup used to measure maximum crack width for various fiber volumes (Haroon et al. 2004)

Table 2-6 Test setup and maximum crack with various fiber volumes (Haroon et al. 2004)

Fiber type (volume)	Compressive strength (psi)	Reinforcement		Maximum crack width (in.) ($0.9f_{pu}$)
		Spiral	Skin	
None (0%)	4050	6	5	0.007
Hooked (1%)	4500	6	-	0.002
Hooked (1%)	4500	3	-	0.002
Hooked (0.75%)	4800	6	3	none

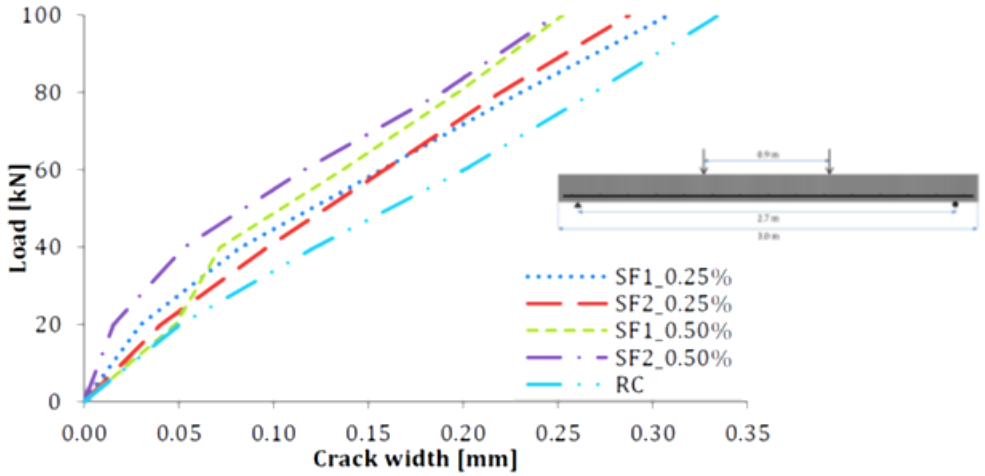

Figure 2-5 Load-crack width for service load region (Blanco 2013)

Evaluation of the effect of fiber reinforcement in prestressed elements indicated that fibers could be effectively used to redistribute stresses during casting and prestress transfer. In addition, end region crack widths were reduced and, in some cases, eliminated. Fibers were shown to be effective as partial replacement of end region reinforcement in reducing construction time and improving element durability.

2.3 Fiber materials

A wide variety of fiber materials and configurations are commercially available. Fibers are typically categorized by their constituent material such as steel, glass, synthetic, or natural fibers (ACI 544.1R-96). ASTM C1116 (2015) categorizes fibers into Type I – Steel, Type II – Glass, Type III – Synthetic, and Type IV – Natural.

Material and geometry selection depend on the intended application and requirements. This section provides a general description of commercially available fiber materials and their geometric and mechanical properties. A more detailed description of the importance and effect of a material and its geometry on the behavior of FRC is presented later in this chapter.

2.3.1 Steel fibers (Type I)

Due to their high strength and stiffness, steel fibers are commonly used in structural applications. These fibers are available in a variety of cross-sections and shapes (Figure 2-6); diameters range from 2.5-3 in. (64-76 mm) with aspect ratios ranging from 20 to 100, other typical properties are:

- Tensile strength: 180-300 ksi
- Modulus of Elasticity: 30,000 ksi
- Specific gravity: 7.85

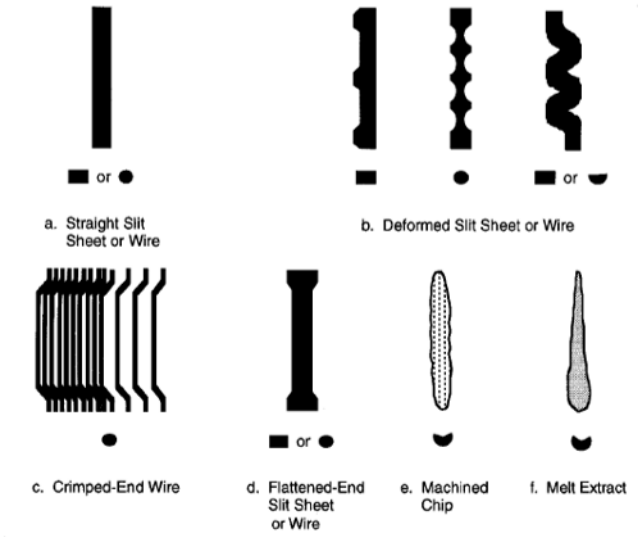

Figure 2-6 Steel fiber configuration (ACI 554.1R-96)

2.3.2 Glass fibers (Type II)

Glass fibers are commonly available in lengths ranging from 0.5 in. (13 mm) to 1.5 in. (38 mm) and can behave as either macro- or microfibers. Advantages of glass fiber-reinforced concrete include its low weight, high moisture resistance, low thermal expansion, and high fire

resistance. A downside of glass fibers is that their mechanical properties can change when exposed to aggressive environmental conditions. Properties of common glass materials are provided in Table 2-7.

Table 2-7 Properties of selected glasses (ACI 554.1R-96)

Material	Specific gravity	Tensile strength (ksi)	Modulus of elasticity (ksi)	Ultimate strain (%)
A-Glass	2.46	450	9400	4.7
E-Glass	2.54	500	10400	4.8
Cem-FIL AR-Glass	2.70	360	11600	3.6
NEG AR-Glass	2.74	355	11400	2.5

2.3.3 Synthetic fibers (Type III)

A wide range of materials are used to produce synthetic fibers (Table 2-8). The most commonly used synthetic fibers are nylon and polypropylene (Folliard et al. 2006). Synthetic fibers can be further subdivided into microsynthetic or macrosynthetic fibers, and, in general, are available in lengths varying from 0.2 in. (6 mm) to 2.5 in. (64 mm). Macrosynthetic fibers are typically longer than 1.5 in., have equivalent diameter (diameter of a circle with area equal to cross-sectional area of the fiber) larger than 0.012 in. (0.3 mm) and modulus of 725-1450 ksi. These fibers are typically dosed at a volume fraction in the range of 0.2% to 1.0% (higher for certain applications) and are commonly referred to as “structural fibers”.

Microsynthetic fibers are typically 0.5 in. (12 mm) to 0.8 in. (20 mm) in length, have equivalent diameter smaller than 0.012 in. (0.3 mm) and modulus of 435 ksi to 725 ksi. These fibers are typically used in volume fractions ranging from 0.05% to 0.2%, and are commonly referred to as “non-structural fibers”.

Table 2-8 Common synthetic fiber types and properties (ACI 554.1R-96)

Fiber type	Equivalent diameter, in. x 10^{-3}	Specific gravity	Tensile strength, ksi	Elastic modulus, ksi	Ultimate elongation, percent	Ignition temperature, degrees F	Melt, oxidation, or decomposition temperature, degrees F	Water absorption per ASTM D 570, percent by weight
Acrylic	0.5-4.1	1.16-1.18	39-145	2000-2800	7.5-50.0	—	430-455	1.0-2.5
Aramid I	0.47	1.44	425	9000	4.4	high	900	4.3
Aramid II†	0.40	1.44	340	17,000	2.5	high	900	1.2
Carbon, PAN HM‡	0.30	1.6-1.7	360-440	55,100	0.5-0.7	high	752	nil
Carbon, PAN HT§	0.35	1.6-1.7	500-580	33,400	1.0-1.5	high	752	nil
Carbon, pitch GP**	0.39-0.51	1.6-1.7	70-115	4000-5000	2.0-2.4	high	752	3-7
Carbon, pitch HP††	0.35-0.70	1.80-2.15	220-450	22,000-70,000	0.5-1.1	high	932	nil
Nylon‡‡	0.90	1.14	140	750	20	—	392-430	2.8-5.0
Polyester	0.78	1.34-1.39	33-160	2500	12-150	1100	495	0.4
Polyethylene‡‡	1.0-40.0	0.92-0.96	11-85	725	3-80	—	273	nil
Polypropylene‡‡	—	0.90-0.91	20-100	500-700	15	1100	330	nil

2.3.4 Natural fibers (Type IV)

Natural fibers are prepared from naturally occurring materials and can be processed to enhance their mechanical properties. These fibers can be obtained at low cost and are available

in large quantities. Many materials are classified as natural fibers, and occur in lengths varying from 0.1 in. to 17 in. and diameters from 0.0001 in. (0.03 mm) to 0.03 in. (0.7 mm). Common natural fibers include coconut, bamboo, sisal, jute, wood fiber, among many others.

Table 2-9 Properties of selected natural fibers (ACI 554.1R-96)

Fiber type	Coconut	Sisal	Sugar cane Bagasse	Bamboo	Jute	Flax	Elephant grass	Water reed	Plantain	Musamba	Wood fiber (kraft pulp)
Fiber length, in.	2-4	N/A	N/A	N/A	7-12	20	N/A	N/A	N/A	N/A	0.1-0.2
Fiber diameter, in.	0.004-0.016	N/A	0.008-0.016	0.002-0.016	0.004-0.008	N/A	N/A	N/A	N/A	N/A	0.001-0.003
Specific gravity	1.12-1.15	N/A	1.2-1.3	1.5	1.02-1.04	N/A	N/A	N/A	N/A	N/A	1.5
Modulus of elasticity, ksi	2750-3770	1880-3770	2175-2750	4780-5800	3770-4640	14,500	710	750	200	130	N/A
Ultimate tensile strength, psi	17,400-29,000	40,000-82,400	26,650-42,000	50,750-72,500	36,250-50,750	145,000	25,800	10,000	13,300	12,000	101,500
Elongation at break, percent	10-25	3-5	N/A	N/A	1.5-1.9	1.8-2.2	3.6	1.2	5.9	9.7	N/A
Water absorption, percent	130-180	60-70	70-75	40-45	N/A	N/A	N/A	N/A	N/A	N/A	50-75

Note: N/A = properties not readily available or not applicable.
Metric equivalents: 1 in. = 25.4 mm; 1 ksi = 1000 psi = 6.895 MPa

2.3.5 Basalt fibers

Basalt fibers are a more recent type of inorganic fiber (Kizilkanat et al. 2015). These fibers have a high modulus of elasticity and a tensile strength comparable to steel fibers. In addition, they have high thermal and chemical stability, and have been observed to easily disperse in concrete mixtures without segregation or clumping occurring (Ayub et al. 2014, Patniak 2013). Unlike steel fibers, basalt fibers are corrosion-resistant and have been found to be resistant to alkaline environments. Another advantage is their low weight (three times lighter than steel, Krassowska and Lapko 2013). Typical properties include:

- Tensile strength: 160 ksi
- Modulus of Elasticity: 6380ksi
- Specific gravity: 2.0

2.3.6 Hybrid fibers

When fibers of differing aspect ratio, material, or strength are combined, they are referred to as hybrid fibers. FRC produced from an effective combination of fibers can surpass the performance of FRC produced with the individual fibers (ACI 544.3R-08).

An example of this interaction is the combination of short and long fibers. When concrete is subjected to tension, microcracks form in the interfacial zone between aggregate and cement matrix. As tension increases, microcracks coalesce to form larger cracks, which may cause tensile failure to occur. In members with “hybrid fibers,” short fibers influence more effectively the initial formation of microcracking. Once macrocracks occur, the long fibers become more active in bridging, since shorter fibers are being pulled out as crack width increases

(Figure 2-7). It has been observed that fibers shorter than 1.4 in. (35 mm) are more effective at controlling crack widths lower than approximately 0.006 in. (Blanco 2013).

Most common fiber combinations are made based on constitutive properties, fiber dimensions, or function. Fibers combinations based on constitutive properties use a stiff fiber to increase strength and a flexible fiber to improve toughness and strain capacity. Fiber combinations based on fiber dimensions use a smaller fiber to control microcracks and increase tensile strength and a larger fiber to control macrocracks and increase fracture toughness. Fiber combinations based on function use one fiber type to improve fresh and early age properties and another to enhance mechanical properties of hardened concrete (ACI 544.3R-08, Mobasher 2011, Qian and Stroeven 2000). Some fiber combinations may be detrimental to one or more properties. Consequently, consideration of desired properties should be taken into account when selecting fiber properties to use (Nehdi and Ladanchuk 2004).

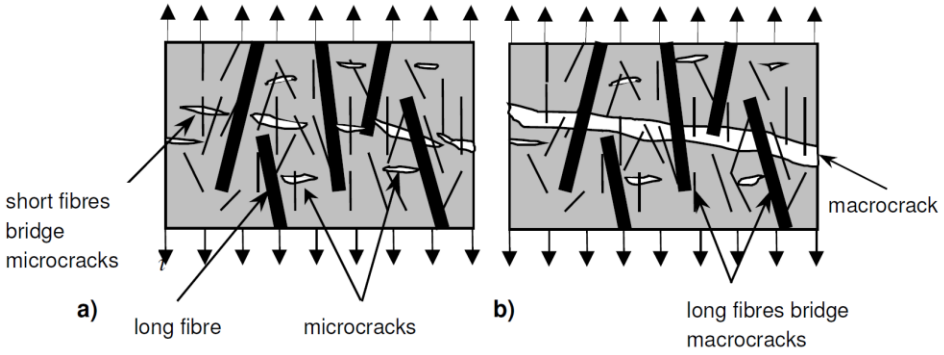

Figure 2-7 Influence of short (a) and long (b) fibers in bridging of cracks (Markovic 2006).

2.4 Typical fiber properties

Commercially available fibers have a diverse range of length and mechanical properties. Table 2-10 shows common fiber materials along with typically available geometric and mechanical properties. Most common fiber use involves nonstructural application such as control of plastic shrinkage cracking and when used for structural applications they are most commonly used as secondary reinforcement. Application of each fiber varies with mechanical properties and available geometries, common application for each fiber type are also provided in Table 2-10. In general, low fiber volumes between 0.1% and 0.3% are often used to control early age cracking, while at volumes above 0.3% post-cracking behavior of concrete is improved (Banthia et al. 2012).

Table 2-10 Typical fiber properties and applications

Material	Equivalent diameter (mm)	Length range (mm)	Aspect ratio	Tensile strength (ksi)	Applications
Steel	0.5-1.00	6-74	30-100	160-300	Tunnel linings, rock slope stabilization, slabs on grade, bridge decks, shotcrete, SIFCON
Glass	0.005-0.15	13-38	13-38	145-246	Cladding materials and thin sheet components.
Polypropylene	0.02-0.4	12-20	50-100	20-100	Residential, commercial and industrial slab on grade, floor overlays, shotcrete
Nylon	0.02-0.3	19-50	50-100	140	
Polyester	0.02-0.40	19-50	50-100	30-175	Slab on grade
Basalt	0.01-0.65	12-100	50-100	150-200	Shotcrete, slabs, thin sheets components, precast products
Carbon	0.008-0.02			70-580	Corrugated units , single or double curvature membrane structures, curtain walls

2.5 FRC implementation

2.5.1 FDOT Structures Design Guidelines (FDOT 2016)

FDOT Structures Design Guidelines (FDOT 2016) specify that the use of structural fiber reinforcement be limited to wet-cast concrete in two shapes: circular structures with inside diameter of less than 12 ft., and rectangular structures with maximum inside wall length of 6 ft. (3.17.10). Design for these structures should be made in accordance with fib Model Code 2010 (Sections 5.6 and 7.7), or as an alternative structure can be designed based on evaluations records from providers accredited to ISO/IEC Guide 65. Residual strength must be determined in accordance with ASTM C1399 (2015) (described in 2.10.1) and must meet a minimum requirement of 215 psi. Fibers allowed to be used include carbon steel fibers for slight/moderate aggressive environments, galvanized, stainless steel, or carbon FRP in all environments while other non-corrosive materials may be considered with FDOT approval.

2.5.2 ACI 318-14

Current Building Code Requirements for Structural Concrete (ACI 2008), hereafter referred as “ACI 318-14”, allows the use of steel fibers in specific conditions as an alternative reinforcement for prescriptive minimum shear reinforcement (Table 2-11). Currently the code covers only the use of fiber reinforcement as prescriptive shear reinforcement and has no design approach for structural or nonstructural applications.

Table 2-11 Cases where minimum area of shear reinforcement is not required (ACI 318-14 Section 9.6.3.1)

Beam type	Conditions
Constructed with steel fiber-reinforced normal weight concrete conforming to 26.4.1.5.1 (a), 26.4.2.2 (d), and 26.12.5.1 (a) and with $f'_c \leq$6000 psi	$h \leq$ 24 in. and $V_u \leq \emptyset 2\sqrt{f'_c} b_w d$

Where 26.4.1.5.1 (a) provides fiber requirements, 26.4.2.2 (d) provides minimum dosage and 26.12.5.1 (a) gives acceptance criteria. Fiber and minimum dosage requirements state that fibers used must be deformed, conform to ASTM A820, have an aspect ratio of 50 but less than 100, and a quantity of at least 100 lb/yd^3. For acceptance, the mixture must comply with compressive strength criteria and residual strength criteria given in Table 2-12.

Table 2-12 Conditions for residual strength, based on results of ASTM C1609 (26.12.5.1 (a))

Midspan deflection	Conditions for residual strength (RS)
L/300	RS is at least the greater of: 90 % of measured first-peak strength from flexural test 90 % of $7.5\sqrt{f'_c}$
L/150	RS is at least the greater of: 75 % of measured first-peak strength from flexural test 75 % of $7.5\sqrt{f'_c}$

2.5.3 ACI 544.7R-16 Tunnel lining design

ACI 544.7R-16 covers a design approach and design parameters for SFRC for tunnel lining applications. Key design parameters include compressive strength, residual flexural strength determined by ASTM C1609 or EN 14651 and splitting tensile strength. Flexural strength parameters determined in accordance with ASTM C1609 or EN 14651 is scaled by a factor of 0.33-0.37.

Required average residual strength is determined as follows

$$f^D_{150r} = f'^D_{150} + 1.34 s_s \qquad \text{Equation 2-1}$$

$$f^D_{600r} = f'^D_{600} + 1.34 s_s \qquad \text{Equation 2-2}$$

Where f^D_{150r} and f^D_{600r} are the required average residual flexural strength at net deflection of L/150 and L/600 (psi) respectively, f'^D_{150} and f'^D_{600} are the specified residual flexural strength at net deflection of L/150 and L/600 (psi) respectively, and s_s is the sample standard deviation of the test results.

Conventional reinforcement can be replaced partially or completely by fiber reinforcement only when the requirements established in Equation 2-3 and Equation 2-4 are satisfied.

$$\frac{f_{600}^{D}}{f_1} > 0.4 \qquad \text{Equation 2-3}$$

$$\frac{f_{150}^{D}}{f'^{D}_{600}} > 0.5 \qquad \text{Equation 2-4}$$

Where f_{150}^{D} and f_{600}^{D} (psi) are the residual flexural strengths at net deflections of L/150 and L/600 respectively, and f_1 is the first peak flexural strength (psi).

2.6 Fiber behavior

Fiber tensile resistance is controlled by either fiber rupture strength or pullout strength, or both. Fiber pullout is the preferred behavior since it provides a more ductile failure mode (ACI 544.4R-88). For straight fibers the pullout process occurs in two main stages: debonding and frictional pullout (Markovic 2006). When a crack forms in the concrete surrounding the fiber, fiber force *P* is controlled by the adhesive and mechanical bond between the fiber and concrete, which fails progressively from the crack face to the end of the fiber (Figure 2-8a and b). When bond is completely broken, then the fiber force *P* is controlled by the frictional force between the fiber and concrete as the fiber is pulled from the concrete (Figure 2-8c).

The debonding process for deformed fibers is more complex. For deformed fibers, plastic deformation of the fiber must occur at the hook bends before frictional pullout is possible (Figure 2-9c and Figure 2-9d). Plastic deformation must occur along the hooked length of the fiber to continue to pull the fiber from the concrete, which increases the pullout force *P*. Consequently, more force and energy are required to pull out a deformed fiber than a straight fiber, leading to improved post-cracking ductility and residual strength.

When the bond strength is greater than the fiber strength, then the failure mode will be governed by fiber rupture. In such cases, ductility and residual strength are controlled by fiber mechanical properties.

Fiber bond strength can be improved by providing better mechanical anchorage or larger interfacial surface area, or both. For instance, Grünewald et al. (2016) found that pullout strength was maximized by using fibers 2-4 times longer than the maximum aggregate size. Aspect ratios greater than 100, however, have been observed to cause workability problems and non-uniform fiber distribution (ACI 544.4R-4). Hydrophilic nature of the fibers with large surface areas will affect workability, the concrete hydration process, and the chemical bond between the fiber and paste. Such effects must be considered when adjusting mixture proportions to accommodate fiber addition.

SCC can be used to offset workability problems associated with the addition of fibers. Indeed, Ferrara et al. 2007 and Markovic (2006) found that the use of SCC with fibers improved the mechanical bond strength of fibers compared to traditional concrete mixtures.

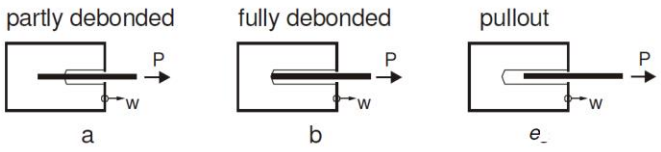

Figure 2-8 Debonding and pullout of straight fiber (Markovic 2006)

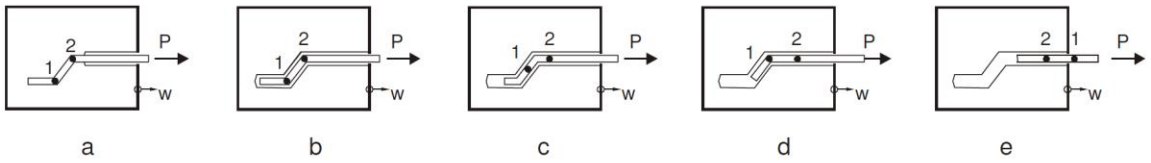

Figure 2-9 Debonding and pullout of hooked end fiber (Markovic 2006).

2.7 Effect of fibers on fresh concrete

Fiber addition can greatly affect fresh properties of the mix, causing placement and consolidation problems. Factors that determine the extent to which fresh properties are affected by the addition of fiber reinforcement include fiber volume fraction, aspect ratio, fiber shape, and fiber material. A review of work performed on the effect of fiber addition on fresh properties of concrete and methods to test FRC workability is provided in the following section.

2.7.1 Workability test methods

Workability of fresh concrete is significantly affected by the addition of fibers. Consequently, appropriate test methods are important for the development of new mixture designs, as well as quality control during production. Several test methods are available, each vary on approach, results obtained, and in their intended application. Some of the more common methods includes inverted slump cone and Vebe tests.

ASTM C995 (2001) provides the methodology to determine the inverted slump-cone time of fiber-reinforced concrete, which gives a measure of workability and consistency. This test can be performed in either a laboratory or field setting, but is not applicable to concrete that flows freely through the cone. Figure 2-10 shows the test setup in which an inverted standard slump mold is filled and vibrated. The time required for FRC to flow through the inverted cone when subjected to internal vibration is measured. Vibration is applied with a vibrator having a head diameter of 1 in. $\pm$ 1/8 in. at a frequency of least 150 Hz. This standard was withdrawn without replacement in 2008.

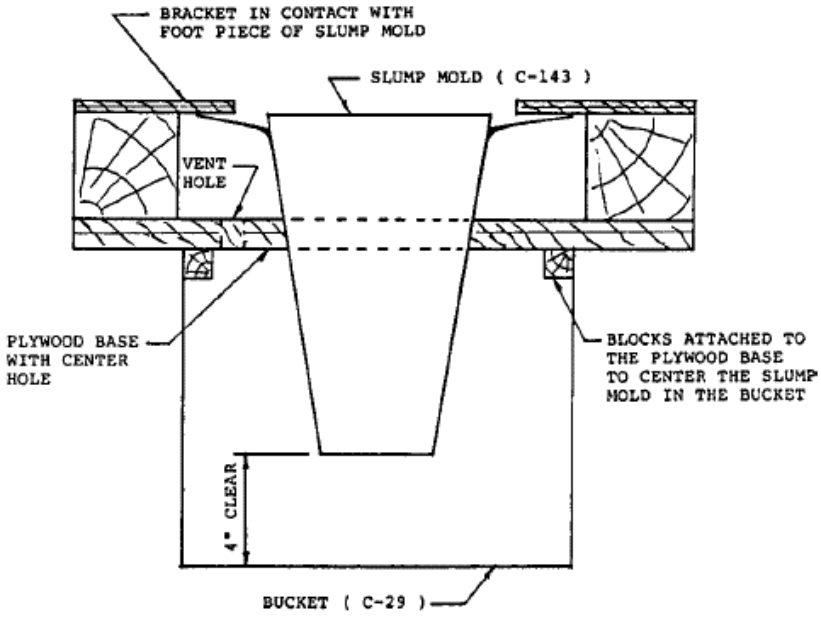

Figure 2-10 Test setup: ASTM C995

The Vebe test (BS EN 12350 2009) provides another method to determine consistency of fresh FRC. The test setup consists of a container placed over a vibrating table (Figure 2-11). Concrete is compacted into a slump mold, which is placed inside the container. Once compaction is complete, the mold is lifted and the clear disc is rotated into place and lowered onto the concrete surface. Then the vibrating table is started; the time taken for the lower part of the disc to be in full contact with the concrete is the Vebe time.

Figure 2-11 Test setup (EN 12350-3 2008)

2.7.2 Workability

Workability is a measure of the ease with which fresh concrete can be placed, consolidated, and finished. In general, an increase in volume, aspect ratio, or change in surface characteristics of fibers decreases the workability of the mixture (Yin et al. 2015, Iyer et al. 2015, Balaguru and Ramakrishnan 1988, Bayasi and Soroushian 1992, Ramakrishnan et al. 1980). Large fiber surface areas and the presence of deformations on the surface will increase friction generated between fibers and coarse aggregates, which decreases flowability.

Figure 2-12 and Figure 2-13 show the effect of deformed fiber shape on workability for a given fiber reinforcement index (product of the fiber volume and aspect ratio). Fibers with circular cross-sections have less contact area per fiber volume when compared to non-circular sections, which results in better workability. For example, a 50% increase in fiber volume will result in a decrease in slump of up to 60% (Yin et al. 2015).

Kizilkanat et al. (2015) found that 0.5-in. (12 mm) glass fibers (0.5-1% volume fraction) could cause up to a 55% reduction in slump when compared with conventional concrete. Hooked-end 1.2-in (30-mm) long steel fibers (0.5-1% volume) reduce slump by more than 50% (Table 2-13) when compared to control mixtures (Yazdani et al. 2002). For the same length (1.2 in.) and a volume of 0.425%, polypropylene fibers reduced slump by 7%, while hooked end steel fibers caused a reduction of 20% (Bolat et al. 2014). When compared to control samples, slump was reduced by 70% and 50% when using polypropylene and basalt fibers (Jiang et al. 2014).

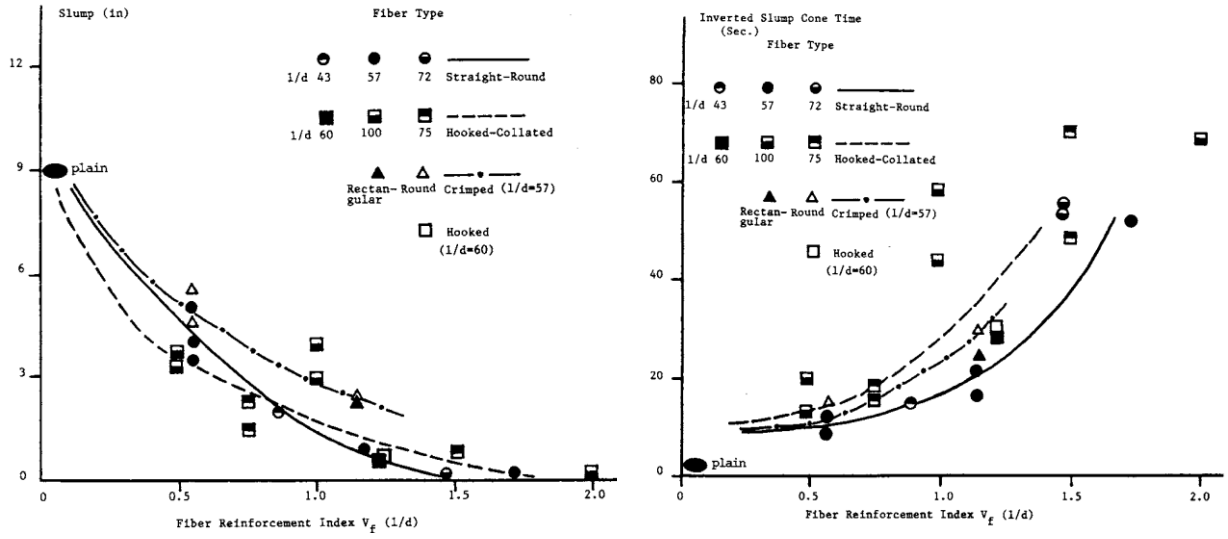

Figure 2-12 Effect of fiber volume and aspect ratio on slump and inverted slump time (Yazdani et al. 2002)

Table 2-13 Slump for conventional concrete and various FRC mixtures (Yazdani et al. 2002)

Fiber	Fiber length (in.)	Fiber length (mm)	Fiber volume (%)	Slump (in.)
No fiber	-	-	0	7.0
Steel crimped fiber	1.5	38	0.5	3.0
			0.75	2.5
			1.0	1.5
Hooked end steel fiber	1.2	30	0.5	2.5
			0.75	1.5
			1.0	1.0
Synthetic fiber	1.5	38	0.5	2.
			0.75	2.0
			1.0	1.5

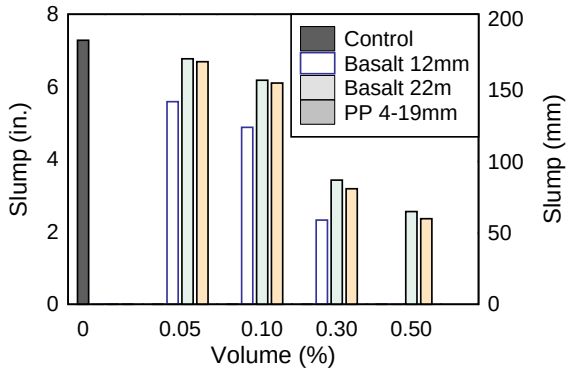

Figure 2-13 Volume and fiber length effect on slump (Jiang et al. 2014)

2.7.3 Plastic shrinkage cracking

Plastic shrinkage occurs prior to initial set of concrete. Shrinkage occurs due to volumetric change from moisture loss, and depends on relative humidity, properties of the materials, concrete age, and volume. .

Extensive work has shown fibers to be effective at reducing crack width and area due to plastic shrinkage by increasing the tensile capacity of concrete while in its plastic state (Branston et al. 2016, Eren and Marar 2010, Majdzadeh et al. 2006, Naaman et al. 2005, Qi et al. 2003). The use of polypropylene fibers with lengths of 0.25 in. and 0.5 in., at 0.1-0.3% volume fiber fraction (Table 2-14) showed a reduction in total crack area (product of average crack width and length) by over 50% when compared to control specimens (Banthia et al. 2006). In general, longer and finer fibers were found to be more effective at reducing crack widths (Banthia et al. 2006). Basalt fibers reduced crack area by over 50% when used at 0.1% (Branston et al. 2016). Use of hybrid fibers composed of synthetic and steel fibers showed a reduction in crack area of 50-99% when compared to plain concrete (Sivakumar and Santhanam 2007).

Table 2-14 Plastic shrinkage using polypropylene fibers (Banthia 2006)

Type	Diameter (denier)	Length (in.)	Length (mm)	Volume (%)	Crack area (in^2)	Crack area (mm^2)
Control	-		-	-	0.51	329.9
Monofilament	3	0.5	12.5	0.1%	0.19	120.9
				0.2%	0.01	3.8
Monofilament	6	0.5	12.5	0.1%	0.33	216.0
				0.2%	0.19	119.5
				0.3%	0.16	101.9
Monofilament	6	0.3	6.35	0.1%	0.40	257.8
				0.2%	0.38	242.8
				0.3%	0.24	154.4
Fibrillated	1000	0.5	12.5	0.1%	0.27	172.9
				0.2%	0.07	42.9
				0.3%	0.05	31.0

2.7.4 Fiber clumping

When introduced into the concrete mixture, fibers can become tangled with each other in a clump, resulting in a phenomenon known as "fiber clumping." Fiber clumping decreases workability; causes segregation and bleeding; prevents complete fiber dispersion; and creates voids (Figure 2-14). Ideally, fibers are added to the mixture in a controlled manner to ensure that the fibers are adequately dispersed into the mixture. Fortunately, if the fibers are initially dispersed into the mixture ball-free they tend to remain that way. The tendency for a mixture to have fiber clumping is affected primarily by fiber properties such as shape and length, mixture composition, fiber dosage and mixing procedures.

Figure 2-14 Fiber clumping during mixing (Macrosynthetic fiber with length 2.3 in. (58 mm) at volume of 0.7%)

As larger aspect ratios and/or larger volume fractions are used, clumping is more likely to occur since fibers are more easily tangled. In general, mixtures with synthetic fibers and rigid fibers with an aspect ratio of less than 50 are less susceptible to fiber clumping. Mixtures with volume fractions higher than 2% by volume are more susceptible to fiber clumping. Similarly,

fiber clumping occurs more frequently when using fibers with high (>1%) volume fraction (ACI 544.3R), but there has been work with 0.35-4% per volume where no clumping is reported (Patniak 2013). Rigid fibers with aspect ratios larger than 60 may require the use of a fiber blower to prevent clumping from occurring.

Figure 2-15 Fibers added to truck mixer using fiber blower (ACI 544.3R-08)

Fiber clumping may occur when the fibers are not dispersed evenly into the mixture during dosage. Adding fibers at a rate faster than they can be incorporated into the mixture, or when the mixture is not fluid enough, causes the fibers to form clumps. Fiber clumping can also occur when fibers are added before all of the other mixture constituents have been added. This results in too little water and aggregate to maintain the fiber dispersion. Overmixing after fiber dosage is another cause of fiber clumping. (544-3R-08)

Coarse aggregate contents of more than 55% of total combined aggregate by volume can also lead to fiber clumping. Furthermore, as the maximum aggregate size is increased there is more potential for fiber clumping to occur. ACI 544-1R-96 and 544-3R-08 provide a recommended gradation for mixtures containing macrofibers to avoid fiber clumping and workability issues.

Table 2-15 Recommended combined aggregate grading for macrofiber reinforced concrete (ACI 544.3R-08)

U.S. standard sieve size	Percent passing for maximum size of				
	3/8 in. (10 mm)	1/2 in. (13 mm)	3/4 in. (19 mm)	1 in. (25 mm)	1-1/2 in. (38 mm)
2 in. (51 mm)	100	100	100	100	100
1-1/2 in. (38 mm)	100	100	100	100	85 to 100
1 in. (25 mm)	100	100	100	94 to 100	65 to 85
3/4 in. (19 mm)	100	100	94 to 100	76 to 82	58 to 77
1/2 in. (13 mm)	100	93 to 100	70 to 88	65 to 76	50 to 68
3/8 in. (10 mm)	96 to 100	85 to 96	61 to 73	56 to 66	46 to 58
No. 4 (5 mm)	72 to 84	58 to 78	48 to 56	45 to 53	38 to 50
No. 8 (2.4 mm)	46 to 57	41 to 53	40 to 47	36 to 44	29 to 43
No. 16 (1.1 mm)	34 to 44	32 to 42	32 to 40	29 to 38	21 to 34
No. 30 (600 µm)	22 to 33	19 to 30	20 to 32	19 to 28	13 to 27
No. 50 (300 µm)	10 to 18	8 to 15	10 to 20	8 to 20	7 to 19
No. 100 (150 µm)	2 to 7	1 to 5	3 to 9	2 to 8	2 to 8
No. 200 (75 µm)	0 to 2	0 to 2	0 to 2	0 to 2	0 to 2

*Combined grading for shotcrete should be in accordance with ACI 506R or ASTM C1436.

Stiffer fibers such as steel and some macrosynthetic fibers can form blockage or clumping when used in highly congested elements. Care should be taken in selecting fiber length and volume to avoid this issue, ACI 544.3R recommends that, unless a full-scale test is performed, fiber length should not exceed half the clear spacing between reinforcement (ACI 544.3R**,** Grünewald 2004). Little data are available on this topic; however, work with 1.2-in. (30-mm) steel fibers to evaluate blocking concluded that the minimum gap width between reinforcement depends on the fiber length, aspect ratio, and volume (Groth 2000). Based on the work performed, guidelines to avoid blocking using SFRC were developed (Table 2-16).

Table 2-16 Guidelines for assessing blocking of SFRC (Groth 2000)

Reinforcement spacing to fiber length ratio	Fiber aspect ratio	Fiber content (lb/ft^3)
3	80	1.9
	65	3.8
2	65	1.9
	45	3.8
1	45	1.9

2.7.5 Bleeding and segregation

Increases in cumulative bleed water volumes of over 20% and 30% were seen when using steel hooked end fibers of 1.2-in. (30-mm) and 2.4-in. (60-mm), respectively (Figure 2-16) (Uygunoglu 2011). Dhonde et al. (2005), however, reported that no segregation or bleeding occurred when using steel fibers of 1.2 in. (30 mm) and 2.4 in. (60 mm) length at volume fraction ranging from 0.5-1.5%. VSI index of 0-1 was reported for all mixture prepared. Furthermore, Patniak (2013) reported that no bleeding or segregation was observed when working with 0.35-4% volume fraction of basalt fibers of 1.7 in. (43 mm) length.

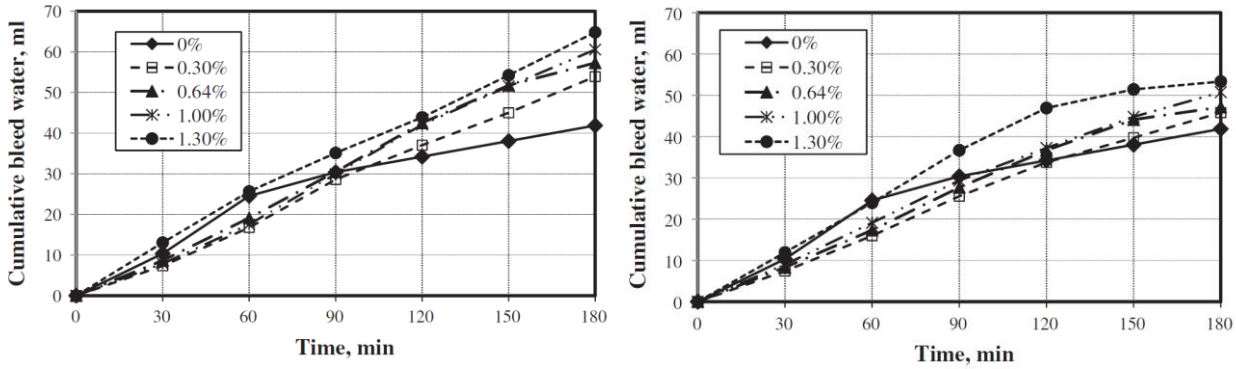

Figure 2-16 Cumulative bleeding in steel fiber-reinforced concrete: (a) 2.4 in. (60 mm), and (b) 1.2 in. (30 mm) (Uygunoglu 2011)

2.8 Effect of fibers on mechanical properties

The use of fibers in concrete are thought to provide an overall improvement in mechanical properties. While this is generally true, the relative improvements in individual properties may not be uniform with an increase in fiber volume. This chapter presents research on the effect of fibers on mechanical properties, examining each property individually to understand the effect of fibers on that property.

2.8.1 Compressive strength

Behavior of compressive strength of FRC has been extensively investigated. Typical fiber dosage levels do not substantially increase compressive strength when compared to control samples (Arslan 2016, Ayub et al. 2014a, Jiang et al. 2014 , Krassowska and Lapko 2013, Yin et al. 2015, ACI 544.1R- 96, Kizilkanat 2015). Variation in compressive strength of 0-25% for up to 1.5% volume fraction has been reported (Figure 2-17 through Figure 2-19). The increase in compressive strength is most likely due to control of micro-cracking provided by fibers, while decrease is often attributed to increased percentage of entrapped air when using high volumes of fibers (Folliard et al. 2006).

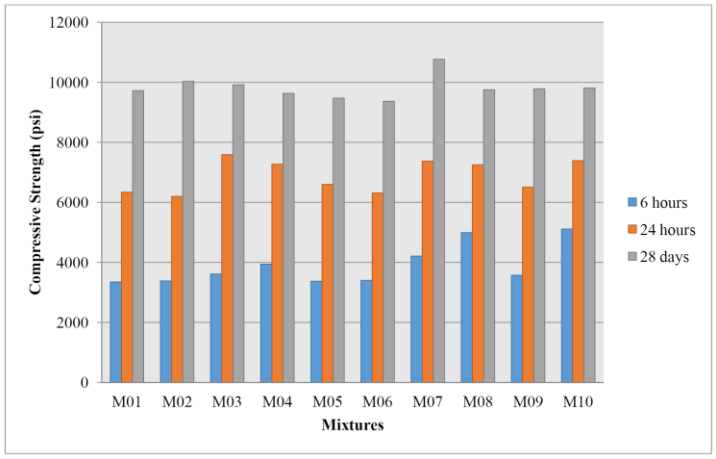

Mix	Fiber Type	Fiber Volume fraction (%)
M01	None	0
M02	Polypropylene 0.5" multifilament	0.1
M03	Steel 0.5" monofilament	0.1
M04	Glass 0.5" monofilament	0.1
M05	Basalt 0.5" monofilament	0.1
M06	Nylon 0.5" monofilament	0.1
M07	Polypropylene 1.5" macro synthetic	0.1
M08	Polypropylene 3/4" fibrillated	0.1
M09	Nylon 0.5" monofilament	0.3
M10	Polypropylene 3/4" fibrillated	0.3

Figure 2-17 Compressive strength for different fibers (N Suksawang et al. 2014)

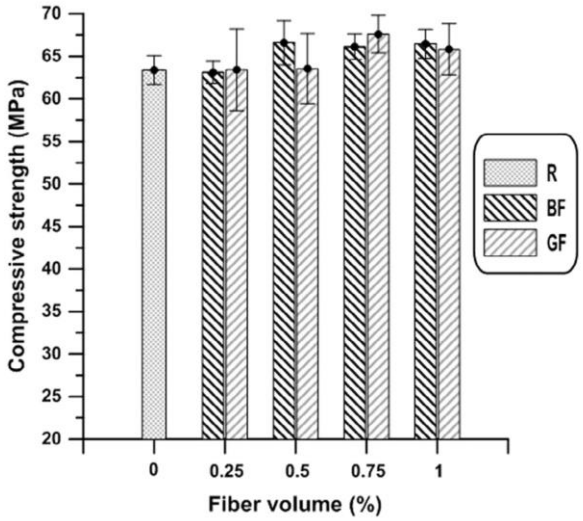

Figure 2-18 Compressive strength for basalt and glass fibers (Kizilkanat et al. 2015)

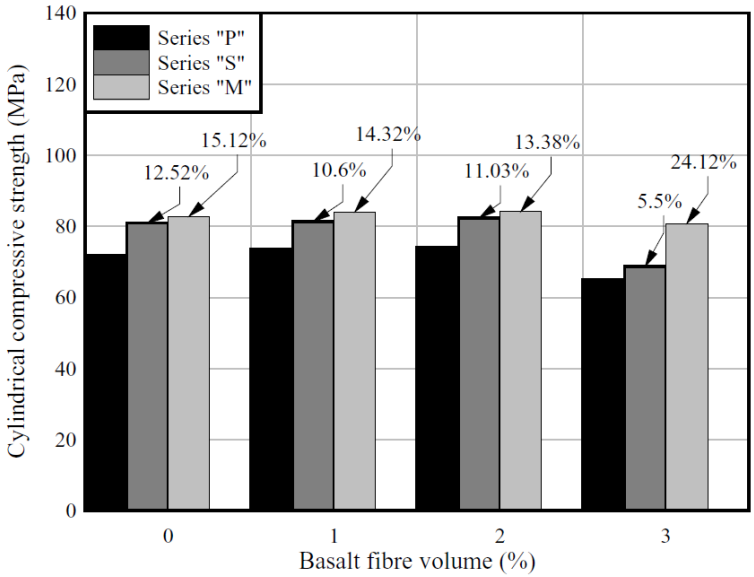

Figure 2-19 Compressive strength for basalt fibers, using plain concrete (series P), 10% silica fume (series S) and 10% met kaolin (series M). (Ayub et al. 2014)

2.8.2 Tensile strength

Concrete is a brittle material with low tensile strength; tensile strength is commonly in the range of 10-15% of its compressive strength. In FRC, however, fiber-bridging action can result in improved crack control and tensile strength

Yazici et al. (2006) found that tensile strength (using split-cylinder tensile strength) was improved by 11-54% using steel fibers with aspect ratio of 80 and volume of up to 1.5%. Kizilkanat et al. (2015) reported an increase of up to 40% using 1% volume fraction of basalt fiber and 27% using 0.75% volume fraction of glass fiber when testing the split tensile strength (Figure 2-20). Yurtseven (2004) reported that polypropylene and carbon fibers at 0.6% volume fraction improved splitting tensile strength by 19.5% and 31.6%, respectively. An increase in

splitting tensile strength (tested in accordance with BS 1881-117: 1983 1983) of up to 30% was seen using basalt fibers of 1 in. (25 mm) length (Ayub et al. 2014) while Patnaik (2013) reported an increase of up to 50% in flexural tensile strength when using 1.7-in. (43 mm) basalt fibers (Figure 2-21).

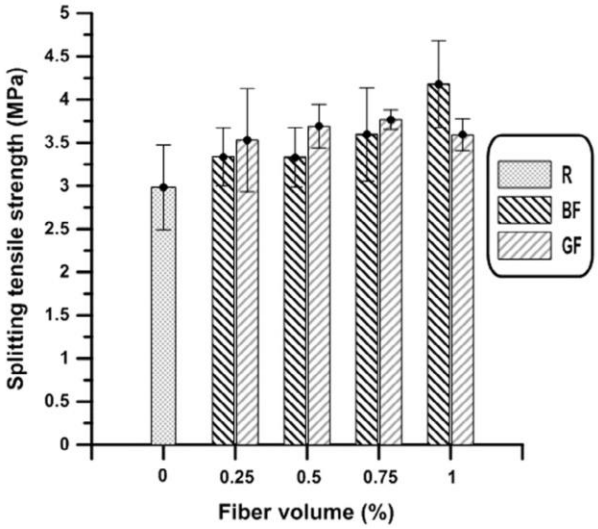

Figure 2-20 Splitting tensile strength for basalt and glass samples (Kizilkanat et al. 2015)

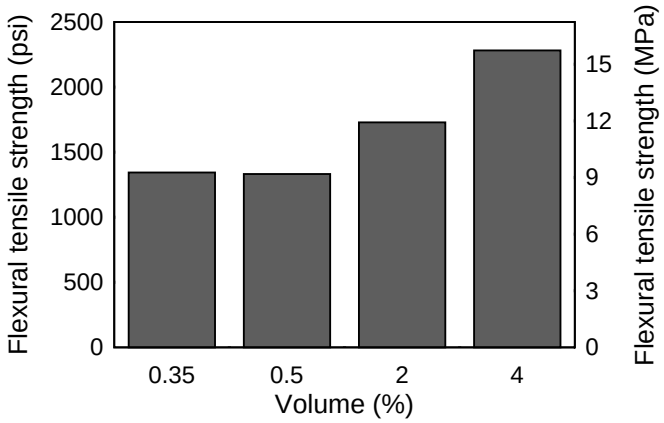

Figure 2-21 Flexural tensile strength for basalt fibers at varying percent volume (Patnaik 2013).

2.8.3 Flexural strength

Flexural strength increases of 50-70% have been reported when incorporating fiber reinforcement (Tadepalli et al. 2009, Yazici et al. 2006). Improvement depends on fiber material, properties, volume, and bond strength between the fiber and the matrix. Fiber properties such as length and shape affect the strength of mechanical bond between the fibers and the matrix; longer and deformed fibers provide better mechanical bond, which increases flexural strength (Figure 2-22, Figure 2-24).

When compared with plain concrete, steel fibers added at 1.5% volume fraction showed an increase in flexural capacity of 40%, while basalt fibers showed an increase of about 60% (Krassowska and Lapko 2013). Yazici et al. (2006) performed work with steel fibers at different

volumes and aspect ratios. Increase in flexural strength of 30-60% for aspect ratios varying from 45 to 80 was reported (Yazici et al. 2006).

Glass fibers performed better than basalt fibers of 0.5 in. (12 mm) length, but glass fibers showed no significant improvement as volume was increased beyond 0.5% (Figure 2-23). When compared with polypropylene fibers, basalt fibers showed higher flexural strength and improved post-crack response (Figure 2-24).

Due to the improved mechanical bond between fiber and concrete, when the volume and aspect ratio are increased, flexural strength is increased. At a higher volume fraction (1%), increases of up to 32% and 34% was reported when using glass and basalt fibers, respectively (Kizilkanat et al. 2015). As fiber volume of steel fibers is increased from 0.5% to 1.5%, flexural strength is increased by 20- 60% (Yazici et al. 2006). For increased aspect ratio from 45 to 80 the flexural strength can be increased by up to 70% (Yazici et al. 2006).

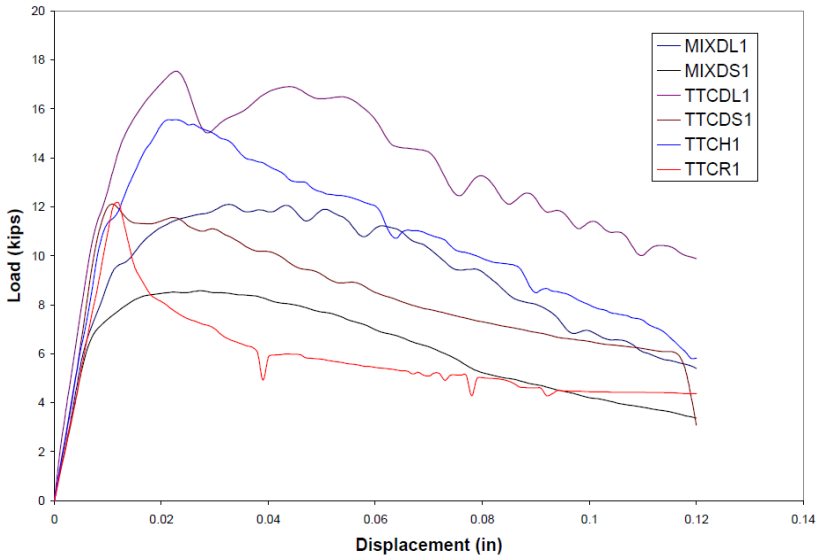

Figure 2-22 Load-displacement for different steel fibers at 0.5% content (Tadepalli et al. 2009)

Table 2-17 Fiber designation followed by Tadepalli et al. 2009

Mix	MIXDL1	MIXDS1	TTCDL1	TTCDS	TTCR1	TTCH1
Fiber shape	Hooked end					Twisted
Manufacturer	Dramix				Royal	Helix
Aspect ratio	80	55	80	55	53	50

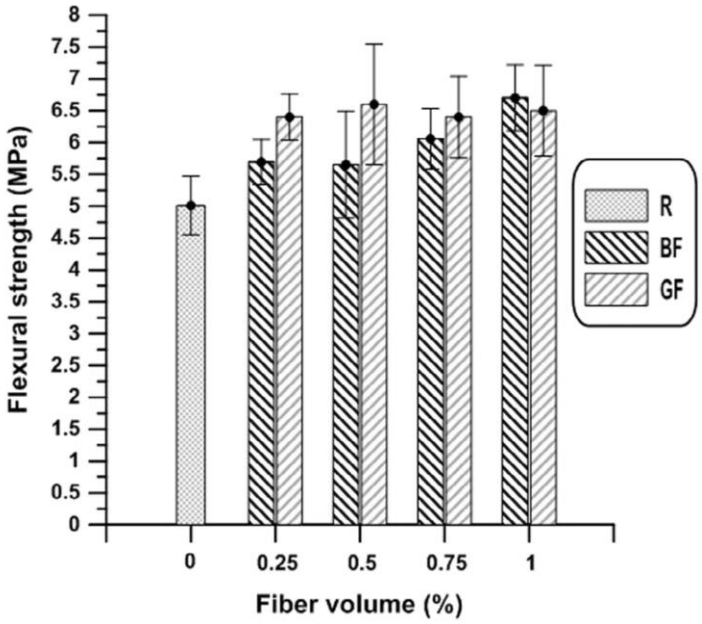

Figure 2-23 Flexural strength for basalt and glass samples (Kizilkanat et al. 2015)

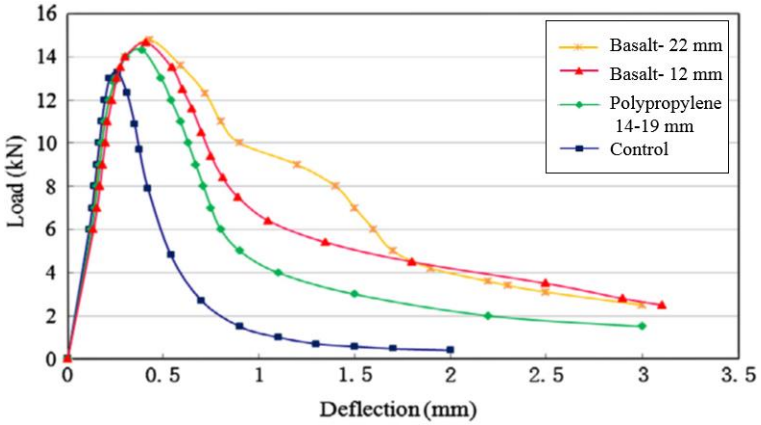

Figure 2-24 Load-deflection curve for various fibers at 0.3% volume (per ASTM C1609) (Jiang et al. 2014)

Jiang et al. 2014 performed work with polypropylene and basalt fibers at volumes less than 0.3%. Less than 10% increase in flexural strength was noted as fiber material or length was changed (Figure 2-24). Nevertheless, a difference between the post-cracking response of conventional concrete and FRC was seen. The longer fibers showed a more gradual decrease in post-cracking load when compared with both conventional concrete and FRC with shorter fibers (Figure 2-22 and Figure 2-24).

Limited work has been performed to evaluate the behavior of FRC produced with hybrid fibers. Blending of fibers with varying characteristics may provide greater improvement in flexural capacity than single fiber FRC (Mobasher 2011, Markovic 2006, Lawler et al. 2005 and Yao et al. 2003). Mixtures containing blended steel fiber lengths of 0.5 in. and 2.4 in. (13 mm and 60 mm) has shown higher flexural strength and a more ductile response (Figure 2-25; Markovic 2006).

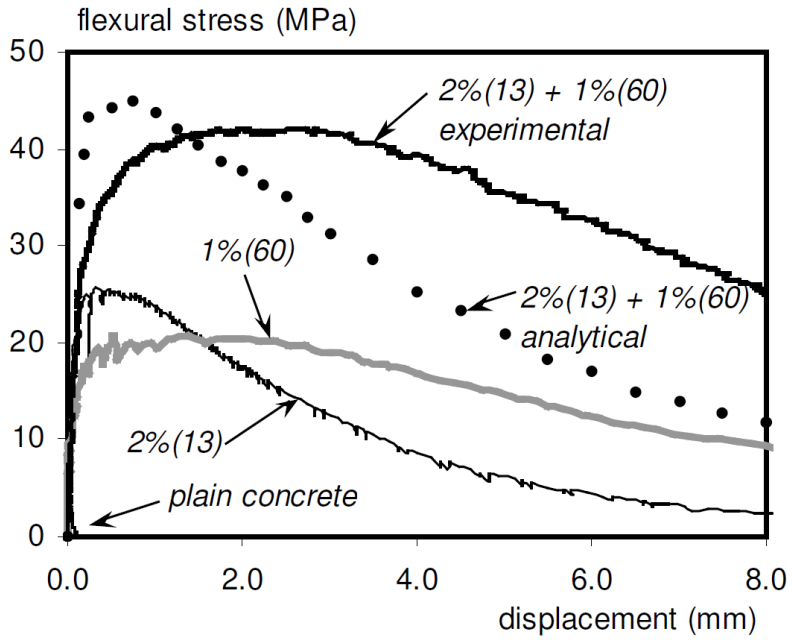

Figure 2-25 Flexural behavior of concrete with 0.5 in. (13 mm) long straight steel, 2.4 in. (60 mm) long hooked end steel fiber and a combination of both. (Markovic 2006)

2.8.4 Residual strength

Materials that are brittle in nature such as concrete have negligible post-cracking ductility. The mechanical property that is predominantly affected by fiber reinforcement is the residual strength. Residual strength describes the post-cracking response of the material and is due to the bridging action of the fiber reinforcement. Enhancement of concrete mechanical properties such as tensile and flexural strength is due to the improved post-cracking capacity and improved ductility that fibers provide.

Suksawang et al. (2014) and Yazdani el al. (2002) performed work with different fiber types and lengths. They determined that steel fibers provided improvement of residual strength when compared with microsynthetic fibers (Figure 2-26). Residual strength was increased as the fiber shape changed and volume fraction was increased. This improvement was due to enhanced bond and more fibers crossing cracks (Figure 2-26 and Figure 2-27). Hybrid fiber FRC in some cases can provide better improvement in residual strength than single-fiber FRC (Figure 2-28).

Polypropylene fibers chemically enhanced to bond with concrete have been developed (Attiogbe et al. 2014). Compared with a reference fiber (only mechanical bond provided) of similar physical and mechanical properties, residual tensile strength (ASTM C1399) was increased by 37% (Figure 2-29).

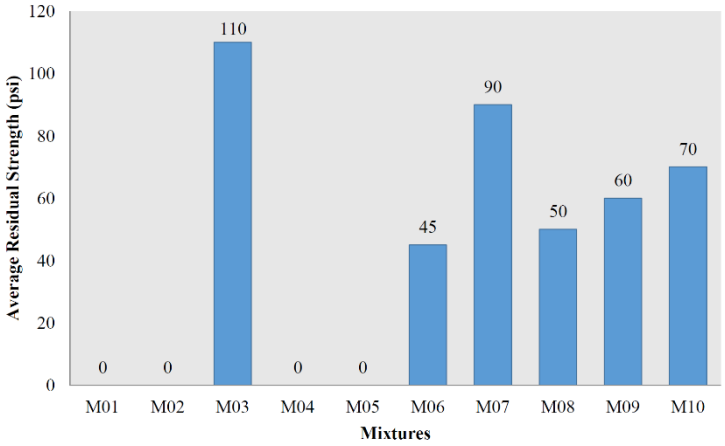

Mix	Fiber Type	Fiber Volume fraction (%)
M01	None	0
M02	Polypropylene 0.5" multifilament	0.1
M03	Steel 0.5" monofilament	0.1
M04	Glass 0.5" monofilament	0.1
M05	Basalt 0.5" monofilament	0.1
M06	Nylon 0.5" monofilament	0.1
M07	Polypropylene 1.5" macro synthetic	0.1
M08	Polypropylene 3/4" fibrillated	0.1
M09	Nylon 0.5" monofilament	0.3
M10	Polypropylene 3/4" fibrillated	0.3

Figure 2-26 Average residual strength using different fibers (per ASTM C1399) (Suksawang et al. 2014)

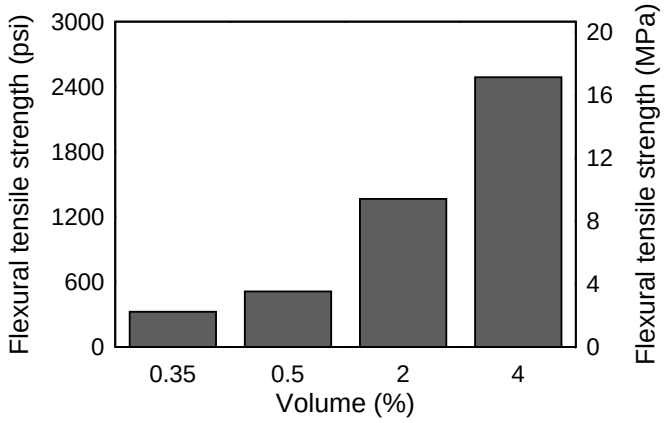

Figure 2-27 Average residual strength using 1.7 in. (43 mm) basalt fibers (per ASTM C1399) (data obtained from Patnaik 2013)

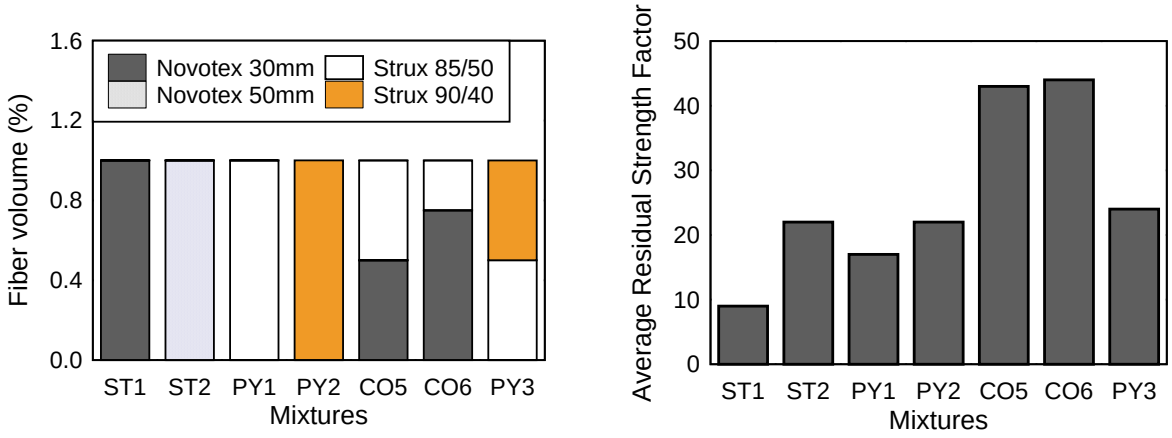

Figure 2-28 Average residual strength for hybrid fibers (Nehdi and Ladanchuk 2004)

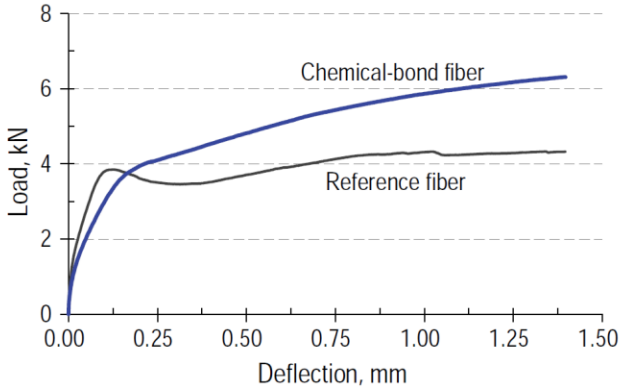

Figure 2-29 Load-deflection curve (ASTM C1399) for polypropylene fibers at 5 lb/cy (Attiogbe et al. 2014)

2.8.5 Creep

Creep is time-dependent deformation that occurs under sustained stress and can result in excessive deflections and loss of prestress force among other serviceability issues. Due to the relatively low volume of fibers used in FRC, the effect of fibers on compressive creep is typically negligible. Furthermore, fibers typically benefit the post-cracking behavior of concrete. Kurtz et al. (2000) indicated that creep failure occurred in cracked micro-synthetic FRC for sustained stress levels. Micro-synthetic FRC could only sustain a small percentage of the post-crack stress. Creep of the fiber/matrix interface bond was an important aspect because most FRC mixtures are designed to fail in pullout mode rather than fiber-fracture mode.

While a reduction in flexural creep is possible with the use of high-modulus fibers, Serna et al. 2015 found that creep rate increased in samples with synthetic fibers and decreased in samples containing steel fiber (Figure 2-30). Bernard 2010b found that at volume fractions less than 1% no measurable creep occurred.

After long-term loading and different levels of environmental exposure there was no substantial reduction in residual flexural tensile strength in samples with synthetic fibers, but a reduction of approximately 60% was noted in samples containing steel fibers and immersed in seawater (Figure 2-31).

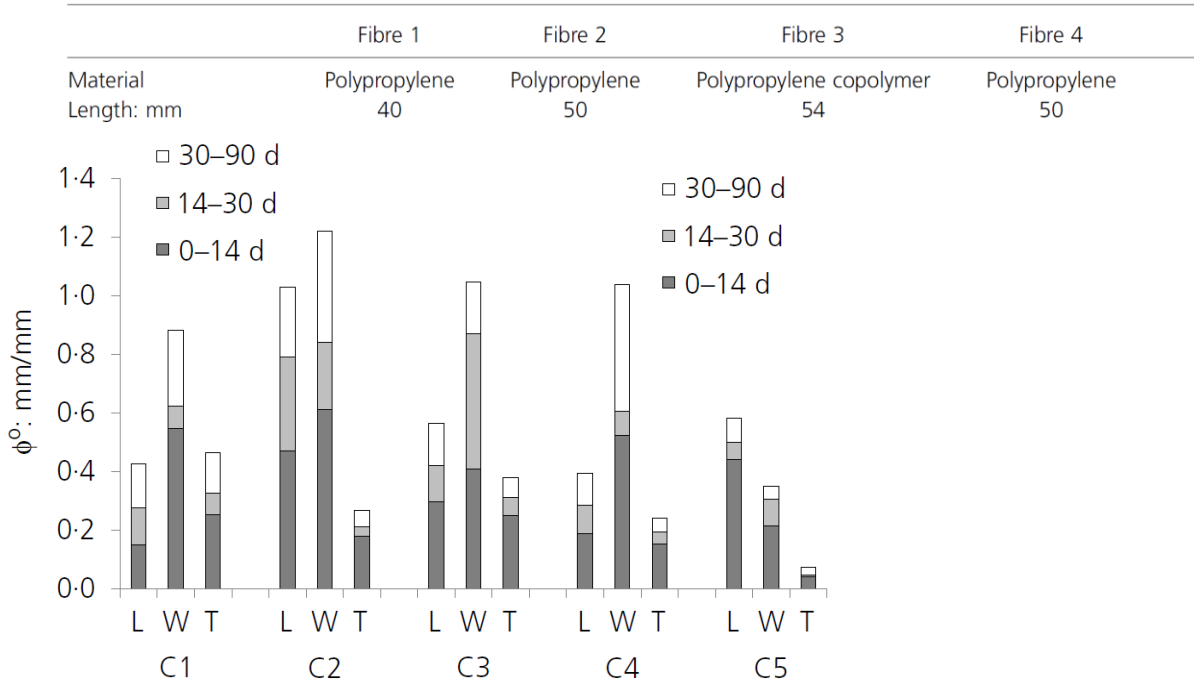

Figure 2-30 Creep coefficient after 14, 30 and 90 days for different ambient exposures (Ros et al. 2015)

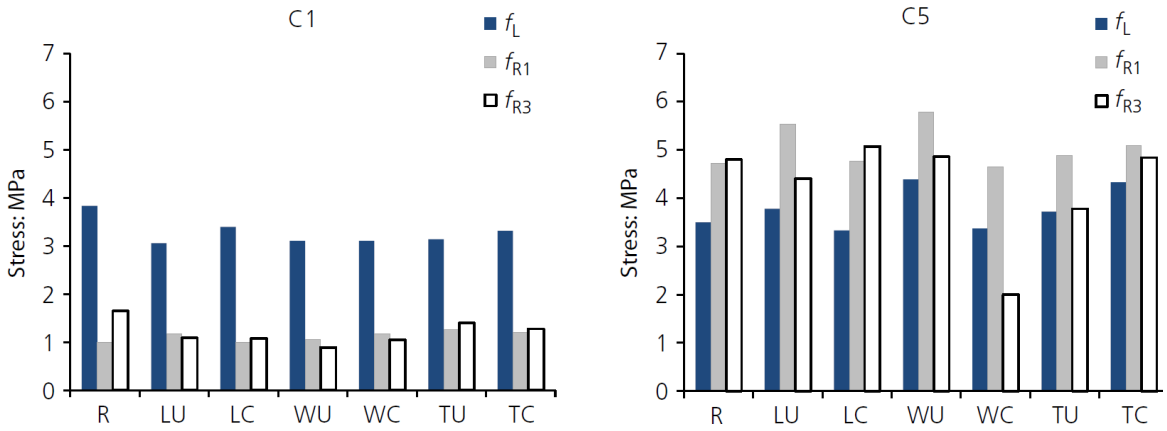

Figure 2-31 Comparison of first-peak strength and residual first-peak strength (Ros et al. 2015)

2.8.6 Drying shrinkage cracking

Volumetric change due to the loss of moisture in hardened concrete leads to shrinkage. Internal or external constraints prevent the change in volume from occurring, which may result in the development of tensile stresses and, ultimately, cracking of the matrix. Because of the bridging action across the cracks, fibers have been found to help control crack length and width (ACI 544.1R), which can improve durability.

In restrained ring testing, control samples showed average crack widths of 0.35 in. while average crack widths on samples containing fibers (5-10 lb/yd^3) varied from 0.005-0.008 in. (Ideker et al. 2014).

Compared with other fibers, at the same volume fraction, polypropylene fibers shown improved ability to reduce early age crack width (Suksawang et al. 2014). Polypropylene fibers at volumes ranging between 0.1% and 0.2% showed a reduction in maximum cracked width of up to 80% (Figure 2-32) compared with control specimen (Suksawang et al. 2014,Soroushian et al. 2004).

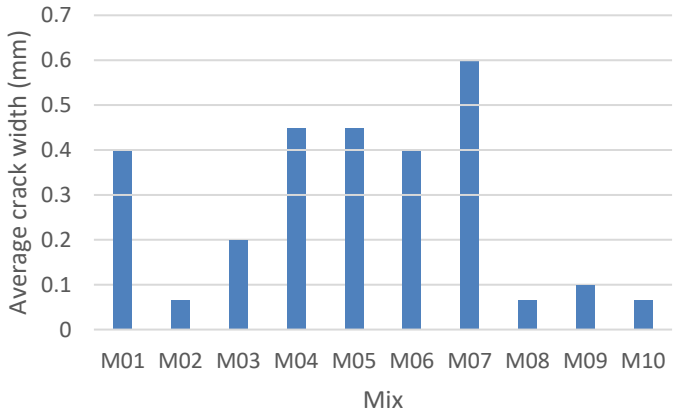

Mix	Fiber Type	Fiber Volume fraction (%)
M01	None	0
M02	Polypropylene 0.5" multifilament	0.1
M03	Steel 0.5" monofilament	0.1
M04	Glass 0.5" monofilament	0.1
M05	Basalt 0.5" monofilament	0.1
M06	Nylon 0.5" monofilament	0.1
M07	Polypropylene 1.5" macro synthetic	0.1
M08	Polypropylene 3/4" fibrillated	0.1
M09	Nylon 0.5" monofilament	0.3
M10	Polypropylene 3/4" fibrillated	0.3

Figure 2-32 Restrained shrinkage average crack width (per ASTM C1581) (Suksawang et al. 2014)

2.8.7 Corrosion

Concrete typically provides the embedded steel reinforcement with excellent corrosion protection. The high alkaline environment combined with the durable low permeability covering provides a system that is generally very durable. One source of problems, however, are cracks that, when not properly controlled, can lead to reinforcement corrosion due to the carbonation of the concrete and the intrusion of moisture, oxygen, and chloride ions or other corrosive elements. The exact role of cracking in the corrosion process, however, is not clear.

Corrosion can affect both deformed steel reinforcing bars and steel fibers. Unchecked corrosion will eventually result in further cracking and spalling of concrete due to the expansion of the corrosion products. Minimizing crack widths is thought to provide improved corrosion protection by slowing the ingress of corrosive agents. Through bridging action, fibers help control crack growth, resulting in reduced corrosion rates of steel reinforcement compared to conventional concrete (Blunt et al. 2015, Jen et al. 2016, Sanjuán et al. 1997, 1998, Solgaard et al. 2013). Jen et al. (2016) performed work using hybrid fiber combination of polyvinyl alcohol microfiber of 0.3 in. (8 mm) length and steel fiber of 1.2 in. (30 mm) length. Work was performed to verify the effect of fibers on corrosion of reinforcing steel using pre-damaged and undamaged samples. Figure 2-33 shows both pre-damaged and undamaged FRC samples had lower chloride content.

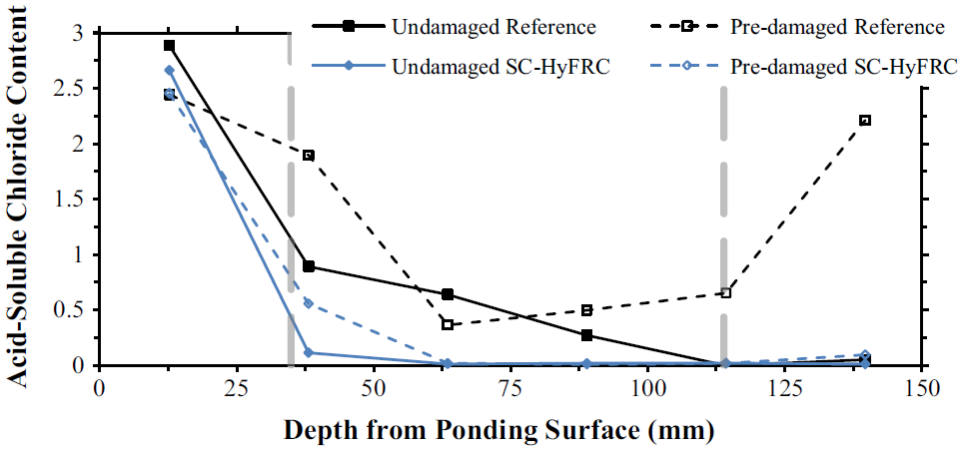

Figure 2-33 Chloride content profile of core sample (vertical lines are centerline of reinforcing steel) using combination of steel and polyvinyl alcohol fibers (Jen et al. 2016)

Steel fiber corrosion can cause volumetric change and toughness reduction of fibers, causing the failure mechanism to change from pullout to fiber rupture due to section loss from corrosion (Frazão et al. 2015, Kosa and Naaman 1990). For uncracked sections with compressive strengths over 3000 psi, well-consolidated, and with water-to-cement ratios in compliance with ACI 318, corrosion of fibers has been shown to occur only at the samples' surfaces, with no propagation of corrosion beyond 0.1 in. below the surface (ACI 544.1R). In cracked sections with crack widths less than 0.004 in., no corrosion was found along the fibers bridging the cracks (ACI 544.1R).

Narrow, shallow cracks are not expected to reduce strength (ACI 544.1R and ACI 544.4R). Cracks wider than 0.004 in., however, can cause up to a 30% reduction in residual strength (Bernard 2010a, Berrocal et al. 2016).

Frazão et al. (2015) found that volumetric change of fibers due to corrosion can cause microcracking in the surrounding concrete in extremely aggressive environments (Figure 2-34). Such volumetric change, however, is not large enough to cause concrete spalling (ACI 544.4R).

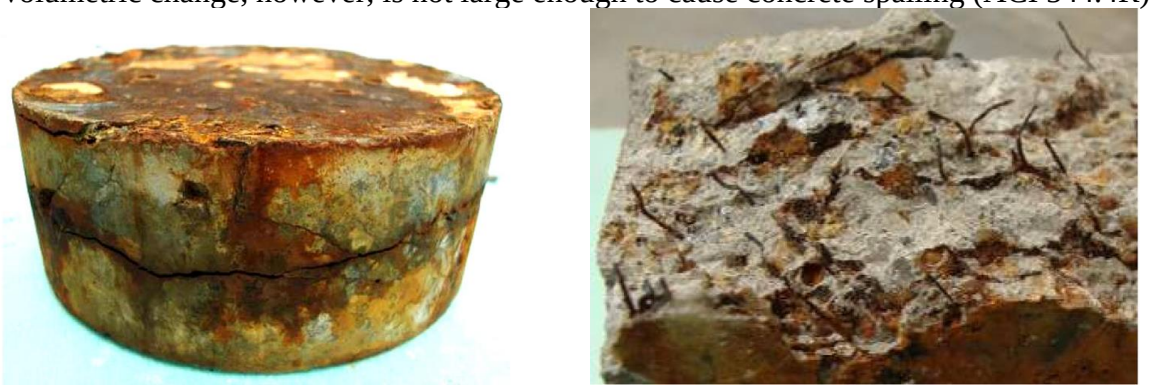

(a) (b)

Figure 2-34 Micro crack in steel fiber-reinforced SCC samples (a) and fracture surface (b) (Frazão et al. 2015)

2.9 Self-consolidating concrete and fibers

Self-consolidating concrete (SCC) is a highly fluid mixture that, unlike conventional concrete, can flow around reinforcement and consolidate within formwork by its own weight, without vibration. Its high flowability make it ideal for use in heavily reinforced elements where space is limited for placement and consolidation. Due to increased workability and ductility, fiber-reinforced self-consolidating concrete (FRSCC) is potentially a solution to problems due to poor workability and cracking. In addition, due to SCC high compactness and fine particle content, mechanical bond between the fiber and concrete matrix can be improved, leading to increased toughness and residual strength.

For SCC to comply with workability requirements, a mixture should possess three main properties: filling ability, passing ability, and segregation resistance. The performance requirements for each of the SCC properties should be determined by addressing the method of placement, form geometry, reinforcement density and configuration, and compliance requirements of the applicable local agencies. Some of the methods to measure these properties, and the limits on such measurements, are presented in this section.

2.9.1 Test methods for fresh properties

For SCC to comply with workability requirements, a mixture should possess three main properties: filling ability, passing ability, and segregation resistance. Where flowability is the ability to flow and fill the formwork under its own weight, passing ability is the ability to flow around obstructions such as around reinforcement, and segregation resistance measures the ability to remain homogenous during mixing, transport, and placement. Various test methods can be used to measure fresh properties of a SCC mixture.

Table 2-18 lists the most common standardized methods to assess SCC fresh properties and the property measured, Figure 4-36 shows the test setup for each method.

Table 2-18 Common testing for SCC fresh properties

Test	Standard	Property measured
Slump flow	ASTM C1611	Flowability
VSI	ASTM C1611	Segregation
J-Ring	ASTM C1621	Passing ability
Bleeding	ASTM C232	Bleeding
Segregation	ASTM C1610	Segregation
Static segregation	ASTM C1712	Segregation
V-funnel	BS EN 12350-9	Filling ability
L-box	BS EN 12350-10	Passing ability

(a)

(b)

(c)

(d)

(e)

(f)

Figure 2-35 Common testing for SCC fresh properties: (a) ASTM C1611, (b) ASTM C1621, (c) ASTM C1610, (d) ASTM C1712, (e) BS EN 12350-9 and (f) BS EN 12350-10

2.9.2 FDOT requirements for fresh properties

FDOT Materials Manual (FDOT 2015) section 8.4 provides instructions for use and acceptance of SCC mixtures for manufacturing of precast/prestressed concrete products. This document provides guidelines for quality control, mixture design requirements, and properties. Tests required to be performed to determine SCC fresh properties and the respective limit are listed in Table 2-19.

Table 2-19 FDOT (2015) specified limits for fresh properties of SCC for precast/prestressed concrete products

Standard	Parameter	Limit
ASTM C1611	Slump flow	Shall be less or equal to 27.0 inches ($\pm$2.5 in.)
ASTM C1611	VSI	Shall be less or equal to 1
ASTM C1611	T_{50}	Recommended 2-7 seconds
ASTMC1621	Passing ability	Shall not exceed 2.0 inches
ASTM C1610	Segregation	Shall not exceed 15%

2.9.3 EFNARC criteria for fresh properties

The European Federation of Producers and Contractors of Specialist Products for Structures (EFNARC) provides technical reports and guidelines for concrete construction. In early 2002, EFNARC developed specifications and guidelines for SCC with requirements for material composition. These guidelines recommend the evaluation of the workability parameters shown in Table 2-20.

When compared to the requirements established by the FDOT, EFNARC has a broader variety of acceptable test methods to determine the properties of SCC. In addition, it provides a wider range of acceptance for slump flow, allowing for mixes with less filling ability. Requirements for T_{50} are in similar range. Another difference is seen in passing ability assessment; while both EFNARC and FDOT use the same test methodology, assessment is made using different criteria. EFNARC specifies use of J-Ring where the criterion is the difference between the concrete surface in the center and in the edge of the ring. While FDOT follows ASTM C1621standard where assessment of passing ability is made based on the difference between the unrestrained flow (ASTM C1611) and obstructed flow (ASTM C1621).

Table 2-20 EFNARC acceptance criteria for SCC.

Property	Method	Typical range of values
Filling ability	Slump flow	25.5-31.5 in. (650-800 mm)
	T_{50}	2-5 sec
	V Funnel	8-12 sec
	Orimet test	0-5 sec
Passing ability	J Ring	0-0.4 in. (0-10 mm)
	L Box	0.8-1.0
	U Box	0-1.2 in. (0-30 mm)
	Fill Box	90-100%
Segregation resistance	GTM Screen Stability	0-15%
	V Funnel $T_{5\,minutes}$	0-3 sec

2.9.4 PCI Determination of performance requirements

Precast/Prestressed Concrete Institute (PCI) provides guidelines for the use of self-consolidating concrete in precast/prestressed elements. Based on element characteristics such as element shape or reinforcement level, PCI provides guidelines of placement difficulty for

different workability properties. Recommendations are shown in Table 2-21, where the dark blocks represent situations that could lead to issues during placement.

Table 2-21 Parameter determination based on member characteristics (TR-6-03)

		Slump flow (in.)			T50 time (sec)			Passing ability		
	Level of difficulty	< 22	22-26	>26	< 3	3-5	>5	<15	10-15	>10
Reinforcement level	Low									
	Medium	■			■					■
	High	■			■				■	■
Element shape	Low									
	Medium						■			
	High	■					■		■	■
Element depth	Low	■	■							
	Medium									■
	High				■				■	■
Surface finish importance	Low									
	Medium	■					■			
	High	■	■				■			
Element length	Low									
	Medium	■								■
	High	■	■		■				■	■
Wall thickness	Low	■	■				■			
	Medium	■								
	High									
Coarse aggregate content	Low									
	Medium									
	High								■	■
Placement energy	Low	■	■						■	■
	Medium	■								■
	High				■					

2.9.5 Effect of fibers on SCC fresh properties

Decrease of workability of SCC with the addition of fibers is expected. Siddique et al. (2016) performed work with steel fibers in volumes varying from 0.5% to 1.5% and reported that increased fiber content resulted in decreased slump flow and increased flow time and blocking (Figure 2-36). Observed slump flow was 10% less than that of the control mixture when using 1.5% steel fibers. However, the work conducted by Sahmaran et al. (2006) and Siddique et al. (2016) showed that is possible to satisfy requirements for SCC fresh properties as defined by EFNARC (2002) using steel fibers at volume fractions less than 1.5% (Figure 2-36 and Figure 2-37). Work by Sahmaran and Yaman (2007), Strauss et al. (2014), Khaloo et al. (2014), and

Gurjar (2004) showed that steel fiber reinforcement at a dosage of 0.5-2%, no segregation of aggregates was reported.

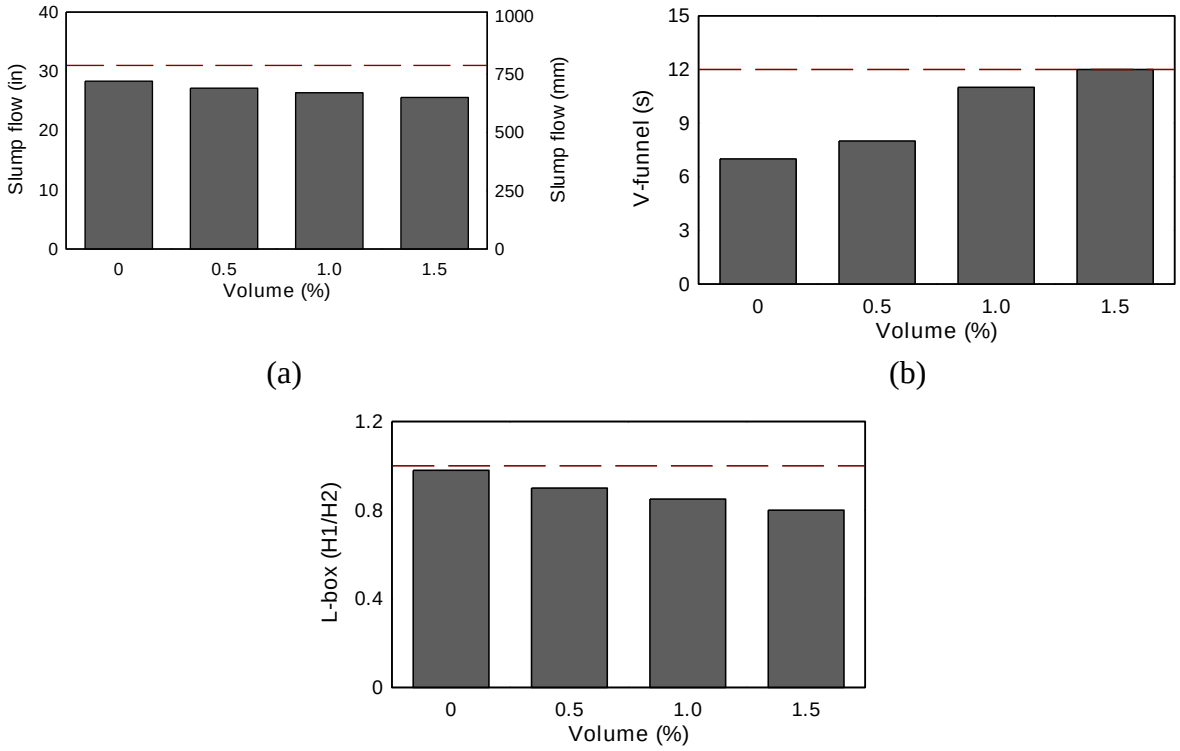

Figure 2-36 Fresh properties for SCC mixtures prepared with 30mm steel fibers (Siddique et al. 2016): (a) slump flow, (b) V-funnel and (c) L-box (maximum limits from EFNARC 2005 are shown in red dashed line).

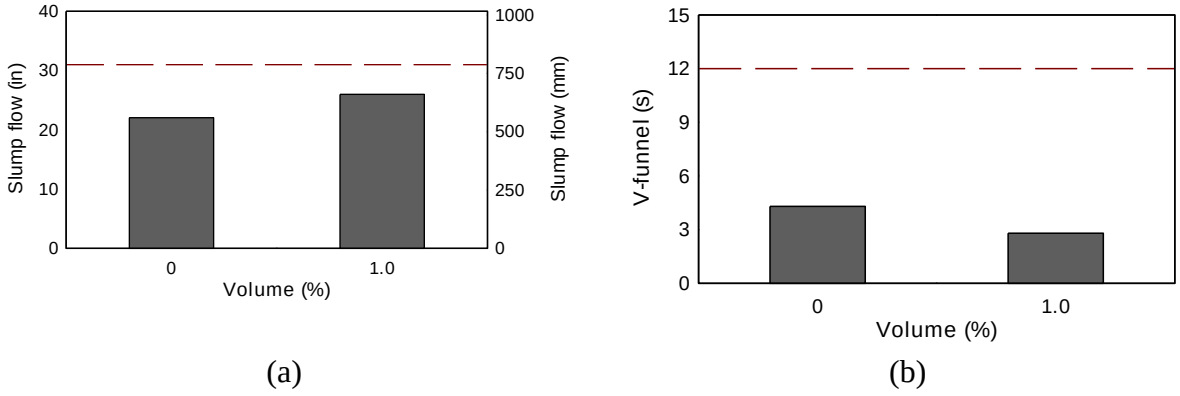

Figure 2-37 Fresh properties for SCC mixtures prepared with 30mm hooked end steel fibers (Sahmaran and Yaman 2007): (a) slump flow, and (b) V-funnel (maximum limits from EFNARC 2005 are shown in red dashed line).

Gencel et al. (2011), Forgeron and Omer (2010), Soutsos et al. (2012), and Aydin (2007) performed work using synthetic fibers (carbon, polypropylene, polyethylene, polyolefin). Similar behavior can be seen as with steel fibers where workability is reduced as dosage and

length are increased. Aydin (2007) performed work with carbon fibers, steel fibers, and a hybrid combination of the two (Figure 2-38). For the same mixture proportions, slump flow decreased when using carbon fibers and steel fibers at 2% volume fraction by 46% and 29%, respectively. Passing ability was reduced by 50-60% compared with control sample, and no segregation was reported. All FRSCC mixtures prepared for the study complied with slump flow, T_{50} range, and passing ability requirements of the FDOT.

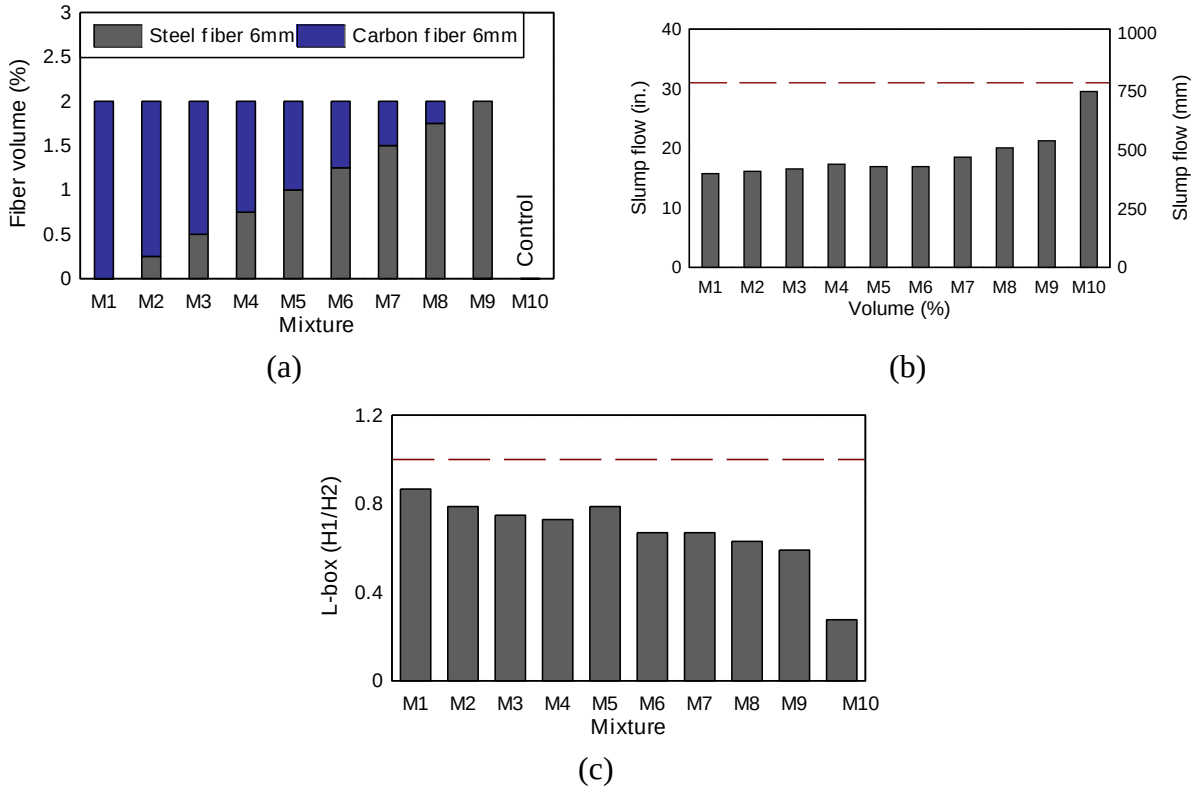

Figure 2-38 Fresh properties for SCC mixtures prepared with steel and carbon fibers (Aydin 2007): (a) mixture proportions, (b) slump flow and (c) L-box.

Experimental work has shown that it is possible to develop SCC mixtures including fiber reinforcement that maintains self-compacting characteristics. To maintain resistance to segregation of the aggregates and fibers, special attention should be given to ensure viscosity is maintained (Ozyurt et al. 2007). Fiber length should be carefully selected to avoid obstruction and ensure good flowability of the mixture.

2.9.6 Effect on mechanical properties

Use of SCC is meant to affect fresh properties of concrete and has negligible effect on hardened properties when compared to conventional concrete. Siddique et al. (2016), Ning et al. (2015), Sahmaran and Yaman (2007), and Soutsos et al. (2012) performed work on mechanical properties in FRSCC. Similar fresh properties was observed as with conventional concrete. Figure 2-39 shows work performed by Siddique et al. (2016), negligible effect is observed on compressive strength, increase in tensile strength and flexural strength is observed due to increased post-cracking capacity.

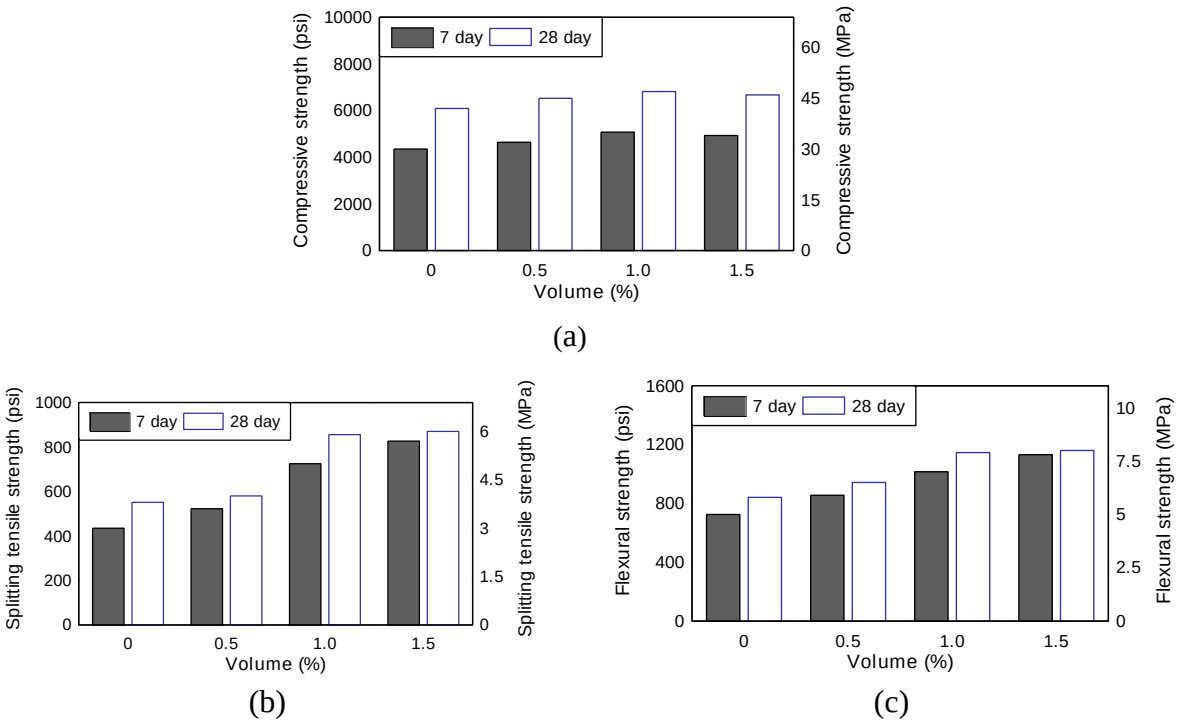

Figure 2-39 Results from Siddique et al. 2016: (a) compressive, (b) splitting tensile and (c) flexural strength of FRSCC mixture with steel fibers

2.9.7 Fiber segregation

Ozyurt et al. (2007) investigated fiber dispersion and segregation in FRSCC and FRC. Alternating current-impedance spectroscopy was used to determine fiber segregation of mixtures prepared with 1% volume of 1.6 in. (40 mm) steel fibers and a viscosity-modifying agent. Variation of fiber content along the height of the samples was found to be less in FRSCC than in FRC (Figure 2-40). FRSCC was found to have better resistance to fiber segregation, good placeability, and higher capacity when compared to FRC.

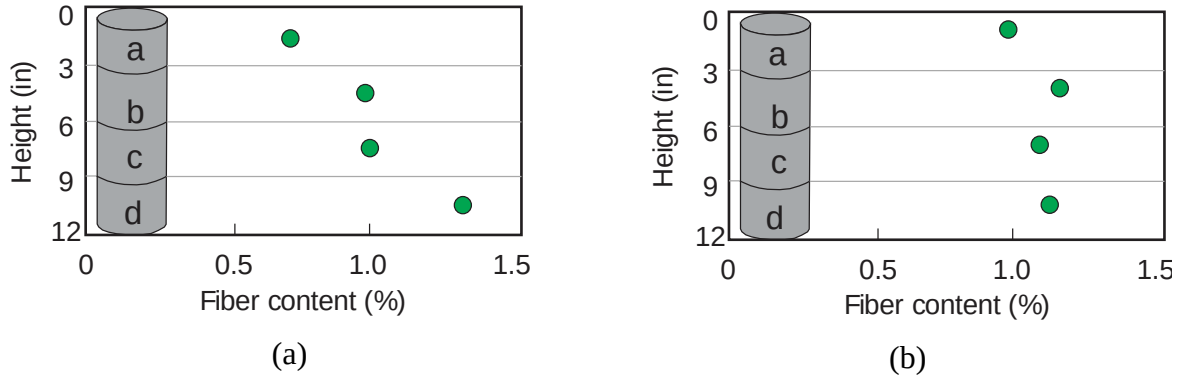

Figure 2-40 Fiber content profile containing 1.6 in. (40 mm) steel fiber for mixture of (a) FRC and (b) FRSCC (Ozyurt et al. 2007)

To avoid segregation, special attention should be given to mixture viscosity. Viscosity modifying admixtures (VMAs) are used to increase viscosity, causing an increase in resistance to segregation of SCC (Ozyurt et al. 2007).

2.10 Test methods for FRC mechanical properties

Various test methods to characterize FRC mechanical properties are available. The methods vary in approach, results obtained, geometry of samples used, and variability of the results. Some of the most common methods and their corresponding methodology are presented in this chapter.

2.10.1 Average residual strength (ASTM C1399)

ASTM C1399 (2010) provides test procedures to determine the average residual strength (ARS) of FRC beam. ARS is the post-cracking flexural strength of a 4 x 4x 14 in. sample beam (Figure 2-41). The sample can either be molded to the specified dimensions or cut from a larger molded specimen.

The sample is tested in two stages. First, the sample is loaded up to initial cracking using a steel plate to control the initial crack width. The sample is unloaded and the steel plate is removed. The beam is then reloaded to a deflection of 0.05 in. to complete the test. Load and deflection are measured during the test (Figure 2-42).

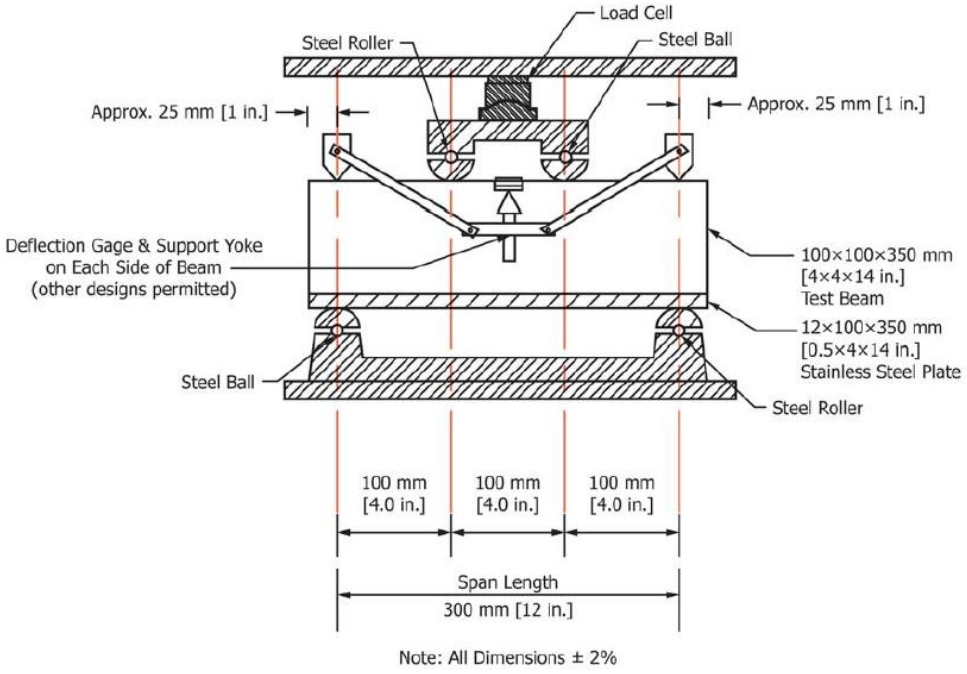

Figure 2-41 Test setup for average residual strength (ARS) (ASTM C1399/C1399M-10)

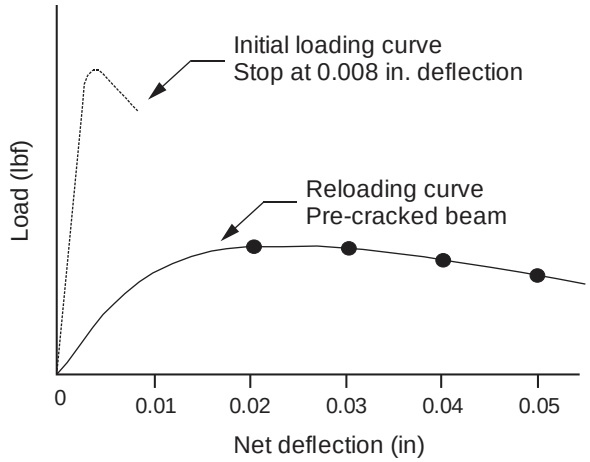

Figure 2-42 Load-deflection curves: ASTM C1399/C1399M-10

Loads corresponding to deflections of 0.02, 0.03, 0.04, and 0.05 in. are used to compute the ARS following Equation 2-5.

$$ARS = \left(\frac{P_A + P_B + P_C + P_D}{4}\right) \times \frac{L}{bd^2} \qquad \text{Equation 2-5}$$

Where ARS is the average residual strength (psi), $P_A + P_B + P_C + P_D$ is the sum of recorded load at the specified deflections (lb.), L is the span length (in.), d is the depth of the beam (in.), and b is the width of the beam (in.).

2.10.2 Flexural performance (ASTM C1609)

ASTM C1609 (2012) provides test procedures to evaluate the flexural performance of FRC samples including first-peak strength, residual strength, and toughness. The preferred sample size is either 4 x 4 x 14 in. or 6 x 6 x 20 in. A specimen size different from the two preferred specimen sizes is permissible. Samples may be either molded or cut from a larger molded sample. Results are expected to vary with the size of the specimen. The specimen is subjected to third-point loading using a closed-loop system (Figure 2-41) at a constant rate (Table 2-22). Load and deflection are measured during the test.

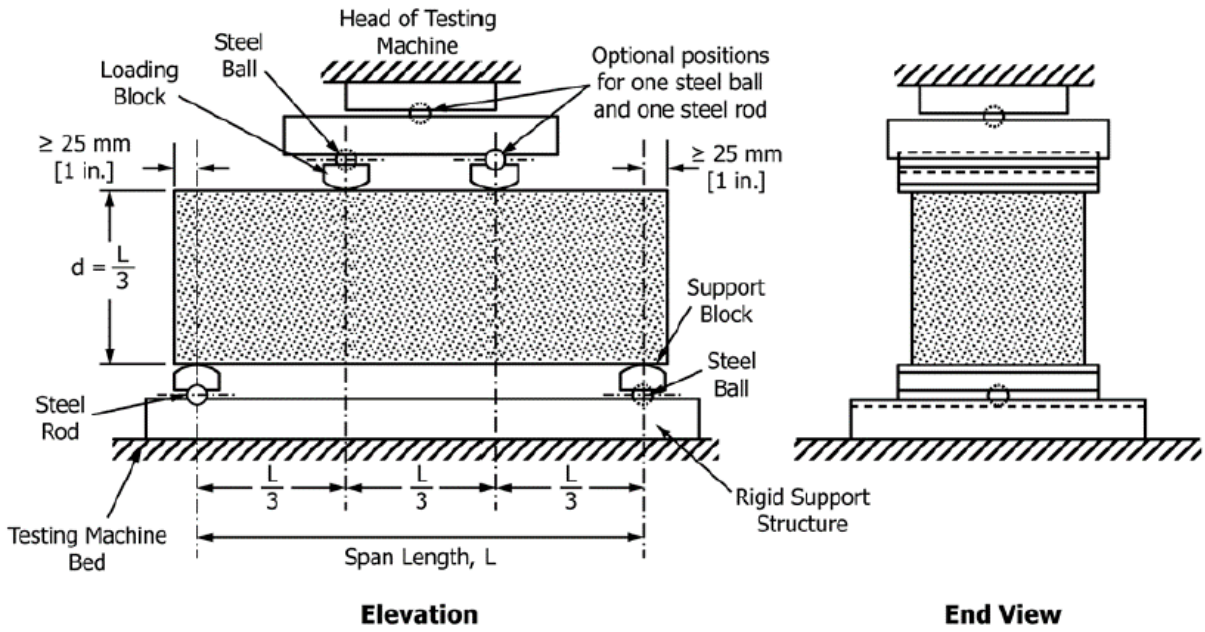

Figure 2-43 Test setup: ASTM C1609/C1609M

Table 2-22 Rate of Increase in net deflection (ASTM C1609/C1609M-12)

100 by 100 by 350 mm [4 by 4 by 14 in.]	0.025 to 0.075 mm/min [0.001 to 0.003 in./min]	0.05 to 0.20 mm/min [0.002 to 0.008 in./min]
150 by 150 by 500 mm [6 by 6 by 20 in.]	0.035 to 0.10 mm/min [0.0015 to 0.004 in./min]	0.05 to 0.30 mm/min [0.002 to 0.012 in. min]

[A]The initial loading rate up to deflection of L/900 for other sizes and shapes of specimens shall be based on reaching the first-peak deflection 40 to 100 s after the

Residual strength is determined using the loads measured at the specified deflections (Figure 2-44) in Equation 2-6.

$$f = \frac{PL}{bd^2}$$ Equation 2-6

where f is the strength, P is the load at given deflection, L is the span length, d is the average depth of the specimen at fracture, and b is the average width of the specimen at the fracture.

Toughness is determined by the area under the load-deflection curve.

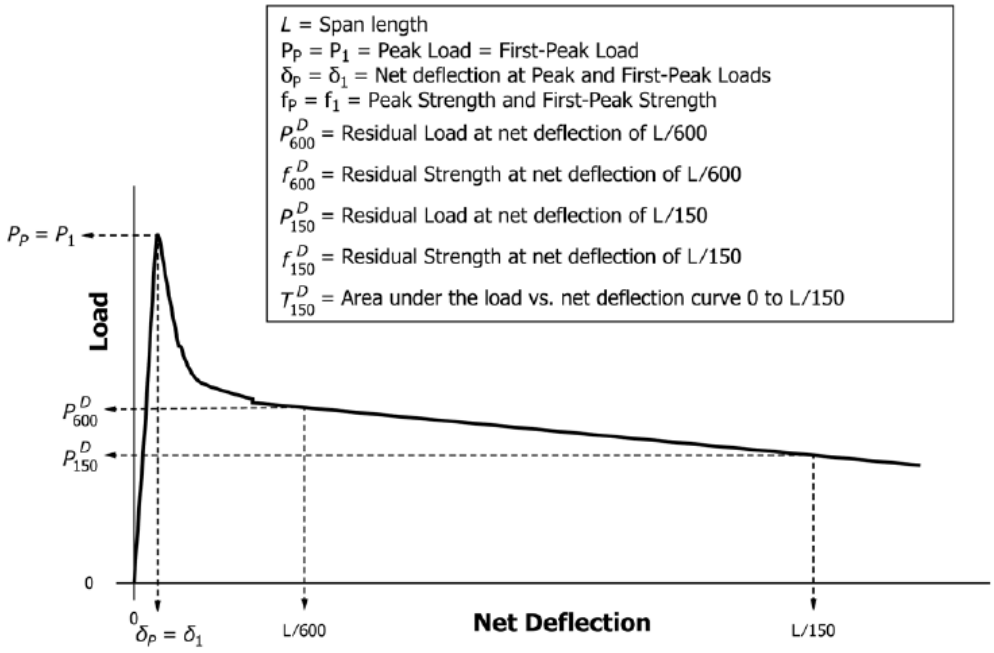

Figure 2-44 Load-deflection curve, and parameters (ASTM C1609/C1609M-12)

2.10.3 Flexural toughness (ASTM C1550)

ASTM C1550 (2012) provides test procedures to determine the flexural toughness of a round FRC plate sample, which is 3 in. (75 mm) thick and 31.5 in. (800 mm) diameter. The panel is supported on three pivots symmetrically placed around the panel circumference and is subjected to a central point load (Figure 2-45).

Load and deflection are recorded and are used to generate a load-deflection curve (Figure 2-46). Flexural toughness is determined as the area under the curve from the origin to the specified central deflection. Toughness in this test is generally defined at central deflections of 0.2, 0.4, 0.8, and 1.6 in. (5, 10, 20, or 40 mm).

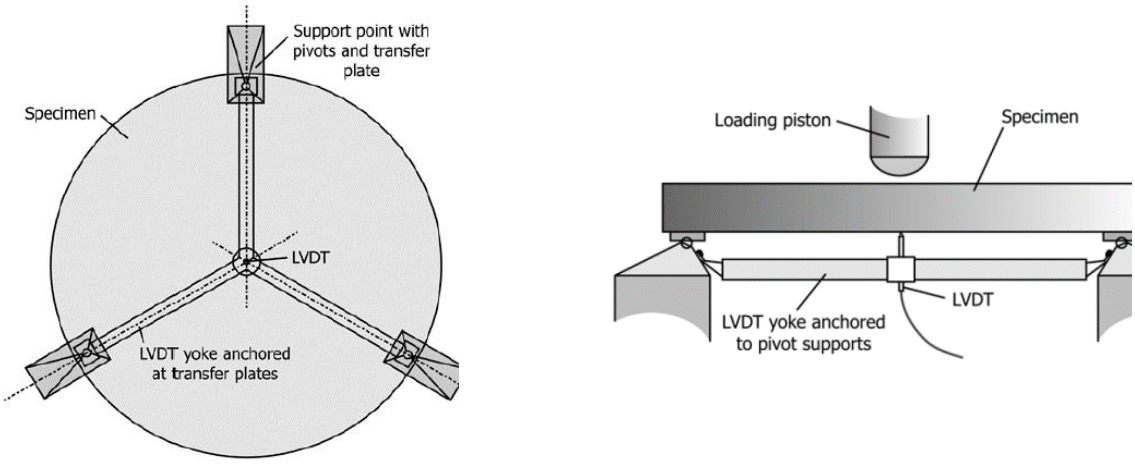

Figure 2-45 Test setup: ASTM C1550 (2012)

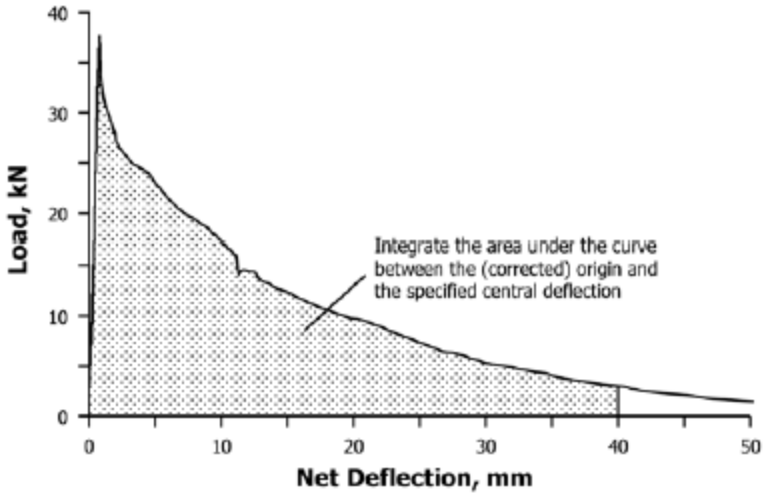

Figure 2-46 Load-net deflection curve (ASTM C1550 2012)

2.10.4 Limit of proportionality (EN 14651)

EN 14651 (2005) provides test procedures to determine the limit of proportionality (LOP) and a set of residual strength (RS) values for a beam sample loaded in flexure. This method is intended primarily for FRC using metallic fibers. Beam specimens are 5.9 in. x 5.9 in. x 21.7 in. (150 mm x150 mm x 550 mm); after samples are formed, a notch is sawn at midspan (Figure 2-47).

Samples are loaded in three-point bending. Crack mouth opening displacement (CMOD) measurements are made at the notch and are used to control the test load rate. RS is determined by Equation 2-7 using the loads for specified CMOD values of 0.02, 0.06, 0.10, and 0.15 in. (0.5, 1.5, 2.5 and 3.5 mm).

Equation 2-7

$$f_{R,j} = \frac{3F_j l}{2bh_{sp}^2}$$

Where $f_{R,j}$ is the residual strength corresponding with $CMOD = CMOD_j$ or $\delta = \delta_j$ (j=1,2,3,4) in Newton per square millimeter, F_j is the load corresponding with $CMOD = CMOD_j$ or $\delta = \delta_j$ (j=1,2,3,4) in Newton, l is the span length in millimeters, and b is the width of the specimen in millimeters and h_{sp} is the distance between the tip of the notch and the top of the specimen in millimeters. LOP is determined following Equation 2-8.

Equation 2-8

$$LOP = \frac{3F_L l}{2bh_{sp}^2}$$

Where LOP is the limit of proportionality in Newton per square millimeter, F_L is the load corresponding to the LOP in Newton, l is the span length in millimeters, and b is the width of the specimen in millimeters and h_{sp} is the distance between the tip of the notch and the top of the specimen in millimeters. In addition, the standard provides a correlation among the CMOD and deflections as described in Equation 2-9.

Equation 2-9

$$\delta = 0.85CMOD + 0.04$$

Where δ is the deflection in millimeters, and $CMOD$ is the crack mouth opening displacement in millimeters.

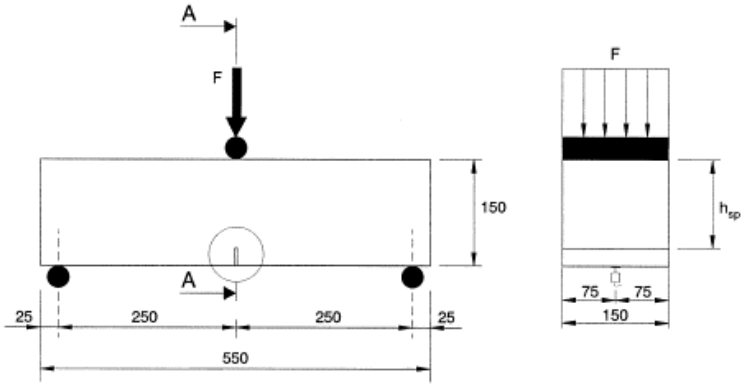

Figure 2-47 Test setup: EN 14651

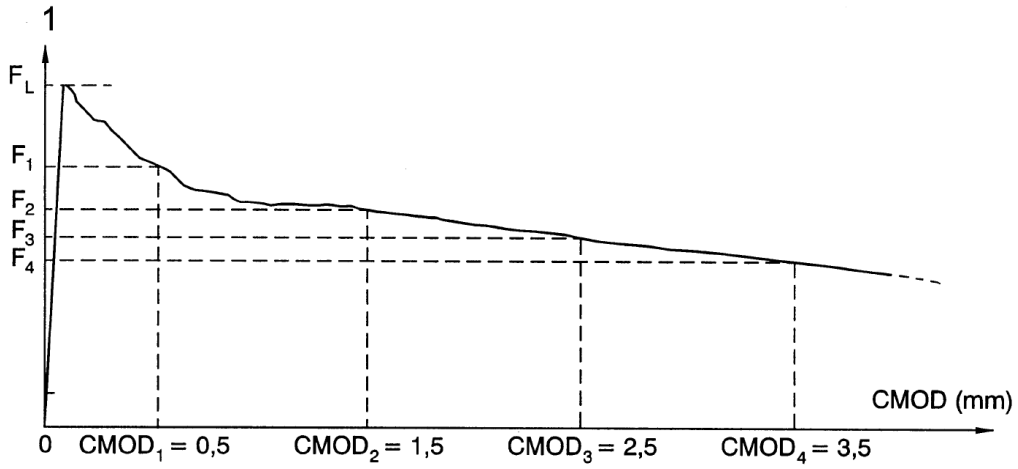

Figure 2-48 Load-CMOD plot

2.10.5 Barcelona test (PrUNE 83515)

PrUNE 83515 (2010) provides test procedures to determine the cracking strength, ductility, and residual strength of FRC. This test is based on the double punch test of a cylindrical specimen as developed by Chen (1969) and is commonly referred to as the Barcelona Test. The test specimen is a molded cylindrical specimen of height and diameter approximately equal to 5.9 in. (150 mm).

The test is an indirect measurement of tensile strength by using steel punch device to split the concrete cylinder transversely (Figure 2-49). Total crack opening displacement (TCOD) of the sample is measured as compressive axial load is applied at a constant rate of 0.02 in/min (0.5 mm/min). The loading is applied until TCOD is equal to 0.24 in. (6 mm) (relative to beginning of the test). Residual strength is determined using Equation 2-10 using the loads for specified values of TMOD of 0.08, 0.10, 0.16 and 0.24 in. (2, 2.5, 4, and 6 mm).

$$f_{ctRx} = \frac{3P_{Rx}}{9\pi aH}$$ Equation 2-10

where f_{ctRx} is the residual strength in Newton per square millimeter, P_{Rx} is the load corresponding with $TCOD_{Rx}$ in Newton, a is the diameter of the punches in millimeters, and H is the height of the specimen in millimeter.

The cracking load is determined with Equation 2-11 and ductility is determined as the area under the load-TCOD curve.

$$f_{ct} = \frac{4P_f}{9\pi aH}$$ Equation 2-11

where f_{ct} is the unit cracking load in Newton per square millimeter, P_f is the load produced by the crack in Newton, a is the diameter of the punches in millimeters, and H is the height of the specimen in millimeter.

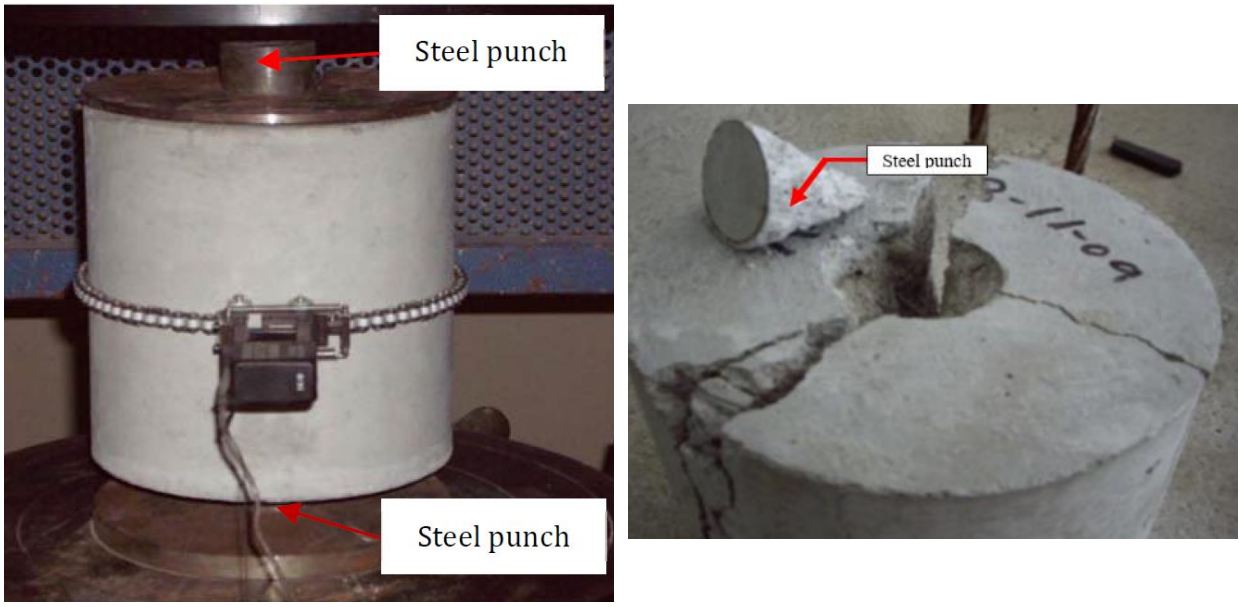

Figure 2-49 Test setup: PrUNE 83515 (2010)

2.11 Findings

The key findings from FRC research over the last ten to fifteen years relevant to this research can be summarized as:

- Adding fibers to concrete can reduce slump flow by up to 60%;
- Flexural tensile strength can be increased by up 70%,
- Fibers can effectively be used to control crack width and length; it has been shown that end region crack width can be reduced by up to 70% by adding steel fibers,
- Shear capacity can be increased by over 30% when incorporating synthetic fibers at 1% volume fraction

- Distributed fibers provide a much more closely spaced grid of reinforcement than is possible with traditional reinforcement;
- Residual tensile strength of concrete is greatly improved; and
- Crack widths are reduced, which improves shear-friction strength.

Macrofibers introduced in the last ten years with higher modulus of elasticity and tensile strength offer several benefits over microfibers including:

- higher post-cracking strength and ductility
- improved fiber pullout resistance

Steel FRC (SFRC) shows higher strength when compared to synthetic fiber FRC using the same fiber volume and length; however, benefits of using macrosynthetic fibers over steel fibers include:

- Improved workability
- Eliminates risk of damage due to corrosion
- Macrosynthetic fibers are lighter than steel fibers, which can reduce the possibility of segregation from occurring

Nevertheless, much work is needed to incorporate fiber reinforcement in design as primary reinforcement. FRC behavior depends greatly on fiber orientation and distribution, which can be affected by concrete fresh properties, casting, placement procedures, and wall effects due to formwork. The development of SCC has helped remove some of the issues that can occur due to placement and consolidation, which also removes the need for external vibration. This can help to ensure that a more uniform distribution of the fibers is obtained, improving the effectiveness of fiber reinforcement to improve concrete mechanical properties. Due to increased workability, compactness, high fine particle content and ductility, FRSCC is a potential solution to problems due to poor workability and cracking.

3 FRC mixture development

3.1 Introduction

Precast prestressed bridge girders can sometimes contain large quantities of reinforcement within the end of the girders, which may result in concrete consolidation problems. FRC has the potential to eliminate the need to include such high level of reinforcement within the end region. The addition of fibers, however, can negatively affect the fresh properties of concrete. The use of fiber-reinforced self-consolidating concrete (FRSCC) is potentially a solution to problems due to poor workability of FRC while improving end region resistance to cracking. FRSCC combines the improved mechanical properties of FRC with flowability of SCC. SCC provides a benefit over conventional mixtures since its high flowability makes it ideal for use in heavily reinforced elements where space is limited for placement and consolidation.

This chapter covers the work conducted to develop mixtures for use in full-scale girder testing. Mixtures were developed for several different fiber types and volume fractions. The mechanical properties including the post-cracking response of each mixture was evaluated to determine the capacity of each fiber to improve end region resistance to cracking. In addition, because the goal is to use the mixtures in prestressed bridge girder construction, flowability and passing ability properties of the mixture were a key aspect of the mixtures selected to produce the girders. Final mixture selection for end region crack testing was made considering both the fresh properties and residual strength.

3.2 Constituent materials

All mixtures were prepared and tested for fresh properties at a local precast facility in Florida. Commonly available materials were used to develop the mixtures to maintain realistic conditions for concrete mixing when casting real girders for bridge construction. Table 3-1 shows a summary of general properties for materials used in the mixtures prepared, and later in this chapter more details of each constituent material are provided.

Table 3-1 Material properties

	Type	SG
Cement	Type I/II	3.15
Flyash	Class F	2.17
CA-1	#67	2.42
CA-2	#89	2.4
FA	Astatula	2.63
Water	Tap	1

Detailed constituent properties:

(a) *Fibers* – Two types of steel fibers were tested, SH is a hooked end steel fiber with length of 1.4 in. (35 mm) and CR is a steel crimped fiber with length of 1.5 in. (38 mm). Two types of synthetic fibers from different manufacturers were used; PP and P2 are both polypropylene fibers with length of 2.1 in. (54 mm). PP, however, chemically bonds with the concrete, which supplements the mechanical bond. Basalt fibers of length of 1.2 in. to

2.2 in. (30 mm to 55 mm) were included in the investigation but were not included in full-scale batches due to lack of availability in the U.S. Fiber designation and details are shown in Table 3-2.

(b) *Cementitious materials* - FDOT allows the use of cement Types I, II, II (MH), III, IV and V (AASHTO M85), or IP, IP (MS), IS (AASHTO M 240) (Section 921). Cement used for this study is classified as AASHTO Type I/II meeting ASTM C150 and AASHTO M 85 standards. Maximum allowed quantity of fly ash to be used as supplementary cementitious material is 25% by weight, while for extreme environmental conditions a minimum of 18% should be provided (Standard Specifications for Road and Bridge Construction 2016). Fly ash classified as a Class F fly ash meeting ASTM C618 and AASHTO M 295 standards was used as supplementary cementitious material.

(c) *Chemical admixtures* – For SCC in precast concrete products, FDOT specifications require the use of Type I, II, F, or G admixtures. In use of Type F or G admixtures, aggregate distribution should be verified in accordance with ASTM C1610 (Standard Specifications for Road and Bridge Construction 2016). High-range water-reducing admixture (HRWR) Type F meeting ASTM C494 requirements was used for the mixtures prepared. In addition, an admixture to retard initial setting time was added. The use of air entrainment admixtures is required by the FDOT for construction of precast products, except for Class I and II concrete (Standard Specifications for Road and Bridge Construction 2016). Air-entraining admixture meeting requirements of ASTM C260, AASHTO M 154, and CRD-C 13 was used.

(d) Coarse and fine aggregates - FDOT requires that coarse aggregate with Size No. 57, 67 or 78 be used for all concretes. With the engineer's approval, however, Size No. 8 or 89 can be used alone or blended with the previously mentioned coarse aggregates. Most mixtures were prepared either using a blend of No. 67 and No. 89 or using No. 89 to improve fresh properties of FRC.

(a) (b) (c)

(d) (e)

Figure 3-1 Fibers used to prepare mixtures: (a) B, (b) B3, (c) PP, (d) PP2, (e) SH, and (f) CR.

Table 3-2 Fiber properties

Fiber designation	B	B2	B3	PP	PP2	SH	CR
Material	Basalt	Basalt	Basalt	Polypropylene	Polypropylene	Steel	Steel
Length (in.)	1.2	1.8	2.2	2.1	2.1	1.4	1.5
Length (mm)	30	45	55	54	54	35	38
Tensile strength (ksi)	156	156	156	85	83-96	160	140
SG	2.1	2.1	2.1	0.91	0.91	7.85	7.85

3.3 Mixture requirements

FDOT specifications require that Class VI concrete be used in precast prestressed bridge production. Mixtures prepared in the study were designed to meet requirements for Class VI (Table 3-3). Due to the high congestion of reinforcement in prestressed bridge girders and the loss of workability when fibers are incorporated, all mixtures developed were self-consolidating concrete (SCC). FDOT requirements for fresh properties of SCC mixtures were used as a gage to determine if mixtures had adequate workability to be incorporated into bridge production (Table 3-4).

Table 3-3 Mixture proportioning requirements for Class VI concrete (FDOT 2016)

28-Day Compressive Strength (psi)	8,500
Water/ CM	0.37*
Minimum CM (lb/cy)	752
Maximum Fine/Total aggregate	0.50*
Minimum Fine/ Total aggregate	0.45*

*Mass ratio

Table 3-4 Current FDOT limits for fresh properties of SCC mixtures

Test Result	ASTM	Limit
Slump flow	C1611	Shall be less or equal to 27.0 inches ($\pm$2.5inches)
VSI	C1611	Shall be less or equal to 1
T_{50}	C1611	Recommended 2-7 seconds
Passing ability	C1621	Shall not exceed 2.0 inches
Static segregation	C1610	Shall not exceed 15%

3.4 Mixture proportions

SCC mixtures incorporating fibers were prepared using an FDOT approved mixture as a starting point; this mixture will be referred to as the control (CT). The control mixture was modified to incorporate fibers while still complying with FDOT requirements for proportioning, as well as hardened properties. Fiber dosage was adjusted based on recommended dosages provided by each of the fiber manufacturers. Table 3-5 contains a summary of mixture proportions used for the investigation, including the mixture designations used through the report. Fiber volumes ranging between 0.1-0.7% were used. Volume of coarse aggregate was reduced to accommodate the respective fiber volume.

Table 3-5 Mixture proportions

	Proportions (lb/cy)							Properties tested	
Mixture	Cement	Flyash	#67	#89	FA	Water	Fiber	Fresh	Hardened
0	735	165	1370	0	1265	279	-	-	-
1	790	175	578	774	1212	279	14	X	X
2	790	175	575	776	1212	279	3.8	X	-
3	735	165	1370	0	1265	279	7	-	-
4	790	175	565	776	1212	279	11	X	-
5	790	175	584	774	1212	279	40	X	X
6	790	175	0	1354	1212	279	4.6	X	-
7	790	175	575	776	1212	279	3.8	X	X
8	735	165	16370	0	1265	279	7	X	X
9	790	175	565	774	1212	279	7	X	X
10	790	175	0	1320	1063	244	8	-	-
11	790	175	565	774	1212	279	11	X	X
12	790	175	0	1320	1063	279	11	-	X
13	790	175	0	1320	1063	279	93	X	X
14	790	175	0	1320	1063	279	93	X	X

*Not performed (-)

* Performed (X)

3.5 Specimen naming

The specimen naming format was selected to include details regarding fibers (Figure 3-2) and concrete mixture proportions. Figure 3-2 and Table 3-6 provide naming details used to label laboratory specimens and for referencing in this report. The first two characters refer back to the fiber designation (Table 3-6), these were assigned considering the different fiber material and fiber length combinations. The second set of characters refers to the volume of fibers used multiplied by a factor of 100, and the third set of characters identifies the mixture number as specified in Table 3-5. The last character is a numeric value, represented by "*X"* in Figure 3-2, and denotes the specimen number. For simplicity, specimens might also be referred to by using only the fiber designation and volume.

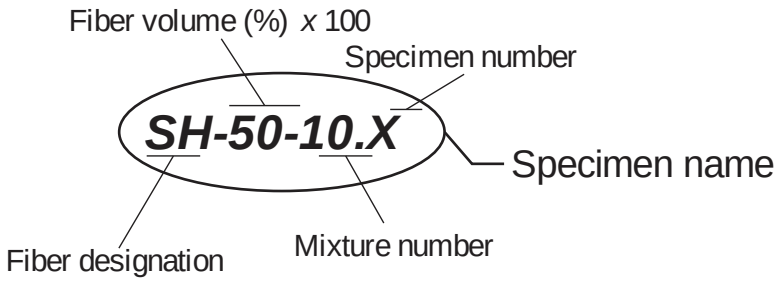

Figure 3-2 Specimen naming format

Table 3-6 Summary of specimen name and description

Mixture #	Fiber	Volume (%)	Name
0	-	-	CT
1	SH	0.10	SH-10-01
2	B2	0.10	B2-10-02
3	B3	0.20	B3-20-03
4	B	0.30	B-30-04
5	SH	0.30	SH-30-05
6	PP2	0.30	PP2-30-06
7	PP	0.25	PP-25-07
8	PP	0.45	PP-45-08
9	PP	0.45	PP-45-09
10	PP	0.50	PP-50-10
11	PP2	0.70	PP2-70-11
12	PP	0.70	PP-70-12
13	SH	0.70	SH-70-13
14	CR	0.70	CR-70-14

3.6 Batching procedures

Trial mixtures of 1.6 to1.8 cubic feet were prepared in the precast plant laboratory using a 4-cf drum mixer in accordance with the mixing procedures shown in Table 3-7. Fibers were added after all ingredients were mixed and good SCC consistency was obtained. Based on preliminary work, this method appeared to provide better workability and fiber distribution than adding fibers to aggregates at early stages of the mixing procedures.

Table 3-7 Mixing procedure

Order	Action
1	Butter mixer using concrete, water and coarse aggregates
2	Empty mixer
3	Coarse aggregates
4	Fine aggregate
5	Air entrainment admixture
6	Retardant admixture
7	Half of water content
8	Fly ash
9	Cement
10	HRWR
11	Fibers
12	Remaining water

3.7 Test program

In order to determine the adequacy of each mixture the test program involved evaluation of fresh and hardened concrete properties. Mixtures were tested for fresh properties to determine compliance with FDOT requirements and to determine the optimum fiber length and volume that could be incorporated. Test procedures were performed in accordance with applicable specifications as stipulated in Table 3-8. Hardened properties of each mixture were tested to evaluate the effect of fiber reinforcement. As part of the experimental program, compressive strength tests were conducted at the precast plant and testing to quantify residual strength was conducted at the University of Florida. Test procedures were performed in accordance with applicable specifications (Table 3-9). Table 3-8 and Table 3-9 contain chapter correspondence for discussion of each test procedure.

Table 3-8 Fresh properties tests

Test	Standard	Chapter
Slump flow	ASTM C1611	2.9.1
VSI	ASTM C1611	2.9.1
T_{50}	ASTM C1611	2.9.1
Passing ability	ASTM C1621	2.9.1

Table 3-9 Tests for hardened properties

Test	Standard	Chapter
Compressive strength	ASTM C39	-
Average residual strength	ASTM C1399	2.10.1
Flexural tensile strength	EN 14651	2.10.4

Table 3-10 Tests conducted for each mixture

	Properties tested	
	Fresh	Hardened
CT	no	no
SH-10-01	yes	yes
B2-10-02	yes	no
B3-20-03	no	no
B-30-04	yes	no
SH-30-05	yes	yes
PP2-30-06	yes	no
PP-25-07	yes	yes
PP-45-08	no	no
PP-45-09	yes	yes
PP-50-10	yes	yes
PP2-70-11	no	yes
PP-70-12	no	no
SH-70-13	yes	yes
CR-70-14	yes	yes

3.8 Fresh properties — results

Results of fresh property testing during mixture development are summarized in Table 3-11 and Figure 3-3 through Figure 3-6. Maximum FDOT limits are represented in blue (when available) to show compliance of each mixture. During mixing, B3-20-03, PP-45-08, PP-70-12, and PP2-70-11 showed excessive fiber clumping (Figure 3-7). On this basis, these mixtures were eliminated from further consideration. In general, steel fibers showed the best passing ability and VSI among all fibers.

Except for B2-10-02, P1-25-07, SH-50-10, and CR-70-14, all mixtures met the requirement for maximum unrestricted flow, which is 27 inches. Despite lack of compliance by SH-50-10, no issues with consistency or bleeding were observed. With the exception of mixture SH-70-13, all mixtures complied with FDOT passing ability requirements for SCC mixtures. SH-70-13, however, showed no fiber clumping within the J-Ring. Clumping occurred in the J-ring test for the mixture with fibers with length of 2.1 in. (54 mm) with volumes between 0.3% and 0.7% (Figure 3-8). This can lead to potential issues with placement of mixtures into highly reinforced specimens.

All remaining mixtures showed good consistency, no bleeding, and good resistance to segregation. VSI (visual stability index) was between zero and one, and T-50 varied between 2 and 5 seconds, which is well within the recommended values for SCC. Fiber clumping was apparent, however, inside the J-Ring. Mixtures B2-10-02, SH-10-01, and P1-25-07 contained fiber volumes that were deemed too low, and no further testing was conducted using these mixtures.

Table 3-11 Fresh properties for mixtures prepared in laboratory mixer

Mixture	Slump flow (in.)	J-Ring flow (in.)	Passing ability (in.)	T-50 (seg)	VSI	Air content (%)
SH-10-01	26.75	27	-0.25	3	0	3
B2-10-02	30	29.25	0.75	5	0	5
B3-20-03	-	-	-	-	-	-
B-30-04	29	28.75	0.25	5	0	5
SH-30-05	27.75	26.25	1.5	2	0	4
PP2-30-06	21	20.25	0.75	5	1	5
PP-25-07	30.5	30.5	0	4	0	4
PP-45-08	-	-	-	-	-	-
PP-45-09	26.5	26.5	0	-	1	-
PP-50-10	32	30.5	1.5	3	1	3
PP2-70-11	-	-	-	-	-	-
PP-70-12	-	-	-	-	-	-
SH-70-13	28.25	24.5	3.75	3	0	3
CR-70-14	31	29.5	1.5	3	0	3

* Not performed (-)

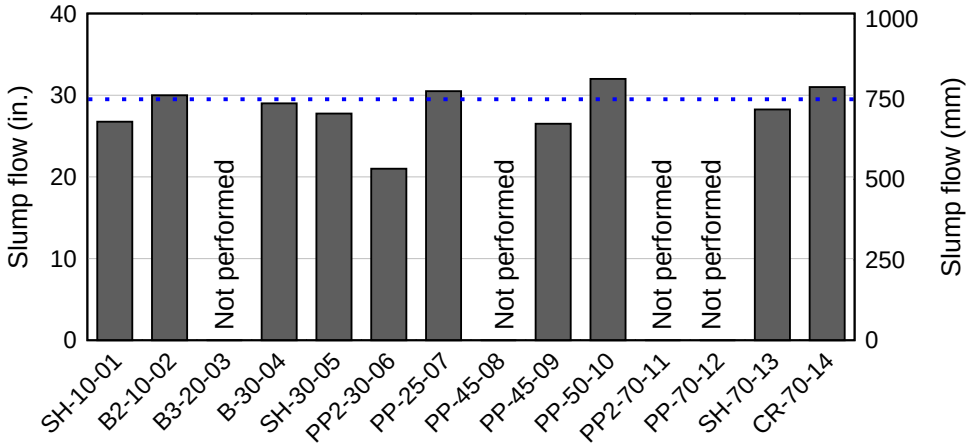

Figure 3-3 SCC properties: slump flow for laboratory mixtures

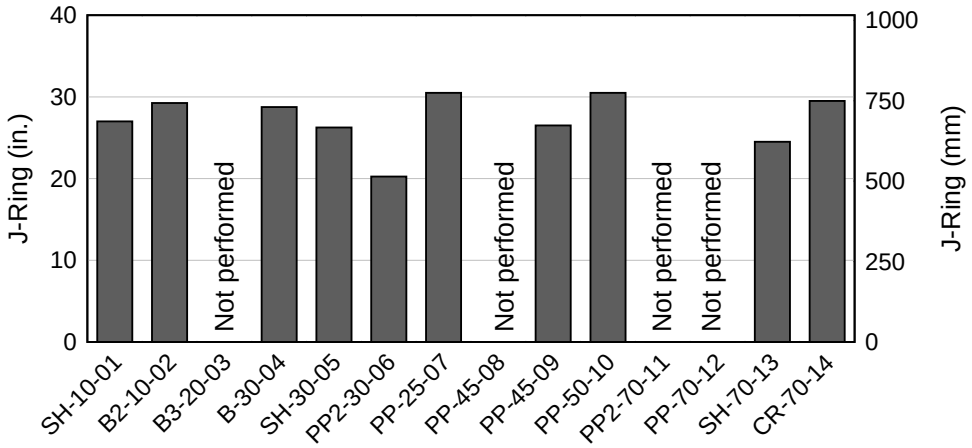

Figure 3-4 SCC properties: J-Ring for laboratory mixtures

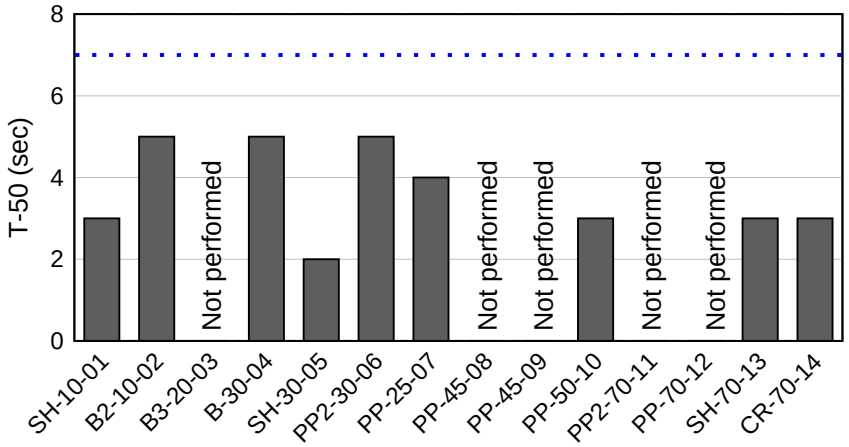

Figure 3-5 SCC properties: time for spread to reach 50mm diameter

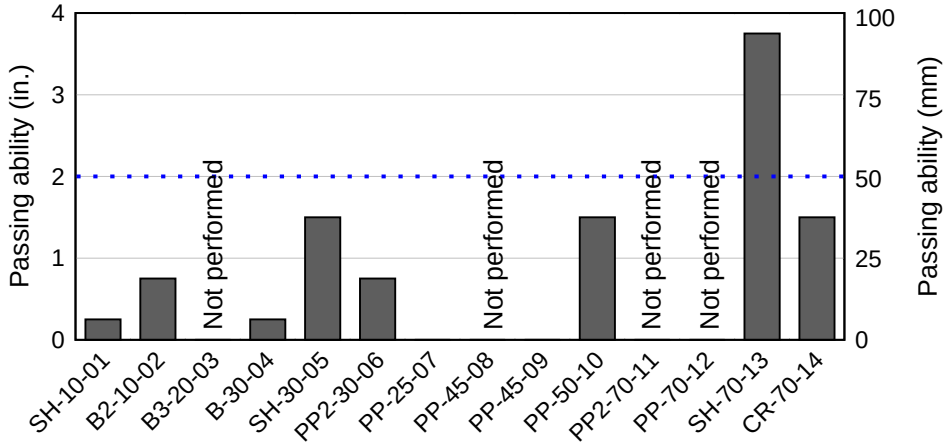

Figure 3-6 SCC passing ability for laboratory mixtures

Figure 3-7 Fiber clumping during mixing procedures (Mixture 8)

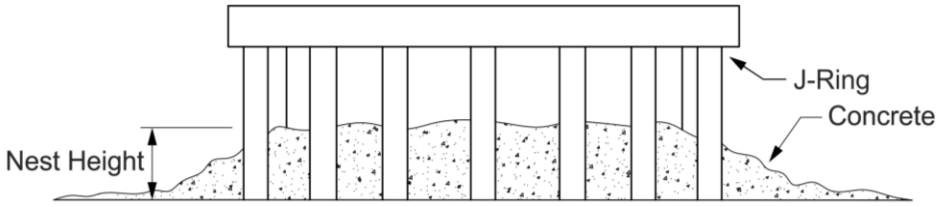

Figure 3-8 Illustration of fiber clumping inside J-Ring

(a)

(b)

Figure 3-9 J-Ring Flow; (a) Good passing ability (B2-10), (b) Excessive fiber clumping (PP2-70)

3.9 Hardened properties — results

3.9.1 Compressive strength (ASTM C39)

For each mixture prepared in the laboratory mixer, seven 4 in. x 8 in. cylinder specimens were prepared to determine the average compressive strength; two were tested at 24 hours, two at 7 days, and three at 28 days.

Compressive strength of cylinders exceeded the specified 28-day specified compressive strength of 8,500 psi (Table 3-12). Figure 3-10 shows graphic representation of the compressive strength of mixtures prepared in the laboratory mixer. In general, early age strength (24 hours) was increased by as little as 5% to up to 65% when compared to the control mixture; this was likely due to the confinement provided by the fiber reinforcement. The effect of fiber reinforcement on 28-day strength was found to be negligible (up to 12.5% difference).

Table 3-12 Compressive strength (laboratory mixtures)

	24 hours (psi)	7 days (psi)	14 day (psi)	28 day (psi)
SH-10-01	4,090	7,700	9,020	10,120
B2-10-02	4,050	8,870	10,400	10,840
B-30-04	4,880	9,240	-	11,050
SH-30-05	5,300	8,110	-	9,440
PP2-30-06	3,390	7,210	-	9,390
PP-25-07	3,770	9,150	-	10,760
PP-45-09	3,620	9,240	-	10,280
PP-50-10	6,740	9,050	-	10,970
PP2-70-12	4,280	9,870	-	10,080
SH-70-13	5,240	9,050	-	10,907
CR-70-14	5,950	8,080	-	10,060

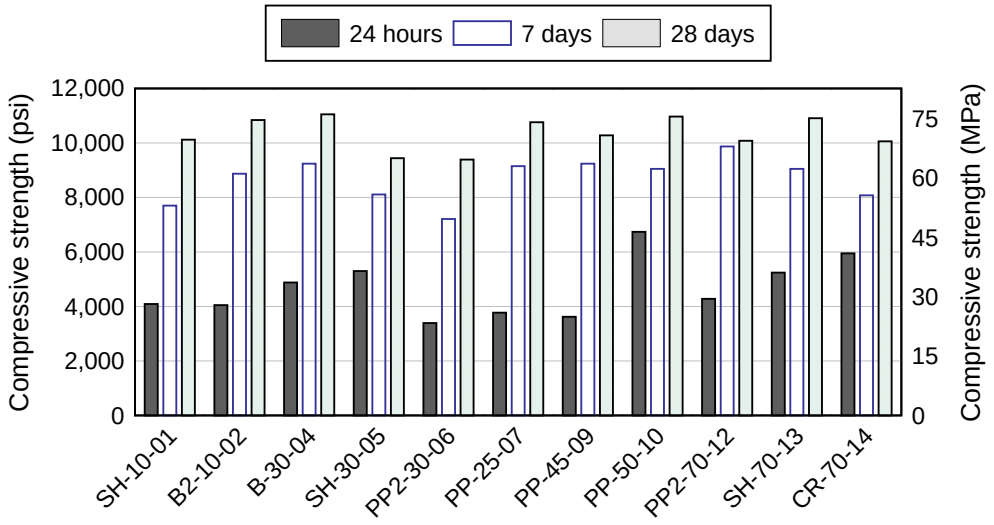

Figure 3-10 Compressive strength at 24 hours, 7 days, and 28 days

3.9.2 Average residual strength (ASTM C1399)

Average residual strength tests to evaluate the effect of fibers on the post cracking behavior of concrete were performed. Test equipment problems delayed testing such that the test age was beyond 28 days (Appendix A); however, these are not expected to have a significant effect on the relative comparison of the results.

Figure 3-12 shows an example of typical cracking patterns seen in FRC specimens after testing. Cracking typically occurred within the middle third of the span for specimens. Fiber bridging (Figure 3-13) provided residual flexural strength well beyond cracking and up to a deflection of 0.05 in. where the test was terminated. Residual strength varied with fiber material and fiber volume used. In general, higher fiber volumes and the use of stiffer fibers led to a higher value of average residual strength (ARS) (Figure 3-14).

Because end region is a serviceability issue, this investigation focuses particularly on the response of each mixture right after cracking is initiated. For the ASTM 1399, which uses

displacement as control variable, it has been differentiated between residual stress at service level as a deflection of 0.02 in. or less.

Figure 3-14 shows residual strength at the specified displacements of 0.02, 0.03, 0.04 and 0.05 in. SH-70-13 and CR-70-14 had the highest residual strength under service conditions, with only 6% difference between the two. At a volume fraction of 0.3%, hooked end steel fibers (SH-30-05) provided 60% higher residual strength than macrosynthetic fibers (PP2-30-06) and 90% higher than basalt fibers (B-30-04). S1-10-01 provided similar residual strength under service stress as PP2-30-06. Nonetheless, PP2-30-06 required a volume higher volume and almost twice the length of the fiber used in S1-10-01. Under service stress, similar residual strength is obtained from using PP at 0.45% (PP-45-09) and PP2 (PP2-30-06) at 0.30%, however, PP provided higher residual strength at all other stress levels.

Figure 3-15 shows ARS results for molded specimens. Some samples showed relatively low ARS, which is thought to be due to the low volume of fibers used. SH-70-13 provided the maximum ARS, with CR-70-14 being the second highest ARS with a difference of 38% in ARS. At the same volume fraction of 0.30%, steel fibers (SH-30-05) provided a 90% higher residual strength than basalt (B-30-04) and 60% higher than the synthetic fiber (PP2-30-06). PP-45-09 and PP2-30-06 had similar load-deflection responses and a difference of 2.3% in ARS.

Figure 3-11 ARS test specimens (after testing)

Figure 3-12 ARS test specimens cracked surface

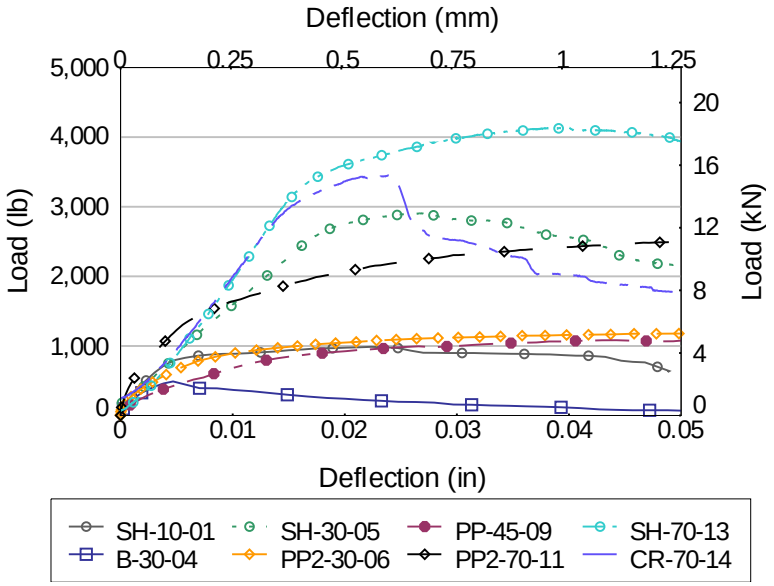

Figure 3-13 Reloading curves for molded specimens

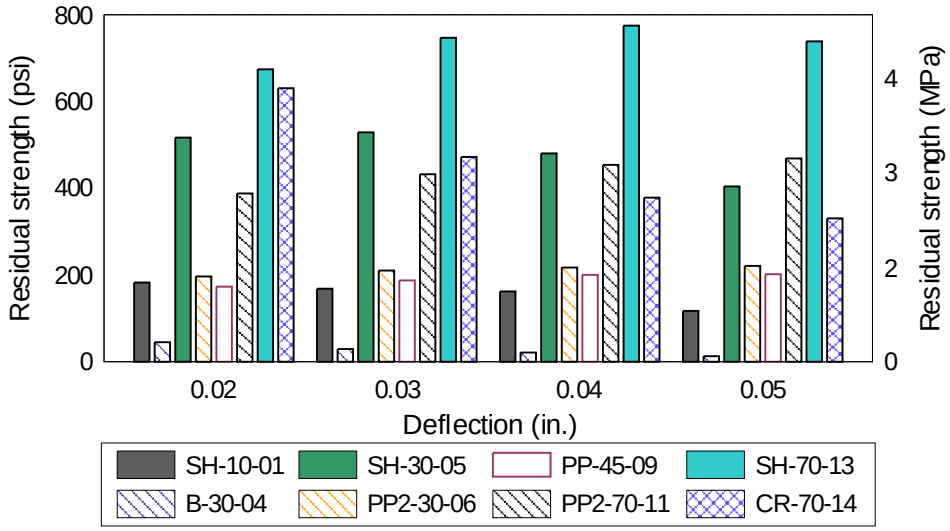

Figure 3-14 Residual strength at specified displacements for molded specimens

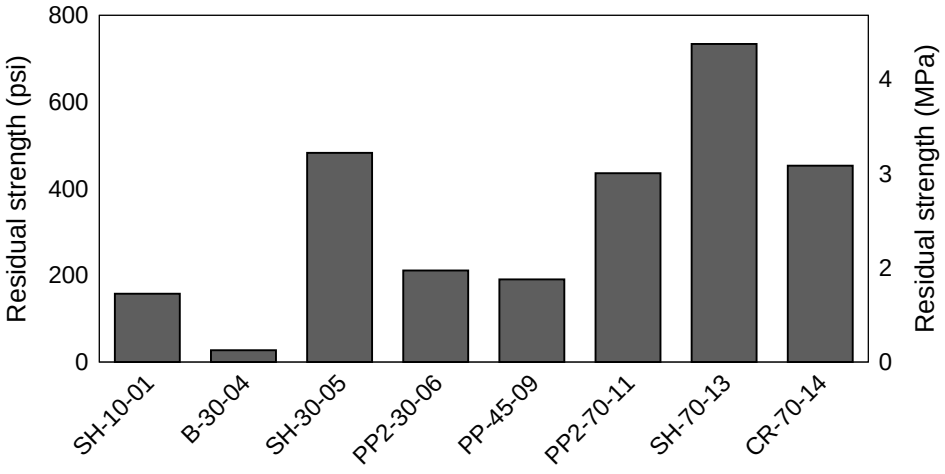

Figure 3-15 Average residual strength for molded specimens

3.9.3 Flexural tensile strength (EN 14651)

Flexural tensile residual strength testing was performed to evaluate the effect of fiber in the post cracking behavior of concrete. Test equipment problems delayed testing such that the test age was beyond 28 days (Appendix A); however, these are not expected to have a significant effect on the relative comparison of the results.

Typical behavior showed a sudden decrease in stiffness once cracking occurred with the exception of specimen's using higher fiber volume (0.7%) or stiffer fibers (SH and CR). For the case of mixtures exhibiting softening, the residual strength was generally less than 30% of the limit of proportionality (LOP) after CMOD reached 0.04 in. (1 mm). In case of mixtures exhibiting hardening after cracking, residual strength reached between 30-100% of LOP.

Figure 3-17 shows typical load-CMOD curves for molded specimens. Peak loads were between 1.1 kip and 2.0 kip, after which most specimens showed a rapid loss in stiffness. Figure 3-17 and Figure 3-18 show LOP and residual strength at specified CMOD increments of 0.02, 0.06, 0.10, and 0.15 in. (0.5, 1.5, 2.5 and 3.5 mm). B-30-04 and S1-10-01 showed residual strength less than 5% of LOP after CMOD reached 0.04 in. (1 mm). This low strength is likely due to the low fiber dosage used for these mixtures. PP2-30-06 and P-45-09 showed similar LOP, P1-045-06 had residual strength almost 50% higher than P2-030-11 at all stress levels. Both synthetic macrofibers, however, showed a more ductile behavior than B2-030-05 and S1-010-07. Specimens with steel fibers showed hardening behavior, which can be attributed to the high stiffness and tensile strength of steel (SH and CR) fibers. Residual strength for this mixtures was in the range of 30% to 100% of LOP.

Figure 3-19 shows residual flexural tensile strength for crack mouth opening displacement (CMOD) increments of 0.02, 0.06, 0.10, and 0.15 in. (0.5, 1.5, 2.5 and 3.5 mm). The focus of this research project is on the service level cracking that occurs in the end region. Consequently, the post-cracking flexural strength between first cracking and $f_{R,1}$ (EN 14651) is of the most interest (Figure 3-20), at CMOD value of 0.02 in. (0.5 mm). CR-70-14 had the highest residual strength under service stress, followed by SH-70-13. CR-70-14 had residual strength 20% higher than SH-70-13. At the same volume fraction of 0.30%, SH-30-05 showed higher residual stress at all stress levels when compared with B-30-04 and PP2-30-06 specimens, this can be attributed to steel fibers (SH) high tensile strength and stiffness. Residual stress at

CMOD of 0.02 in. (0.5 mm) ($f_{R,1}$) of B-30-04 and PP2-030-06 was 80% and 75% less than that of SH-30-05. PP2-30-06 and PP-45-09 showed similar residual strength under service stress. Similar to results for ASTM 1399 testing, mixtures 03, 06, 80, 09, and 11 were selected based on fresh and hardened properties. However, due to limited availability of macro-configured basalt fibers, these fibers were not included in the full-scale testing.

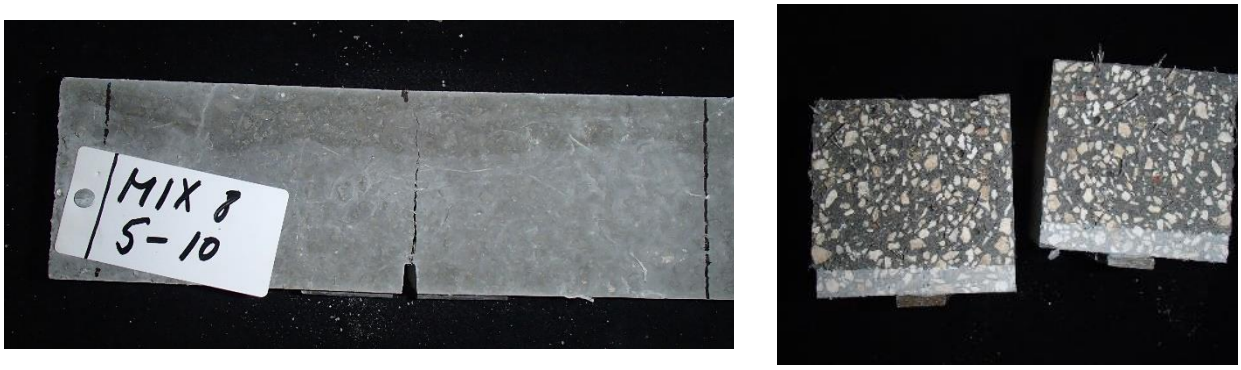

Figure 3-16 Test specimens (after testing)

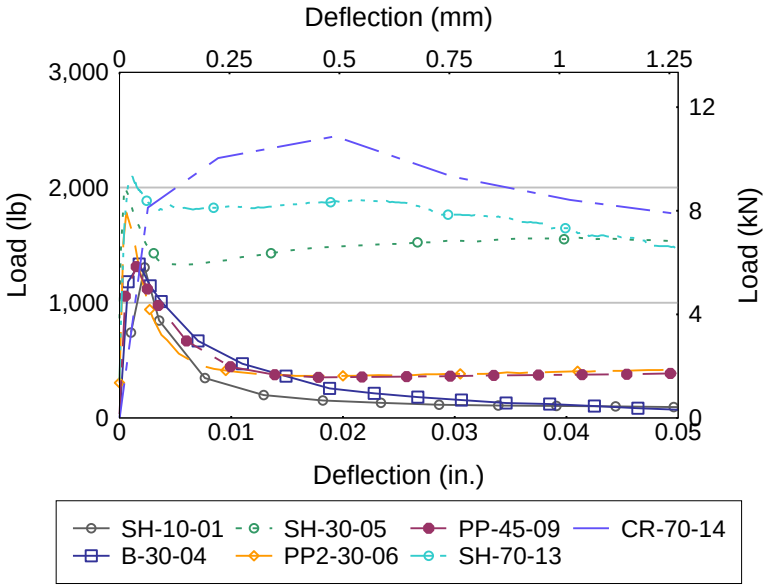

Figure 3-17 Load-CMOD curves for molded specimens

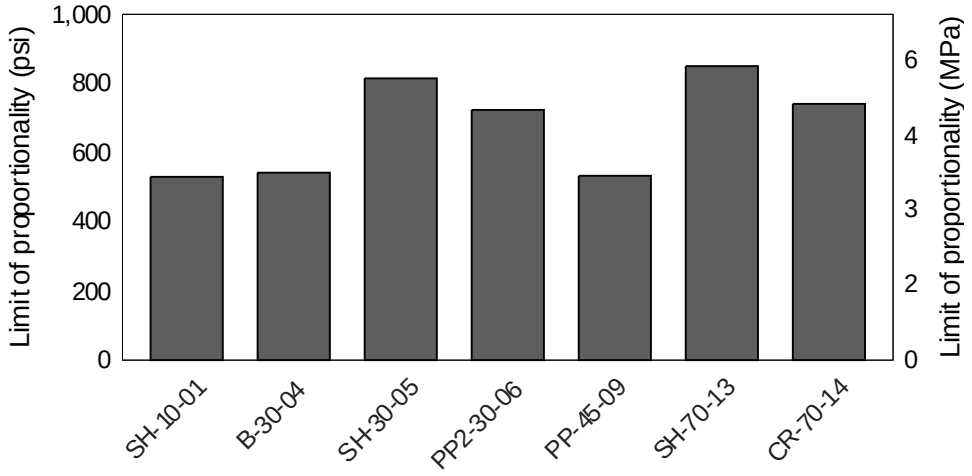

Figure 3-18 Limit of proportionality (LOP) for molded specimens

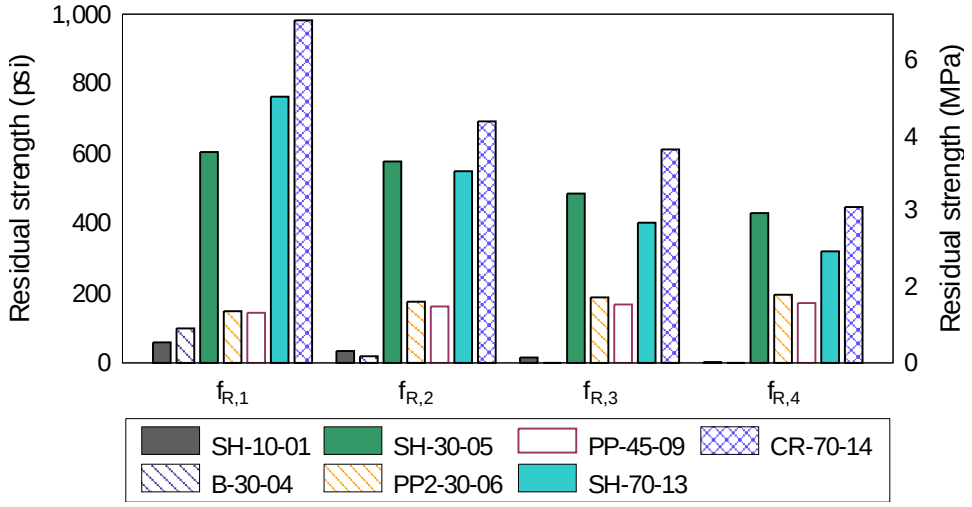

Figure 3-19 Residual flexural tensile strength for molded specimens

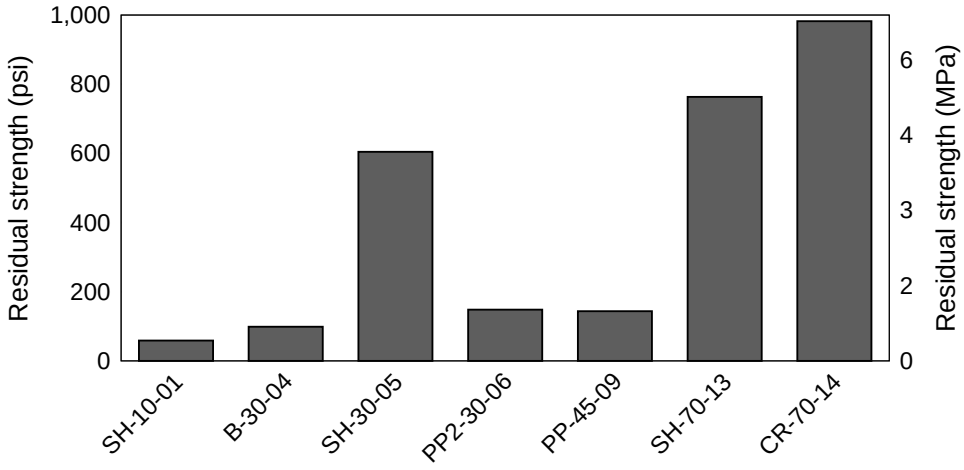

Figure 3-20 Residual stress ($f_{R,1}$) for molded specimens

3.10 Findings

FRC mixtures were developed and tested to evaluate the effect of including fiber reinforcement on fresh and hardened concrete properties. Key findings from the mixture development work include:

- For mixing in a laboratory setting, fiber addition into the mixture after all ingredients were mixed and good SCC consistency was obtained provided better workability and fiber distribution than adding fibers along with aggregates at early stages of mixing,
- FRSCC mixtures were developed using fiber reinforcement at volumes ranging between 0.1-0.7% while still maintain flow and passing ability properties of SCC,
- FRSCC mixtures with macrosynthetic fiber at volumes higher than 0.5% had issues with fiber clumping during mixing procedures and/or fiber nesting inside the J-Ring. This is a concern for placeability and passing ability of mixtures when incorporated into precast production,
- In general, higher fiber volumes and the use of stiffer fibers led to a higher residual strength,
- At volume fraction of 0.3%, hooked end steel fibers (SH) provided average residual strength 90% higher than basalt fibers (B) and 60% than macrosynthetic fibers (PP2),
- Hooked end steel fibers (SH) at volume of 0.3% provided similar average residual strength than the synthetic macrofiber (PP2) at a volume of 0.7%. However, under service stress, hooked end steel fibers provided residual strength up to 70% higher than the macrosynthetic fiber,
- Chemically enhanced macrofiber (PP) at a volume of 0.45% and synthetic macrofiber (PP2) had similar load-displacement response and residual strength, therefore the chemically enhanced bond did not provide significant increase in post cracking response. However, fiber PP was easier to handle and include during mixing procedures compared to PP2,
- Steel fibers (SH and CR) at volume of 0.7% provided higher residual strength than other fibers while still maintaining flowability and passing ability properties of SCC,

3.11 FRC mixture selection

Workability (section 5.8), and residual strength (section 3.9) were considered while making the final selection for fiber type and volume to be tested in full-scale production of precast prestressed girders. Residual strength results were normalized by the maximum value and assigned a rating on a scale of 0 to 10 based on the performance obtained for the respective test. Ease of mixing, passing ability results, and fiber clumping/nesting were also assigned a rating on the same scale. As an example, as shown in Figure 3-21, a 10 was assigned to a mixture with good passing ability and no fiber clumping or clumping, while a zero rating would be assigned to mixtures that showed issues during mixing and/or excessive fiber nesting. Figure 3-21 and Figure 3-22 show the cumulative rating for each mixture, considering workability and strength performance at various stress levels. Table 3-13 shows a summary of the details for the recommended mixtures. From the fibers used in mixtures with the highest total rating, basalt fibers were not included in full-scale testing due to limited availability of macro-configured basalt fibers, this led to the final selection of hooked end steel fibers at a volume of 0.3% and 0.7%, steel crimped fibers at a volume of 0.7% and chemically enhanced macrofibers at a volume of 0.45%.

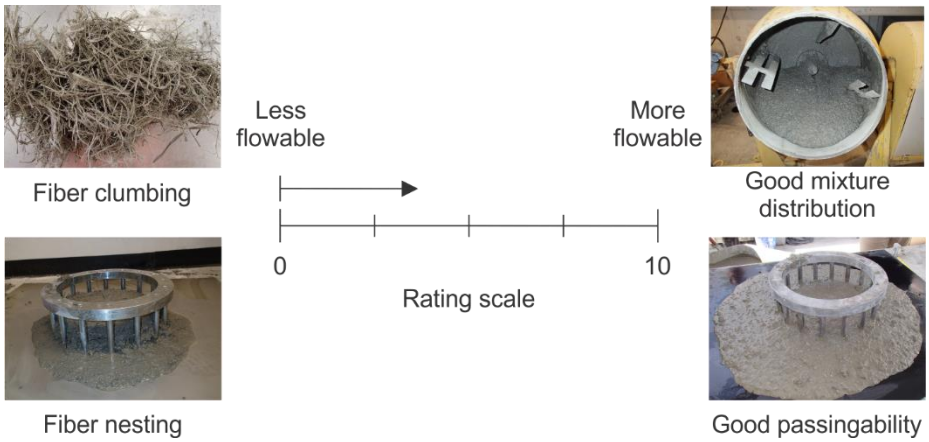

Figure 3-21 Workability rating

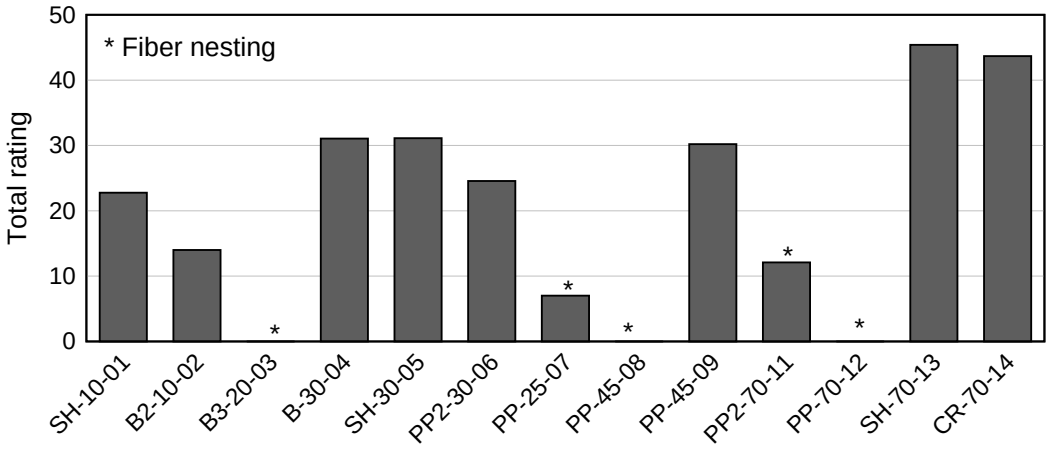

Figure 3-22 Total rating: considering mixture workability and residual strength

Table 3-13 Mixtures selected for use in full-scale testing

Mixture	Fiber	Length (in.)	Length (mm)	Volume (%)
05	SH	1.4	35	0.30
09	PP	2.1	54	0.45
13	SH	1.4	35	0.70
14	CR	1.5	38	0.70

PP – polypropylene macrofiber chemically enhanced
PP2 – polypropylene macrofiber
SH – hooked-end steel fiber
CR – crimped steel fiber

4 End region crack control test

4.1 Introduction

Five 78-in. deep Florida I-Beam (FIB-78) girders with 20-ft spans were fabricated and tested to evaluate the effectiveness of FRC in controlling end-region cracking. This chapter covers the specimen design, construction, test procedures, and results from the experimental investigation conducted to evaluate the effectiveness of FRC at controlling end region cracking.

4.2 Specimen design

Five 78-in. deep Florida I-Beam (FIB-78) girders with 20-ft spans were fabricated and tested to evaluate the use of FRC to control end-region cracking (Table 4-1). Because the length of the end region is 1 to 1.5 times the height of the specimen, a 20 ft. total length provided sufficient length to capture end-region cracking behavior independently at both ends of the specimen. Of the five specimens constructed, specimen CT served as control and was constructed using FDOT Class VI concrete mixture as would typically be used in prestressed bridge girders. The other four specimens were cast using the same reinforcement layout as specimen CT but incorporating varying fibers and/or fiber volume.

Table 4-1 Specimen description.

Specimen	Fiber volume fraction (%)	End region reinforcing arrangement		Girder
		End C	End M	
CT	-	Conventional	Modified	1
PP	0.5	Conventional	Modified	2
SH	0.3	Conventional	Modified	3
SH	0.7	Conventional	Modified	4
CR	0.7	Conventional	Modified	5

PP – Polypropylene macrofiber chemically enhanced
SH– Steel hooked-end fiber
CR – Steel crimped fiber

Specimens had (57) 0.6-in. diameter fully bonded prestressing strands in the bottom flange and (4) 3/8-in. diameter strands in the top flange (Figure 4-1). Prestressing pattern and level were chosen based on typical prestress pattern used for FIB-78 cross-sections. Calculated and allowable longitudinal stresses due to prestressing and self-weight are shown in Figure 4-2. Allowable stresses were calculated according to FDOT and AASHTO LRFD requirements. As shown in Figure 4-2, allowable stress limits were exceeded in tension. This was to ensure that cracks formed within the end region so that the effectiveness of the fiber reinforcement would be tested.

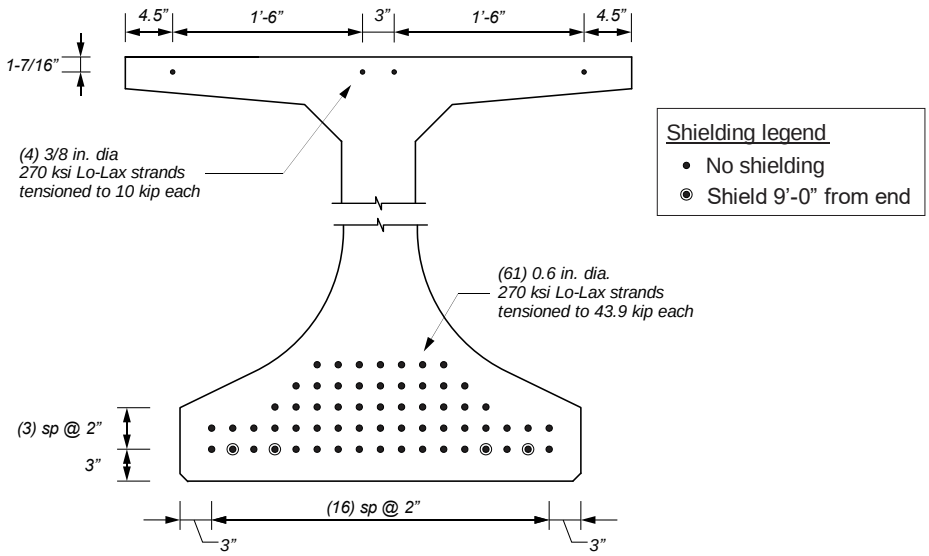

Figure 4-1 Strand layout and prestressing details

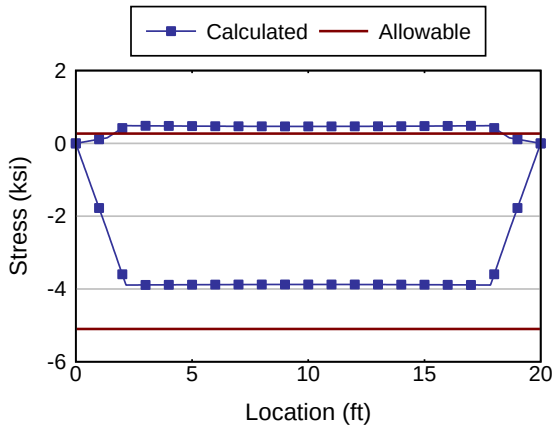

Figure 4-2 Longitudinal stress due to prestress and self-weight

One end of each specimen (C-end) had end region detailing following conventional FDOT reinforcement layout. The other end (M-end) used modified end region detailing. C-end was designed following the guidelines provided by AASHTO LRFD and FDOT without accounting for fiber contribution to strength. As shown in Figure 4-3, vertical end zone reinforcement for C-end consisted of 12 #5 bars placed within 20.5-in. of the girder end. Six of the twelve #5 bars were placed within 9.75-in. of the girder end. Figure 4-4 shows that 100% of the required resistance in AASHTO LRFD was provided by the mild steel reinforcement.

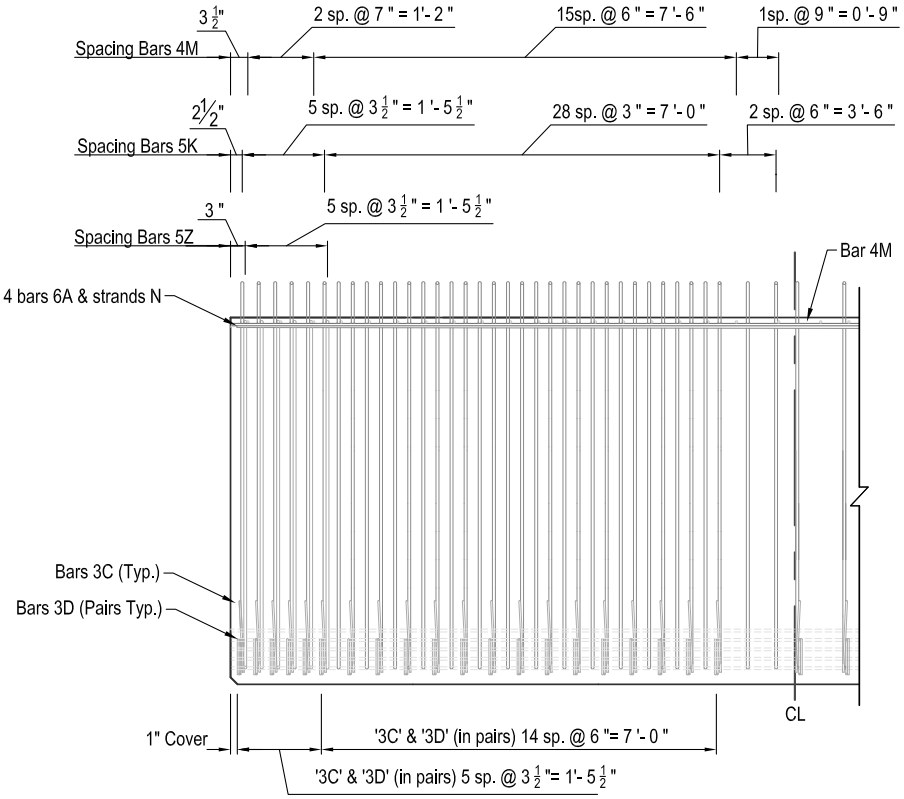

Figure 4-3 Conventional end region detailing (C-end)

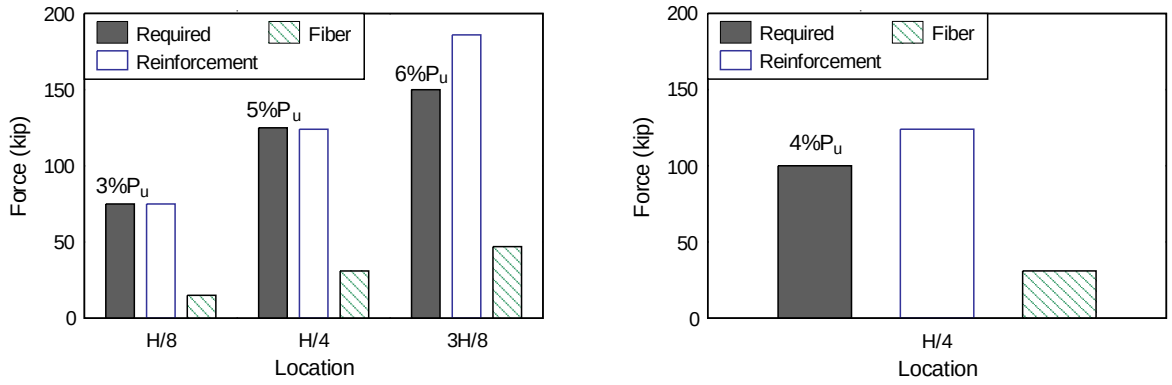

Figure 4-4 Strength provided by conventional end region detailing (C-end): (a) FDOT and (b) LRFD requirements

M-end was designed following the guidelines provided by AASHTO LRFD and FDOT for strength requirements and accounting for fiber contribution. The fiber contribution was estimated using the results from laboratory testing of residual tensile strength. To ensure that enough cracking occurred to be able to compare the effectiveness of the fibers at controlling end-region cracking less than 50% of the required reinforcement was used (Figure 4-4). Vertical end zone reinforcement for the M-end consisted of six #5 bars placed within 20.5-in. of the girder end. Of the six #5 bars, two were placed within 9.75-in. of the girder end. Figure 4-6

shows that about 60% of the required resistance was provided by the mild steel and the fiber reinforcement.

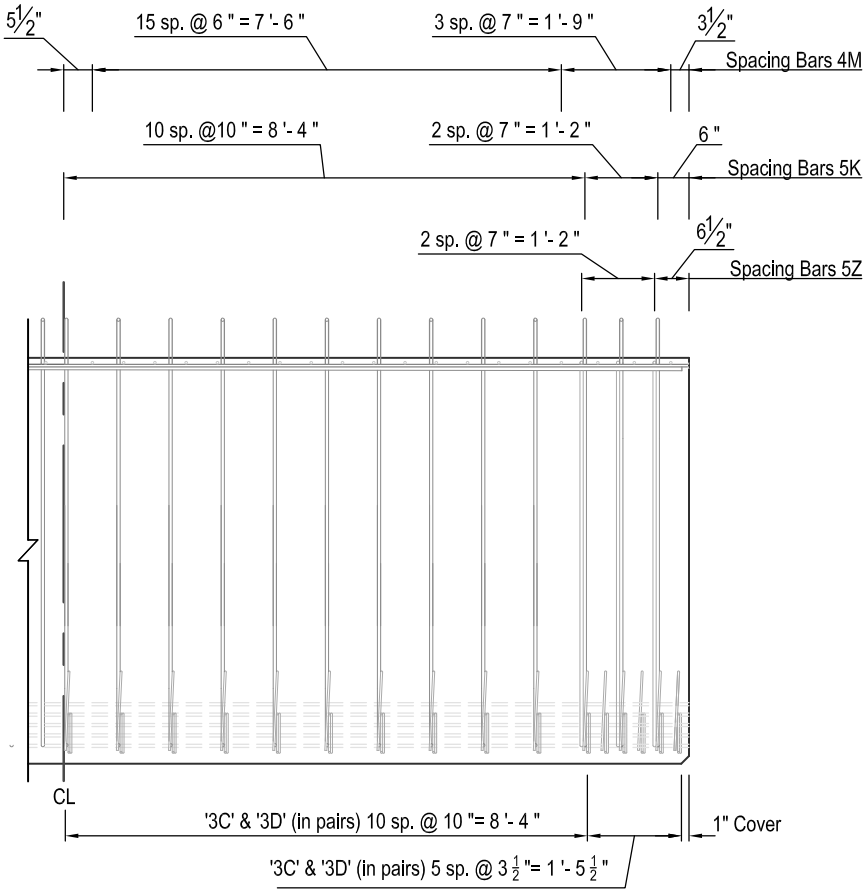

Figure 4-5 Modified end region detailing (M-end)

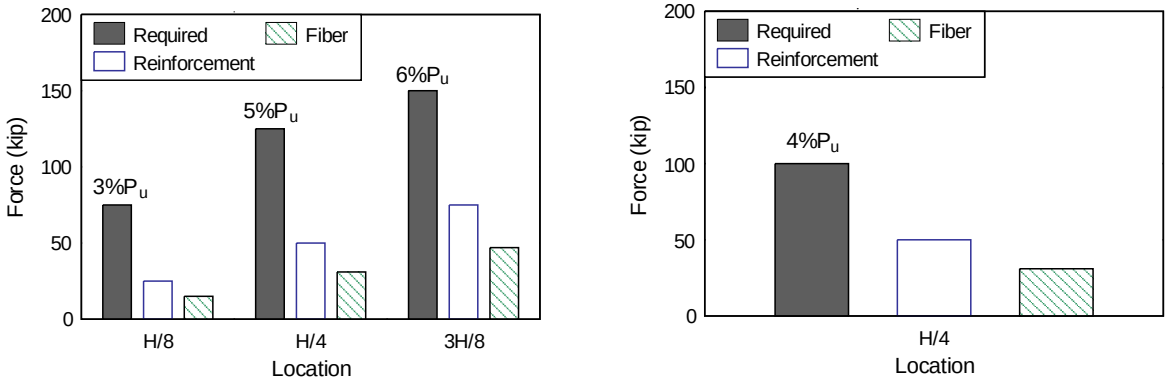

Figure 4-6 Strength provided by modified end region detailing (M-end): (a) FDOT and (b) AASHTO LRFD requirements

4.3 Specimen construction

The five specimens were fabricated at Dura-Stress in Leesburg, FL during August and September of 2018. To maintain realistic construction practices, specimens were cast in line with production bridge girders. Specimens were poured in stages; for each pour, one specimen was placed in the bed alongside a girder for real bridge production of 145-ft span, as shown Figure 4-7. This chapter contains details about the schedule and fabrication procedures.

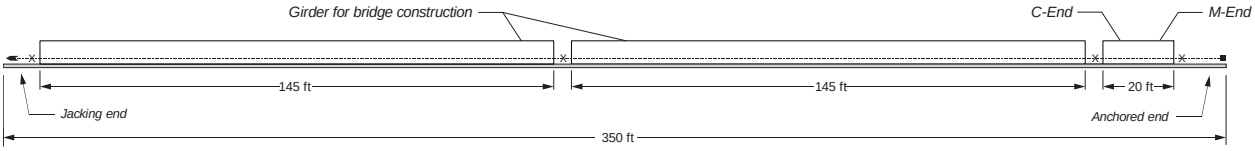

Figure 4-7 Layout of specimen casting

Construction began by placing steel and plywood bulkheads and laying out strands. Plastic tubes for shielding strands were then placed on the strands prior to tensioning. Once strands and shielding were in place, strands were tensioned using a hydraulic jack. Strands in the top flange were tensioned first. The bottom strands were tensioned starting from bottom layer and working up to the topmost strand layer. Figure 4-8 shows prestressing strands after tensioning of all strands was completed. Appendix F shows strand stress report for each specimen constructed.

Figure 4-8 Prestressing strands after tension was applied

Mild reinforcement was placed in each specimen after strands were tensioned. Selected reinforcing bars were instrumented with strain gages prior to placement in girders. Figure 4-9 and Figure 4-10 show the reinforcement layout used for each girder. Lifting hoops are also shown in Figure 4-10, which were used for lifting and transporting girders. Lifting loops consisted of (6) 0.5-in. diameter looped strands centered at 3 ft. from each girder end. Size, configuration and placement of the lifting loops were consistent in all specimens.

Figure 4-9 Mild steel reinforcement installation

(a) (b)

Figure 4-10 Mild steel reinforcement: (a) C-end and (b) M-end

Fifty-foot long modular steel forms were used for the specimen construction. Once reinforcement and internal instrumentation were installed, steel forms were oiled and placed as shown in Figure 4-11. The steel forms were squared and set in place using cross-ties as shown in Figure 4-12.

Figure 4-11 Steel form placement.

Figure 4-12 Form cross-tie.

Concrete mixtures used for the construction of the specimens were designed based on Class VI concrete (f'_c=8500 psi), which is typically used in bridge girder production. Concrete was mixed in the precaster's batch plant using a 6-cy mixer. Fibers were introduced into the mixtures by hand following the addition of the coarse and fine aggregate. Freshly batched concrete was transported from the batch plant and placed using the fabricator's truck, as shown in Figure 4-13a. Since specimens were cast using self-consolidating mixtures, no vibration was used in any of the girders. After concrete was placed, the top surface was finished using a rake finish, as is typical in FDOT girder production (Figure 4-13b). Heavy tarps were used to cover the girders for curing until the day prior to strand detensioning in which tarps were removed to allow installation of external gages

(a) (b)

Figure 4-13 Concrete placement and finish: (a) concrete delivery to forms and (b) top flange finish

Figure 4-14 Tarp cover used for curing

Flame cutting was used to release the prestressing strands (Figure 4-15). Strands were cut individually following the prestress detension sequence as shown in Figure 4-16. Top flange strands were cut first, followed by the fully bonded strands in the bottom flange starting from the lowest row and moving upwards. Lastly the fully debonded strands were cut starting from the lowest row and moving upwards. This strand release sequence is typical in the state of Florida, and was used so that the stress distribution during prestress transfer matched those of production bridge girders.

Figure 4-15 Flame cutting of prestressing strands

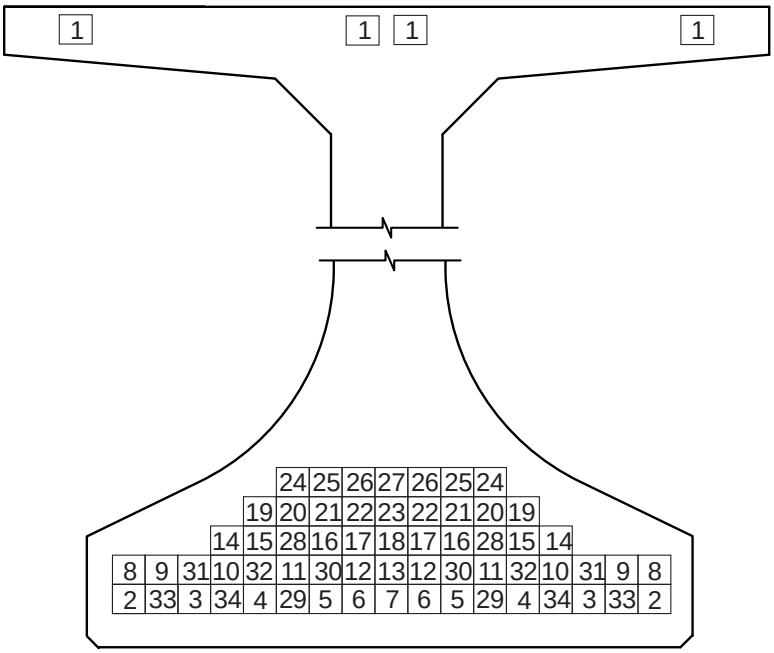

Figure 4-16 Detensioning sequence

After prestress transfer, specimens were lifted off the prestressing bed and transported to the storage area within the precast facility while cracks were monitored. Figure 4-17 shows the relative location of casting (highlighted in blue) and the long-term location for storing each girder. The south face of girders CT and SH-30 were under direct sun exposure during storage. The girder orientation during storage could have led to additional cracking in the south face of CT and SH-30 specimens due to thermal effects. The north face of specimen CT and SH-30 had limited sun exposure because of cover provided by nearby girders. Girders SH-70, CR-70, and PP-50 were stored between other girders. This limited the effect of differential temperatures among the faces of each girder.

Three of the girders were moved twice during the crack monitoring period. Lifting of the girders can cause crack widths to increase (Okumus and Oliva 2014), this was reflected by an increase in effective crack width and crack area noted after these girders were moved. No

significant difference was seen in total crack length after the specimens were moved, indicating no new cracks formed. More detailed information regarding specimen construction schedule and storage is provided in Appendix A.

Table 4-2 Age of specimens at transport

	Age after casting (days)	
Girder	Moved from prestressing bed	Moved within yard
CT	9	21
SH-30	6	8
SH-70	6	-
CR-70	7	-
PP-50	6	62

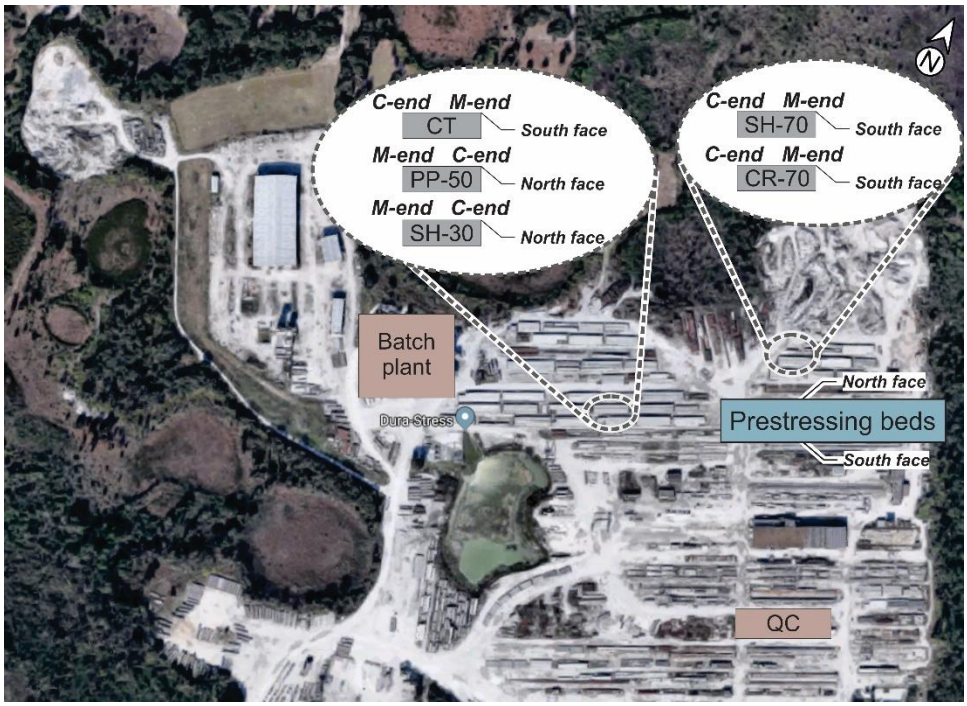

Figure 4-17 Girder location within the precast plant

4.4 Mixture proportions

Concrete mixtures were prepared at the precast batch plant. Specimen CT was cast using a conventional FDOT Class VI mixture. For the remaining specimens, the selected FRSCC mixture proportions were used. Mixture proportions used for each girder are summarized in Table 4-3.

Table 4-3 Mixture proportions used in full-scale FIB girder

	Mixture proportions (lb/cy)				
	CT	SH-30	SH-70	CR-70	PP-50
Cement	750	790	790	790	790
Flyash	170	175	175	175	175
CA #67	1089	0	0	0	0
CA #89	314	1335	1320	1320	1320
Fine agg	1210	1063	1063	1063	1063
Water	258	279	279	279	244
Fiber	0	39.68	92.58	92.58	7.67

4.5 FIB Specimen naming

Specimens were designated by the fiber type, volume, and end region detailing. Table 4-4 and Table 4-5 show the designation used for each fiber and for each end region detailing. Figure 4-18 shows an example of specimen naming format, which includes the fiber and volume used along with the end region detail in the specimen.

Table 4-4 Fiber designation and description

Fiber designation	Fiber Material	Fiber Type
PP	Polypropylene	Chemically enhanced
SH	Steel	Hooked end
SC	Steel	Crimped
CT	no fiber added	

Table 4-5 Detailing designation

Detailing	Designation
Conventional	C
Modified	M

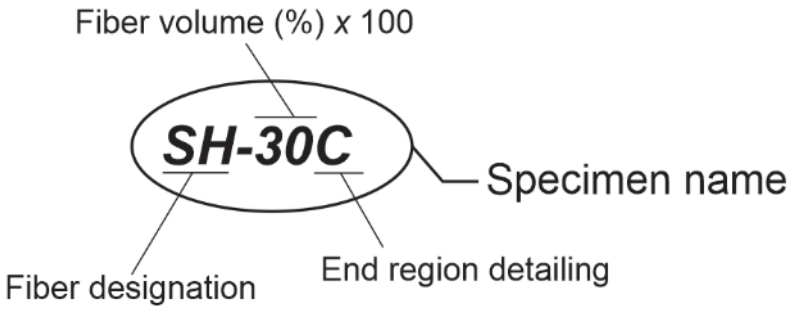

Figure 4-18 Example of girder end designation

4.6 Results of fresh properties testing

Typically, self-consolidating concrete (SCC) is used in construction of bridge girders in Florida. For this reason, the goal was to integrate the fiber reinforcement into the mixture while still satisfying passing ability and flowability requirements for SCC. Slump flow, T50, VSI, air content, density, passing ability testing was conducted for each mixture. Testing was conducted by the precaster following respective ASTM procedures shown in Table 4-6.

Table 4-6 Test for fresh properties

Test	ASTM	Limits
Slump flow	C1611	Shall be less or equal to 27.0 inches (±2.5inches)
Visual Stability Index (VSI)	C1611	Shall be less or equal to 1
T-50	C1611	Recommended 2-7 seconds
Passing ability	C1621	Shall not exceed 2.0 inches
Air content	C231	0-6%
Unit weight	C138	-

Figure 4-20 shows results for flow and passing ability of mixtures used in production of full-scale FIB girders. FDOT limits for each metric is indicated by the red dashed line. Most mixtures exceeded the limit for unrestricted flow of 27 inches (Figure 4-20a). All mixtures, however, showed good consistency, no bleeding, and good resistance to segregation. VSI (Visual Stability Index) was for all mixtures equal to zero and T-50 varied between 2 and 6 seconds (Figure 4-20c), which were well within the required values for SCC. Even though the passing ability limit of less than 2 inches was exceeded by all mixtures except for mixture containing steel crimped fibers (CR-70), no issue with fiber clumping was observed in mixtures containing hooked end or crimped steel fibers. Fiber nesting was apparent, however, inside the J-Ring when synthetic fibers were used (mixture PP-50), as shown in Figure 4-19b.

(a) (b)

Figure 4-19 J-Ring for (a) SH-30 and (b) PP-50

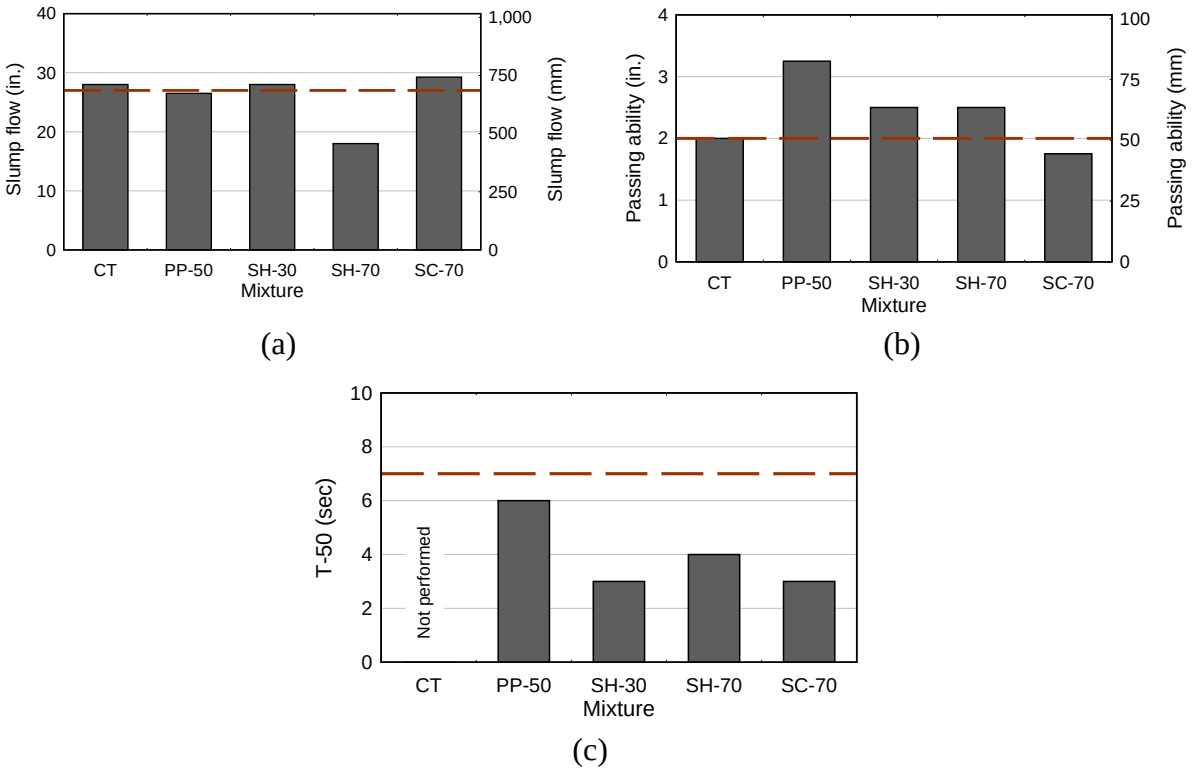

Figure 4-20 SCC properties: (a) slump flow, (b) passing ability, and (c) T-50

4.7 Results of hardened properties testing

4.7.1 Compressive strength

For each mixture, three 4 in x 8 in. cylinder specimens were prepared to determine the average compressive strength at 28 day. Cylinders were prepared and tested at the precast facility. Figure 4-21 shows graphic representation of the compressive strength of mixtures prepared in the laboratory mixer. Compressive strength of cylinders exceeded the specified 28-day specified compressive strength of 8,500 psi. The effect of fiber reinforcement on 28-day strength was found to be negligible, up to 10% difference.

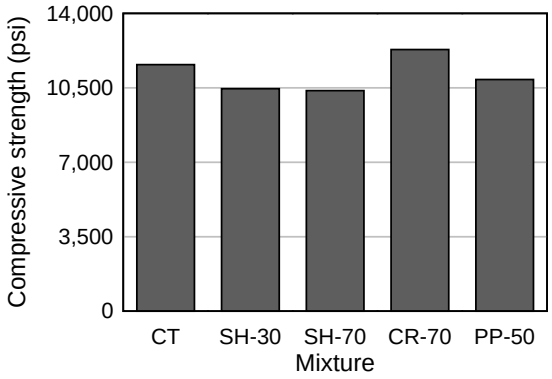

Figure 4-21 Compressive strength test results for concrete used to produce the girders (ASTM C39)

4.7.2 Residual strength ASTM 1399

Figure 4-22 shows average load-displacement curves for each of the mixtures tested; Appendix G contains curves for each specimen tested. Because of the bridging action across the cracked surface provided by the fiber reinforcement, the load carrying capacity continued even beyond test termination at 0.05-in. deflection. In general, higher fiber volumes and the use of stiffer fibers led to a higher residual strength at all loading stages.

Because end region cracking occurs under service loads rather than at extreme loads, the behavior right after cracking has initiated, up to a 0.02-in. beam deflection, was considered more significant than at larger deflections, which are typically related to ultimate strength.

Figure 4-23a shows the residual strength at the four key displacements, and Figure 4-23b shows the average residual strength for each of the mixtures tested. It is apparent that hooked end steel fibers (SH) at 0.70% volume dosage provided the highest residual strength among all fibers tested. This fiber provided up to 40% higher average residual strength than any other fiber. When compared with the crimped steel fibers (SC) at the same volume dosage of 0.70%, SH showed about 25% higher residual strength at service conditions and 30% higher average residual strength. By reducing the fiber volume of hooked end steel fiber from 0.70% to 0.30%, average residual strength was reduced by about 40%. At service level, hooked end steel fiber at a volume of 0.3% showed a load carrying capacity about 15% higher than the synthetic macrofiber (PP) at a volume fraction of 0.50%. At ultimate strength, however, the load-carrying capacity of the synthetic macrofiber was up to 20% higher.

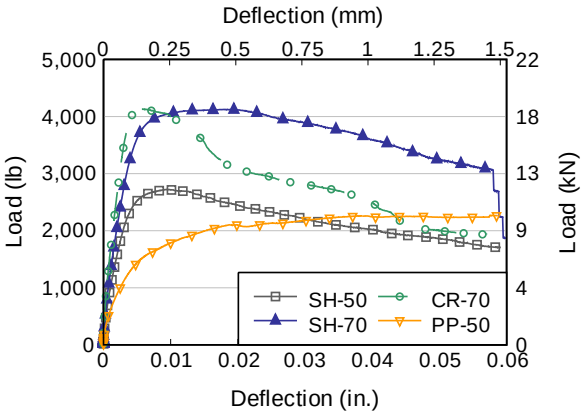

Figure 4-22 ASTM 1399 Load-displacement curve

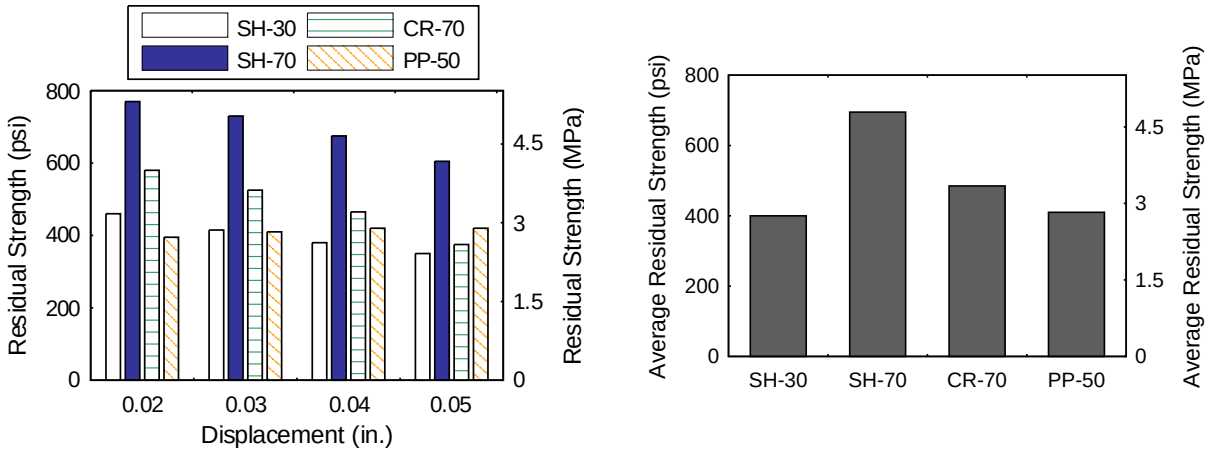

(a) (b)

Figure 4-23 Beam tests results showing (a) residual strength at specified displacements and (b) average residual strength.

4.7.3 Residual strength EN 14651

EN 14651 provides procedures to determine residual strength of a notched beam at various stages of displacement. This test is controlled by the crack mouth opening displacement (CMOD) of the notch. Load and deflection data were collected externally using a LabVIEW program prepared at the University of Florida. Figure 4-24 shows the test setup used during testing.

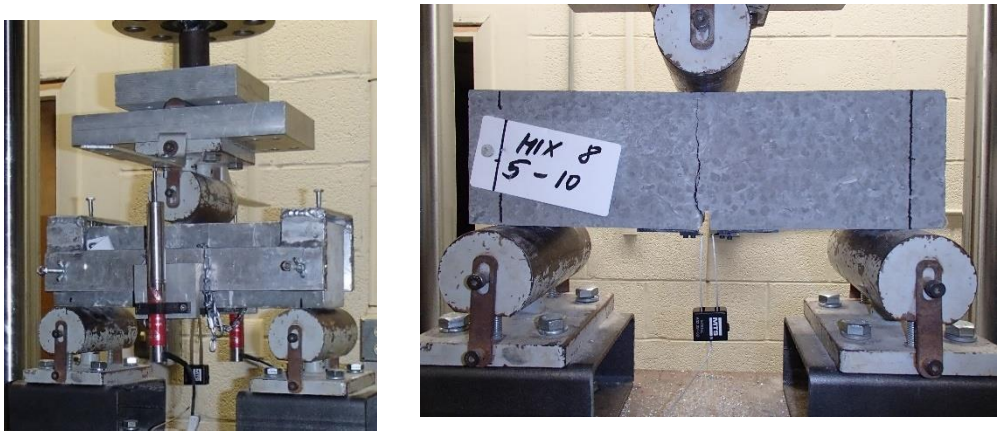

Figure 4-24 EN 14651 test setup

Figure 4-25a shows average load-CMOD curves for each of the mixtures tested. Appendix G contains curves for each specimen tested. Cracking loads obtained ranged between 1.6 and 1.9 kip, after which specimens containing steel fibers showed hardening behavior followed by a gradual loss in stiffness. Synthetic fibers showed a rapid loss in stiffness immediately after cracking (Figure 4-25b). To evaluate service behavior, post-cracking flexural strength between first cracking and $f_{R,1}$,CMOD of 0.02 in. (0.5 mm), was evaluated. Residual strength varied with fiber material and fiber volume used. In general, higher fiber volumes and the use of stiffer fibers led to a larger residual strength.

Figure 4-26 shows residual strength at specified CMOD increments of 0.02, 0.06, 0.10, and 0.15 in. (0.5, 1.5, 2.5 and 3.5 mm). Hooked end steel fibers (SH) at 0.70% volume dosage

provided the highest residual strength among all fibers tested. This fiber provided higher load carrying capacity than any other by up to 40%. When compared with the crimped steel fibers (SC) at the same volume dosage, SH showed higher residual strength by over 15% at service level (CMOD less than 0.5mm) and over 30% at ultimate stress. By reducing the fiber volume of hooked end steel fiber from 0.70% to 0.50% residual strength was reduced by about 30% in stresses at service level and by up to 43% at ultimate stress. In service stress, SH-30 had about 70% higher residual stress when compared with PP-50. At ultimate strength, the hooked end steel fiber showed higher residual strength by up to 37%.

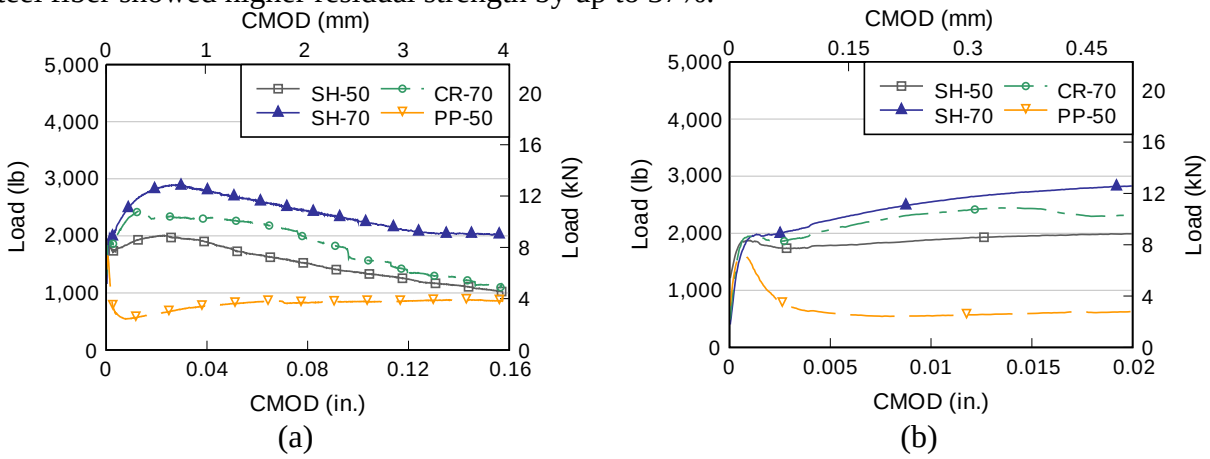

Figure 4-25 EN 14651 (a) Load-CMOD curve and (b) Load-CMOD at service level

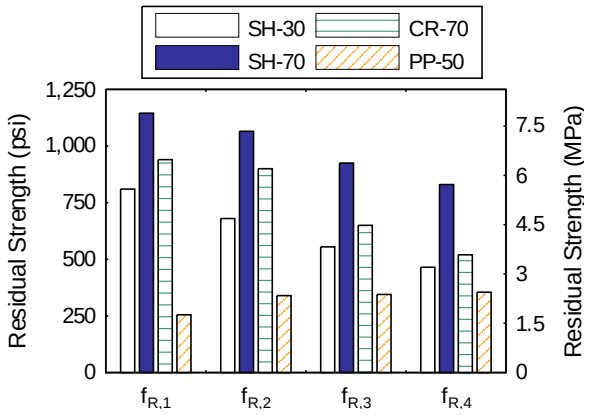

Figure 4-26 Residual strength results when tested in accordance with EN 14651

4.8 Strain during prestress transfer — testing and results

The experimental program included two stages: (1) strain monitoring during prestress transfer and (2) monitoring crack growth after prestress transfer and for a period of 148 days. Table 4-7 contains a summary of the prestress transfer testing. This section outlines the procedures and results of the strain monitoring during prestress transfer.

4.8.1 Test procedures

Prior to prestress transfer, specimens were inspected for cracking and null readings were taken for all strain gages. During prestress transfer, strain in concrete and mild steel

reinforcement within the end region was monitored to evaluate the effect of FRC during prestress transfer. Strain readings were taken at a frequency of 12 Hz for approximately 30 min while prestressing strands were cut. After prestress transfer, strain data was collected until strains in the concrete stabilized, which occurred in approximately 15 min. Crack monitoring was conducted once strain monitoring was completed, Table 4-8 shows the interval for crack monitoring within 148 days after prestress transfer.

Table 4-7 Summary of prestress transfer test procedures

Activity
Null readings for all strain gages
Inspect specimens for cracking prior to prestress transfer
Monitor strains during prestress transfer
Inspect cracking after prestress transfer
Transport specimen to storage location within the precast facility
Inspect cracking after transport
Inspect specimens for cracking for 148 days following prestress transfer

Table 4-8 Interval of crack monitoring during 148 days from prestress transfer

Age (days)	Measurement Interval (days)
0-7	1
7-14	3
14-35	7
35-63	14
63-148	85

4.8.2 Instrumentation

Strain measurements were collected from each specimen during prestress transfer using internal and external strain gages. Table 4-9 contains a list of the types of gages used along with their labels and placement. A consistent coordinate system is used throughout this report to define instrumentation location and direction of strains, stresses and forces. The origin of the coordinate system is located at the bottom of the end containing the conventional end region detailing (C-end) and at the centroid of the cross-section. The x-axis is horizontal across the width of the girder, the y-axis extends longitudinally along the beam and the z-axis is vertical, as shown in Figure 4-27.

Table 4-9 Instrumentation type and placement

Label	Type	Placement
XS	Foil strain gage	Concrete surface
IS	Foil strain gage	Reinforcement
ES	Embedded strain gage	Concrete interior

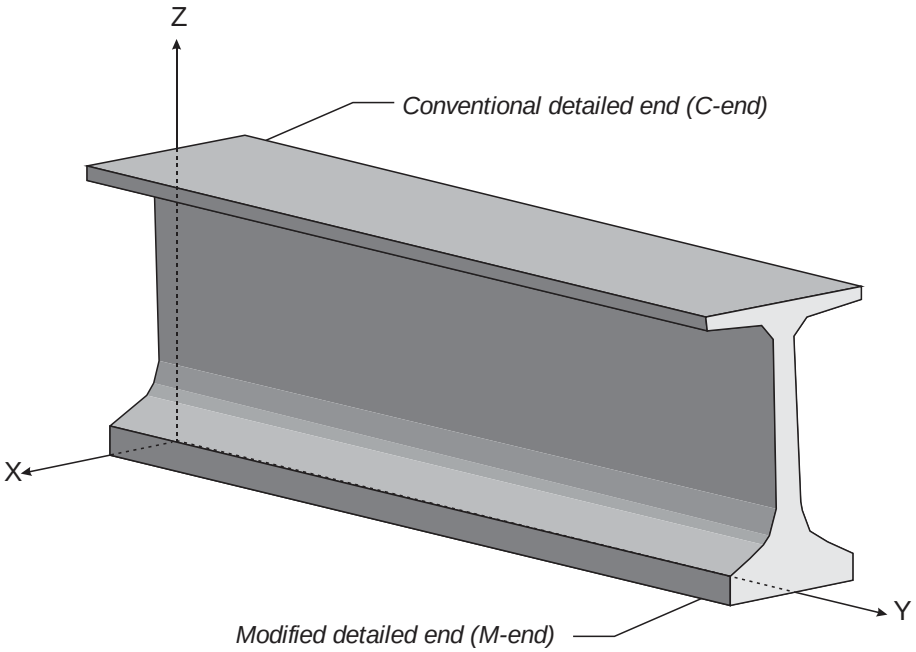

Figure 4-27 Coordinate system

XS strain gages were used to measure concrete strain during prestress transfer (Figure 4-28). These gages had a 2.4 in. (60 mm) gage length and were attached to the concrete surface after formwork was removed. A total of twelve (12) external gages were attached to the concrete surface at each girder end. Appendix E provides coordinates of external gages along with the direction of strain measurement. Figure 4-29 and Figure 4-30 show strain gages before and after attachment to the concrete surface.

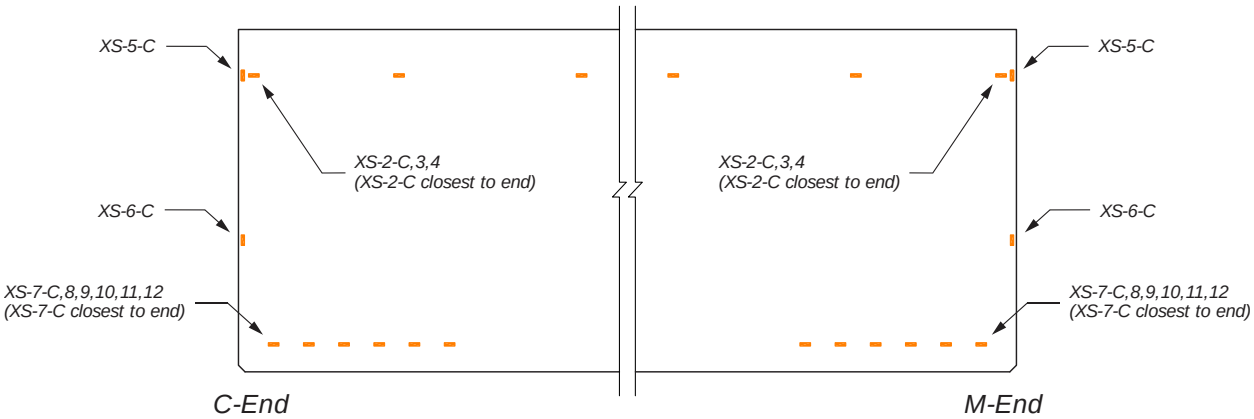

Figure 4-28 External instrumentation layout

Figure 4-29 XS gages prior to installation

Figure 4-30 XS strain gages

Two types of gages were placed internally to the concrete section (Figure 4-33). ES were 2.4 in. (60 mm) long full-bridge strain gages intended to measure the concrete strain during prestress transfer (Figure 4-31). IS were 0.2 in. (5 mm) long quarter-bridge foil gages bonded to the mild steel reinforcement within the transfer length to monitor strain in the mild reinforcement (Figure 4-32). For both IS and ES gages, the wires were tied along the reinforcement and exited the section from the top flange. Two (2) embedded strain gages (ES) and five (5) internal strain gages were placed in each girder end. Detailed information on these gages is located in Appendix E

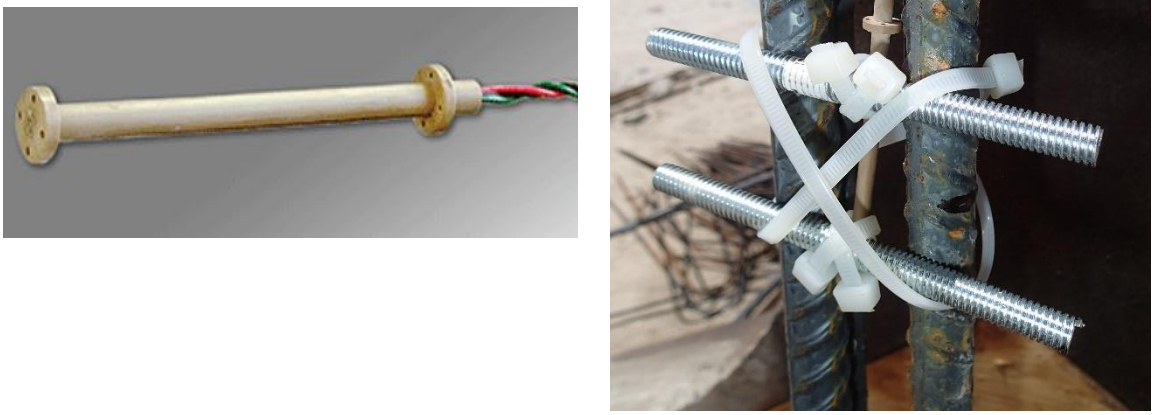

Figure 4-31 ES strain gages

Figure 4-32 IS strain gage prior to reinforcement installation

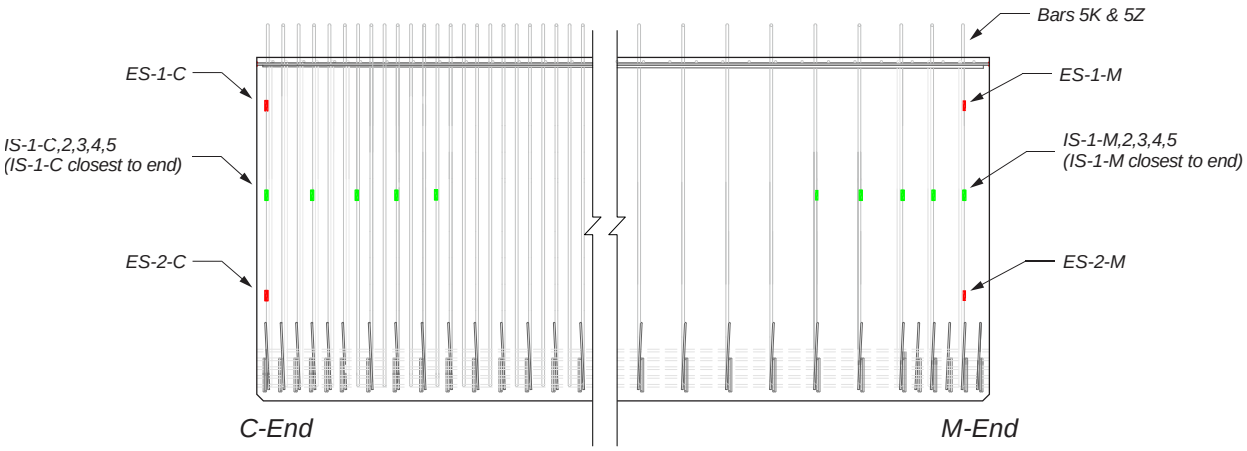

Figure 4-33 Internal instrumentation layout

4.8.3 Reinforcement strain results

Strain gages IS were placed on the steel reinforcement to measure steel strain during prestress transfer. Figure 4-34 shows the general location of the IS gages along the web of the girder (coordinates for each gage are provided in Appendix section F.1). In general, vertical tensile strain in the web was highest near the end of the girder (IS-1) and decreased in magnitude as the distance from the girder end increased.

The magnitude of the tensile strain recorded in the mild steel reinforcement is highly dependent on the location of the end region cracks. Figure 4-35 shows the crack pattern immediately after prestress transfer overlaid with the position of the IS strain gages to aid in the following discussion of the strain measurements recorded during prestress transfer.

Strain measurements taken from the mild steel reinforcement when using conventional end region detailing (Figure 4-36) show that among all specimens, a maximum tensile strain of 730 microstrain was observed in the CT specimen. This strain is well beyond the strain required to initiate concrete cracking, which is estimated at 130 microstrain (based on measured compressive strength and ACI empirical equations). This strain converts to a steel stress of about 20 ksi in the reinforcement, which is well within the working stress level, and is likely the maximum stress that will be subjected to the bar. The maximum tensile strain in all specimens occurred within 15 in. (~h/5) of the girder end. For this reason, the amount of reinforcement provided within this region is critical to effectively controlling end region cracking.

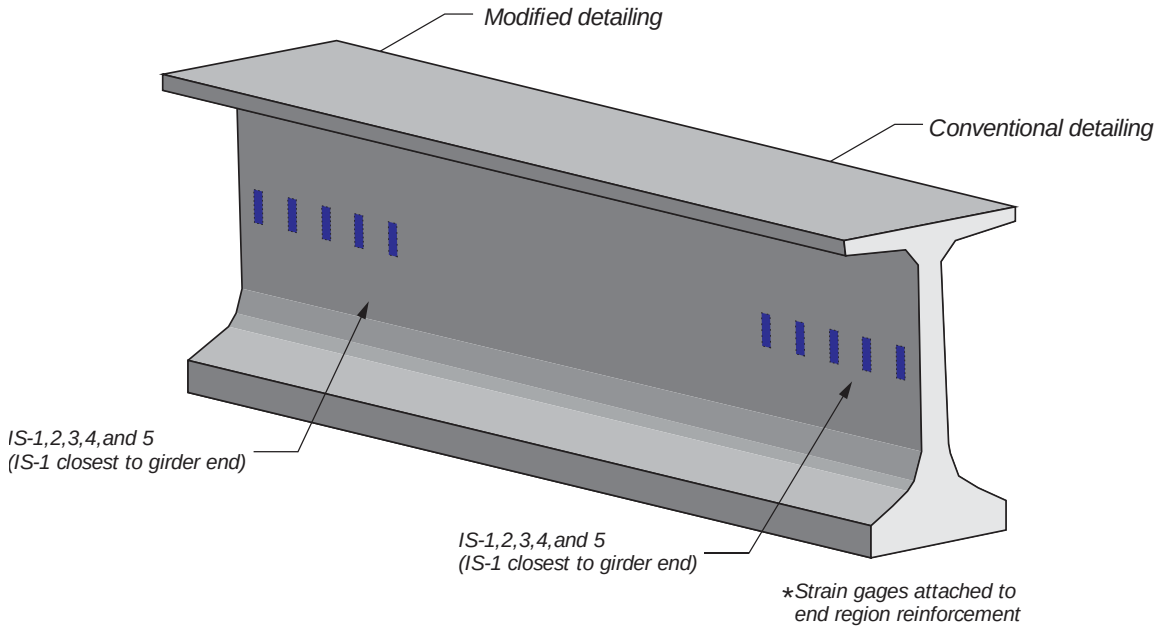

Figure 4-34 Strain gages bonded to vertical reinforcement

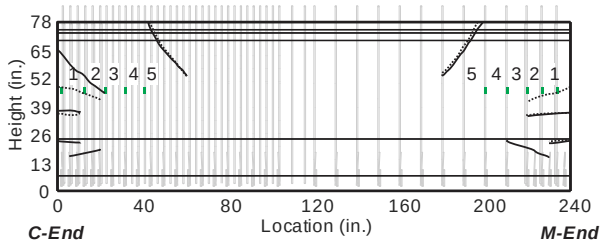

(a)

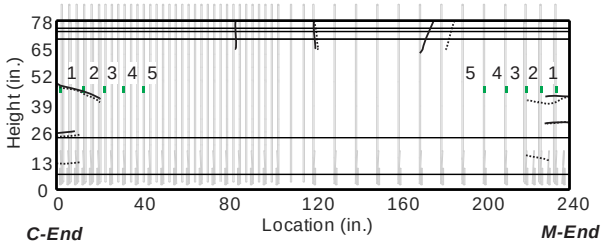

(b)

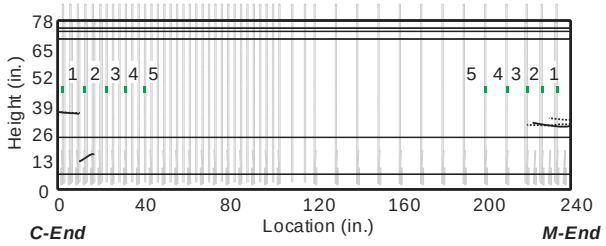

(c)

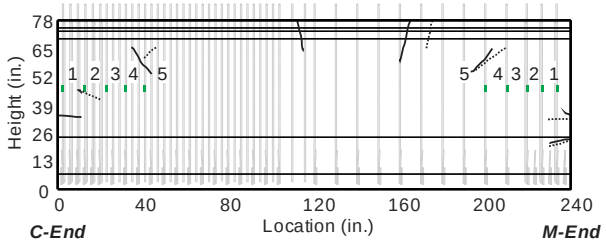

(d)

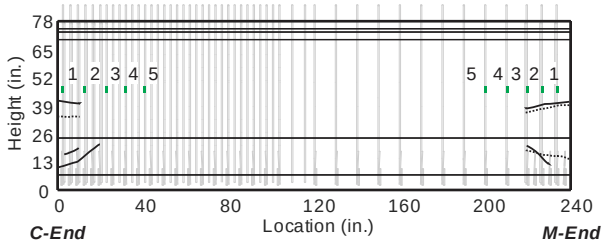

(e)

Figure 4-35 Cracking after prestressed transfer overlaid with IS strain gages location shown on North face of specimen (Solid lines depict cracks visible on the North face and dashed lines depict cracks visible on the South face): (a) CT, (b) SH-30, (c) SH-70, (d) CR-70 and (e) PP-50.

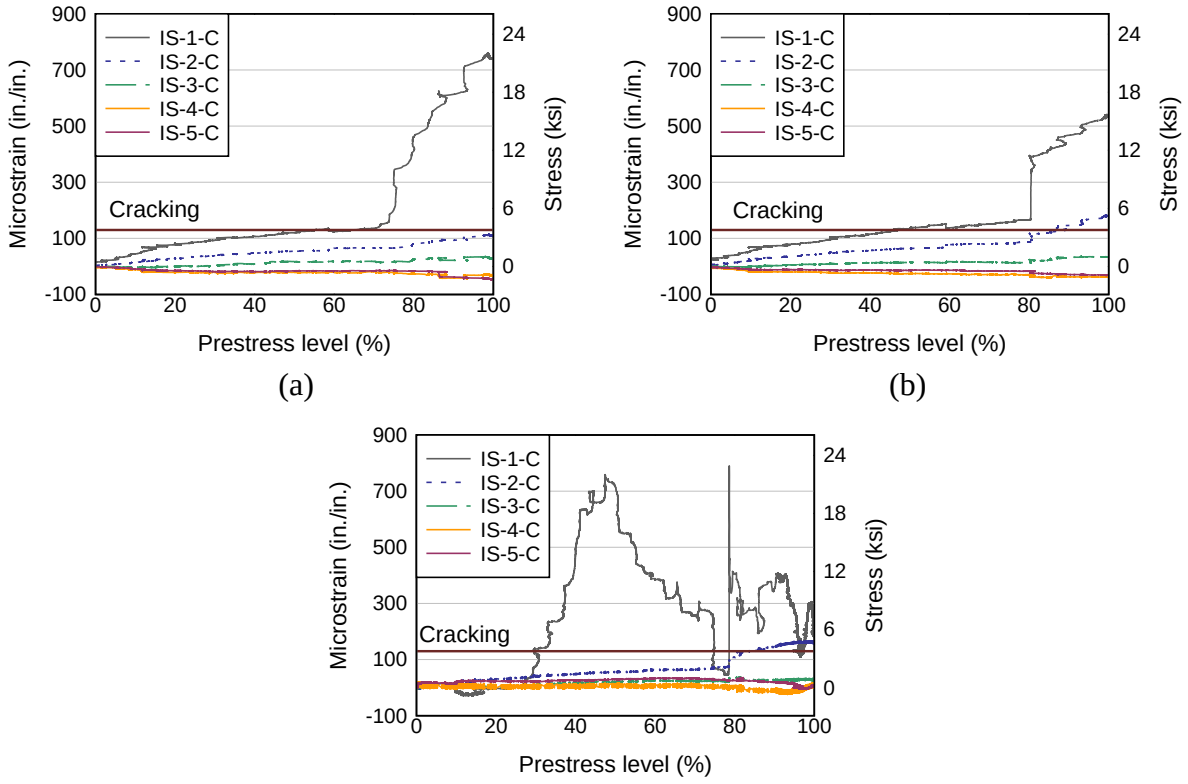

Figure 4-36 Mild steel reinforcement strain during prestress transfer, conventional end region detailing: (a) CT, (b) SH-30, (c) CR-70

Figure 4-37 shows mild steel reinforcement strains during prestress transfer when using a modified end region detailing. No data is available for specimen CT due to strain gage malfunction during prestress transfer. Comparison of strain in FRC specimens showed that maximum tensile strains varied between 130-300 microstrain. This strain converts to a steel stress of about 10 ksi in the reinforcement, which is well within the working stress level. However, based on the end region crack pattern at the end of prestress transfer (Figure 4-35), no cracks occurred near the location of the strain gages, for this reason it is likely that the stress recorded is at the lower bound of the range that occurred in this bar.

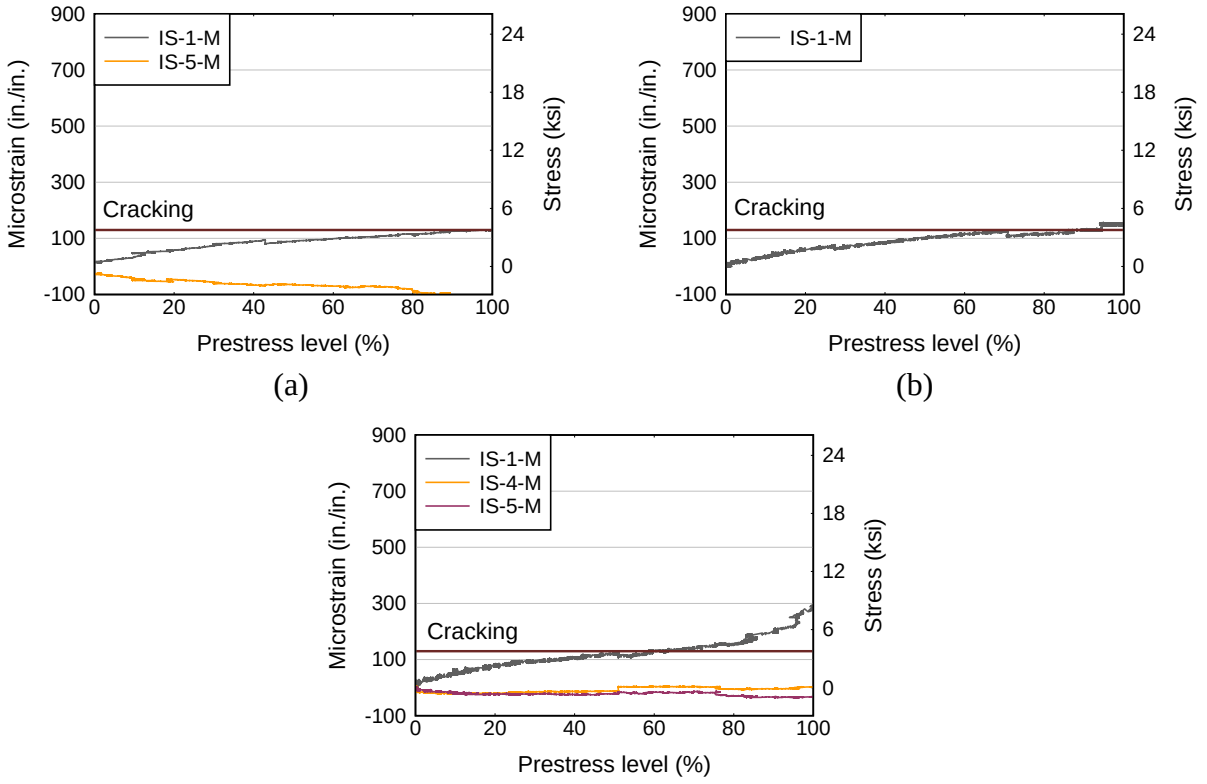

Figure 4-37 Mild steel reinforcement strain during prestress transfer, modified end region detailing: (a) SH-30, (b) CR-70, (c) PP-50

Figure 4-39 compares mild steel reinforcement strain for the conventional and modified end region detailing. The volume of reinforcement at the modified end was about 50% of that in the conventional end. Higher tensile strains, and wider cracks were expected in the modified end because a lesser amount of reinforcement was present. However, the strain recorded in the first line of reinforcement (IS-1) in both SH-30 and CR-70 was higher in the conventional end. The crack pattern after prestress transfer shows that cracks formed at or close to the location of strain gage IS-1 in the conventional end, whereas no such cracks were noted in the modified end (Figure 4-35). This would lead to higher strains locally near the crack in the conventional end compared to that of the modified end. In addition, strain gages in the conventional and modified end were not located at the same distance from the girder end. Table 4-10 shows the distance of each strain gage from each girder end and Figure 4-39 shows maximum strain recorded in the conventional and modified end with respect to the distance from the girder end. IS-1 strain gages, which were located in the region where maximum tensile strains were expected, were placed 3 and 6.5 in. away from the girder end in the conventional and modified end, respectively. The distance at which the strain gages were placed from the girder ends could also explain why larger strains were measured in the conventional end in the first line of reinforcement (IS-1) for both SH-30 and CR-70 specimens.

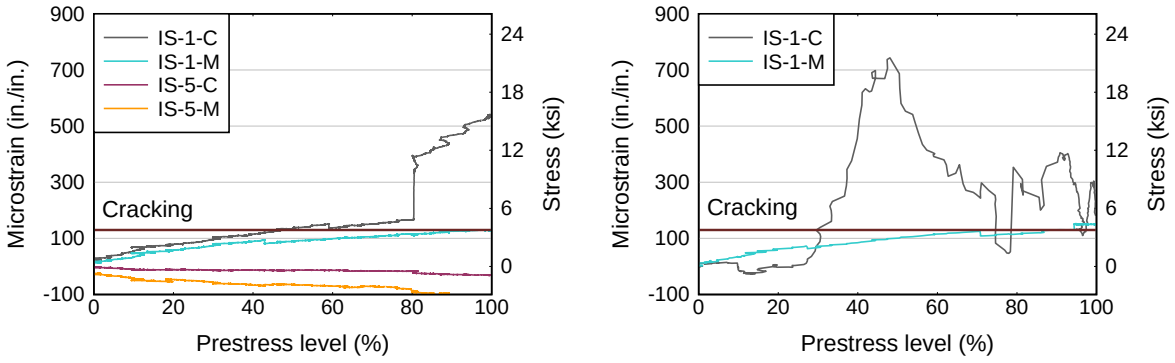

Figure 4-38 Comparison of reinforcement strain for conventional (C) and modified (M) end region detailing: (a) SH-30 and (b) CR-70

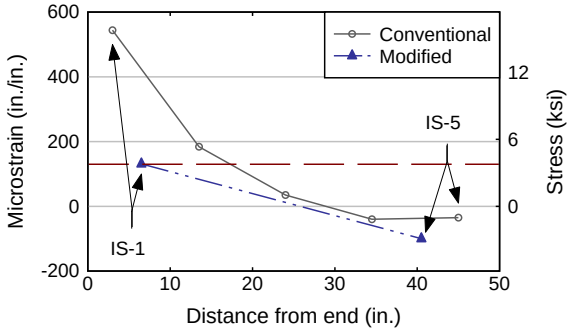

Figure 4-39 Maximum reinforcement strain and distance from girder end for conventional and modified end region detailing for SH-30

Table 4-10 IS strain gage distace from the girder end (y-direction)

Strain gage	Distance from girder end (in.)	
	Conventional	Modified
IS-1	3	6.5
IS-2	13.5	13.5
IS-3	24	20.5
IS-4	34.5	30.5
IS-5	45	40.5

4.8.4 Concrete strain results

External strain gages XS-5 and XS-6 were placed on the side face of the web of each girder to measure concrete strain during prestress transfer. Internal strain gages ES-1 and ES-2 were embedded to measure concrete strain during prestress transfer. Figure 4-40 shows the general location of the XS and ES strain gages (coordinates for each gage are provided in Appendix Section F.1). In general, both internal and external strain gages showed that vertical tensile strain in the web increased as prestress force was transferred. In addition, tensile strain was highest near the transition between the bottom flange and the web compared to strain along the transition between the top flange and the web.

Figure 4-41 and Figure 4-42 show strain measurements from internal and external concrete strain gages, respectively, when using conventional end region detailing. For all specimens, the highest strain was recorded in strain gages placed nearest the transition between the bottom flange and the web (ES-2 and XS-6). Among all specimens, a maximum tensile strain of 260 microstrain was observed in the internal strain gage in specimen SH-30. This strain is well beyond the strain required to initiate concrete cracking, which is estimated at 130 microstrain (based on measured compressive strength and ACI empirical equations). Internal concrete strain gages placed near the transition from the web to the top flange (ES-1 and XS-5) suggest that the concrete near this location remained uncracked during prestress transfer. Overlay of crack pattern with the location of the strain gages confirmed this behavior for all specimens, except for the case of CT in the end with conventional end region detailing. End region cracks occurred during prestress transfer and continued to grow over a period of about 3 months. Initial cracks continued to grow well after prestress transfer, and new cracks continued to form. Crack monitoring was conducted once strain monitoring was completed. One possible explanation for cracking in specimen CT (C-end), where strain measurements were below cracking, is that cracking near the location of XS-5 formed after strain monitoring was completed.

Figure 4-43 and Figure 4-44 show strain measurements from the internal and external concrete strain gages, respectively, when using modified end region detailing. For all specimens, the highest strain was recorded in strain gages placed near the transition between the bottom flange and the web (ES-2 and XS-6). Among all specimens, a maximum tensile strain of 150 microstrain was observed in the external strain gage in specimen PP-50. This strain was of similar magnitude as the strain required to initiate concrete cracking, which is estimated at 130 microstrain (based on measured compressive strength and ACI empirical equations). Internal concrete strain gages placed near the transition from the web to the top flange (ES-1 and XS-5) suggest that the concrete near this location remained uncracked during prestress transfer. Comparison of crack locations with that of the strain gages confirmed this behavior for all specimens.

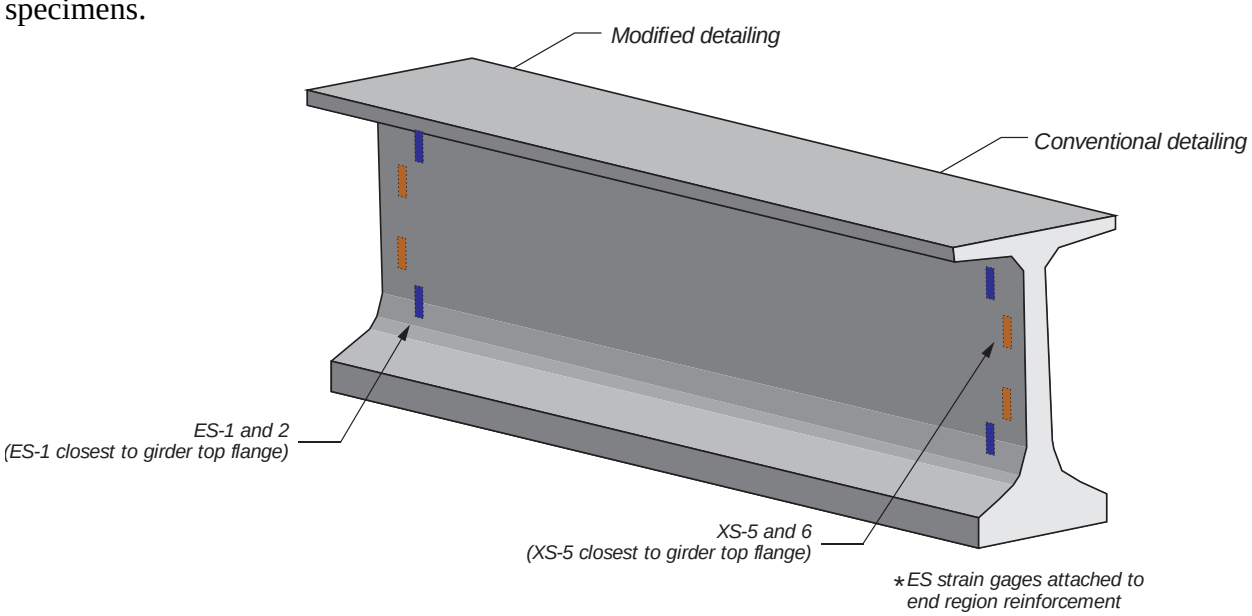

Figure 4-40 ES and XS strain gages for measurement of concrete strains

Figure 4-45 compares internal concrete strain in the conventional end with that of the modified end of SH-30. Similar strain magnitudes were reported near the transition from the web to the top flange (ES-1) for both ends and were well below the strain expected to initiate concrete cracking. No cracks were observed in the region near ES-1 strain gages for specimen SH-30 (Figure 4-46b), which agrees with the low strain measurements. The crack pattern after prestress transfer shows that cracks formed at or close to the location of strain gage ES-2 in the conventional end. In contrast, no such cracks were noted in the modified end (Figure 4-46b), which validates the higher strains recorded in the conventional end.

Figure 4-47a shows a comparison of concrete strain measured using external strain gages at both ends of CR-70. During early stages of prestress transfer, higher strains were recorded in the modified end. After 50-70% of the prestress force was transferred, the maximum strain reported for both ends ranged between 100-130 microstrain, which would be expected initiate concrete cracking. Indeed, cracks were observed in the region near XS-6 strain gages for the conventional and modified end of CR-70 (Figure 4-48d). Figure 4-47b shows concrete strain at both ends of PP-50 measured using external strain gages. Strain reported by gage XS-5 suggests that concrete near XS-5 remained uncracked, which is in agreement with absence of cracks observed in the region near XS-5 (Figure 4-48e). Strains measured at XS-6 were of sufficient magnitude to initiate cracking, but no cracks were observed near XS-6 immediately after prestress transfer (Figure 4-48e).

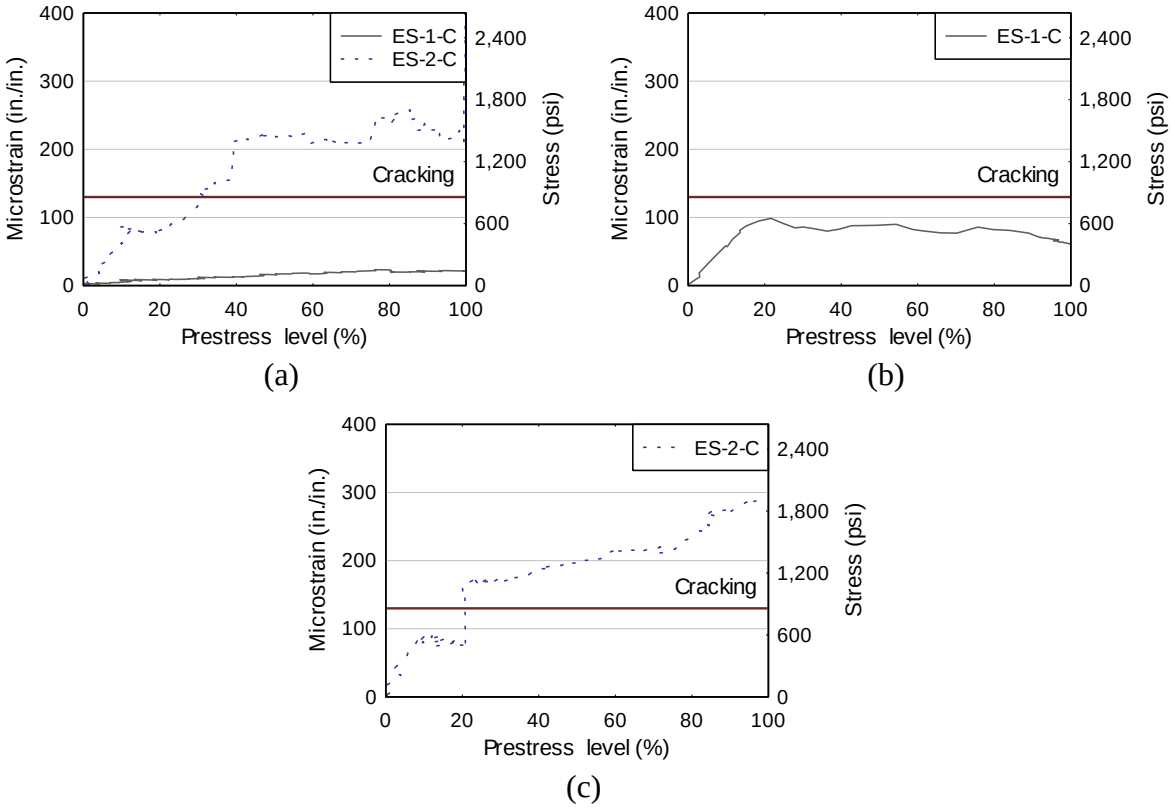

Figure 4-41 Internal concrete strain during prestress transfer, conventional end region detailing: (a) SH-30, (b) CR-70, and (c) PP-50

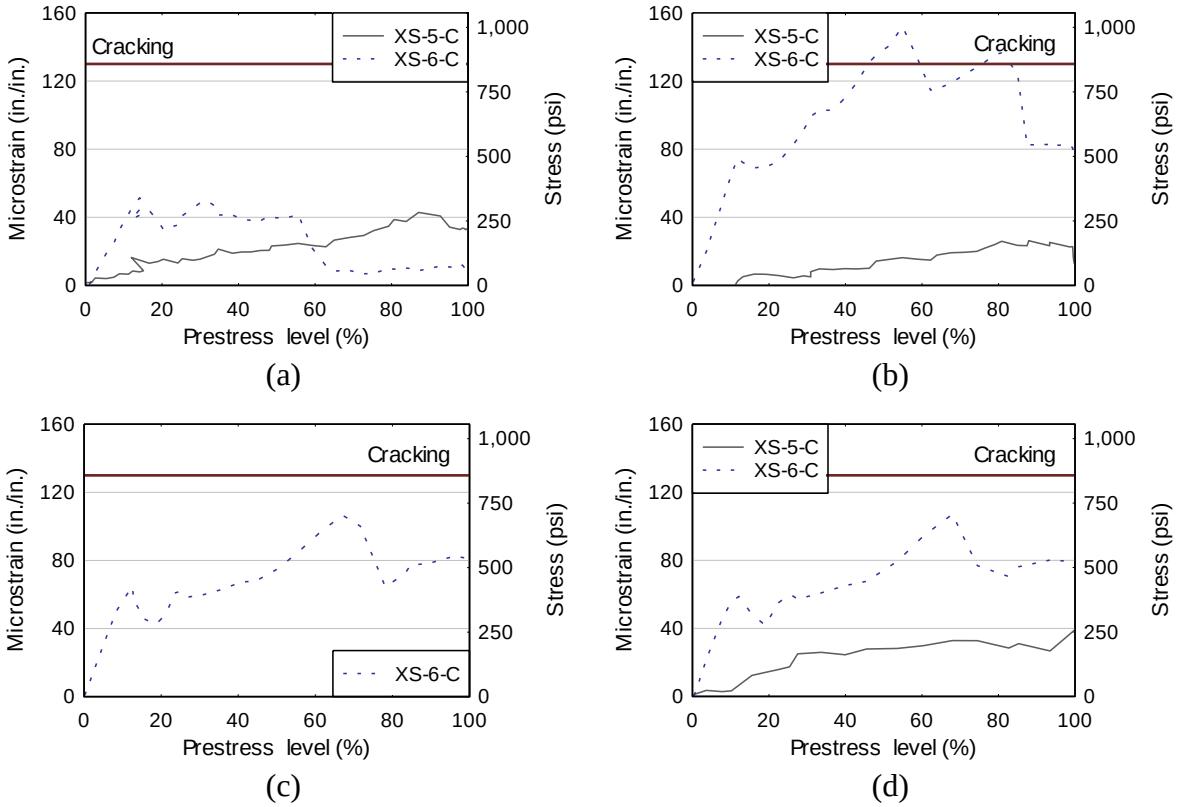

Figure 4-42 External concrete strain during prestress transfer, conventional end region detailing: (a) CT, (b) SH-30, (c) CR-70 and (d) PP-50

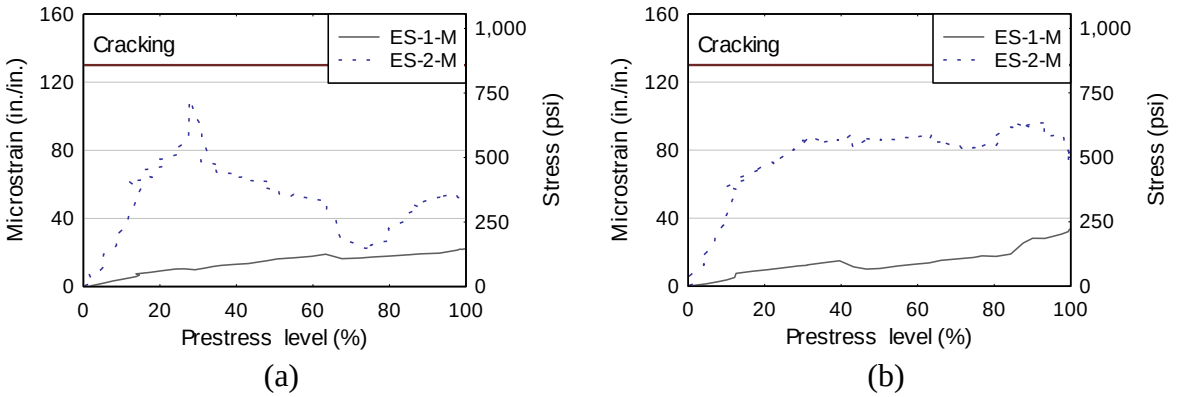

Figure 4-43 Internal concrete strain during prestress transfer, modified end region detailing: (a) CT, and (b) SH-30

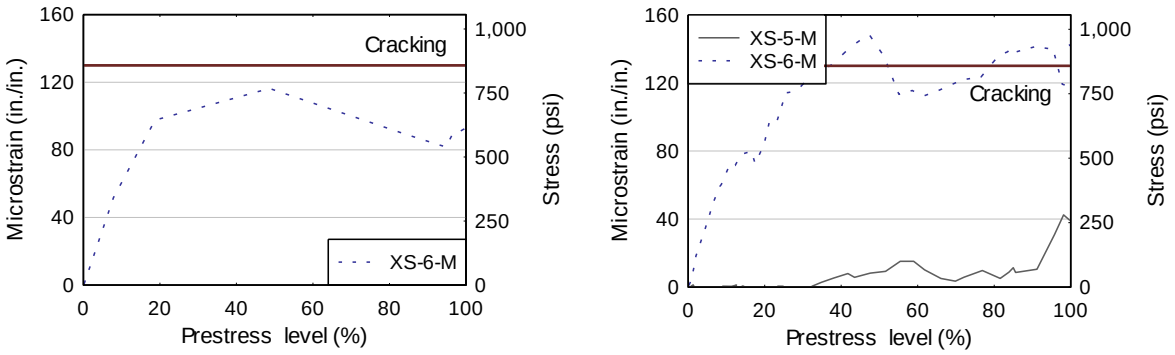

(a) (b)

Figure 4-44 External concrete strain during prestress transfer, modified end region detailing: (a) CR-70, and (b) PP-50

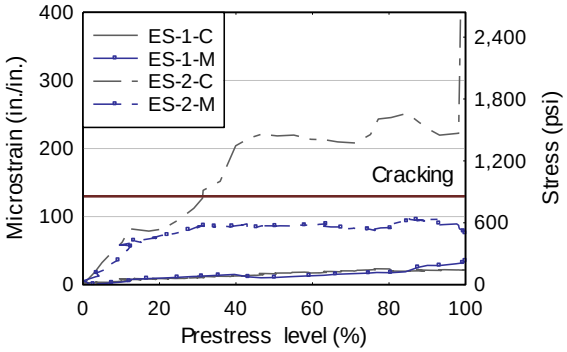

Figure 4-45 Comparison of embedded concrete strain for specimen SH-30 for conventional (C) and modified (M) end region detailing

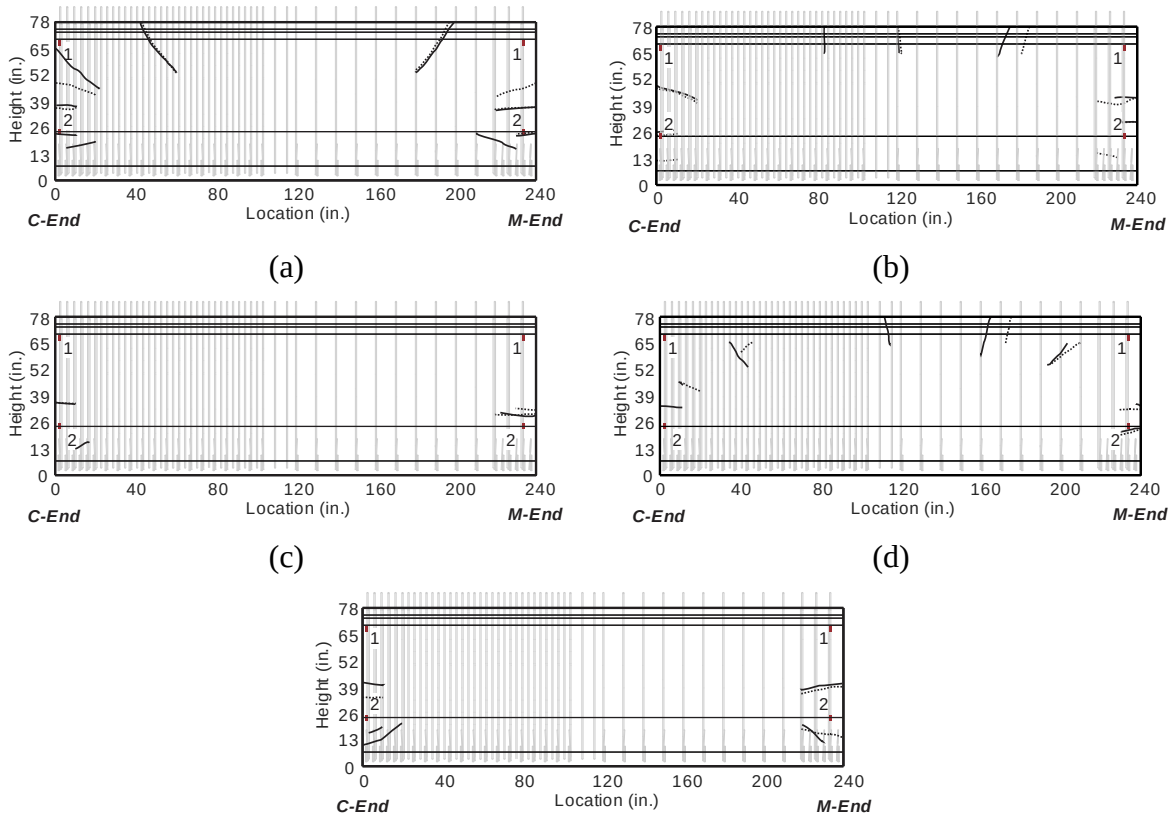

Figure 4-46 Cracking observed after prestressed transfer overlaid with embedded strain gage (ES-1 and ES-2) location shown on North face of specimen (Solid lines depict cracks visible on the North face and dashed lines depict cracks visible on the South face): (a) CT, (b) SH-30, (c) SH-70, (d) CR-70 and (e) PP-50

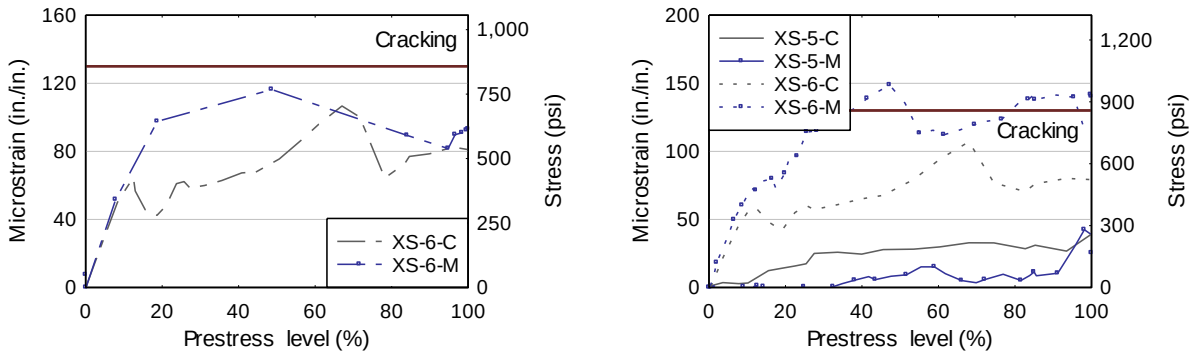

Figure 4-47 Comparison of external concrete strain for conventional (C) and modified (M) end region detailing: (a) CR-70 and (b) PP-50

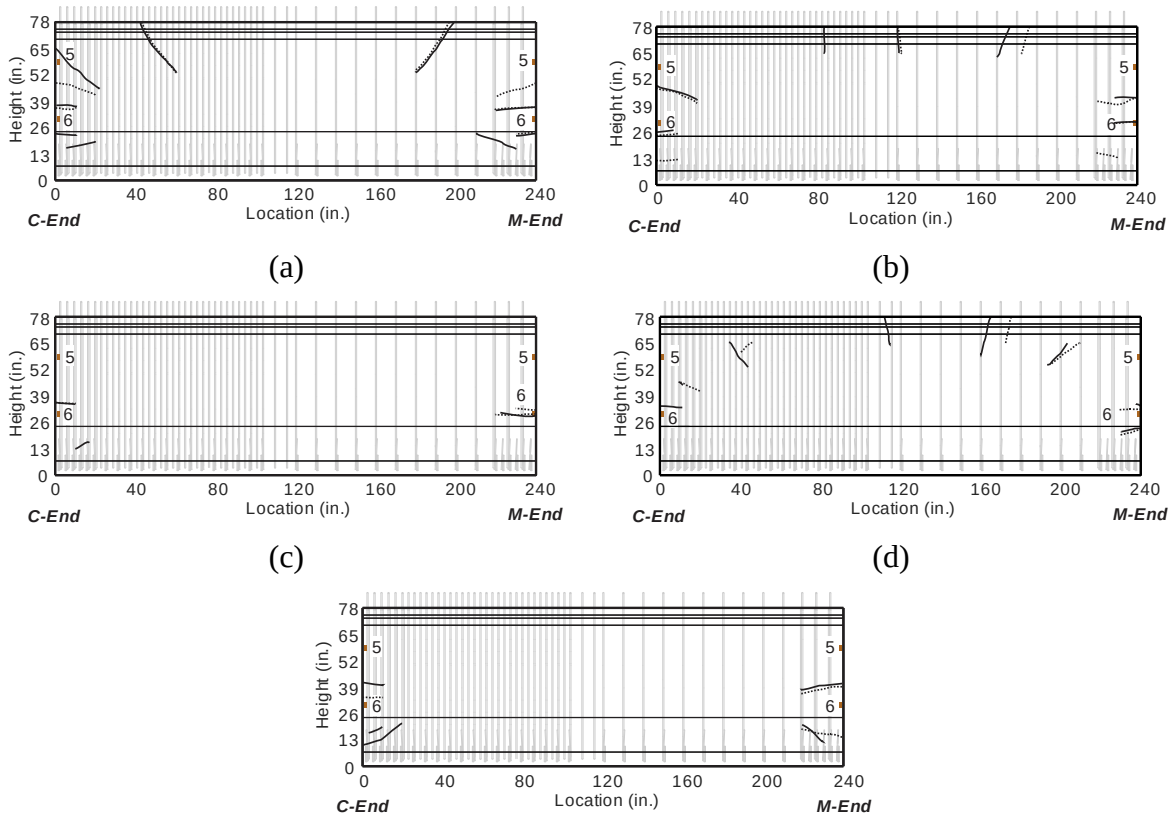

Figure 4-48 Cracking observed after prestressed transfer overlaid with external strain gage (XS-5 and XS-6) location shown on North face of specimen (Solid lines depict cracks visible on the North face and dashed lines depict cracks visible on the South face): (a) CT, (b) SH-30, (c) SH-70, (d) CR-70 and (e) PP-50

4.8.5 Transfer length results

Strain gages XS-7 through XS-12 were placed on the side face of the bottom flange of each girder to experimentally evaluate transfer length (Figure 4-49). The 95% Average Maximum Strain Method (Russel and Burns 1993) was used to estimate the transfer length for each girder from the strain readings taken during prestress transfer (Figure 4-50). For all specimens, concrete strain was observed to increase with increased distance from the girder end. The strain plateaued at about 32 in. from the girder end, which indicates the end of the transfer length. The strain after this point, which is relatively constant was used to estimate the average strain. A line corresponding to the 95% of the average strain is included in the plots. The distance from the girder end in which the 95% of the average strain intersects the experimental curve is defined as the transfer length (Figure 4-50).

Results indicate that the transfer length of the FRC was similar to that of the CT. Furthermore, for CT, no significant difference was observed between the transfer lengths measured at the ends with conventional and modified end region detailing. However, in the case of SH-30 and CR-70 a difference of about 10 in. was observed between transfer length measured at the conventional and modified end. The transfer lengths estimated from the experimental

results are in good agreement with the calculated transfer length of 36 in. based on AASHTO LRFD.

An average transfer length of 31.3 in. was calculated based on the estimated transfer lengths for each girder end. Figure 4-51 shows the distribution of the experimental transfer length measurements with respect to the average transfer length and Figure 4-52 shows the ratio of transfer length measurements to the average transfer length. A ratio less than one indicates that the measurement was smaller than the average transfer length, and a ratio larger than one indicates that the measurement was larger than the average transfer length. The coefficient of variation between the measured transfer lengths was 15%. No data was collected for transfer length in specimen SH-70 due to gage malfunction. Because of the consistency of transfer length measurements in the other FRC specimens, however, similar transfer length was expected as for the remaining girder specimen.

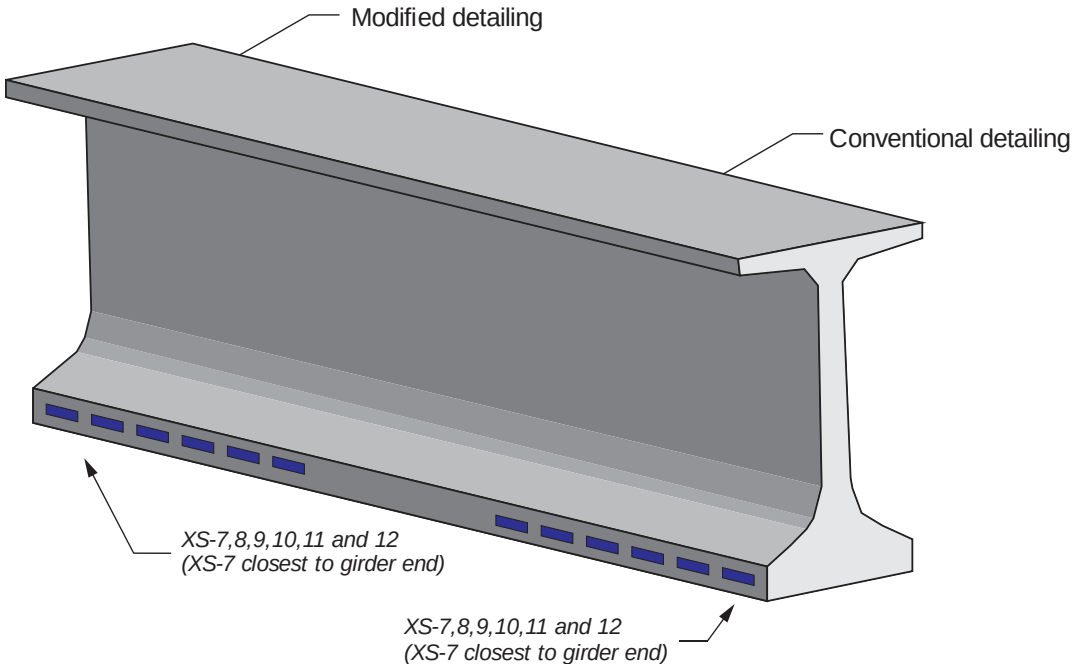

Figure 4-49 External strain gages for measuring transfer length (XS-7 through XS-12)

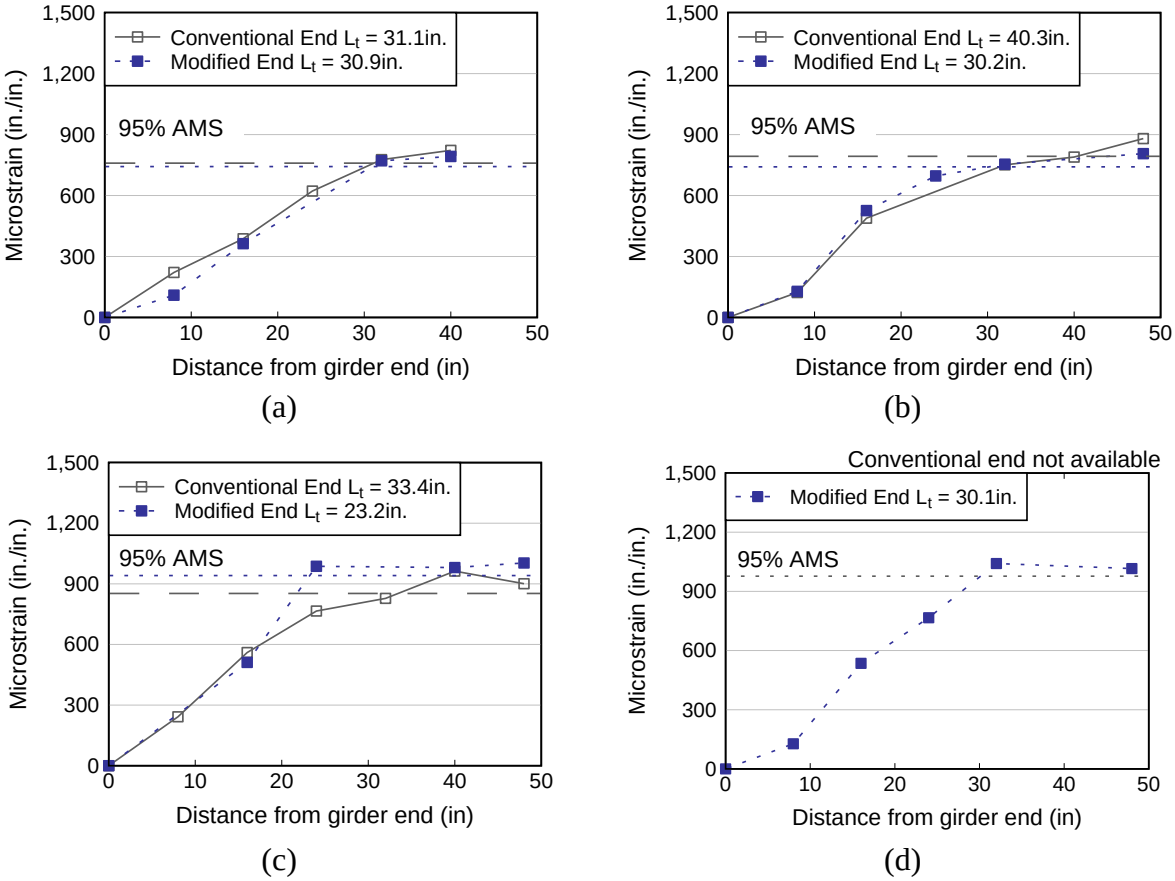

Figure 4-50 Transfer length: (a) CT, (b) SH-30, (c) CR-70 and (d) PP-50

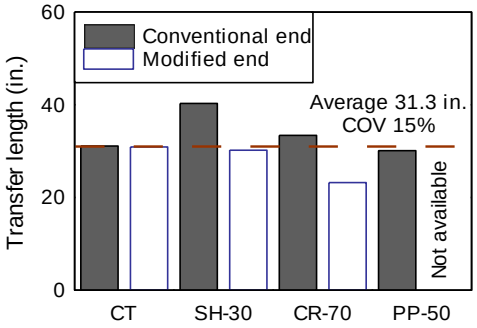

Figure 4-51 Distribution of transfer length measurements with respect to the average transfer length

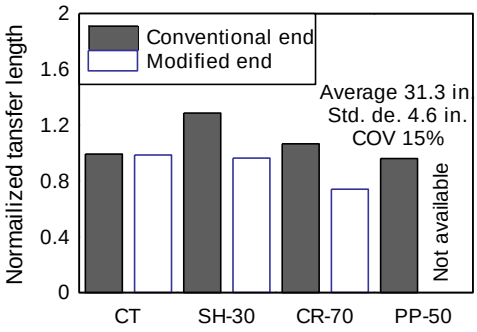

Figure 4-52 Ratio of measured transfer length to average transfer length

4.9 Cracking after prestress transfer — testing and results

The experimental program included two stages: (1) strain monitoring during prestress transfer and (2) monitoring crack width and length after prestress transfer and for a period of 148 days. This chapter outlines the procedures used and results obtained from monitoring end region cracking after prestress transfer.

4.9.1 Test procedures

After form removal and prior to prestress transfer, specimens were visually inspected for cracking; no cracks were observed in any of the specimens. Crack measurements were taken immediately following prestress transfer and measured periodically for 148 days. Crack measurements were taken daily in the week following prestress transfer, followed by less frequent measurements as crack growth stabilized (Table 4-11).

Table 4-11 Frequency of crack measurements

Age (days)	Frequency of measurements (days)
0-7	1
7-14	3
14-35	7
35-63	14
63-148	85

A gridline reference system was established to facilitate locating and monitoring cracks over time (Figure 4-53). From each girder end, a 10 in. x10 in. grid that covered the entire height of the girder and for distance of about 1D from the beam end (80 in.) was marked. To monitor flexural cracks that occurred in the top of the section at mid-length, the remaining of the girder was divided using a grid with 20 in. horizontal spacing and 10 in. vertical spacing. The grid was labelled using numeric characters for horizontal lines and alphabetical characters for the vertical lines, which were used to record and track the crack width and length.

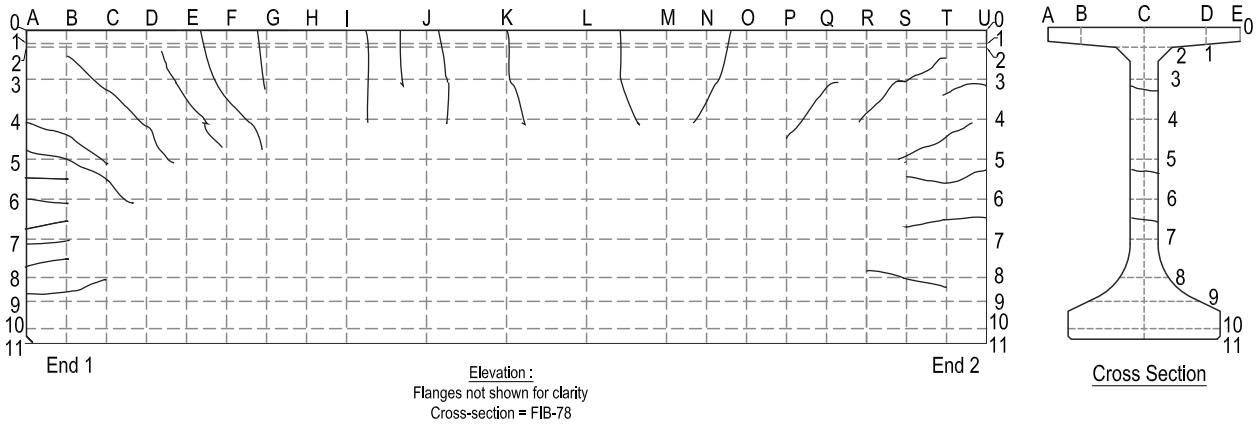

Figure 4-53 Schematic of gridlines used for crack measurements

4.9.2 End region crack monitoring

Specimens were inspected for cracking within one (1) hour after prestress transfer was completed and during the months following transfer. Figure 4-54 and Figure 4-55 show the initial cracking that occurred during prestress transfer and continued to grow over a period of about 3 months. In general, the number of cracks and their length and width grew over time, however, crack patterns varied among the specimens. Detailed figures documenting crack growth for each specimen throughout the entire monitoring period (both North and South face) are included as part of Appendix section F.3.

Cracks formed in the web and bottom flange at each end and in the top flange near mid-length during prestress transfer. In general, the location and characteristics of the cracking were as anticipated. Web cracking is caused due to the prestressing force eccentricity, as prestressing forces are transferred into the concrete, vertical tension forces develop along the web of the girder. The bottom flange cracking occurs due to prestressing eccentricity, and due to Hoyer effect (strands expanding after strand cutting resisted by surrounding concrete).

After girders were moved to storage, monitoring indicated that initial cracks continued to grow in both length and width and that new cracks formed. Figure 4-56 through Figure 4-60 show comparisons of crack patterns immediately following prestress transfer and after beams were lifted for storage. Crack growth continued until about 60 days following prestress transfer. To illustrate this growth, Figure 4-61 through Figure 4-65 show end region cracking visible on both faces of the girders immediately following prestress transfer and 148 days after prestress transfer. Cracks visible on the North face are depicted with solid blue lines and cracks visible on the South face are depicted with dashed green lines (as if seeing through the web). Cracking along the height of the web is the primary focus of this work and is discussed in this chapter.

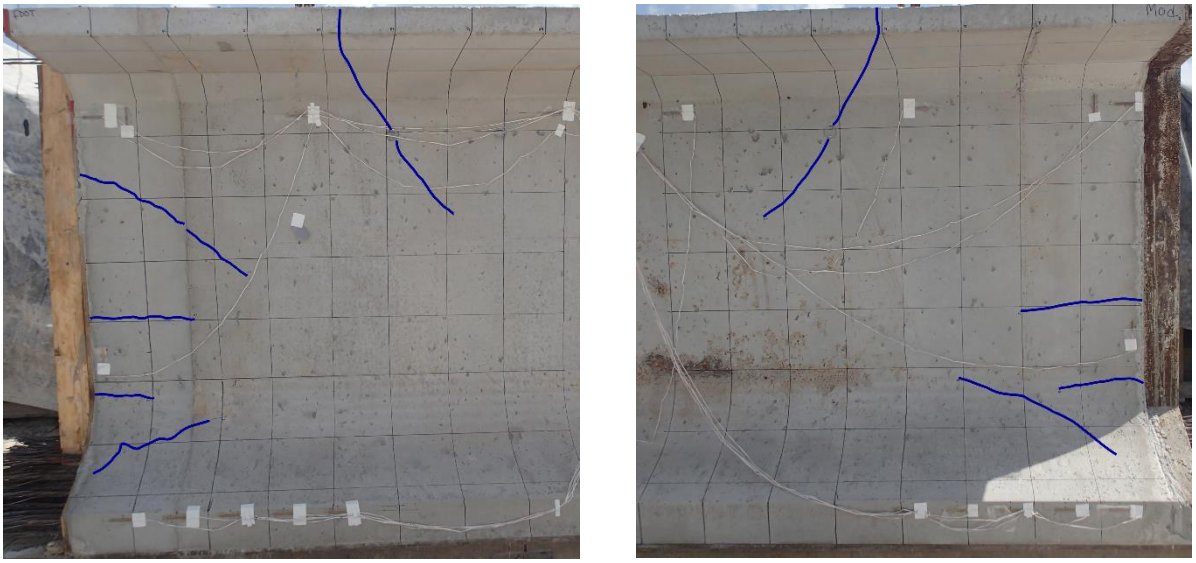

(a) (b)

Figure 4-54 CT end region cracking after prestress transfer in end with: (a) conventional and (b) modified end region detailing

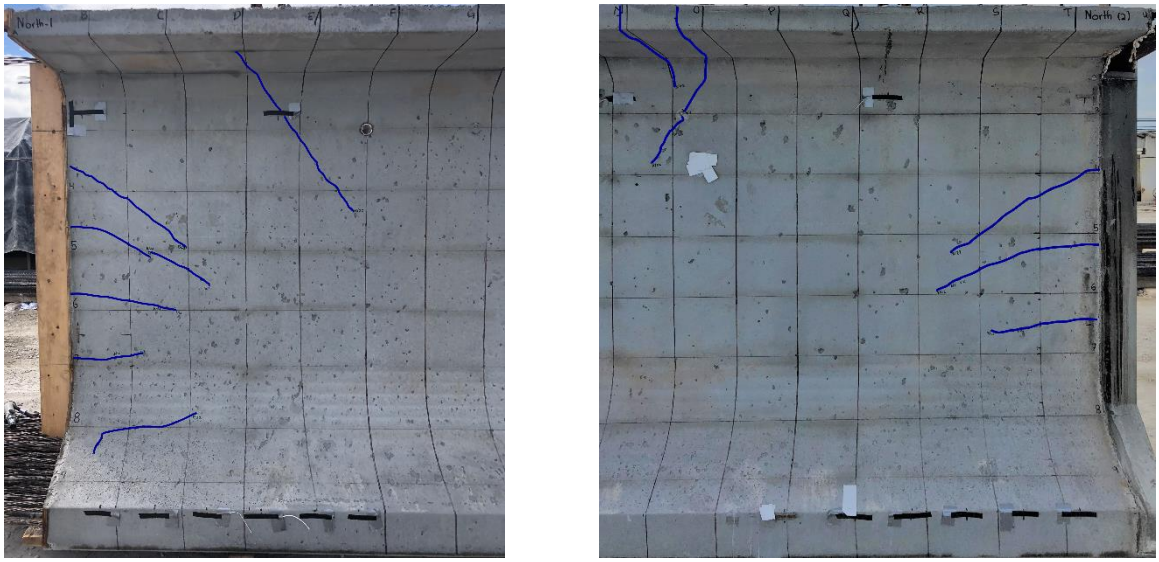

(a) (b)

Figure 4-55 SH-30 end region cracking after specimen lifted off prestressing bed in end with: (a) conventional and (b) modified end region detailing

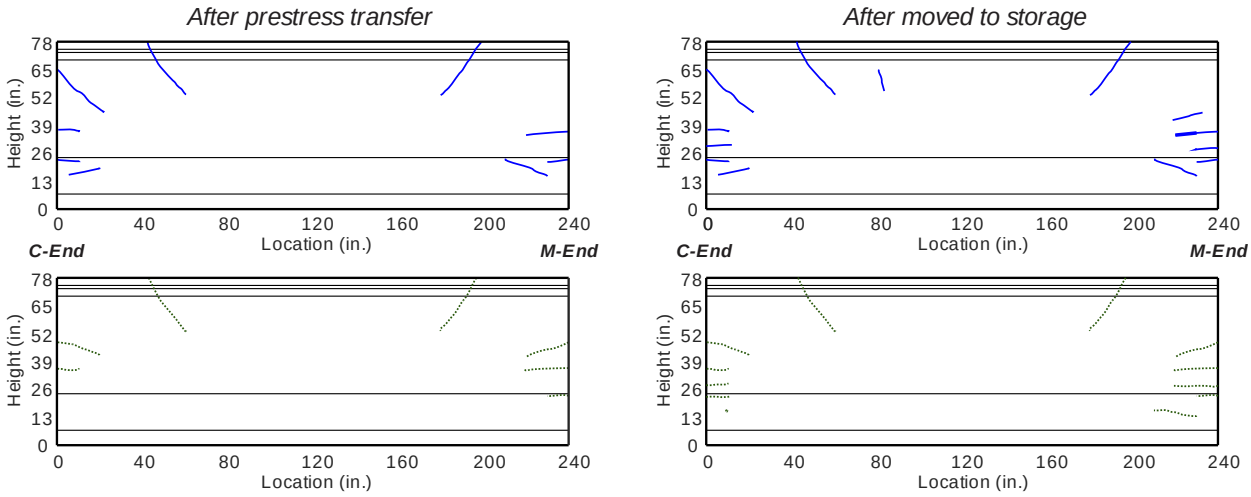

Figure 4-56 CT before and after transporting to storage crack patterns shown on North face of specimen. Solid blue lines depict cracks visible on the North face and dashed green lines depict cracks visible on the South face.

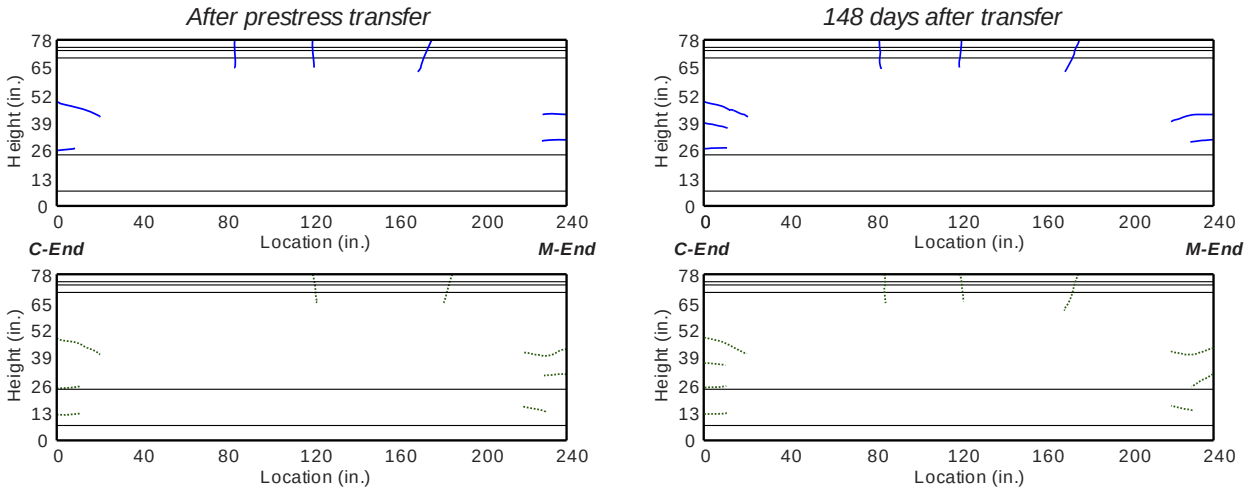

Figure 4-57 SH-30 Crack patterns shown on North face of specimen. Solid blue lines depict cracks visible on the North face and dashed green lines depict cracks visible on the South face.

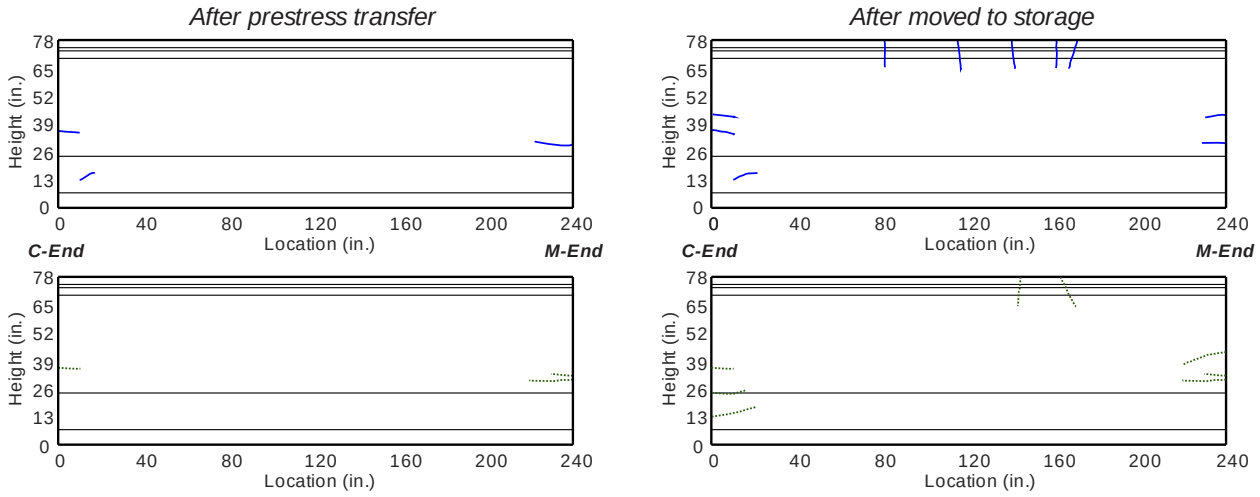

Figure 4-58 SH-70 before and after transporting to storage crack patterns shown on North face of specimen. Solid blue lines depict cracks visible on the North face and dashed green lines depict cracks visible on the South face.

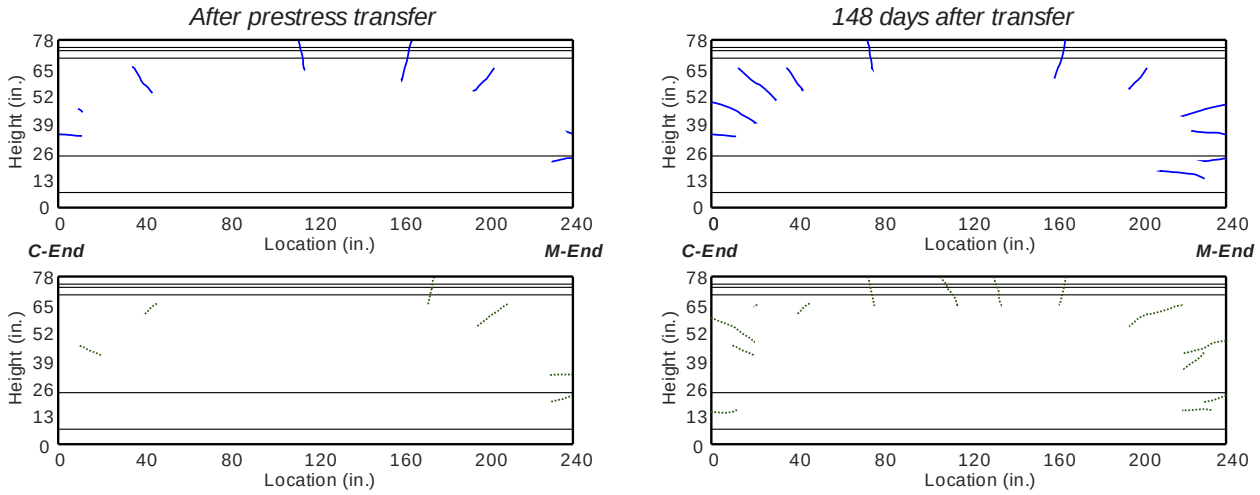

Figure 4-59 CR-70 before and after transporting to storage crack patterns shown on North face of specimen. Solid blue lines depict cracks visible on the North face and dashed green lines depict cracks visible on the South face.

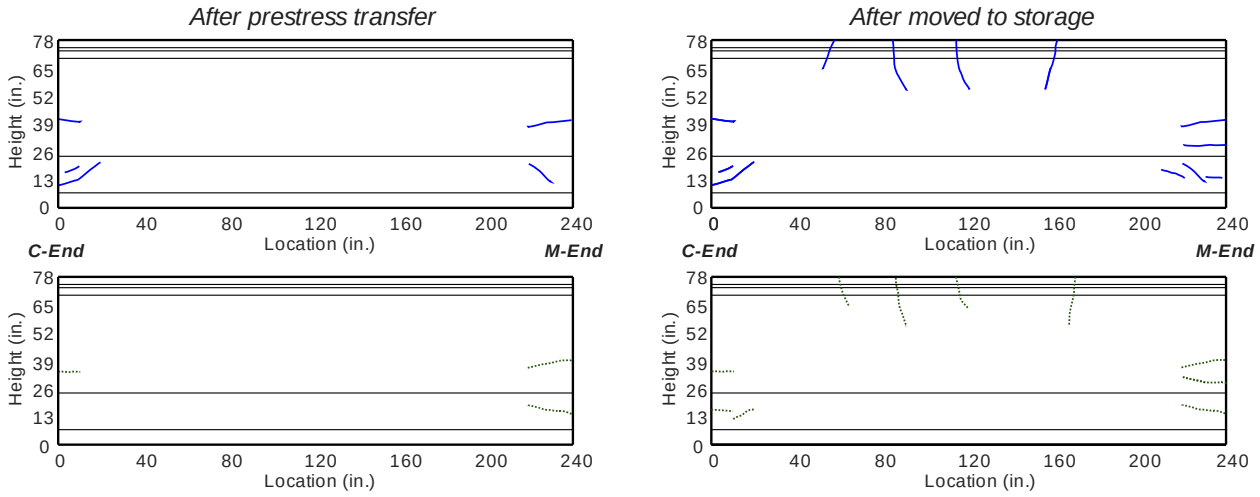

Figure 4-60 PP-50 before and after transporting to storage crack patterns shown on North face of specimen. Solid blue lines depict cracks visible on the North face and dashed green lines depict cracks visible on the South face.

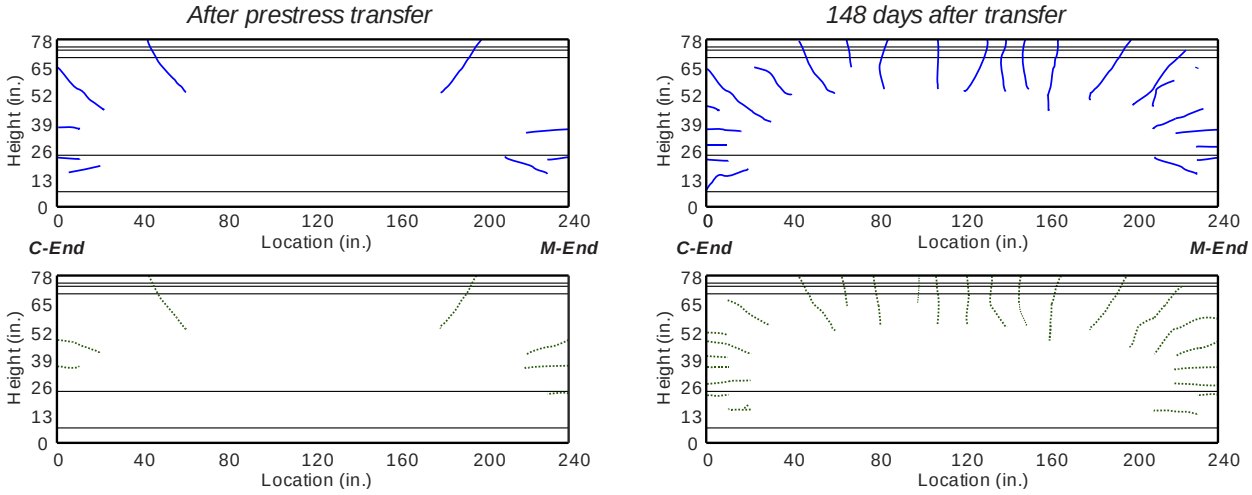

Figure 4-61 CT Crack patterns shown on North face of specimen. Solid blue lines depict cracks visible on the North face and dashed green lines depict cracks visible on the South face.

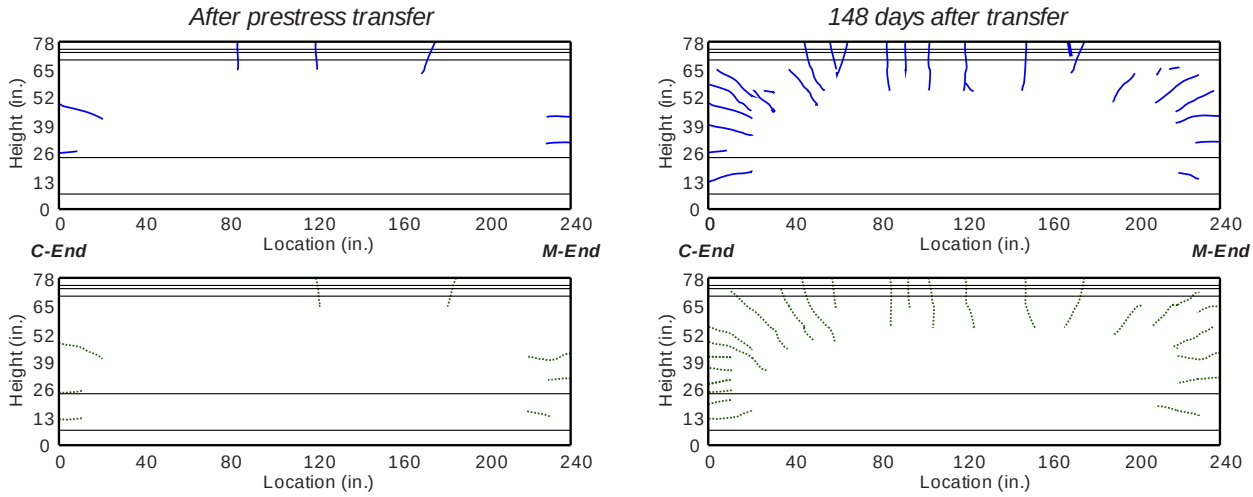

Figure 4-62 SH-30 Crack patterns shown on North face of specimen. Solid blue lines depict cracks visible on the North face and dashed green lines depict cracks visible on the South face.

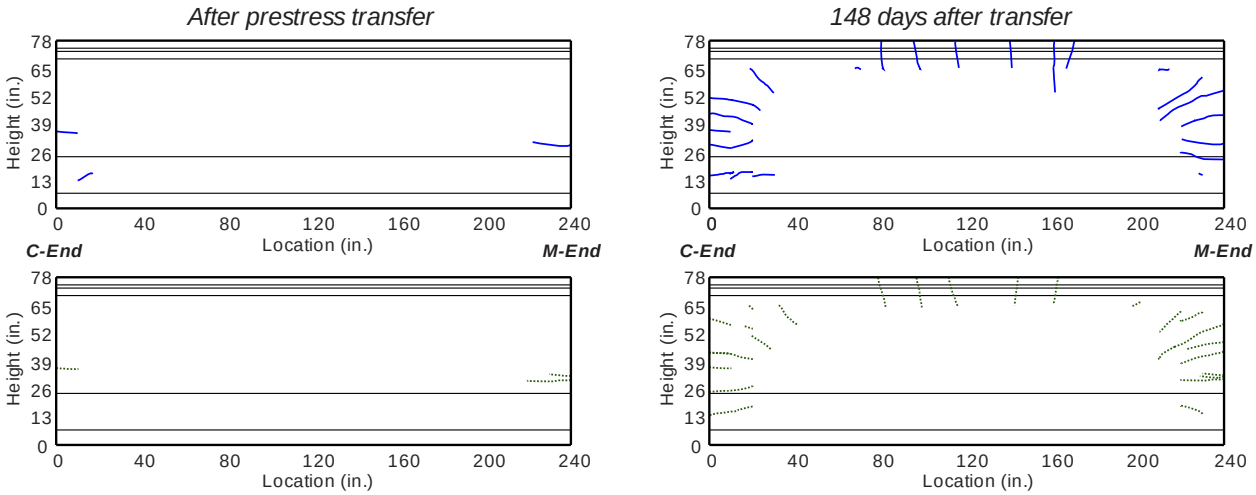

Figure 4-63 SH-70 Crack patterns shown on North face of specimen. Solid blue lines depict cracks visible on the North face and dashed green lines depict cracks visible on the South face.

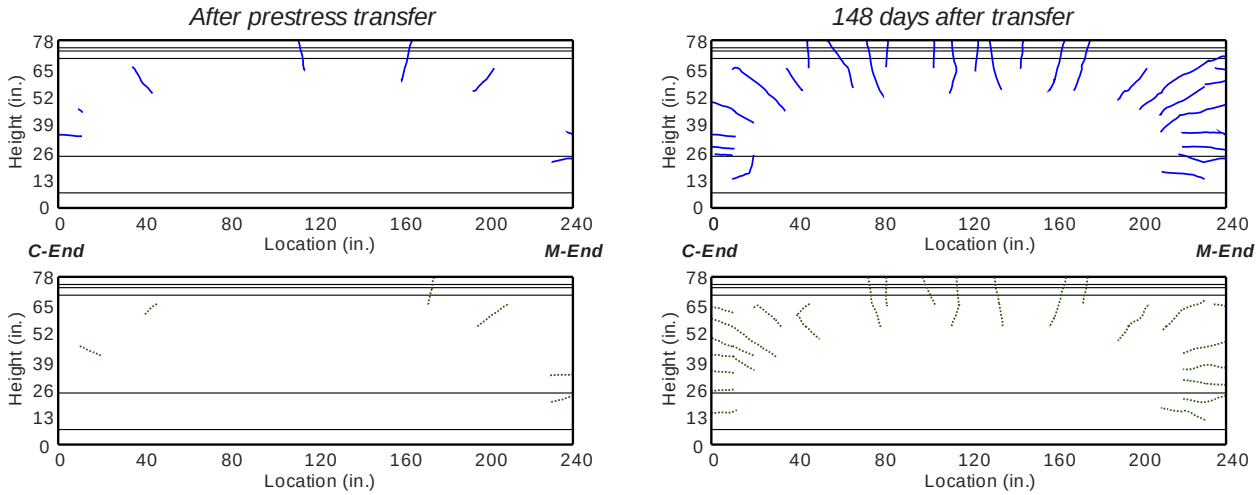

Figure 4-64 CR-70 Crack patterns shown on North face of specimen. Solid blue lines depict cracks visible on the North face and dashed green lines depict cracks visible on the South face.

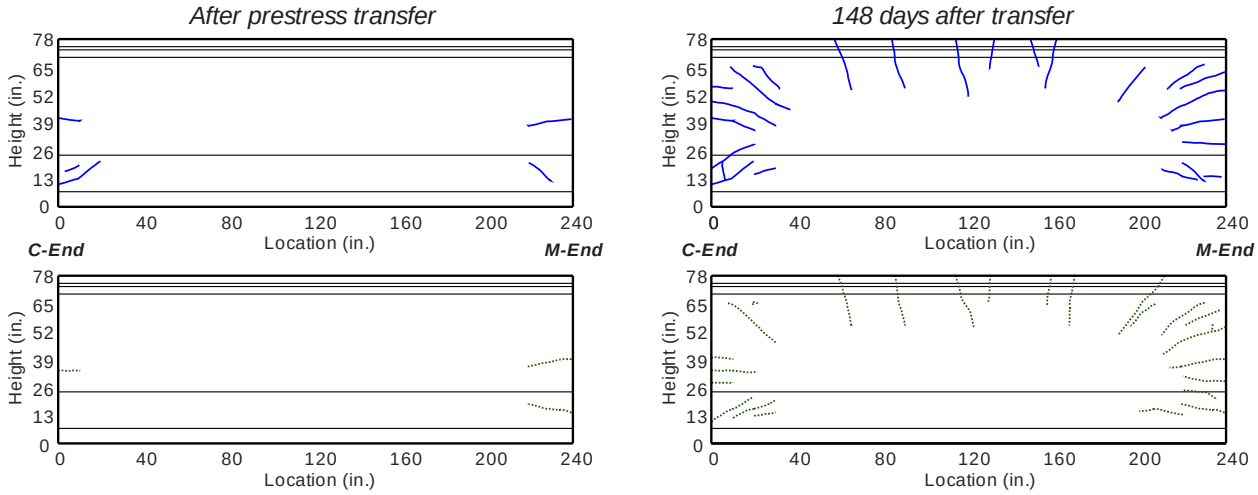

Figure 4-65 PP-50 Crack patterns shown on North face of specimen. Solid blue lines depict cracks visible on the North face and dashed green lines depict cracks visible on the South face.

To evaluate the effectiveness of FRC at controlling end region cracking, four metrics were used: total crack length, total crack area, effective crack width, and maximum crack width. *Total crack length* (L) is the summation of the lengths of all the individual cracks within an end. *Total crack area* (A) is the summation of the crack length multiplied by the respective width. *Effective crack width* (w_e) is the total area divided by the total length. Lastly, in practice, when evaluating whether repair of end region cracking is needed, the maximum crack width is the threshold used. For this reason, the maximum crack width within the end region will be the last metric to evaluate the effectiveness of FRC at controlling cracking. *Maximum crack width* (w_{max}) is the maximum crack width measurement taken, for this case, within the web of each girder end. Figure 4-66 shows an example of the metrics used to quantify effectiveness of FRC at controlling end region cracking. For a period of 148 days measurements were taken at regular intervals. Four metrics were calculated for each measurement to quantify the effectiveness of

FRC controlling end region cracking. The total crack length, total crack area, effective and maximum crack width were evaluated independently for the north and south of each girder.

Inspection of end region cracking for all specimens was conducted at the same age. Because specimens were constructed at different dates, however, measurements for each specimen were taken at different points in time. For this reason, at a given age, specimens could have been exposed to different temperature changes, leading to variable thermal effects that may have affected the results.

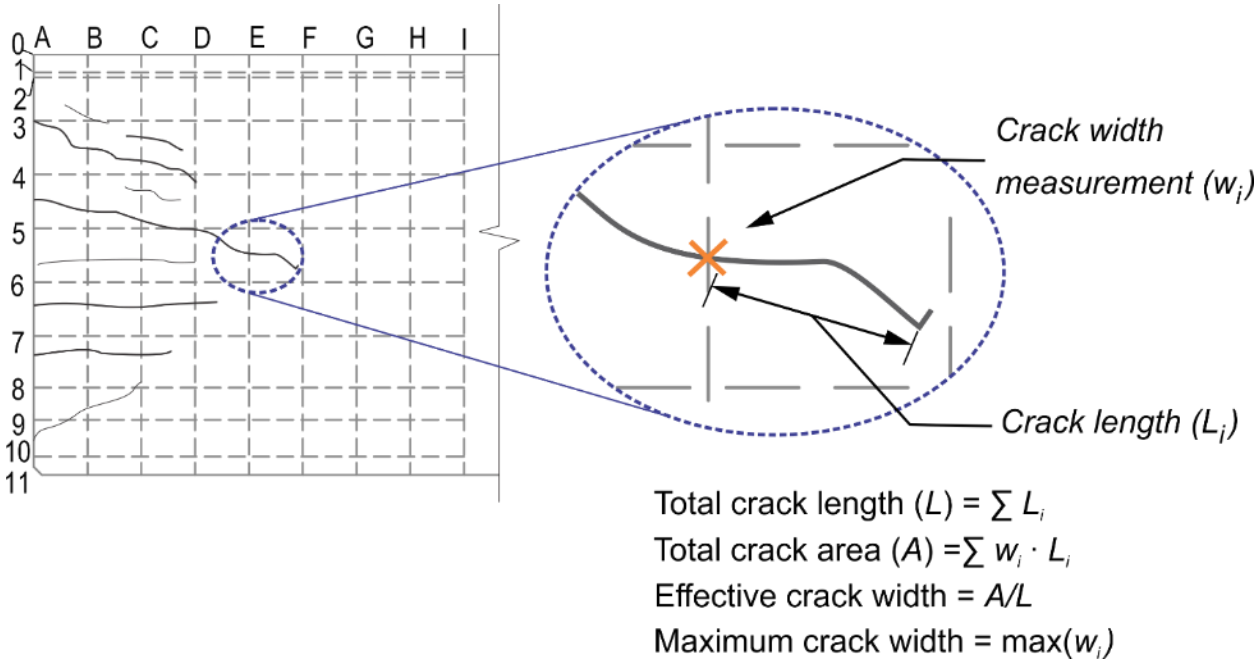

Figure 4-66 Method of computing *total crack length*, *total crack area*, *effective crack width*, and *maximum crack width*

Lifting loops were placed 3 ft from each girder end to allow for specimen transportation. It is likely that the lifting loops provided some resistance to end region cracking. The effect, however, would be similar in all specimens since the configuration of the lifting loops was consistent. In addition, maximum tensile strain during prestress transfer occurs within the first 15 in. from the girder end and the lifting loops are located well beyond this region. The presence of the lifting loops is not expected to affect the evaluation of FRC effectiveness to control end region cracks since the lifting loops were located away from the zone where maximum tensile strain occurred and their configuration was consistent in all specimens.

In bridge construction, it is expected that end region cracking does not continue to grow after the girder is installed on a bridge. Cracks will tend to close when dead loads are applied. As mentioned previously, the test specimens were stored in the precast yard for the duration of the crack monitoring period. Within this time no additional loads were applied to the specimens, this provided the worst-case scenario for end region crack growth, as no reactions from self-weight or deck are present to provide clamping force in the ends, which would control, to some extent, continued crack growth with time.

4.9.3 Effective crack width

Effective crack width (w_e) is defined as the total area divided by the total crack length. (Figure 4-66). In general, effective crack width increased with time, and FRC reduced effective crack widths when compared to the control specimen. Effective crack widths during the first week after prestress transfer varied significantly. Variability in crack widths could be attributed to the small magnitude of the cracks relative to the precision of the crack microscope, in addition to temperature effects. In this section, comparison of each fiber's effectiveness at controlling the effective crack width of each girder is discussed. Appendix section F.4 shows effective crack width for the 148 days of crack monitoring period.

Figure 4-67 and Figure 4-68 show a comparison of the effective crack width at 148 days after prestress transfer. The ratio of the effective crack widths of FRC specimens (w_{e_FRC}) to the effective crack width in CT (w_{e_CT}) was used to allow for direct comparison over time of the effective crack widths of each FRC specimen, relative to CT. Figure 4-69 and Figure 4-70 show this ratio for each specimen. A ratio less than one indicates that the FRC specimen had effective crack widths smaller than CT, and a ratio larger than one indicates that the FRC specimen had effective crack widths larger than CT. Some variability is apparent prior to 40 days. All FRC specimens, however, showed a reduced effective crack width compared to that of CT.

The effectiveness of each fiber mixture were be evaluated by comparing the effective crack width of each FRC specimen to that of CT. Among all specimens, CT had larger effective crack widths than any of the FRC specimens, with SH-70 exhibiting the smallest. Compared to CT, SH-30 (C-end) and CR-70 (M-end) reduced effective crack width by 40% and 20%, respectively. Considering effective crack width computed for the north face after 148 days from prestress transfer, SH-30 provided the most reduction in effective crack width for conventional end region detailing (C-end); whereas, CR-70 provided the most reduction for modified end region detailing (M-end). Considering effective crack width computed for the south face after 148 days from prestress transfer, SH-70 was the most effective at reducing effective crack width. SH-70 reduced effective crack width by 40% and 50%, respectively, when conventional and modified end region detailing were used. Difference in effective crack width between the north and south faces of each girder can be attributed to the orientation during storage (Section 4.3). The south face of girders CT and SH-30 were under direct sun exposure during storage. The girder orientation during storage could have led to additional cracking in the south face of CT and SH-30 specimens due to thermal effects. The north faces of specimen CT and SH-30 had limited sun exposure because of cover provided by nearby girders. Girders SH-70, CR-70, and PP-50 were stored between other girders. This limited the effect of differential temperatures on the faces of each girder.

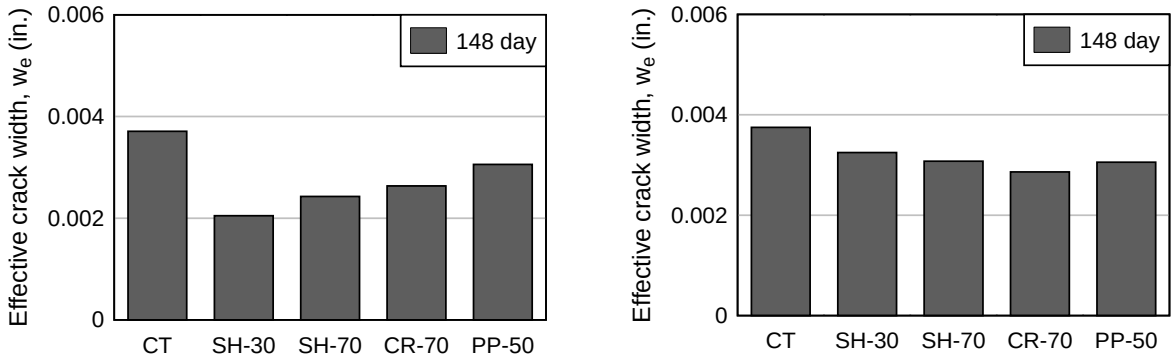

(a) (b)

Figure 4-67 Effective crack width 148 days from prestress transfer: (a) conventional and (b) modified end region detailing (North face)

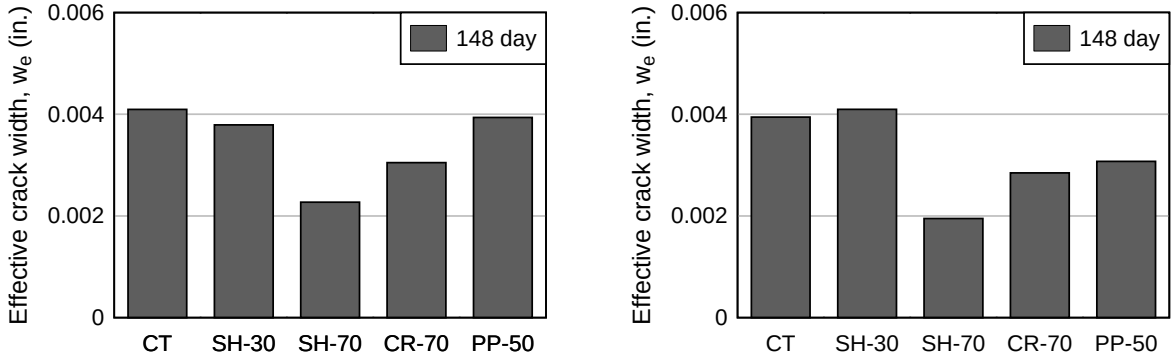

(a) (b)

Figure 4-68 Effective crack width 148 days from prestress transfer: (a) conventional and (b) modified end region detailing (South face)

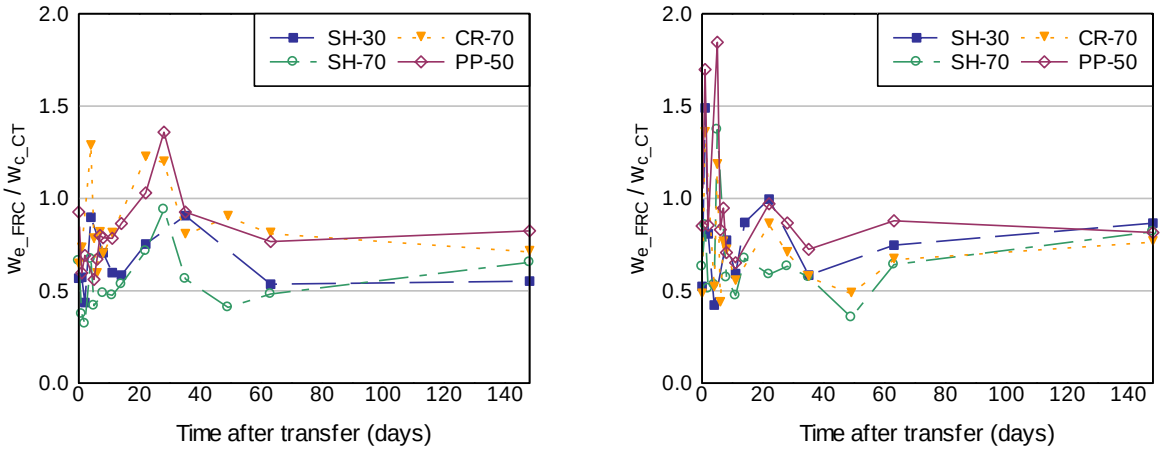

Figure 4-69 Normalized effective crack width through time: (a) conventional and (b) modified end region detailing (North face)

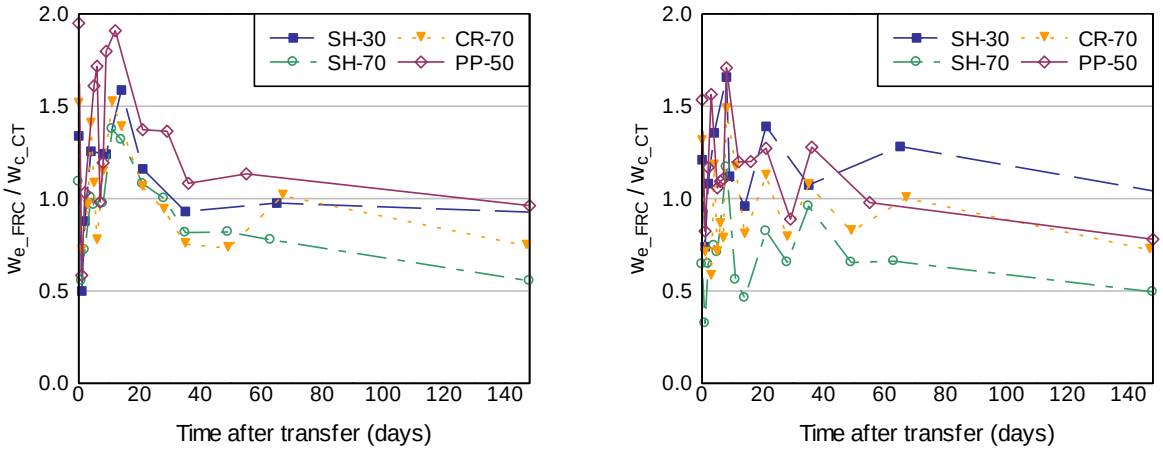

Figure 4-70 Normalized effective crack width through time: (a) conventional and (b) modified end region detailing (South face)

4.9.4 Maximum crack width

Maximum crack width (w_{max}) is defined as the maximum crack width measurement taken within the web of each girder end (Figure 4-66). In general, maximum crack widths increased with time. For conventional end region detailing, all FRC mixtures reduced maximum crack widths compared to CT. For modified end region detailing, however, crack widths were larger in FRC specimens. In this section, maximum crack widths within the web of each girder are compared after 148 days from prestress transfer. Appendix section F.5 shows maximum crack width for the 148 days of crack monitoring period.

Figure 4-71 and Figure 4-72 show comparison of maximum crack width within the web at 148 days after prestress transfer. The ratio of the maximum crack widths of each FRSCC specimen (w_{max_FRC}) to the maximum crack width of CT (w_{max_CT}) was computed. Figure 4-73

and Figure 4-74 show the ratio for each respective specimen. A ratio less than one indicates that the FRC specimen had maximum crack widths smaller than CT, and a ratio larger than one indicates that the FRC specimen had maximum crack width larger than CT. In the conventional end, all FRC mixtures reduced maximum crack widths compared to CT. However, when end region reinforcement was modified, FRC was less effective at controlling maximum crack widths, with little to no reduction in maximum crack width.

The effectiveness of each fiber mixture was evaluated by comparing the maximum crack width of each FRSCC specimen to that of CT. As previously discussed, significant difference in crack widths was observed between the north and south face of each girder. This difference can be attributed to the storage orientation during the crack monitoring period, which could cause differential temperature between the north and south face of each girder (Section 4.3). In general, maximum crack widths were reduced by FRC, however the fibers were less effective at controlling maximum crack widths when end region reinforcement was reduced. Hooked end steel fibers were the most effective at controlling maximum crack widths both when conventional and modified end region detailing were used. Compared to CT, SH-70 had reduced maximum crack width up to 70% of those in CT. Comparing the steel fibers at the same volume of 0.7%, SH-70 fiber provided significantly better control in end region crack widths than CR-70. The better crack control provided by SH-70 can be attributed to the enhanced mechanical bond provided by the hooked end shape of SH fibers. Among all FRSCC specimens, SH-30 and PP-50 were the least effective at controlling maximum crack width. SH-30 had maximum crack widths of up to 90% and 130% of those in specimen CT, for conventional and modified end, respectively. The negligible effectiveness of SH-30 to control maximum crack widths can be attributed to the low volume of fibers used. PP-50 had maximum crack widths of up to 65% and 120% of those in specimen CT, for conventional and modified end respectively. This can be due to the low volume of fibers used compared to the other specimens, in addition to the low stiffness of macrosynthetic fibers compared to steel fibers. To be able to reduce the quantity of end region reinforcement, a higher volume of macrosynthetic fiber would be required. However, the use of higher fiber volume could lead to issues with mixing and mixture fresh properties. CR-70 was the least effective at controlling maximum crack width when conventional end region detailing was used, with maximum crack widths as much as 100% of those in CT.

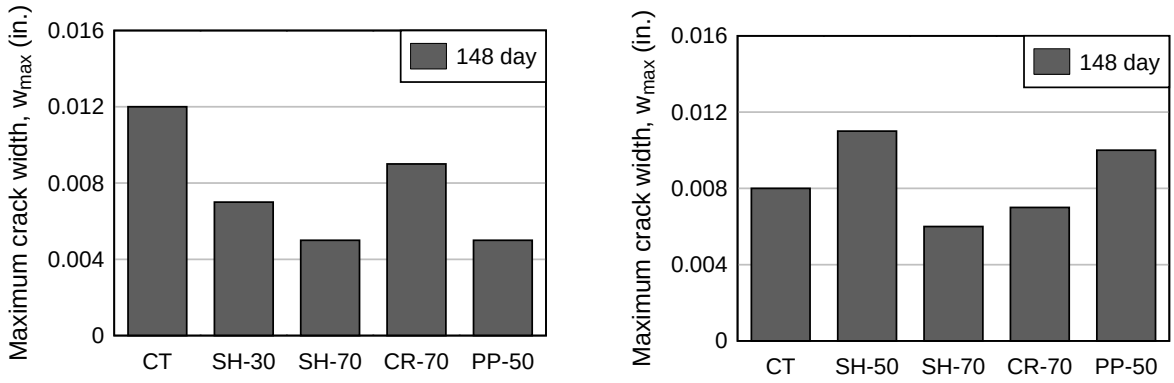

(a) (b)

Figure 4-71 Maximum crack width 148 days from prestress transfer: (a) conventional and (b) modified end region detailing (North face)

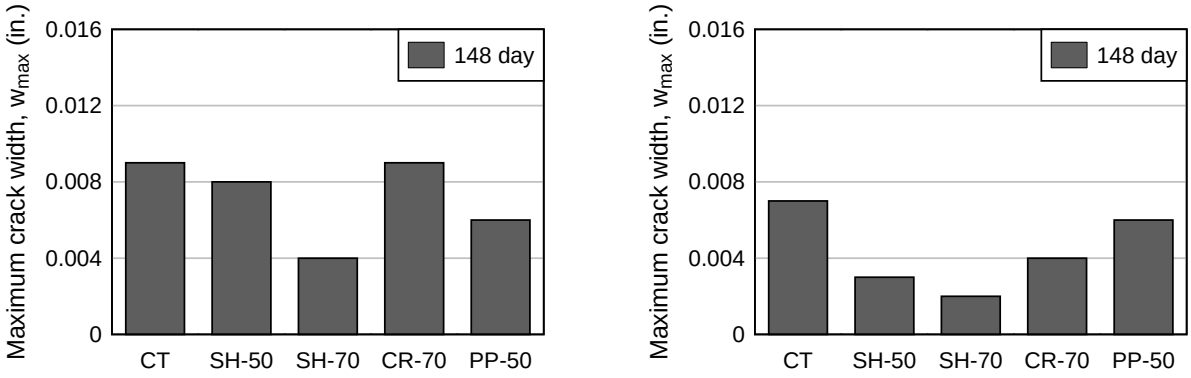

(a) (b)

Figure 4-72 Maximum crack width 148 days from prestress transfer: (a) conventional and (b) modified end region detailing (South face)

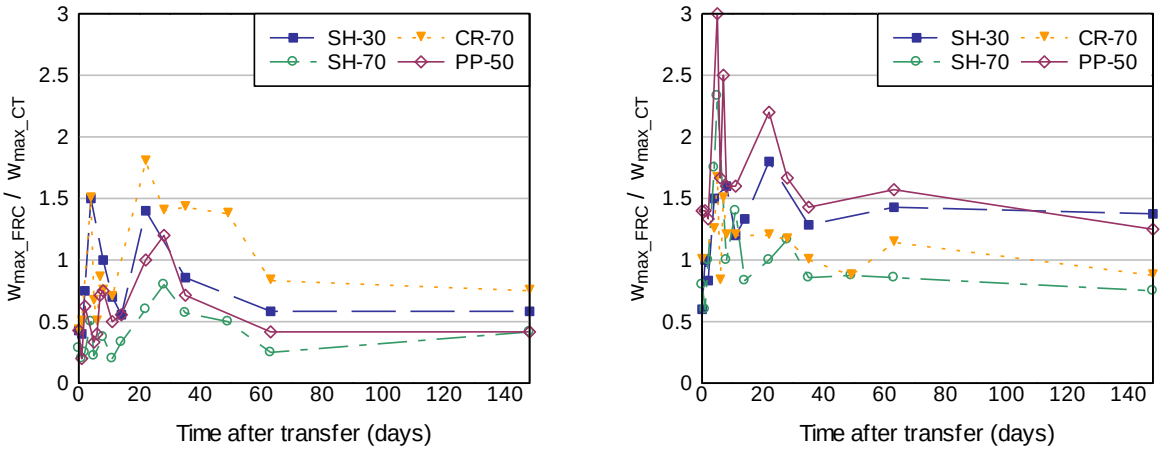

Figure 4-73 Normalized maximum web crack width: (a) conventional and (b) modified end region detailing (North face)

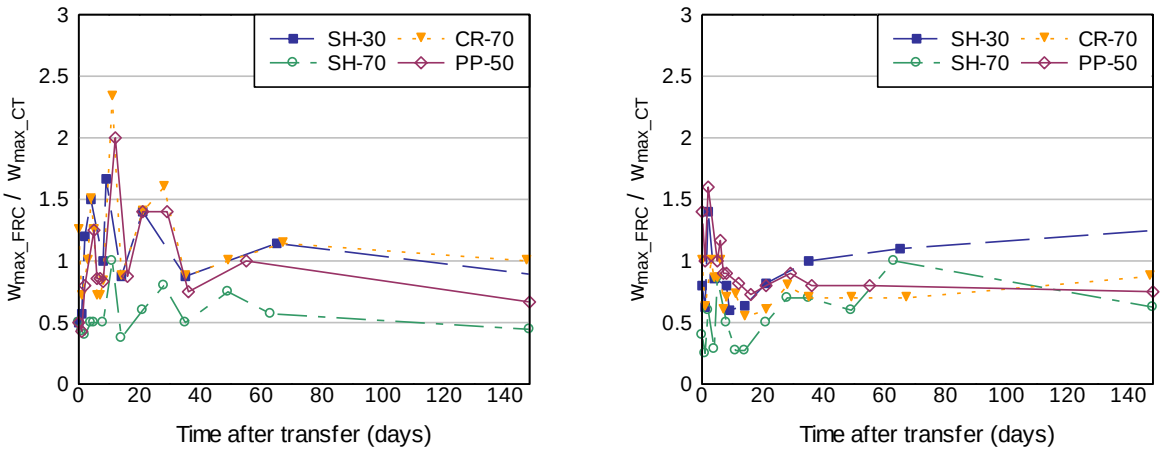

Figure 4-74 Normalized maximum web crack width: (a) conventional and (b) modified end region detailing (South face)

4.9.5 Crack length

Total crack length is the summation of the lengths of the individual cracks within a given specimen end (Figure 4-66). In general, crack length increased over time. In this section, total crack length in each specimen is compared up to 14 days and then at the end of the monitoring period. Appendix section F.6 shows total crack length for the 148 days of crack monitoring period.

Total crack length at 148 days after prestress transfer is shown in Figure 4-75 and Figure 4-76. Figure 4-77 and Figure 4-78 show the ratio of total crack length within an end for each FRC specimens (L_{FRC}) to the total crack length for CT (L_{CT}). A ratio less than one indicates that the FRC specimen had a total crack length shorter than CT, and a ratio larger than one indicates

that FRC had total crack length longer than CT. Comparing total crack length on the north face of the girders, among all specimens, CR-70 had the longer total crack length. For conventional end region detailing, SH-70 had the shorter crack length, while SH-30 had the shorter crack length for modified detailing. Comparing the south face of the girders, SH-30 had the longer total crack length and SH-70 had the shorter total crack length. For modified detailing, SH-70 had the longer total crack length, while SH-30 had the shorter total crack length.

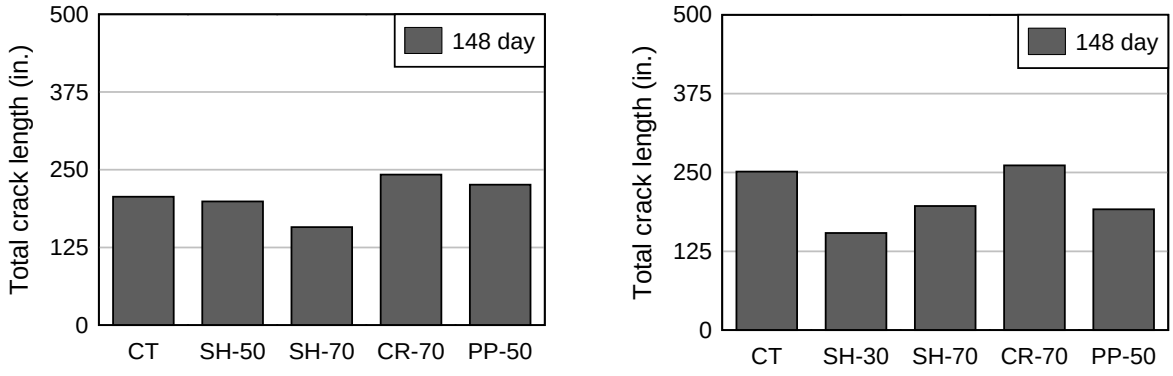

Figure 4-75 Total crack length 148 days from prestress transfer: (a) conventional and (b) modified end region detailing (North face)

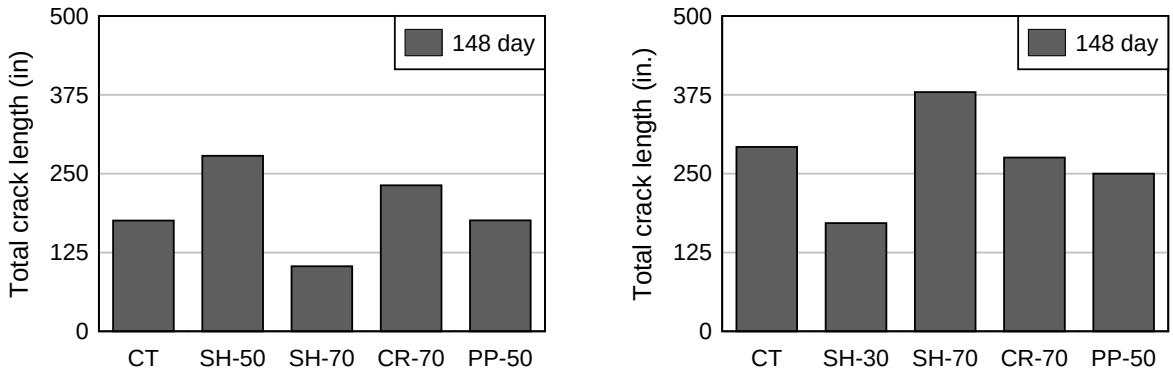

Figure 4-76 Total crack length 148 days from prestress transfer: (a) conventional and (b) modified end region detailing (South face)

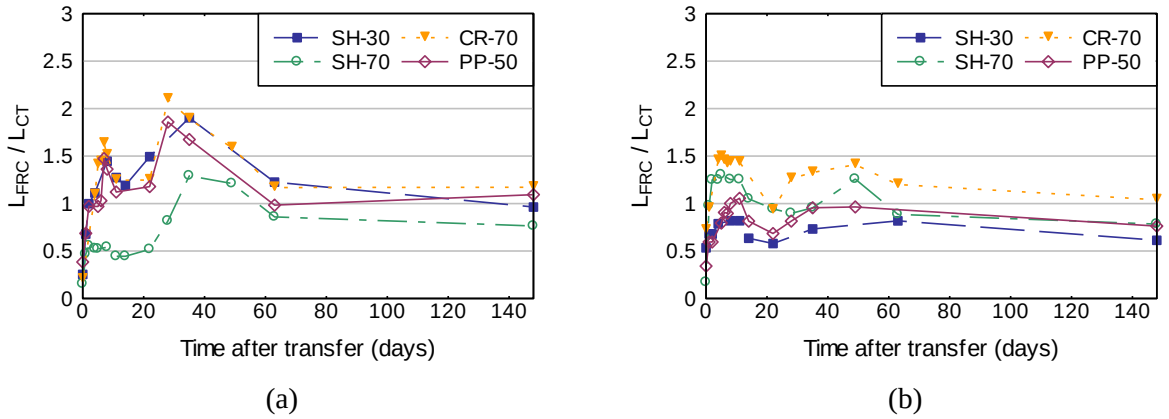

Figure 4-77 Normalized crack length: (a) conventional and (b) modified end region detailing (North face)

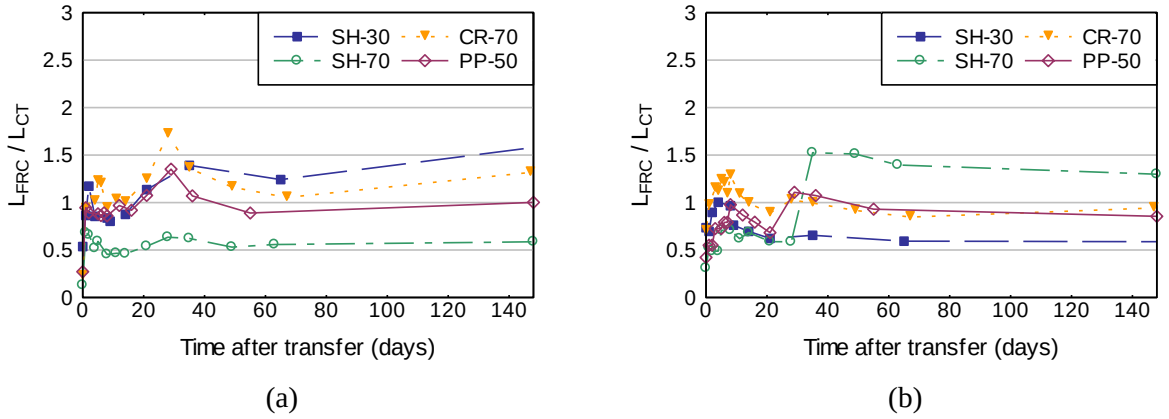

Figure 4-78 Normalized crack length: (a) conventional and (b) modified end region detailing (South face)

4.9.6 Crack area

Crack length and width were used to compute the total crack area in each girder end. *Total area* is the summation of the crack length multiplied by the respective width (Figure 4-66). This section covers the discussion of total crack area for each test girder. Appendix section F.7 shows total crack area for the 148 days of crack monitoring period.

Figure 4-79 and Figure 4-80 show the total crack area recorded 148 days from prestress transfer. Comparing total crack area along the north face, CT had the largest crack area. When conventional end region detailing was present (C-end), specimen SH-70 had the smallest total crack area. However, when end region reinforcement was reduced (M-end), SH-30 had the smallest crack area. Comparing total crack area along the south face, when conventional end region detailing was present (C-end), specimen SH-30 had the largest area and SH-70 had the smallest total crack area. However, when end region reinforcement was reduced (M-end), among all specimens, CT had the largest crack area and SH-30 had the smallest.

Figure 4-81 and Figure 4-82 show the ratio of total crack area for each FRC specimens (A_{FRC}) to the total crack area for specimen CT (A_{CT}). A ratio less than one indicates that the FRC specimen had total crack area smaller than CT, and a ratio larger than one indicates that

FRC had total crack area larger than CT. After 148 days from prestress transfer, all FRC showed reduction in total crack area. For the conventional end (C-end), specimen SH-70 had the smallest total crack area. Compared to CT, SH-70 had up to 50% reduction in total crack area. For the modified end (M-end), SH-30 had the smaller total crack area, with 40% reduction compared to CT.

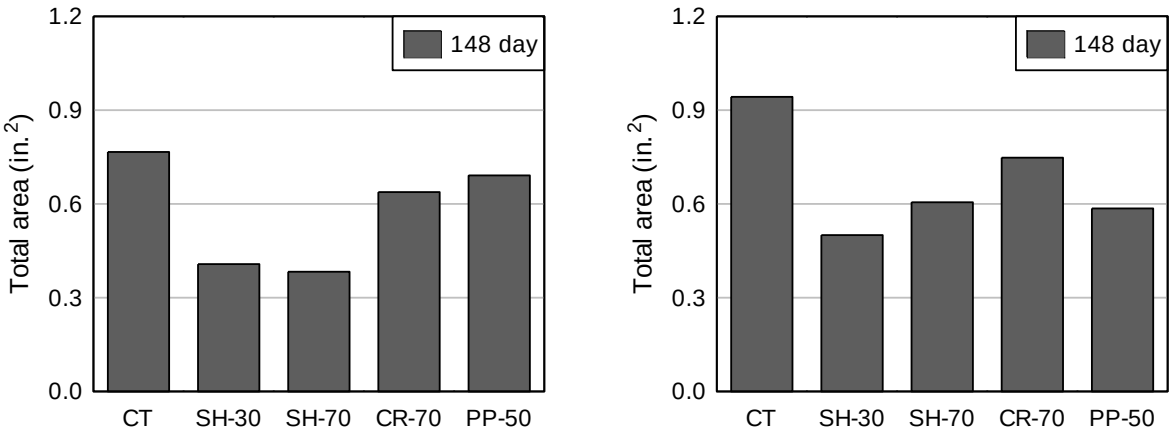

Figure 4-79 Toal crack area 148 days from prestress transfer: (a) conventional and (b) modified end region detailing (North face)

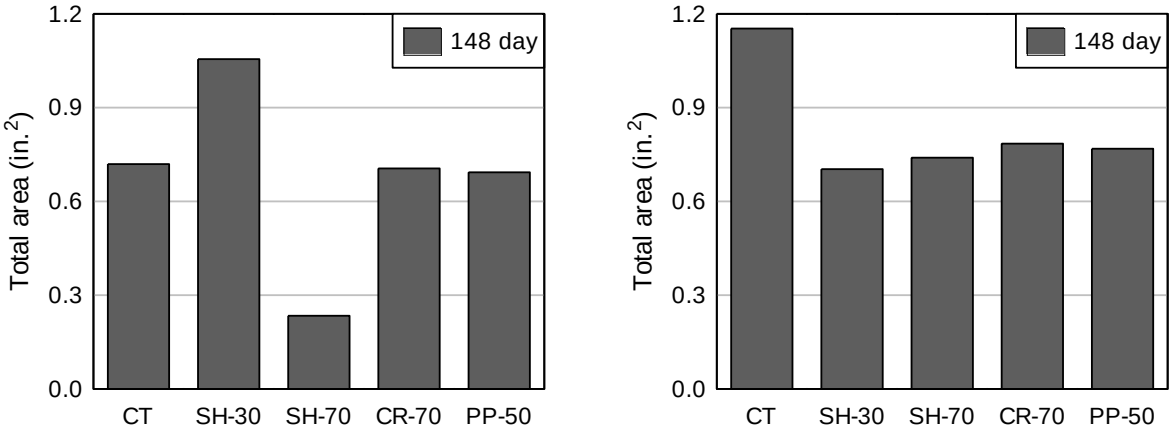

Figure 4-80 Total crack area 148 days from prestress transfer: (a) conventional and (b) modified end region detailing (South face)

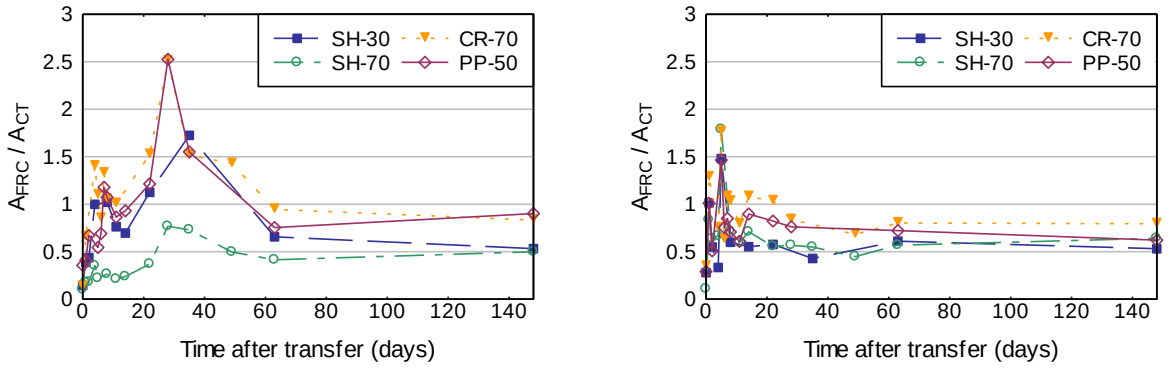

Figure 4-81 Normalized crack area: (a) conventional and (b) modified end region detailing (North face)

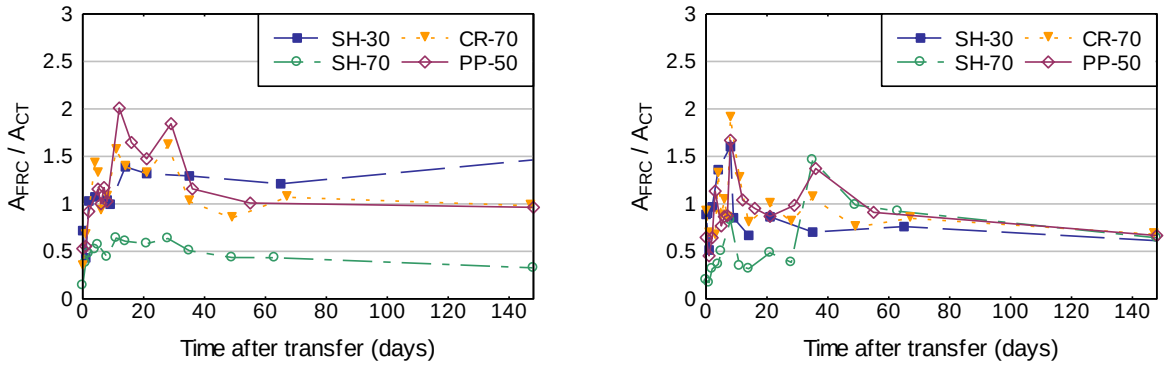

Figure 4-82 Normalized crack area: (a) conventional and (b) modified end region detailing (South face)

4.10 Crack width distribution

Figure 4-83 and Figure 4-84 show the distribution of the crack width measurements taken 148 days after prestress transfer for all specimens. To compute the crack width distribution, both the north and south faces were taken into account. FDOT requires that crack widths wider than 0.006 in. be repaired when exposed to moderate to extreme environmental conditions, and cracks wider than 0.012 in. require engineer evaluation to determine action to be taken. The crack widths of 0.006 in. and 0.012 in. were used as threshold for evaluating the effectiveness of each FRC mixture at controlling crack widths. The efficiency at controlling end region cracks of each fiber varied, but the number of cracks larger than 0.006 in. was reduced when FRC was used. In general, stiffer fibers with higher volume were more effective at controlling the number of crack widths wider than 0.006in.

Figure 4-83 shows crack distribution 148 days after prestress transfer when conventional end region detailing was used. In red, FDOT limit of 0.006 in. has been highlighted. For the control specimen (CT), 13% of measured crack widths were wider than 0.006 in. and 2% wider than 0.012 in. FRC specimens had no cracks wider than 0.012 in. Among all fibers, hooked end steel fibers at volume fraction of 0.7% (SH-70) were the most effective at maintaining crack

widths smaller than 0.006 in. SH-70 had less than 2% larger than 0.006 in. The better crack control provided by SH-70 can be attributed to the enhanced mechanical bond provided by the hooked end shape of SH fibers. PP-50 and SH-30 showed similar effectiveness at controlling end region crack widths. PP-50 was somewhat more effective at controlling end region crack widths than SH-30, with 7% and 9% of crack widths larger than 0.006 in. respectively. However, specimen PP-50 had 40% higher fiber volume and almost twice the length of SH-30. Steel crimped fibers at a volume fraction of 0.7% (CR-70) appeared to be the least effective fiber mixture at controlling crack widths, with 11% of cracks wider than 0.006 in, only 2% less than the control specimen.

Figure 4-84 shows crack distribution 148 days after prestress transfer when modified end region detailing was used. In red, FDOT limit of 0.006 in. has been highlighted. The control specimen (CT) had 19% of measured crack widths larger than 0.006 in. and no cracks wider than 0.012 in. FRC specimens had no cracks wider than 0.012 in. Among all fibers, steel hooked end and steel crimped fibers at a volume of 0.7% were the most effective at controlling end region crack widths. The number of cracks wider than 0.006 in. was reduced to 7% and 6% in specimen's SH-70 and CR-70 respectively. PP-50 had 9% of crack widths larger than 0.006in, whereas SH-30 had 19% of crack widths larger than 0.006 in. Hooked end steel fibers at a volume fraction of 0.3% appeared to be the least effective at controlling end region crack widths when the end region reinforcement was reduced (M-end). Specimen SH-30 showed similar crack width distribution as the control specimen, with 19% of crack widths larger than 0.006 in. The negligible effectiveness of SH-30 to control maximum crack widths can be attributed to the low volume of fibers used. A fiber volume of 0.30% was not sufficient for replacement of FDOT end region reinforcement.

Figure 4-85 shows the distribution of maximum web crack widths along with mean and standard deviation. The maximum web crack width measurement for each date of the crack monitoring period was used to determine the maximum crack width distribution. The maximum crack width measurement taken at both the north and south faces of the girders were considered while determining the crack width distribution. When conventional end region detailing was used, specimen CT had the highest maximum crack widths. Hooked end steel fibers at a volume of 0.7% (SH-70) was the most effective at reducing maximum crack widths. Maximum crack widths measured in specimen SH-70 were smaller than 0.006 in. threshold during the 148 day monitoring period. When modified end region detailing was used, CT and PP-50 specimen showed the larger maximum crack widths. The negligible effectiveness of PP-50 to control maximum crack widths can be attributed to the low volume of fibers used, in addition to the low stiffness of macrosynthetic fibers compared to steel fibers. A higher fiber volume of fiber PP would be required in order to replace end region cracking. However, a higher volume could cause issues during mixing or placement.

Figure 4-86 shows a comparison of crack width distribution observed when conventional concrete is used in conjunction with FDOT end region detailing (C-end) and the crack width distribution observed in FRC specimens when end region reinforcement is reduced (M-end). This allows the evaluation of current end region detailing and the effectiveness of FRC at controlling crack widths when end region reinforcement is reduced. Crack distribution from C-end of specimen CT showed that FDOT end region reinforcement is effective at maintaining the majority of end region crack widths smaller than 0.006 in. However, crack distribution from M-end in FRSCC specimens, showed that PP-50, SH-70 and CR-70 were more effective than FDOT end region reinforcement at maintaining crack widths smaller than 0.006 in. CT in

combination with FDOT detailing had 12% of measured crack widths larger than 0.006 in, and of those 2% were wider than 0.012 in. Whereas, when reinforcement was modified, PP-50 had 9% of measured crack widths larger than 0.006 in, and SH-70 and CR-70 had less than 7% of measured crack widths larger than 0.006 in. No cracks wider than 0.012 in. were measured in FRSCC specimens when reduced end region reinforcement was used. The use of fiber-reinforced concrete in prestressed bridge girders did not completely eliminate the occurrence of end region cracks, however, FRSCC was more effective at controlling end region crack widths than current end region detailing practices.

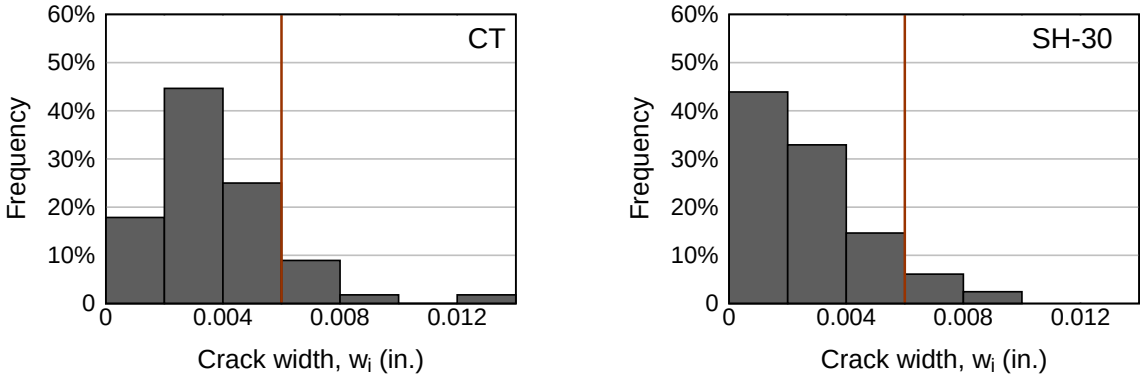

(a)

(b)

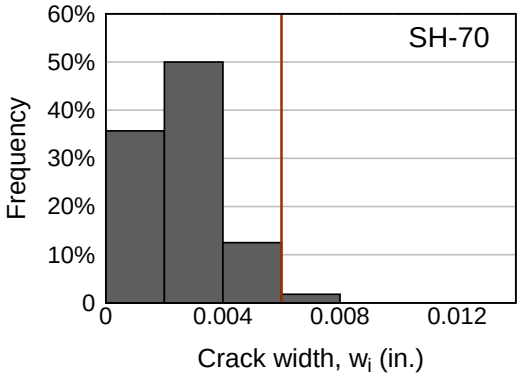

(c)

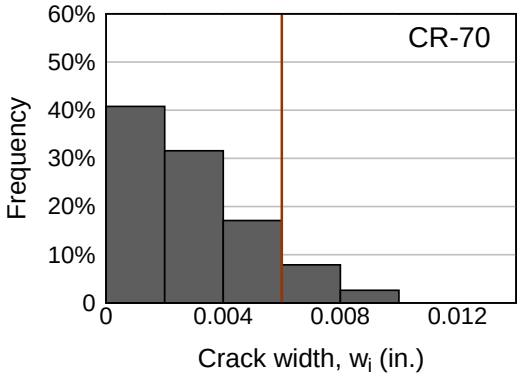

(d)

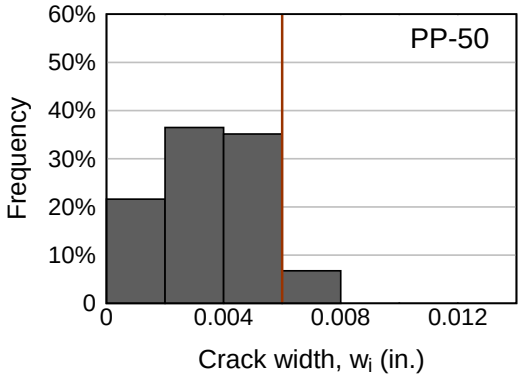

(e)

Figure 4-83 Crack width distribution for conventional end region detailing (C-end) after 148 days from prestress transfer: (a) CT, (b) SH-30, (c) SH-70, (d) CR-70, (e) PP-50

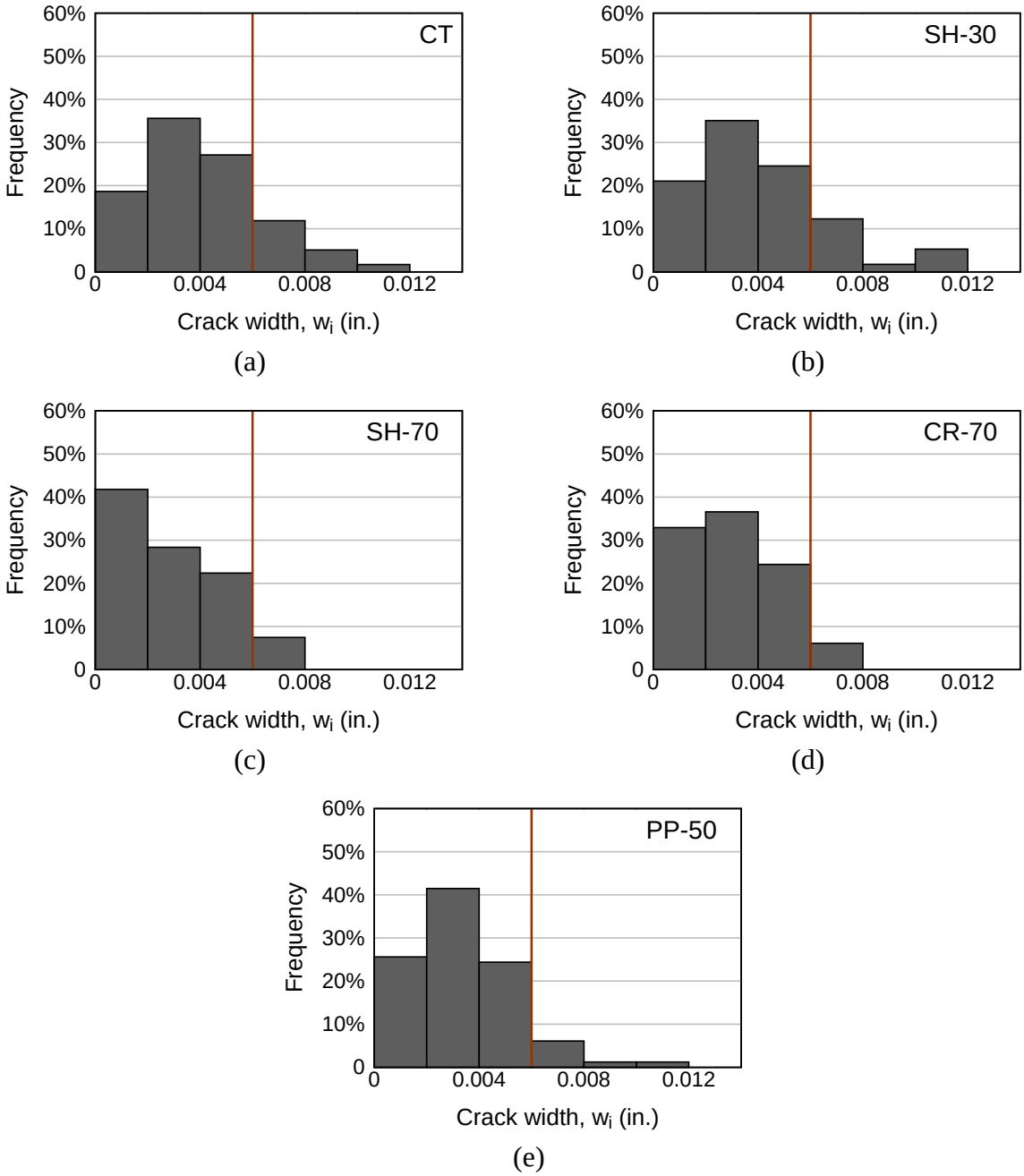

Figure 4-84 Crack width distribution for modified end region detailing (M-end) after 148 days from prestress transfer: (a) CT, (b) SH-30, (c) SH-70, (d) CR-70, (e) PP-50

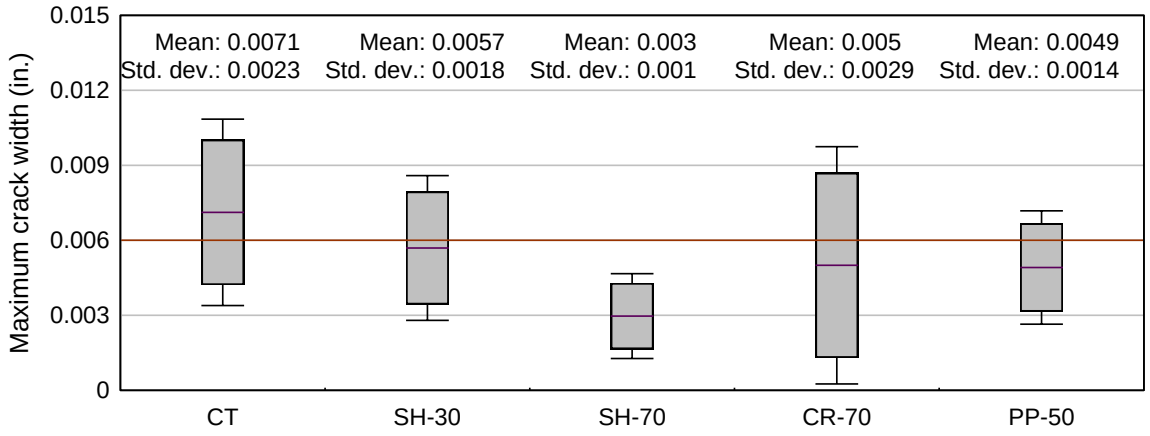

(a)

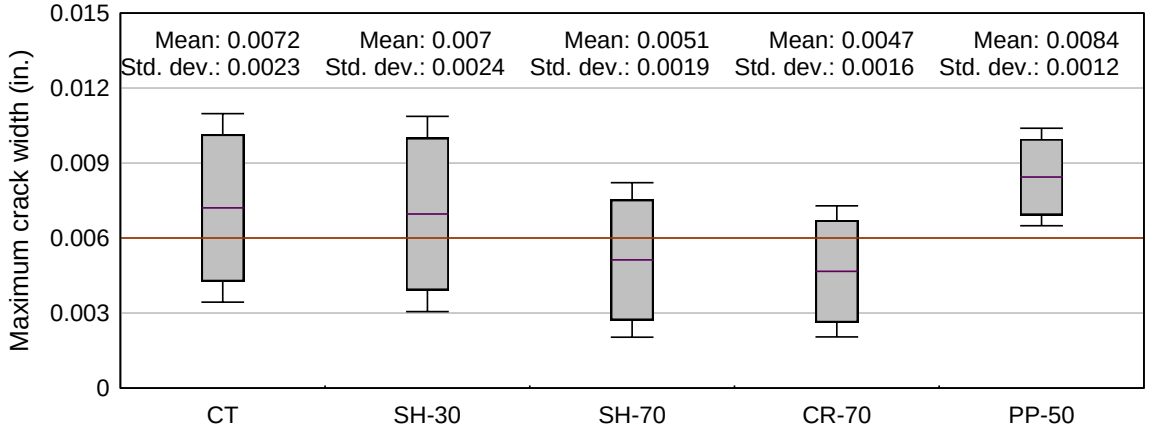

(b)

Figure 4-85 Maximum web crack width distribution: (a) conventional (C-end) and (b) modified end region detailing (M-end)

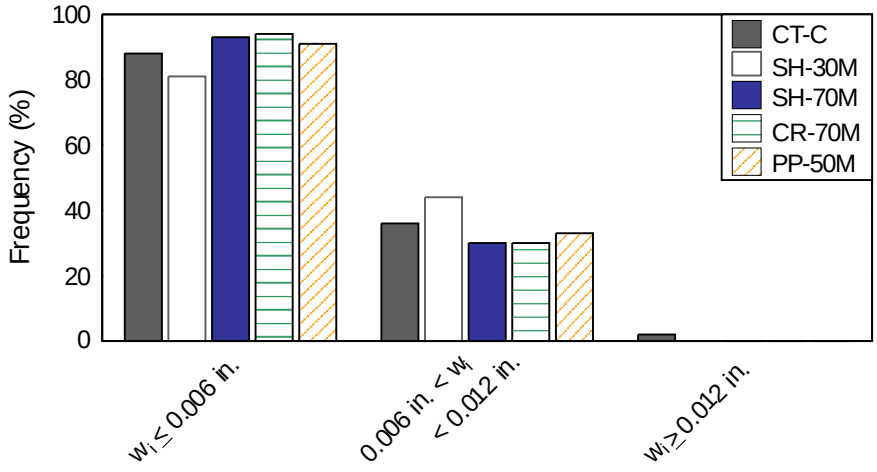

Figure 4-86 Comparison of crack width distribution for CT with conventional (C-end) and modified end region detailing (M-end)

4.11 Findings

Five FIB78 with length of 20 ft were fabricated and tested to evaluate the effectiveness of fiber-reinforced concrete at controlling end region cracking. Concrete and mild reinforcement strains were monitored during prestress transfer and cracking was monitored immediately after prestress transfer and for a period of 148 days.

Key findings based on testing performed during full-scale girder production to assess concrete fresh properties and the monitoring of strains during prestress transfer include:

- Fiber reinforcement reduced flowability and passing ability of SCC mixtures. However, during full-scale production of precast prestressed FIB girders, no issues with placement or consolidation were observed when using FRSCC mixtures with passing ability ranging between 2.5 in. and 3.25 in. Current provisions might be ineffective at assessing passing ability properties of FRSCC.
- Maximum tensile strain during prestress release occurred within first 15 in. from girder end, reinforcement detailing at the end of the girder is critical to effectively controlling end region cracks.
- Maximum tensile strain in mild steel reinforcement was reduced by up to 30% when using hooked end steel fibers at 0.3%.

Key findings when comparing FRC with conventional concrete and detailing:

- The use of FRC reduced maximum crack widths by as much as 50% of those in the specimen with conventional concrete. Similarly, effective crack widths were reduced by as much as 40% of those in the specimen with conventional concrete.
- Hooked end steel fibers at volume fraction of 0.7% (SH-70) were the most effective at maintaining crack widths smaller than 0.006 in. Less than 2% of the cracks in SH-70 were larger than 0.006 in.

Key findings when comparing FRC with conventional concrete and modified end region detailing:

- The use of FRC resulted in reduced effective crack widths as much as 50% of those in the specimen with conventional concrete. Maximum crack widths in specimens with FRC, however, were of similar magnitude to those in the specimen with conventional concrete.
- Steel hooked end and steel crimped fibers at a volume of 0.7% were the most effective of the FRC mixtures at controlling crack widths. The number of cracks wider than 0.006 in. was reduced from 12% in CT to less than 7% in SH-70 and CR-70.

Key findings when comparing the crack width distribution when conventional concrete in conjunction with FDOT conventional end region detailing and FRC specimens with modified end region detailing:

- Conventional concrete and end region detailing had 12% of measured crack widths larger than 0.006 in., and of those, 2% were wider than 0.012 in.
- Fibers at volumes of 0.5% and 0.7% were more effective than FDOT end region reinforcement at maintaining crack widths smaller than 0.006 in. The percentage of measured cracks larger than 0.006 in. when using conventional concrete and FDOT end region reinforcement was 12%. Whereas, when end region reinforcement was reduced, steel hooked end fibers and steel crimped fibers at volume of 0.7% had less than 7% of

measured cracks larger than 0.006 in., while macrosynthetic fibers at volume of 0.5% (PP-50) had 9% of measured cracks larger than 0.006 in.

5 End region finite element analysis

5.1 Introduction

Finite element modeling of end region cracking during and immediately following prestress transfer was conducted to better understand the behavior of the end region of prestressed FIB girders. The modelling was divided into two stages: (1) FRC model calibration using results from laboratory ARS testing and (2) model validation using results from the experimental testing of end region cracking. For the analytical investigation, LS-DYNA processor was used. LS-DYNA is commonly used for impact, and blast analysis. Several concrete models are available in LS-DYNA that have been verified to accurately capture concrete non-linear behavior such as tension strain softening and hardening, and strain rate effects. This software allows for both explicit and implicit analysis. In this investigation, for computational efficacy in analysis, an implicit dynamic analysis was performed. Dynamic analysis was chosen over an implicit static analysis because inertial forces offer an advantage of more stable convergence when there are sudden changes in stiffness on elements, such as the case when cracking of the concrete matrix occurs. Loading rates were adjusted to ensure a quasi-static response was modelled. Accurately representing the behavior of prestress girders at prestress transfer requires a material model that captures FRC post-cracking response and simulation that represents realistic boundary and loading conditions to which girders are subjected under prestress transfer. This chapter covers work conducted to select a material model to represent FRC, along with material calibration using results from the laboratory experimental testing and model validation using results from the full-scale experimental testing conducted.

5.2 Modeling reinforcement

Theoretically, fibers in FRC provide reinforcement uniformly in all directions. In this case the random orientation of fibers was neglected, and fibers were assumed to provide uniform reinforcement along the X, Y, and Z-directions. In general, there are two approaches to model conventional reinforcement in concrete, and the same methods could be applied to model fiber reinforcement. Both methods for modelling reinforcement are discussed in this chapter, along with advantages and disadvantages of each when used to model fiber reinforcement in FRC.

The first method to define concrete reinforcement is by using discrete truss or beam elements with assigned properties for steel reinforcement (Figure 5-1a). For this method, discrete elements are defined by using nodes common to the solid concrete elements and beam elements or by using constraints to provide bond between concrete and reinforcement. Connecting solid concrete element nodes with reinforcement beam elements requires that meshing of the concrete element coincide with lines that define the centroid of the reinforcing elements. No such meshing restrictions are necessary when using constraint definitions.

The second option is the use of a smeared reinforcement approach, in which the reinforcement is integrated into the material model and represented as a fraction of the solid concrete element (Figure 5-1b). The volume-fraction is used to determine properties (e.g., bulk modulus, shear modulus) of the composite material rather than of concrete and/or steel independently. This approach removes the need for compatible nodes or the use of constraint definitions. This approach, however, is better used in cases where small deformations are present, where reinforcement remains elastic or does not stress too far beyond the yield stress

(Schwer 2014). Another downside of this approach is that since the reinforcement is not explicitly defined, there is no stress information for the reinforcement through the simulation. However, because the focus of this investigation is on service loading then a smeared reinforcement approach is believed to be the most effective simulation for fiber reinforcement behavior.

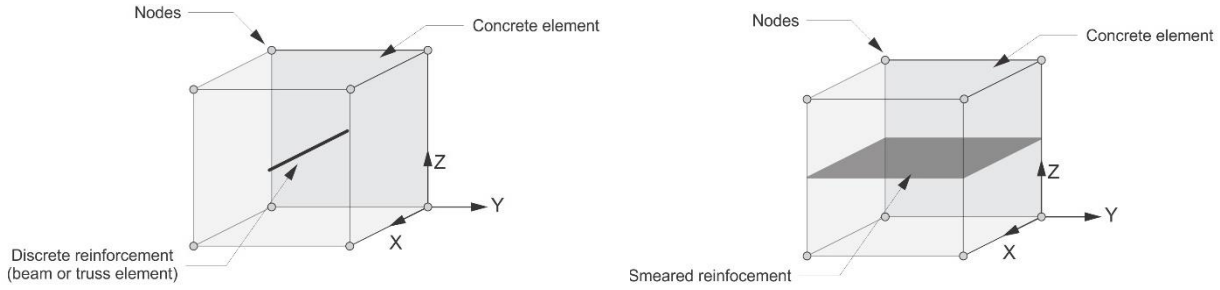

(a) (b)

Figure 5-1 Discrete (a) and smeared (b) reinforcement graphical representation.

To represent the homogeneity of FRC, fiber reinforcement needs to be included along all directions within each concrete element. For this application the use of smeared reinforcement proves effective as it removes the need of creating additional explicit fiber elements, improving the computational efficiency of the model. Conventional reinforcing steel bars, however, were still modelled using discrete beam element. By explicitly defining the mild-steel reinforcement using beam elements, strain during prestress transfer was recovered and was compared with measurements taken in the experimental investigation as means of model validation.

5.3 Concrete material definition

To model full-scale behavior of FRC girders, it is important to use a material model that accurately represents the non-linear behavior of FRC and the redistribution of stresses in the end region after concrete cracks. Concrete was modelled using MAT_WINFRITH_CONCRETE material model, which includes parameters for tension softening behavior and includes smeared reinforcement. In addition, this material model provides up to three orthogonal crack planes per element in which crack widths are calculated. Graphical representation of cracking is also provided during model rendering.

Figure 5-2 shows the required user input parameters for MAT_WINFRITH_CONCRETE definition, which includes: mass density (ro), ultimate compressive and tensile strength (ucs and uts respectively), modulus of elasticity (tm), Poisson's ratio (pr), maximum aggregate size (assize) and either crack width at which concrete tensile stress goes to zero or fracture energy (fe). For smeared reinforcement, the reinforcement is distributed locally over the concrete element in three orthogonal directions (X, Y and Z-direction). Figure 5-2 and Figure 5-3 show input for definition of the smeared reinforcement within Winfrith. The parameters include: modulus of elasticity (e), yield strength (ys), ultimate elongation (uelong), hardening modulus (eh) and reinforcement ratio (ratio of area of reinforcement to gross area) along each direction (xr, yr, zr). The parameters for fiber reinforcement were adjusted based on the fiber material and volume used in order to model the post-cracking response of each FRC mixture.

```
*MAT_WINFRITH_CONCRETE_TITLE
Title
$#     mid        ro        tm        pr       ucs       uts        fe     asize

$#       e        ys        eh    uelong      rate      conm      conl      cont

$#    eps1      eps2      eps3      eps4      eps5      eps6      eps7      eps8

$#      p1        p2        p3        p4        p5        p6        p7        p8
```

Figure 5-2 Winfrith material model input card (MAT_084).

```
*MAT_WINFRITH_CONCRETE_REINFORCEMENT_TITLE
Title
$#eid1/unused  eid2/pid  inc/axis   xr/coor    yr/rqa    zr/rqb
```

Figure 5-3 Winfrith material model input card (MAT_084_REINF).

5.4 Material verification

Prestressed girders are subjected to significant stresses due to the high level of prestress forces. Before implementing the concrete material model MAT_WINFRITH in the analysis for end region cracking on FIB girders, simulations were performed to verify that this material model and the smeared reinforcement can accurately capture response under tension, compression and flexural loading. To verify the response under tension/compression a single element simulation was used, three independent cases were evaluated: response of unreinforced concrete under compressive loading, unreinforced and reinforced concrete response under tensile loading. These simulations served as means to test the smeared reinforcement definition capabilities of MAT_WINFRITH. In all cases, results were compared to theoretical values for determining the accuracy of the concrete material model.

5.4.1 Single element model description

A single element simulation was used to test if the concrete compression and tension response can be accurately represented using the concrete material model MAT_WINFIRTH. In addition, the representation of smeared reinforcement capabilities from MAT_WINFIRTH under tensile loading was verified. Three independent cases were evaluated: (1) response of unreinforced concrete under compressive loading, (2) response of unreinforced concrete under tension, and (3) the response of reinforced concrete (using MAT_WINFIRTH smeared reinforcement) under tensile loading. Geometry, boundary conditions, and material properties were kept constant for the three independent simulations.

A unit cube (1 in. x 1 in. x 1 in.) was used for the three simulations. The element was modelled using 8-node 3D solids, with support and loading conditions applied directly at the nodes as shown in Figure 5-4. Prescribed displacement as defined in Figure 5-5 was assigned to the nodes at the top surface of the element. For verification of response under compression loading (Figure 5-5a), displacement was prescribed to the nodes at the top surface of the element at a rate of 0.001 in./sec to capture concrete failure and 0.0001 in./sec to capture the concrete stiffness drop. To verify response under tensile loading (Figure 5-5b), a displacement rate of 0.00025 in./sec was used prior to concrete tensile contribution to reach zero in order to capture

the change in stiffness due to concrete cracking. After concrete contribution to tension strength reached zero (crack width equal to fe) a rate of 0.005 in./sec was used.

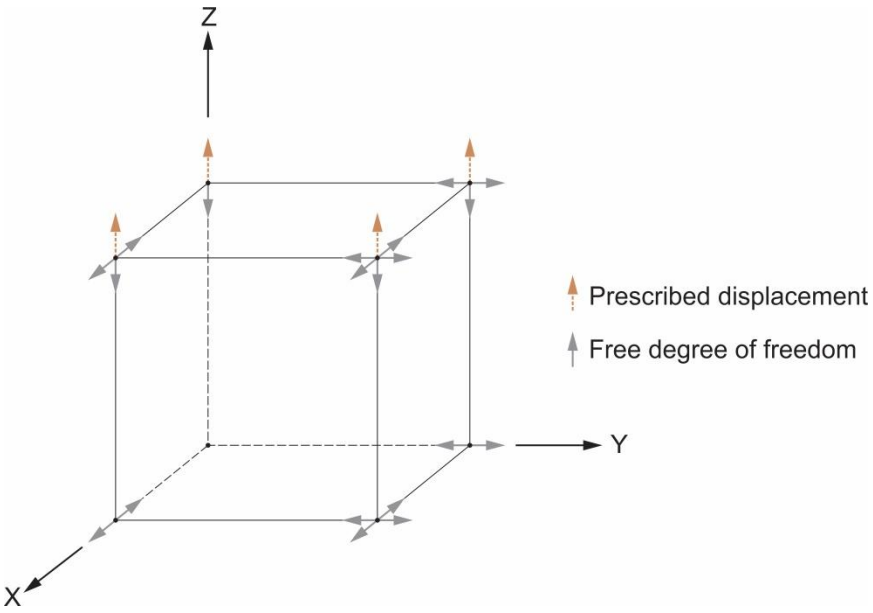

Figure 5-4 Boundary and loading conditions for single element model

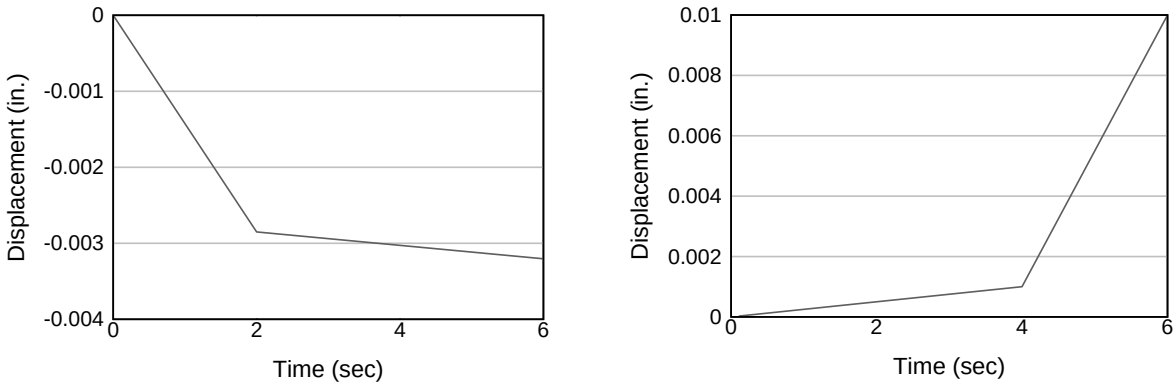

Figure 5-5 Single element prescribed displacement for: (a) compressive and (b) tensile loading

Table 5-1 shows material properties used to define concrete and reinforcement, along with notation for each parameter in parentheses. Concrete compressive strength of 6500 psi was selected and modulus of elasticity and tensile strength were estimated as described in section 5.3. For the case in which reinforcement was included, the reinforcement layer was defined using a smeared reinforcement approach at the center of the element along the z-direction (Figure 5-6).

Table 5-1 Material properties used in analytical model

Concrete properties	
Compressive strength (ucs)	6.5 ksi
Tensile strength (uts)	320 psi
Modulus of elasticity (tm)	4,600 ksi
Poisson's ratio (pr)	0.2
Aggregate size (asize)	0.375 in.
Crack width for tension to reach zero (fe)	6E-4 in.

Reinforcement properties	
Yield strength (ys)	4 ksi
Modulus of elasticity (e)	29,000 ksi
Reinforcement ratio (zr)	0.05

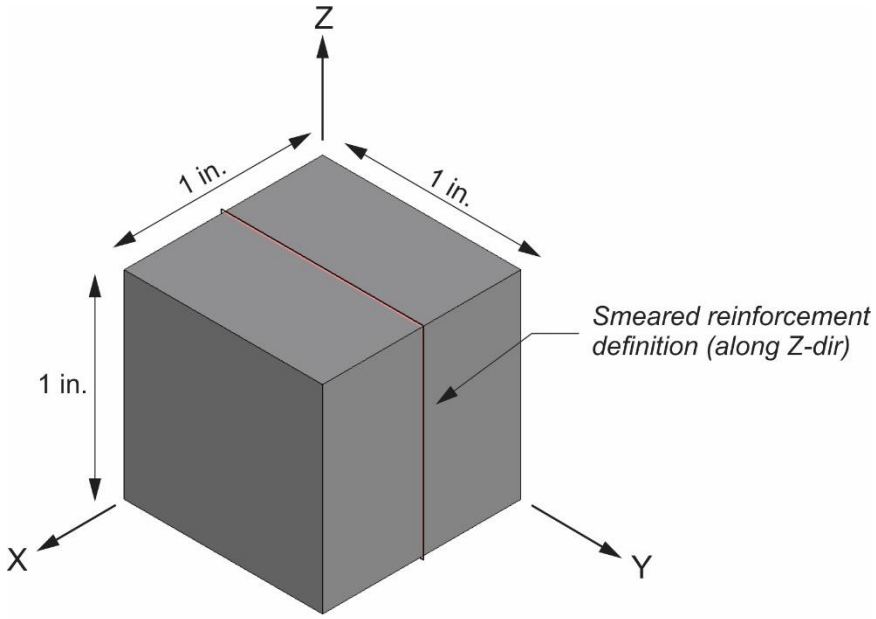

Figure 5-6 Single element reinforcement definition

5.4.2 Verification of MAT_WINFRITH_CONCRETE under tension/compression loading

Compressive loading was applied to verify the response of concrete material model MAT_WINFRITH. The results from the simulation were compared with the theoretical response of unconfined concrete under compressive loading defined following Hognestad (1951). The simulation shows an elastic perfectly plastic response prior to reaching the ultimate compressive strength (ucs) of 6,500 psi. When a strain of 0.0014 in/in (ucs/tm) is reached the simulation shows no additional load carrying capacity, with constant stress until strain exceeds 0.0028 in/in (2ucs/tm) where a brittle failure occurs. At lower than 20% of the compressive strength the simulation is in good agreement with theoretical response. However, for stresses larger than 20% of the ultimate compressive strength this model is observed to overestimate the load carrying capacity of concrete. At ultimate strength this simulation shows significant difference in concrete response under compression when compared to the theoretical values, however, because the focus of this investigation is under service loading, this material model is considered to be suitable to model the post-cracking response of FRC under service loading conditions.

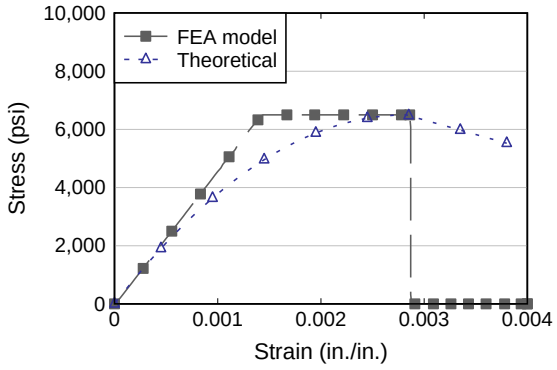

Figure 5-7 Axial stress-strain under compressive loading for a single element simulation

Tensile loading was applied to verify the response of unreinforced concrete material when using MAT_WINFRITH. The theoretical response of unreinforced concrete was defined as elastic perfectly plastic until cracking occurs. After cracking, load carrying capacity is assumed to decrease linearly until the crack width at which concrete tensile contribution equals zero (fe) is reached. After this point, there is no additional load carrying capacity. The concrete cracking stress was assumed to be equal to the ultimate tensile strength (uts), and the strain at which the concrete contribution to tensile strength reaches zero was assumed as the strain at cracking plus the crack width at which concrete contribution reaches zero (fe). The stress-strain curve generated from the theoretical assumptions was compared to the results from the simulation as shown in Figure 5-8a. Good agreement is seen between stress and strain at which concrete cracks, and the strain at which concrete contribution to tension reaches zero, with less than 1% and 10% difference respectively (Table 5-2).

Figure 5-8 (b) shows the comparison between the simulation and theoretical response for the case in which smeared reinforcement is included. The theoretical response was defined by using the transformed section area and stiffness provided from the reinforcement and concrete to define the stress and strain at which cracking of concrete occurs. The contribution of concrete to tension was assumed to be zero after the strain exceeded the strain at cracking plus the crack width at which concrete contribution reaches zero (fe). At this point, the reinforcement has already yielded and the stress after this point is equal to the force carried by the reinforcement (yield strength (ys) times the area of reinforcement provided) distributed over the area of the unit element. As shown in Figure 5-8a and Table 5-2 good agreement is seen between stress and strain at which concrete cracks, and the strain at which concrete contribution to tension reaches zero, with less than 10% difference.

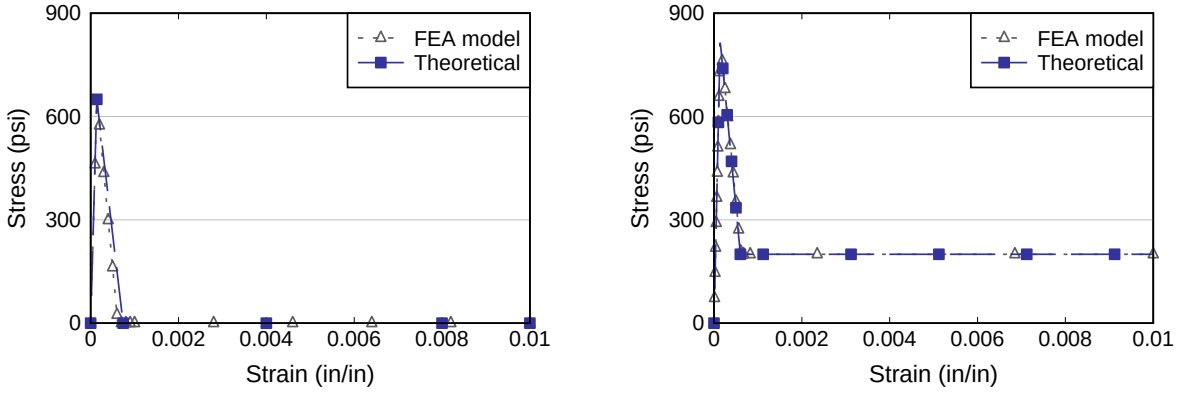

Figure 5-8 Axial stress-strain under tensile loading for: (a) unreinforced, and (b) reinforced single element

Table 5-2 Stress-strain at cracking and point at which concrete contribution reaches zero for single element under tensile loading.

	Cracking		Concrete tensile contribution reached zero	
Analysis	Stress (psi)	Strain (in./in.)	Stress (psi)	Strain (in./in.)
Theoretical unreinforced	650	0.0014	0	0.0007
FEA unreinforced	640	0.0013	0	0.00063
Theoretical reinforced	813	0.0014	0	0.0007
FEA reinforced	808	0.0015	0	0.00063

According to the simulation results, the concrete material model MAT_WINFRITH shows good agreement with theoretical behavior of concrete under compressive and tensile loading, particularly before and right after cracking of concrete occurs. Based on these results, this material model along with a smeared approach are considered to be suitable to model the post-cracking response of FRC under service loading conditions.

5.5 Material model calibration

To model full-scale behavior of FRC girders, it is important to use a material model that accurately represents the post-cracking response of FRC. Results from the laboratory testing conducted as part of the experimental investigation (Section 4.7) were used to calibrate MAT_WINFRITH_CONCRETE input parameters for each FRC mixture. From the experimental investigation conducted, the EN 14651 test proved to provide more repeatable results. This is most likely due to the test procedures in which the load rate is controlled by the crack width, generating a more consistent and stable crack formation and growth and less variable results. This test offers several advantages over the ASTM counterpart. In addition to stability of results, the use of notched specimens causes cracking to initiate away from the surface, which reduces the effect of preferential alignment of the fibers along the molded face. Lastly the testing is not divided in stages, but rather provides continuous data collection for cracking and post cracking behavior. For these reasons, the EN 14651 results were selected for

model calibration. This section briefly provides a description of the analytical model, along with the methodology used for calibration of the material model.

5.5.1 Model configuration

The concrete specimen size and loading conditions were selected based on the experimental work following the EN 14651. A simply supported 4 in. × 2 in. × 14 in. prismatic concrete beam, with a 1/3 in x 2/3 in notch at midspan loaded under third point bending (Figure 5-10) was modelled, and the post-cracking response was used for material calibration.

The concrete beam was modelled using 8-node 3D solids, using a rectangular mesh. Element size of 0.25 in along the X-direction, 0.10 in. along the Y- direction, and 0.12 in. along the Z-direction was used around the area of the notch to ensure that crack propagation can be accurately captured. Single point integration was used for concrete elements, this is necessary as part of the definition of MAT_WINFRITH_CONCRETE. Single integration point offers advantages on computational efficiency over fully integrated elements, however, this introduces the possibility for zero-energy deformation modes to occur (Cook et al. 2014). To control this deformation mode, various hourglass formulations were evaluated for use in the simulations. The most accurate formulation for this application was found to be the stiffness based hourglass control method developed by Belytchko and Bindeman (1993). This is defined in LS-DYNA as hourglass control type 6 with an hourglass coefficient of 0.05. To control hourglassing in the area near the loading fixture (top roller), the elements along the top surface of the beam and for a depth of 0.25 in. were defined using fully integrated elements. MAT_CSCM_CONCRETE (MAT_159), a commonly used material model for concrete (LSTC 2018b, Murray et al. 2007) was used for the elements along the top surface of the beam (Figure 5-9).

Support and loading conditions were modelled by using half cylinders to represent the loading and support fixtures used in the laboratory testing setup. The support rollers were modelled using fully integrated 8-node 3D solids. A rigid material (MAT_020) with steel properties was used to model the core of each roller, this helped reduce the computational time needed in the model. An elastic material with steel properties (MAT_001) was used to model the outer surface of the rollers, this helped control hourglassing in the concrete beam near the area of the rollers. Details of roller geometry and material models used are shown in Figure 5-9.

Boundary and loading conditions were defined in a manner consistent with the conditions present during the experimental testing. Boundary conditions were defined by introducing an automatic surface to surface contact with friction between the roller supports and the concrete element (AUTOMATIC_SURFACE_TO_SURFACE) (LSTC 2018a). A static coefficient of friction of 0.55 and a dynamic friction coefficient of 0.45 were used. A half model was used since the beam cross-section, loading and boundary conditions are symmetric about the Y-Z plane (Figure 5-10). The plane of symmetry was constrained along the X-direction to model a symmetric deformation pattern.

The support rollers are restricted in displacement along all directions with only X-rotation allowed (Figure 5-10). The top surface of the roller is prescribed a displacement along the Z-direction (as shown in Figure 5-9) and is allowed to rotate freely. Loading of the specimen was performed using a prescribed displacement to avoid instability after cracking is initiated. Prior to cracking a loading rate of 0.025 in/sec was used, once cracking occurred the rate was decreased to 0.009 in/sec to maintain a stable crack growth during the analysis (Figure 5-11).

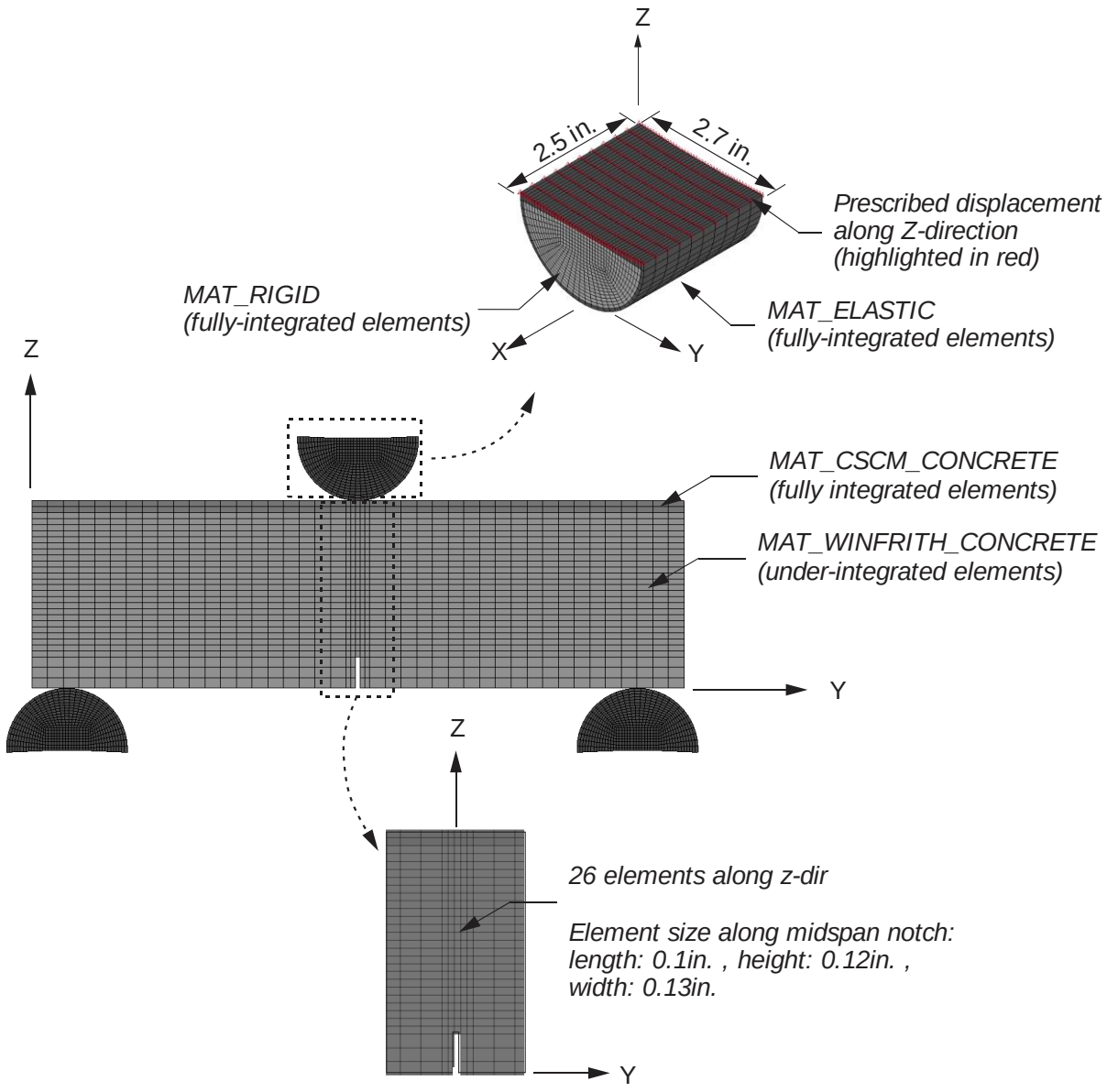

Figure 5-9 FEA model material and mesh details

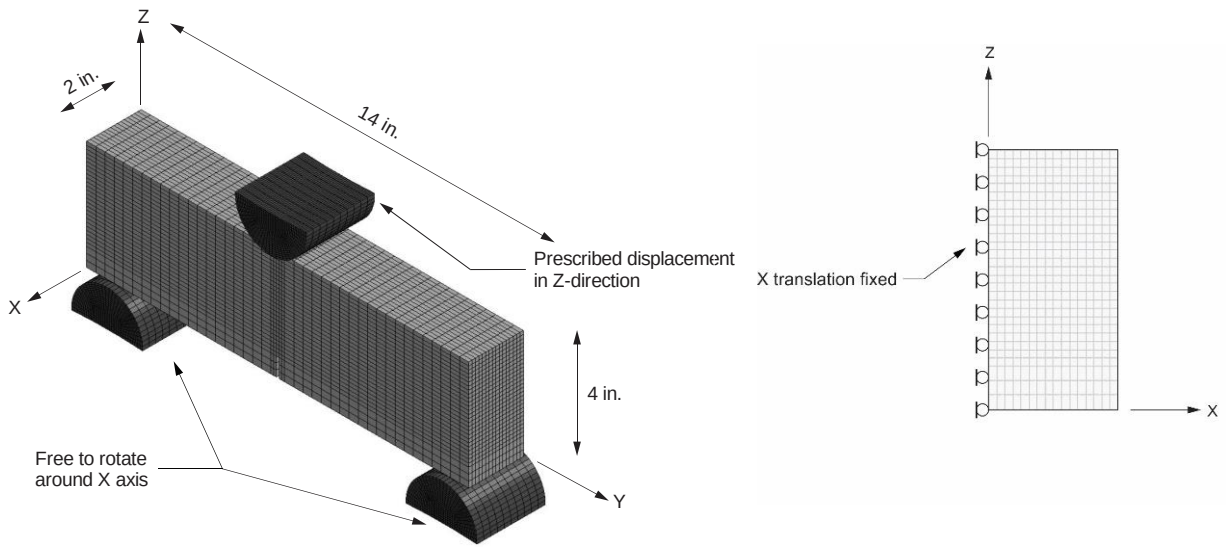

Figure 5-10 Laboratory beam model geometry and boundary conditions

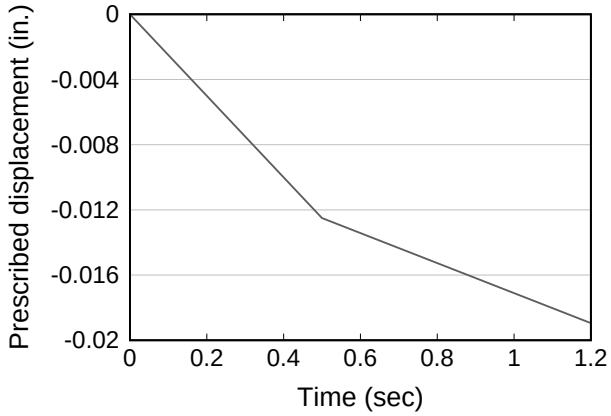

Figure 5-11 Prescribed midspan displacement along Z-direction (downward direction)

5.5.2 Parameters used for material calibration

MAT_WINFRITH CONCRETE material model was used in the beam simulations. Fiber reinforcement was modelled using the smeared reinforcement capabilities of this material model. Compressive strength at 28 days was determined experimentally for all mixtures evaluated. Empirical equations based on concrete compressive strength were used to estimate tensile strength (Equation 5-1), modulus of elasticity (Equation 5-2), and maximum crack width for concrete tensile stress to reach zero (Equation 5-3). Fiber modulus of elasticity and rupture strength were selected based on material and fiber manufacturer specifications (when available). Reinforcement ratio was initially estimated assuming that one-third of the fiber volume was aligned with each of the x, y, and z axes. Reinforcement yield strength, reinforcement ratio and crack width for concrete contribution to reach zero were then adjusted to fit the response from the experimental investigation.

$f_r = 7.5\sqrt{f'_c}$ (ACI 318-14) Equation 5-1

$E_c = 57{,}000\sqrt{f'_c}$ (Pauw 1960) Equation 5-2

$G_F = 73 \cdot f_{cm}^{0.18}$ (fib-Model Code (2010)) Equation 5-3

Where f_r is the concrete modulus of rupture (psi), f'_c is the concrete compressive strength (psi), E_c is the concrete modulus of elasticity (psi), G_F is the fracture energy (N/m), and $f_{cm}$is the mean compressive strength (MPa)

5.5.3 FRC material calibration

For material calibration the parameters that describe concrete post-cracking behavior were modified to fit the post-cracking response of FRC based on the experimental test following procedures for EN 14651. These parameters included crack width at which concrete tensile strength goes to zero; ultimate tensile strength; fiber modulus of elasticity; fiber rupture strength; and fiber volume ratio (Section 5.2). Table 5-3 and Table 5-4 show the parameters used to define concrete and the fiber reinforcement material properties for each specimen.

Because end region cracking is a serviceability issue, the focus of the material calibration was focused at accurately simulating the behavior between crack initiation and a CMOD value of 0.02 in. (0.5 mm). Figure 5-12 shows a comparison of the load versus CMOD response from experimental and analytical testing up to CMOD of 0.03 in. (0.7 mm). The results from the laboratory testing of mixtures used in the construction of the full-scale FIB girders (Section 4.7.3) were used to define the experimental response of each FRC mixture. The experimental curve was determined using the average of the laboratory specimens tested for each mixture. Comparison of the response from the simulation shows good agreement with experimental pre-crack behavior including initial stiffness and cracking load. After cracking load, the simulation captured the post-cracking response of FRC. The results of this work showed that the smeared reinforcement approach is fully applicable to the simulation of end region behavior in FRC beams.

Table 5-3 Concrete mechanical properties used in material definition

Specimen	Compressive strength, ucs (psi)	Tensile strength, uts (psi)	Modulus of elasticity, tm (ksi)	Crack width for crack-normal tensile stress equal zero, fe (in.)
CT	9,330	360	6,600	0.0010
SH-30	7,830	410	5,300	0.0006
SH-70	7,760	260	5,300	0.005
CR-70	9,580	550	5,800	0.0005
PP-50	7,740	410	5,400	0.0013

Table 5-4 Fiber reinforcement mechanical properties used in material definition

Specimen	Modulus of elasticity, e (ksi)	Yield strength, ys (ksi)	Ultimate elongation, uelog (%)	Reinforcement ratio, xr/yr/zr
CT	-	-	-	-
SH-30	30,000	75	0.20	0.0032
SH-70	30,000	95	0.20	0.004
CR-70	30,000	89	0.20	0.0030
PP-50	20,000	15	0.22	0.0025

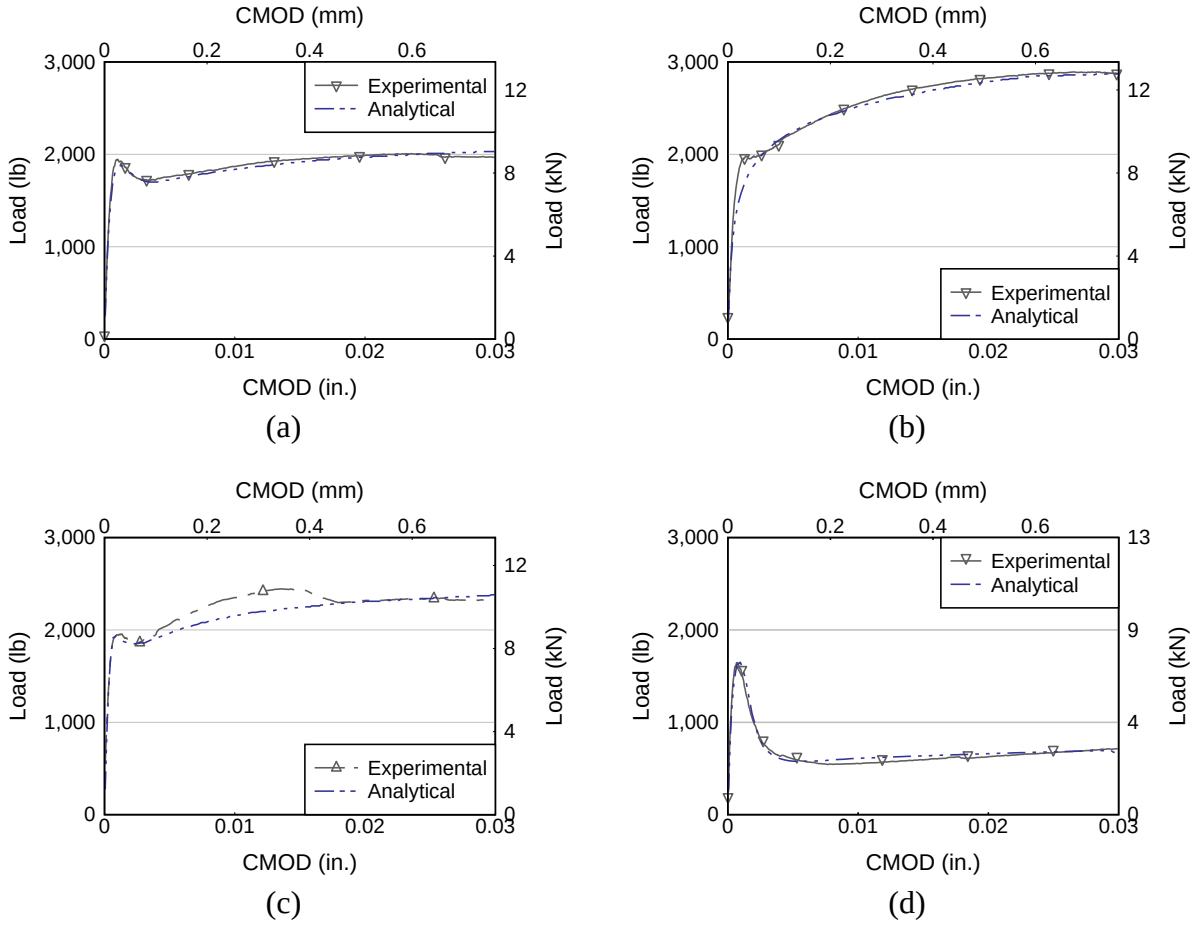

Figure 5-12 Comparison of experimental and analytical response at service level for: (a) SH-30, (b) SH-70, (c) CR-70 and (D) PP-50

5.6 FIB model configuration

The FEA model developed to simulate behavior of FIB bridge girders was developed to simulate cracking of the end region during prestress transfer. The model included transverse and confinement reinforcement following the detailing used in the construction of the FIB-78 specimens. Self-weight and prestress forces were included in the simulation to represent the loading conditions during prestress transfer.

The same coordinate system was used in the analytical model as the one described in Section 0. The origin of the coordinate system is located at the bottom of the end containing the conventional end region detailing (C-end) and at the centroid of the cross-section. The x-axis is horizontal across the width of the girder, the y-direction runs longitudinally along the beam and z-axis is vertical, as shown in Figure 5-13.

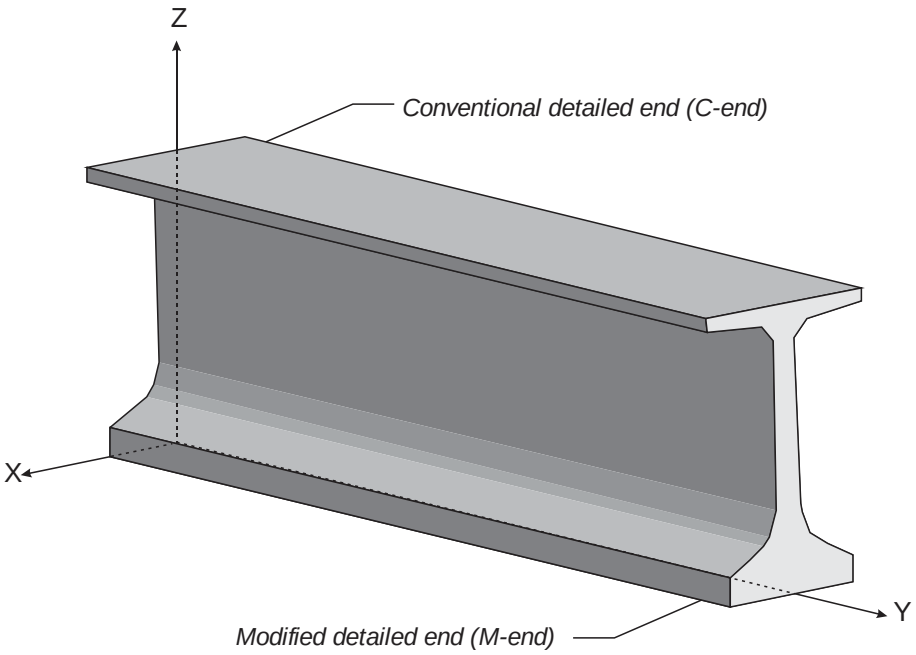

Figure 5-13 Coordinate system

Figure 5-14 shows a schematic of the model configuration, boundary conditions, prestressed reinforcement, and element mesh. The concrete girder was modelled using a rectangular mesh with 8-node 3D solid elements. Single point integration was used for concrete elements, as this is necessary when using MAT_WINFRITH CONCRETE. The material parameters were defined based on the work conducted for material calibration (Section 5.5.3).

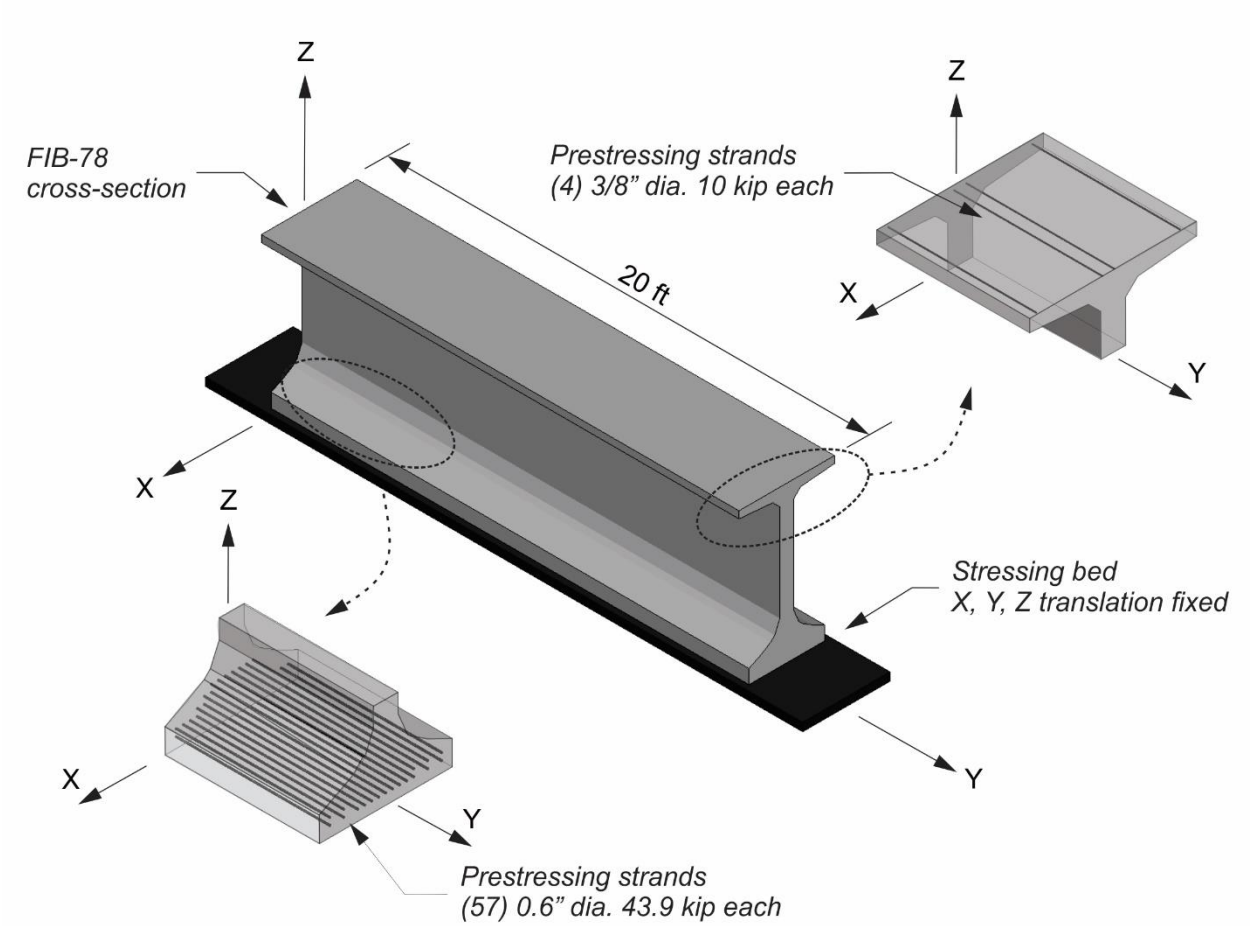

Figure 5-14 FIB-78 Model configuration

The prestressing strands were modelled as discrete cable elements. An initial tensile force was included in the cable to model prestressing force. Perfect bond between the prestressing strands and the concrete elements was modeled by incorporating a constraint based coupling between the beam and the solid elements (CONSTRAINED_BEAM_IN_SOLID). This allowed for the solid elements in the bottom flange to be meshed independently of prestressing strand location (Figure 5-15). MAT_CABLE_DISCRETE_BEAM (MAT_071) was used to model the prestressing strands. This material model allows for an initial tensile force to be specified for each of the elements representing the prestressing strands.

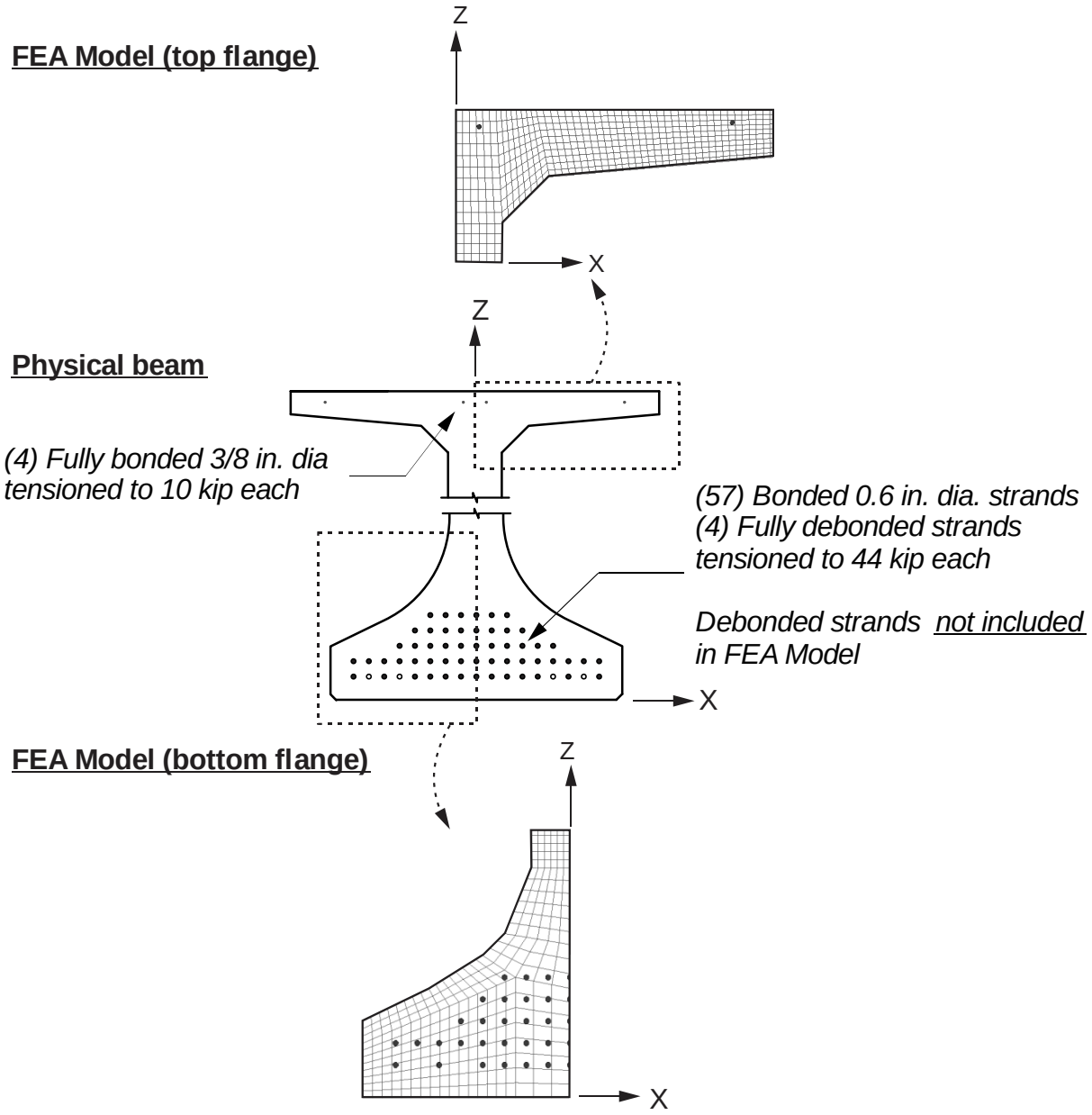

Figure 5-15 Strand layout and concrete element mesh

The confinement and transverse mild steel reinforcement were modelled using discrete beam elements. MAT_PLASTIC_KINEMATIC (MAT_003) was used to model the mild-steel reinforcement, this material model can be used to model elastoplastic material, with option for kinematic, isotropic hardening or a combination (LSTC 2018). Typical material properties for steel were used in the material definition, including: modulus of elasticity of 29,000 ksi, 0.33 Poisson's ratio and 60 ksi yield stress. Perfect bond between the reinforcement and the concrete elements was modeled by incorporating a constraint based coupling between the beam and the solid elements (CONSTRAINED_BEAM_IN_SOLID). This allows the highly reinforced area near the end region to be meshed independently of the solid concrete models. Figure 5-16 shows the reinforcement configuration used in the model, the location for both transverse and confinement reinforcement follow those from the experimental investigation.

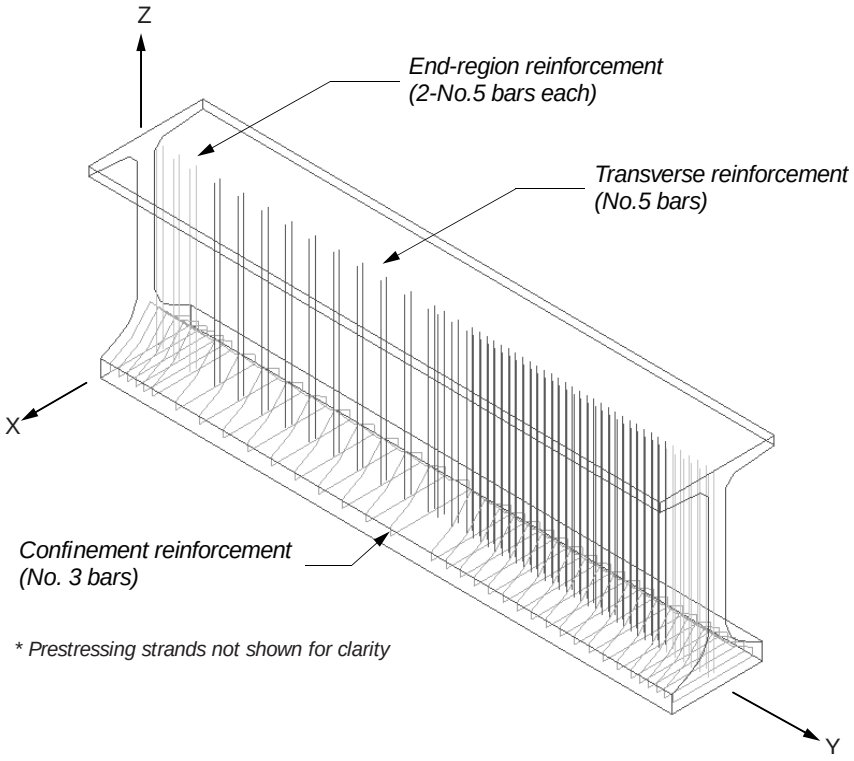

Figure 5-16 FIB-78 Model reinforcement configuration (concrete mesh and prestressing strands not shown for clarity)

Boundary and loading conditions were defined in a manner consistent with the conditions present during prestress release. Boundary conditions were defined by introducing a contact algorithm (AUTOMATIC_SURFACE_TO_SURFACE) between the prestressing bed and the concrete element, and using a static coefficient of friction of 0.55 and a dynamic friction coefficient of 0.45 (Livermore Software Technology Corporation (LSTC) 2016).

Element self-weight is accounted for by using a prescribed body acceleration to define gravity forces. Prestressing force was defined as an initial tensile force in the cable elements as described previously in this section. The prestressing force was sub-divided along the transfer length. As shown in Figure 5-17, transfer length of 30 in. was used for the 0.6-in. diameter strands (bottom flange) and 24-in transfer length for the 3/8-in. diameter strands (top flange), this was determined based on AASHTO LRFD provisions.

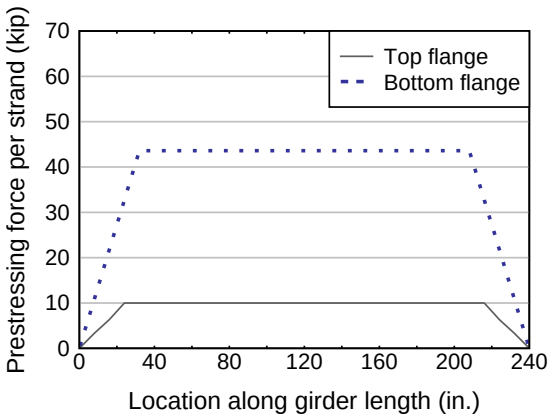

Figure 5-17 Prestressing force in each strand vs. location along beam length

To ensure that static conditions are maintained and hourglass energy is avoided during the simulation, the gravity and prestressing forces were applied in different stages. In addition, by applying the prestress forces in stages, a more accurate representation of the stresses induced during prestress transfer is provided. The sequence in which the prestressing strands were released in the FEA model was determined following the detension sequence used in the experimental procedures (Section 4.3). The loading was divided in stages, as described in Table 5-5 and Figure 5-15. Gravity is introduced initially in the model, followed by the simultaneous release of the prestressing strands in the top flange. Following the release of the prestressing strands in the top flange, at simulation time of 0.2 seconds, the prestressing in the bottom flange are released in pairs (symmetric about the x-axis) following strand detensioning sequence from the experimental investigation (Figure 5-19b and Figure 5-20). Full prestressing force is reached at a simulation time of 7.4 seconds.

The model configuration described above was validated by comparing the results from the analytical work with experimental strain and crack data. The proceeding sections contain details regarding model validation.

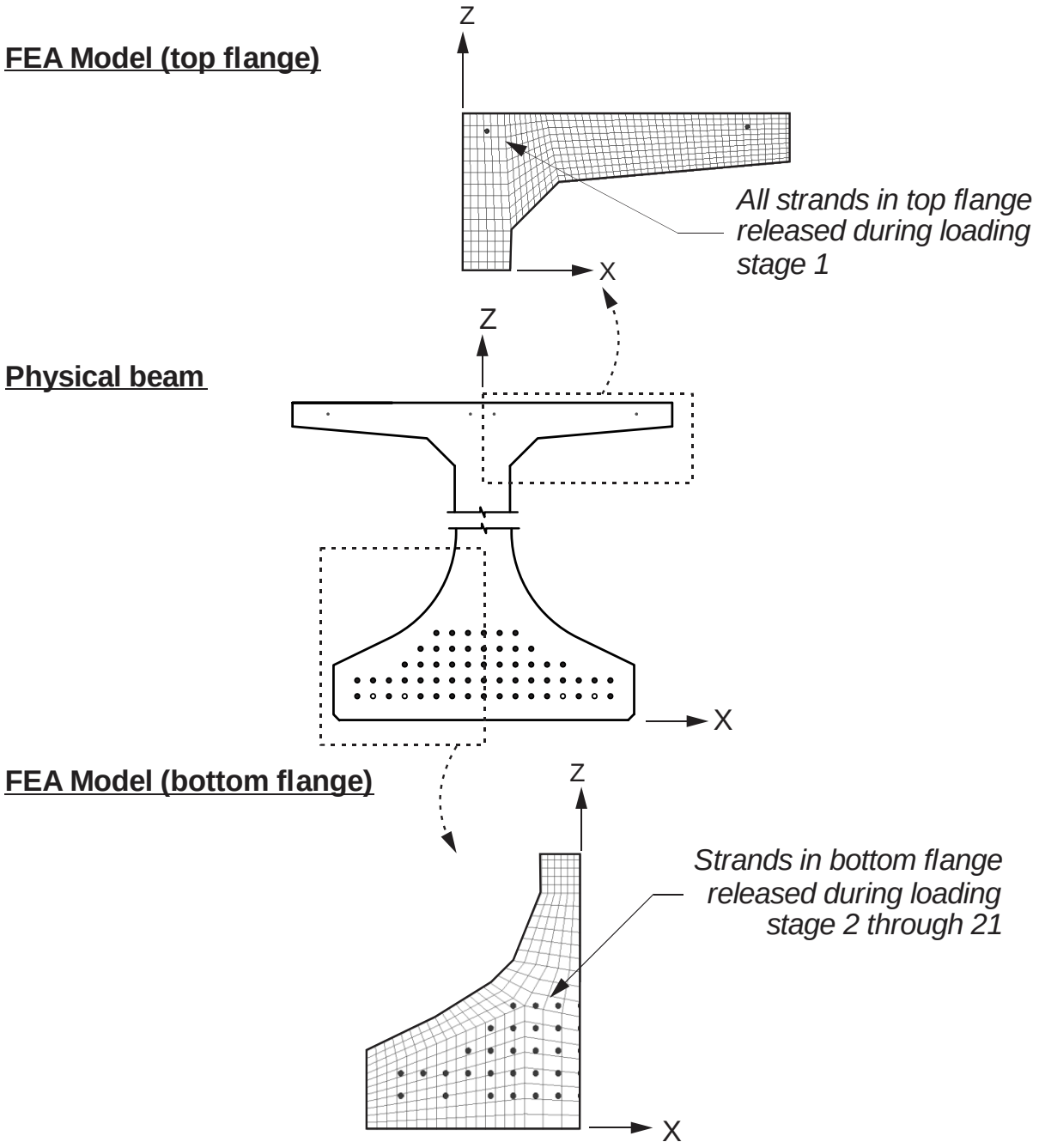

Figure 5-18 Prestress loading definition used in FIB model

Table 5-5 Summary of loading stages for FEA Model

Stage	Loading applied (% of total load)			Simulation time (sec)
	Gravity	Top flange prestressing	Bottom flange prestressing	
0	100	0	0	0
1	100	100	0	0.2
2	100	100	14	0.5
3	100	100	30	1.2
10	100	100	55	3.4
15	100	100	75	5.1
21	100	100	100	7.4

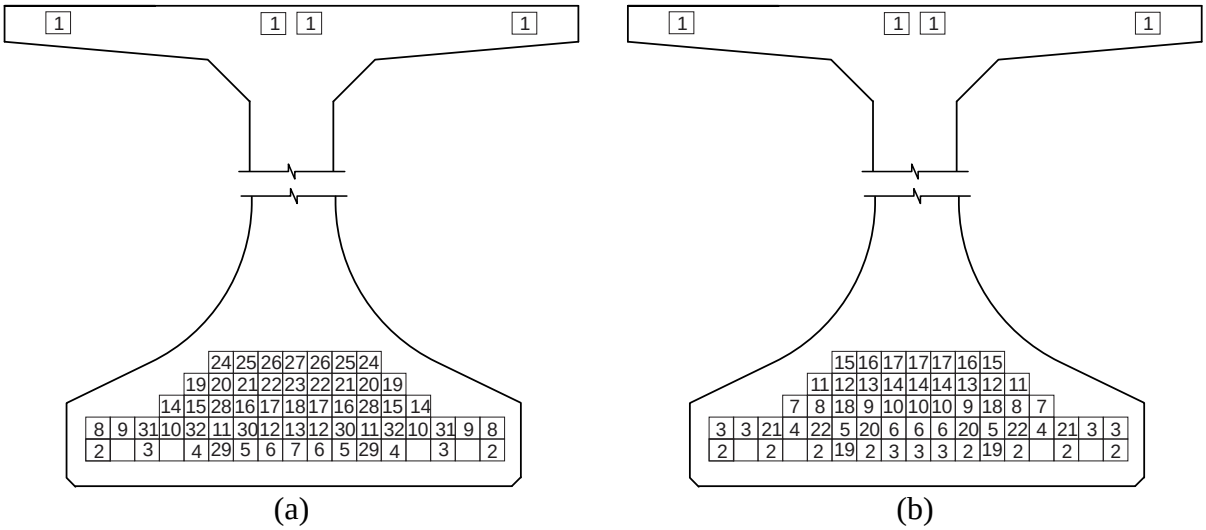

Figure 5-19 Prestressing staging: (a) Experimental test, (b) Model stages

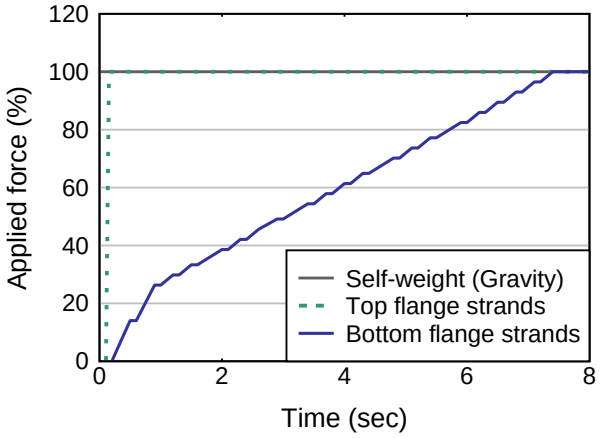

Figure 5-20 Percent of total prestressing force in bottom flange applied (total prestress force in bottom flange of 2485 kips)

5.7 Model validation

Model validation was conducted by evaluating the elastic and post-cracking behavior from the simulation. The elastic region was defined as that prior to end region cracking occurring in the simulation. The first end region cracks occurred in the simulation when approximately 20% of the prestressing force was applied. For validation within the elastic region, concrete and end region reinforcement strains from the simulation were compared to those measured experimentally, until 20% of prestress force was transfered. After cracking in the simulation occurred, the stress in the concrete and steel elements is highly dependent on the location where cracking occurred. For post-cracking validation, the total crack length and area, along with the effective and maximum crack widths were compared to those measured in the experimental program. This section covers the validation of each mixture used, first focusing on behavior prior to cracking and then on cracking after full prestressing was transferred.

5.7.1 Elastic behavior

To validate the FIB model within the elastic region, concrete and end region reinforcement strains from the simulation were compared to those measured experimentally. Figure 5-21 shows the location of the strain gages used for the validation of the FIB model, including strain gages placed in the end region reinforcement (IS gages) and along the concrete surface (XS gages). Appendix E provides coordinates of strain gages. For validation in the elastic range, the comparison focuses on the comparison between analytical and experimental results until 20% of prestressing force was transferred.

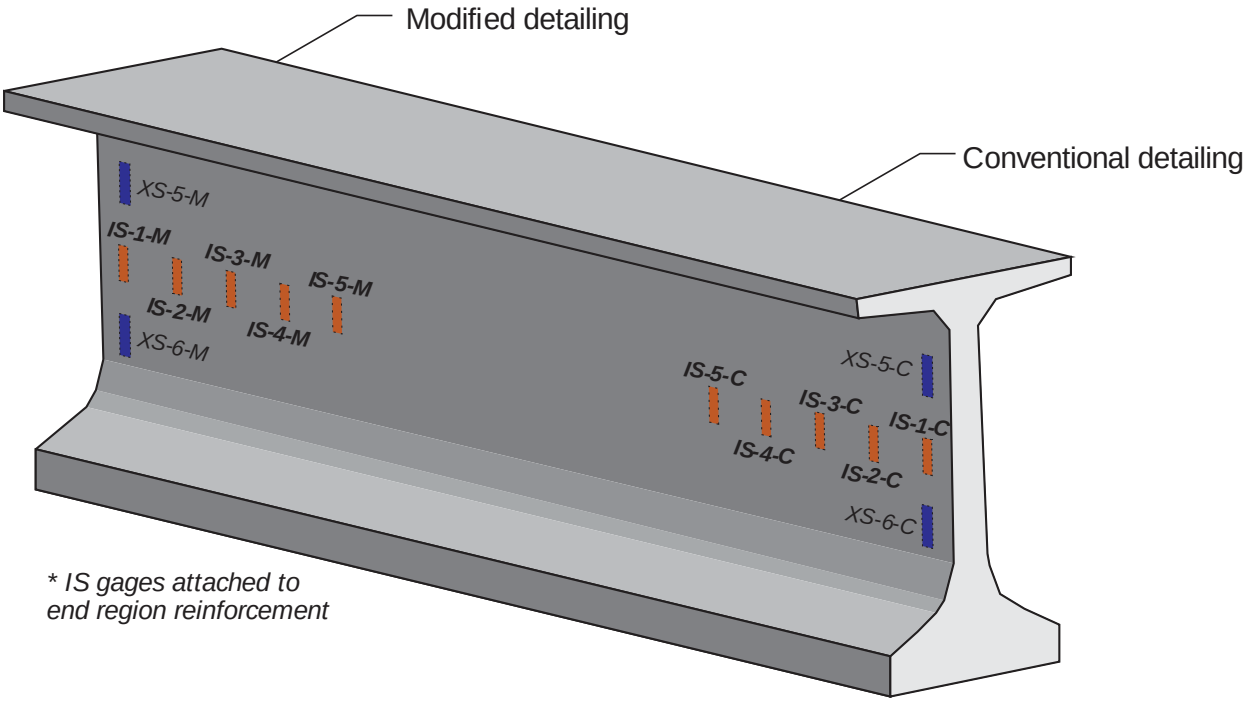

Figure 5-21 Strain gages used for validation of FIB analytical model

Figure 5-22 through Figure 5-24 show comparison of the concrete strain measured experimentally and those obtained from the simulation. Concrete strain from the FEA shows similar pattern as the strain measurements from the experimental program, with strain increasing until cracking occurs. For both the experimental and analytical model, concrete cracking

initiating after 10-15% of the prestress force is transferred. Figure 5-25 through Figure 5-30 show a comparison of experimental and analytical strain recorded in the mild steel reinforcement within the end region. Reinforcement strain from the FEA shows similar pattern as the strain measurements from the experimental program, with vertical tensile strain in the web being highest near the end of the girder (IS-1) and decreasing in magnitude as distance from the girder end increased.

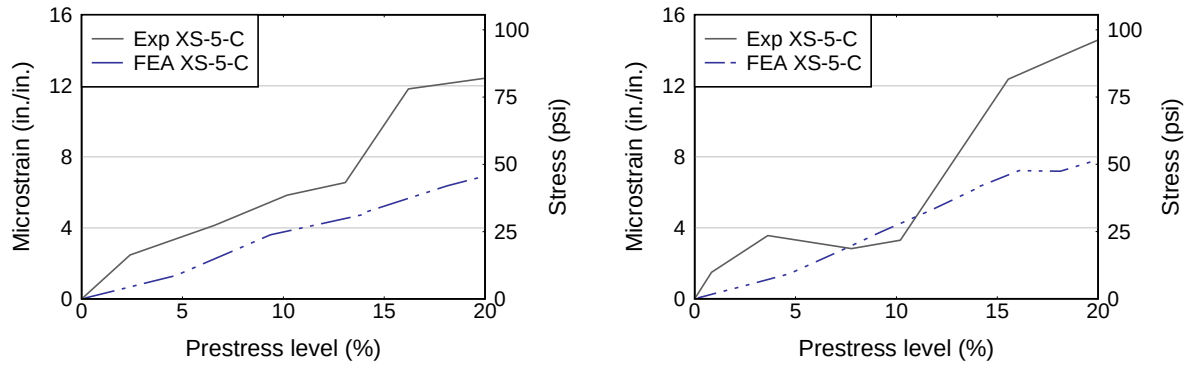

Figure 5-22 Concrete strain (XS-5-C) during prestress transfer in end with conventional end region detailing: (a) CT, and (b) PP-50

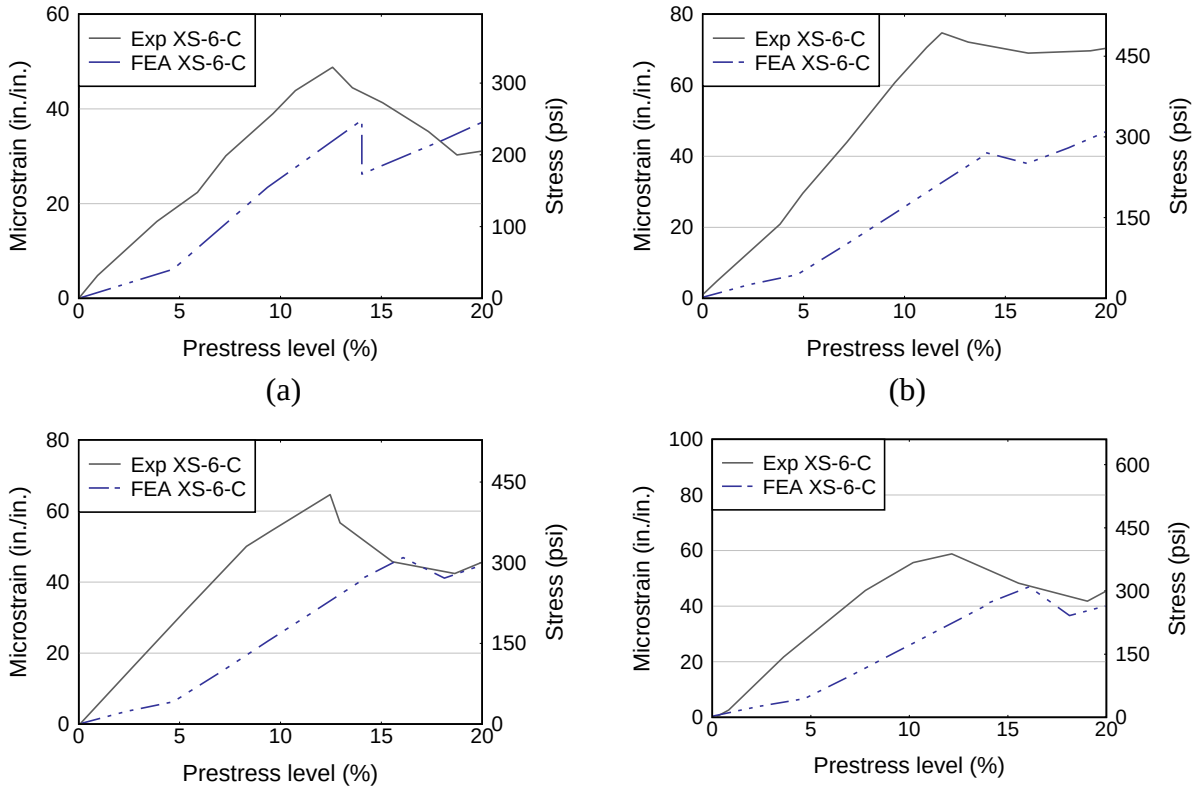

Figure 5-23 Concrete strain (XS-6-C) during prestress transfer in end with conventional end region detailing: (a) CT, (b) SH-30, (c) CR-70, (d) PP-50

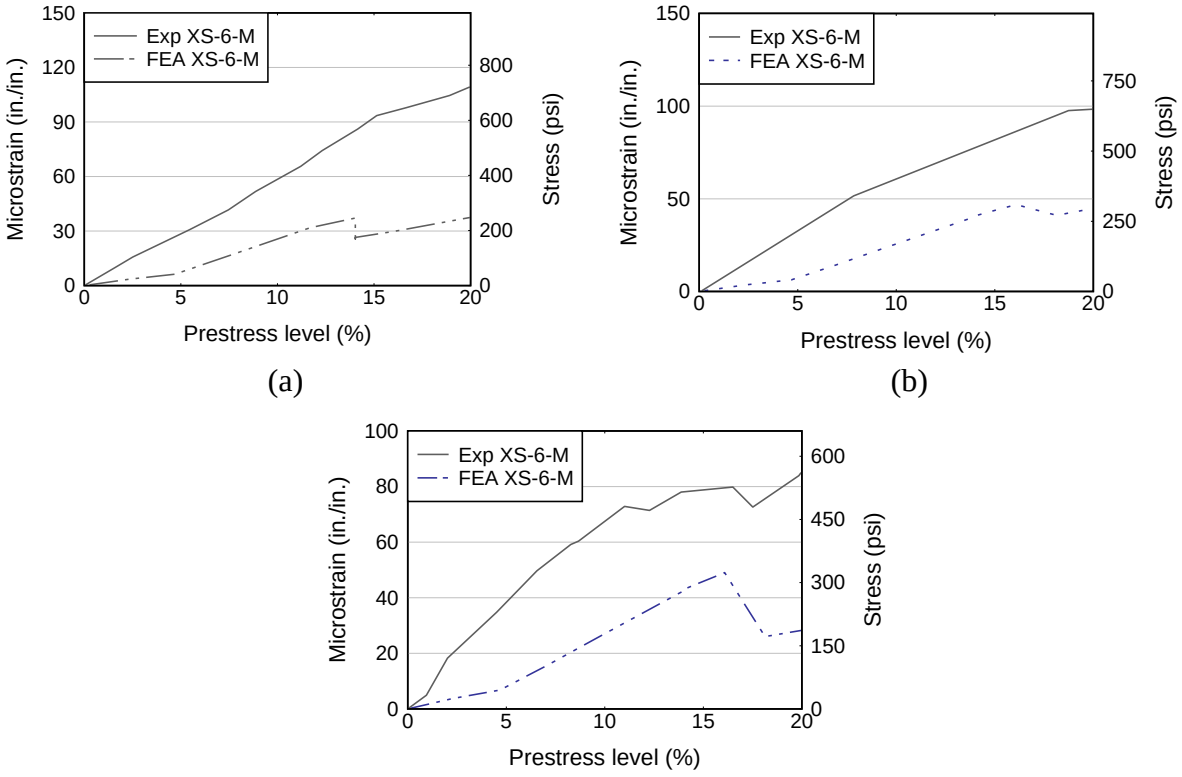

Figure 5-24 Concrete strain (XS-6-M) during prestress transfer in end with modified end region detailing: (a) CT, (b) CR-70, (c) PP-50

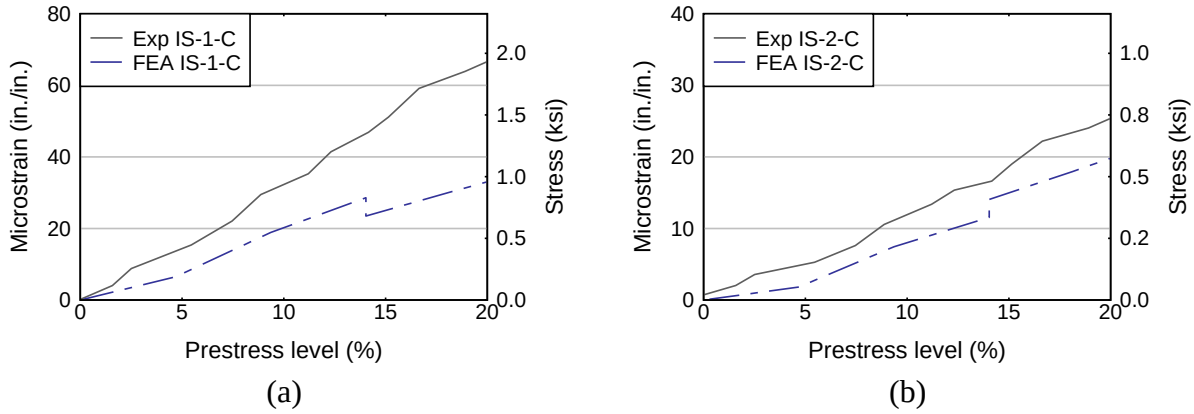

Figure 5-25 CT mild steel reinforcement strain during prestress transfer, conventional end region detailing: (a) IS-1-C, and (b) IS-2-C

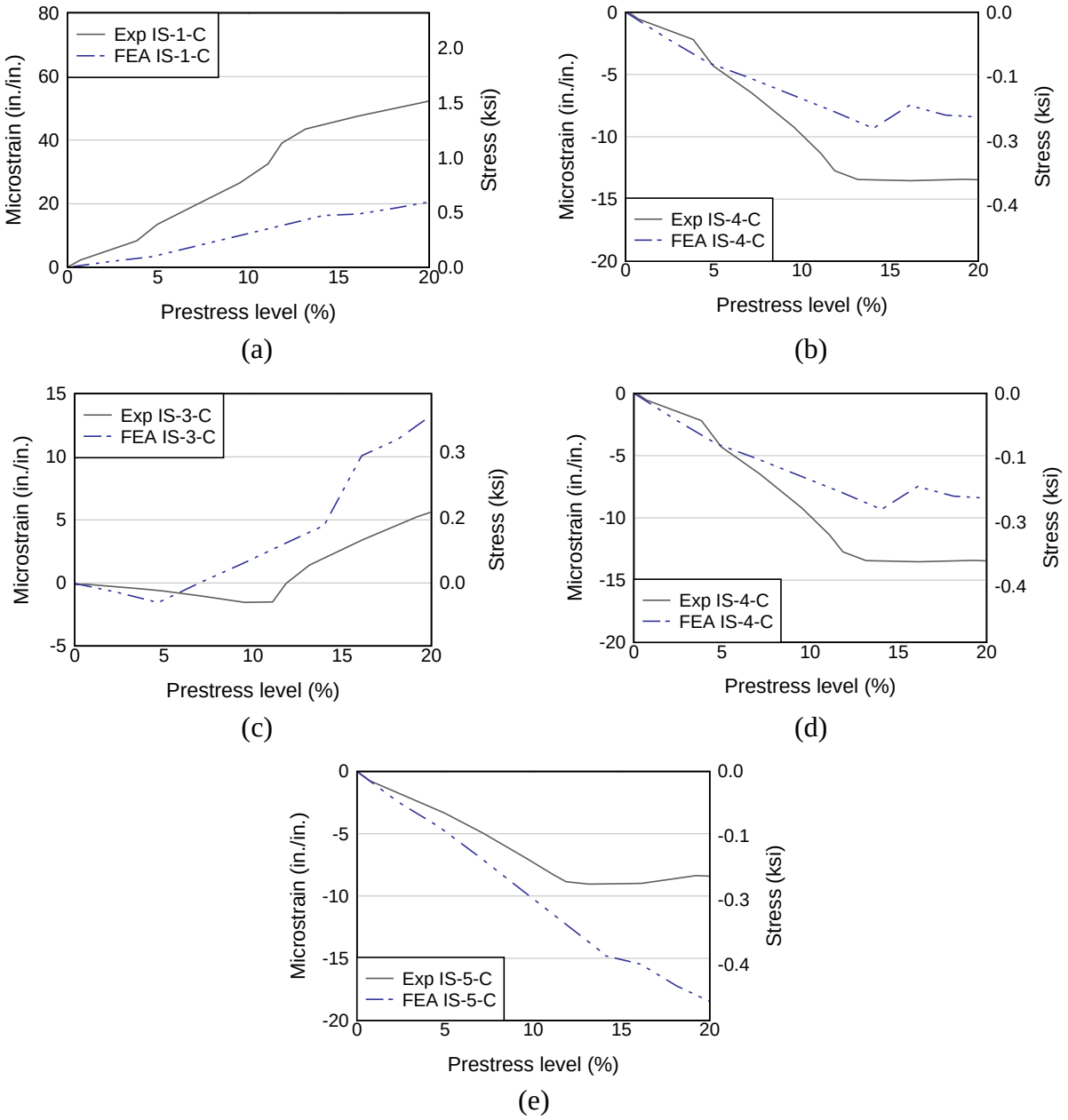

Figure 5-26 SH-30 mild steel reinforcement strain during prestress transfer, conventional end region detailing: (a) IS-1-C, (b) IS-2-C, (c) IS-3-C, (d) IS-4-C, and (e) IS-5-C

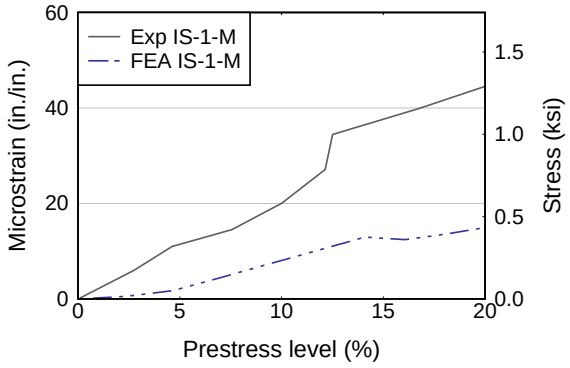

(a)

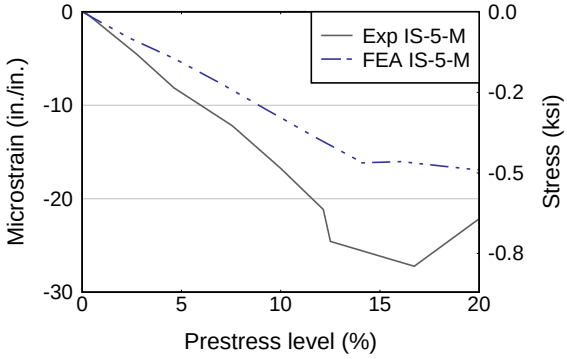

(b)

Figure 5-27 SH-30 mild steel reinforcement strain during prestress transfer, modified end region detailing: (a) IS-1-M, and (b) IS-5-M

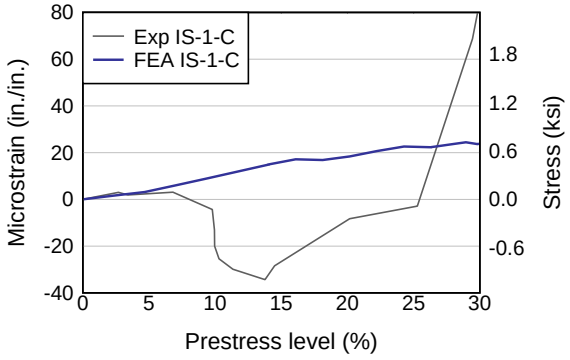

(a)

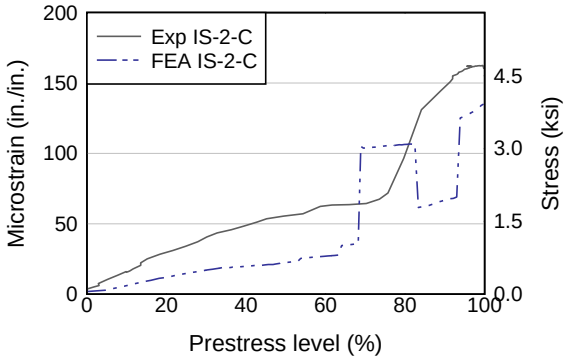

(b)

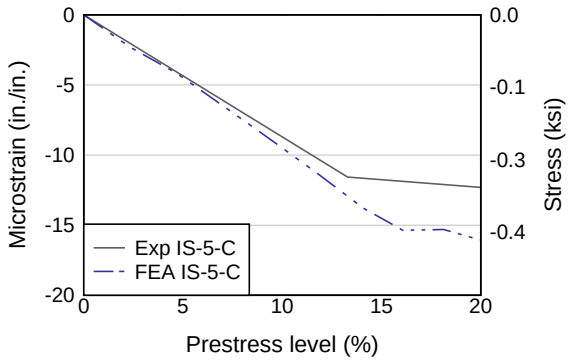

(c)

Figure 5-28 CR-70 mild steel reinforcement strain during prestress transfer, conventional end region detailing: (a) IS-1-C, (b) IS-2-C, and (c) IS-5-C

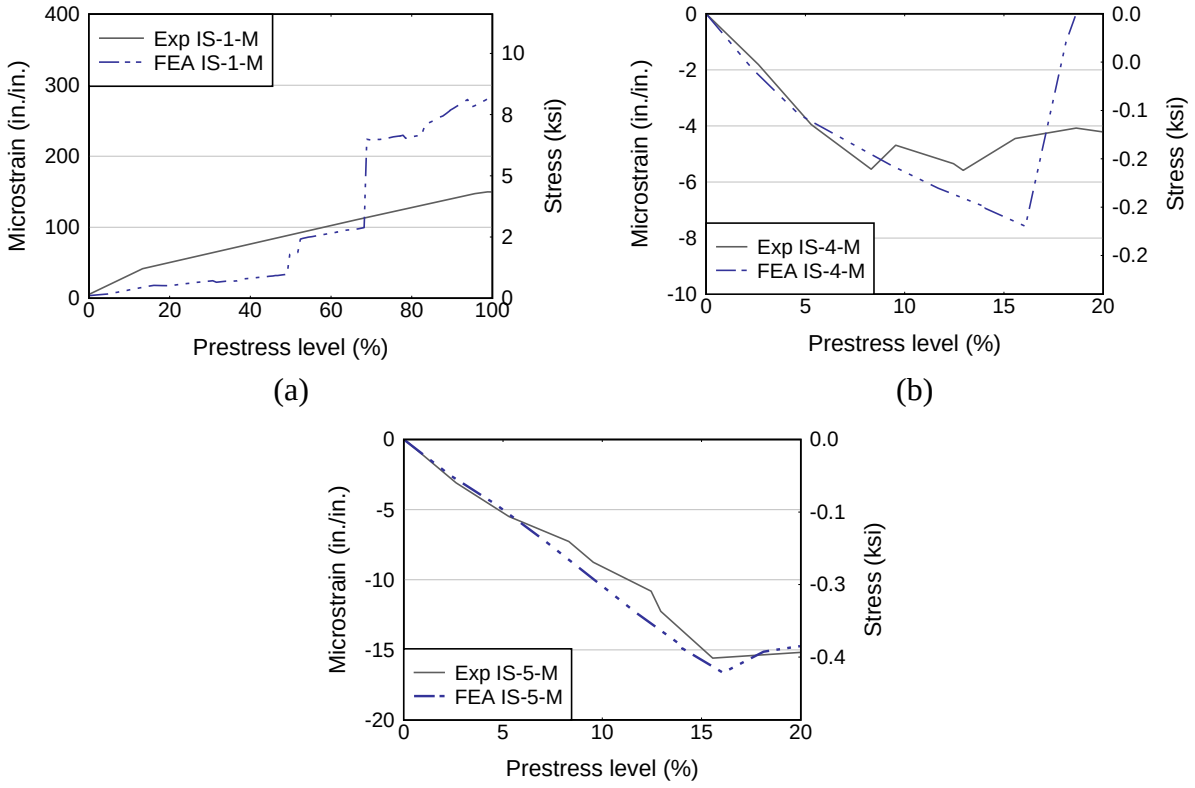

Figure 5-29 CR-70 mild steel reinforcement strain during prestress transfer, modified end region detailing: (a) IS-1-M, (b) IS-4-M, and (c) IS-5-M

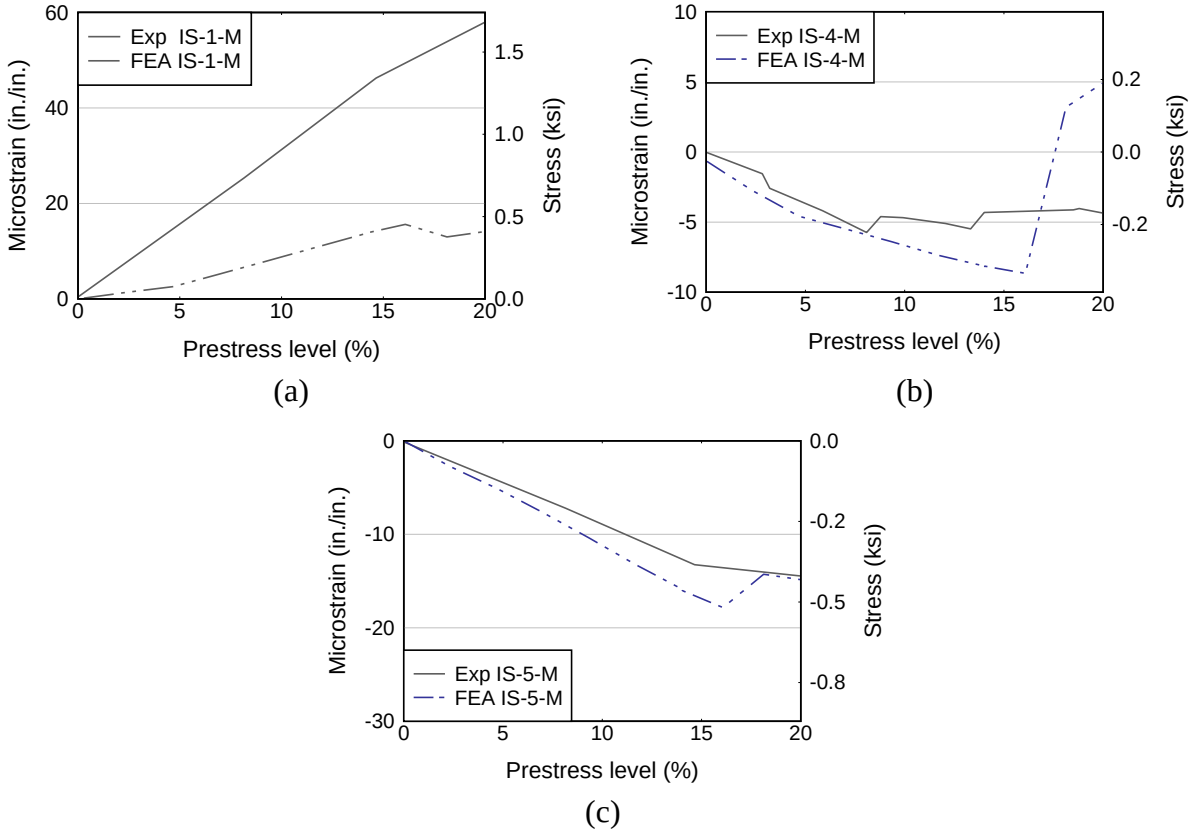

Figure 5-30 PP-50 mild steel reinforcement strain during prestress transfer, modified end region detailing: (a) IS-1-M, (b) IS-4-M, and (c) IS-5-M

5.7.2 Post-cracking behavior

For model validation after cracking occurs, four metrics were used: total crack length, total crack area, effective crack width, and maximum crack width. The same definition for these metrics as described in Section 4.9.2 was followed. Where *total crack length* (L) is the summation of the lengths of all the individual cracks within an end, *total crack area* (A) is the summation of the crack length multiplied by the respective width, e*ffective crack width* (w_e) is the total area divided by the total length and *maximum crack width* (w_{max}) is the maximum measurement taken within the web. To ensure that comparisons between the experimental and analytical crack data is representative, only the crack widths in the elements along the surface of the cross-section (Figure 5-31) were considered to determine the analytical L, A, w_e and w_{max}. In addition, a minimum crack width threshold was established to only consider elements with crack widths that would be visible during field crack monitoring. Minimum crack width threshold of 0.001 in. and 0.0015 in. were established based on the smallest crack widths measurements documented as part of the experimental investigation. Cracks smaller than the established minimum crack width threshold were not considered in the computation of the analytical L, A, w_e and w_{max}.

Figure 5-32 through Figure 5-36 show comparison of effective and maximum crack width between the simulation and the experimental girders. Figure 5-37 and Figure 5-38 show comparison of total crack length and area between the simulation and the experimental girders. In general, the model showed good agreement with effective and maximum crack widths,

however, it seem to overestimate the crack length. Comparing the total crack area, good agreement is seen between the analytical and experimental results. This indicating the simulation had a larger number of fine cracks, consistent with the larger crack length in the simulation. Considering that during the experimental investigation specimens were initially inspected with the naked eye for cracking, it is possible that fine cracks were overlooked. A minimum crack width threshold of 0.0015 in showed better prediction of end region crack widths, area and length immediately following prestress transfer. Figure 5-39 through Figure 5-43 compare end region crack pattern after prestress transfer from the experimental and analytical investigations. In general, FEA simulations showed good agreement with the experimental location and magnitude of end region cracks.

Figure 4-44 and Figure 5-45 show comparison of the strain recorded from the experimental investigation and the analytical model after prestress transfer. The strain at each instrumented reinforcement is shown relative to the bar (or gage) distance to the girder end. Table 5-6 shows the distance of each gage relative to each girder end (same for conventional and modified end). In general, reinforcement strain from the FEA shows similar pattern as the strain measurements from the experimental program, with maximum strain recorded in the bar closest to the girder end. Strain measurements taken from the mild steel reinforcement when using conventional end region detailing show that among all specimens, for both the experimental and analytical, the larger strain was recorded on specimen CT. This strain is well beyond the strain required to initiate concrete cracking. This strain converts to a steel stress of about 20 ksi in the reinforcement, which is well within the working stress level.

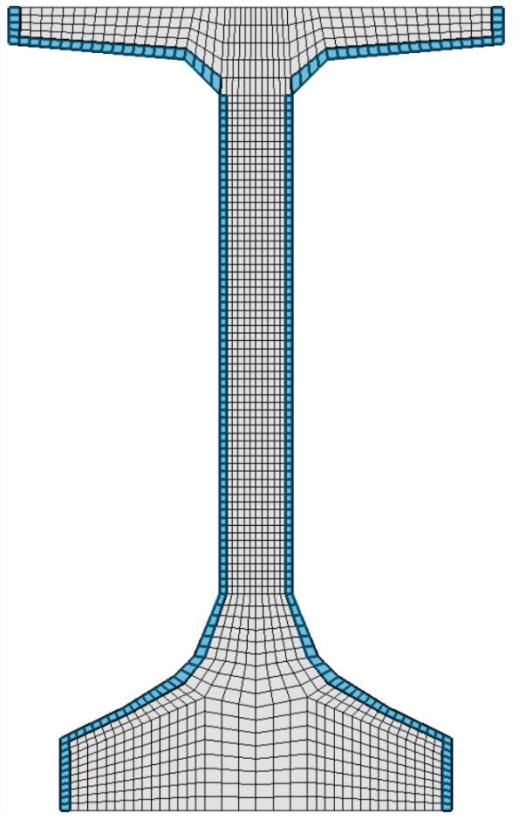

Figure 5-31 Solid elements (highlighted in blue) used to compute total crack length, area, and effective and maximum crack width.

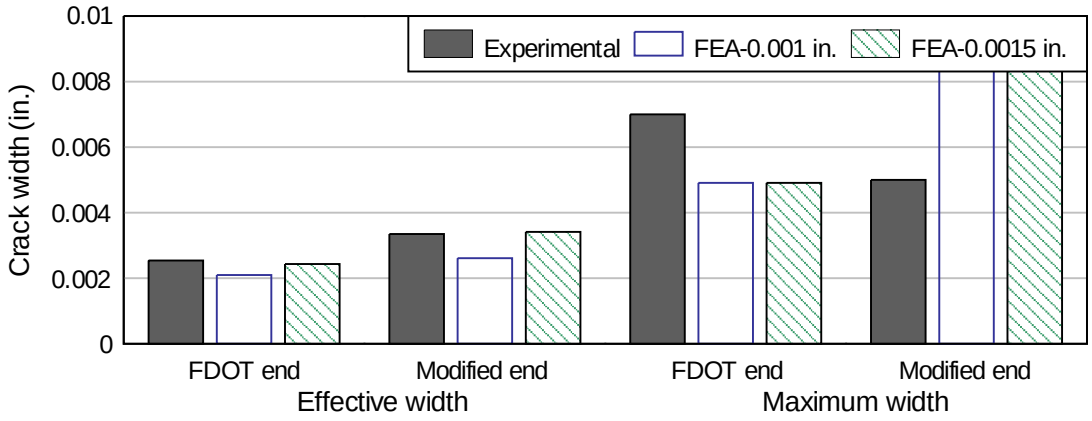

Figure 5-32 Comparison of effective and maximum crack width for specimen CT immediately following prestress transfer.

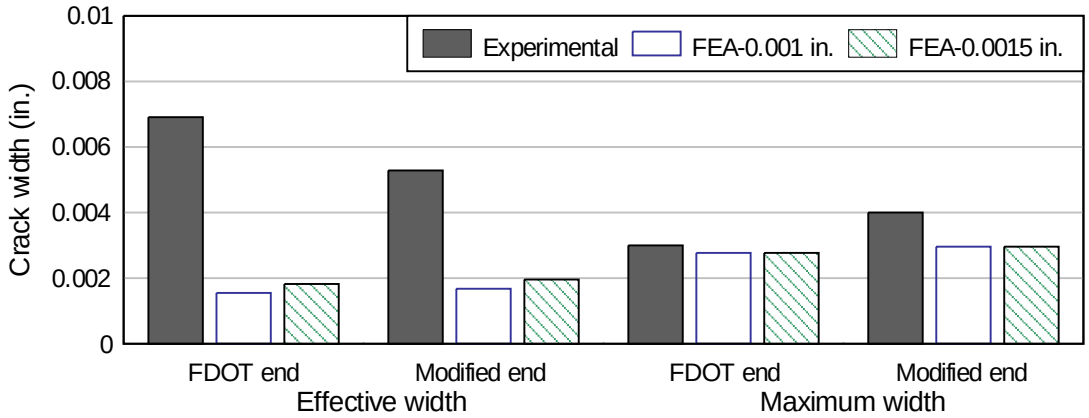

Figure 5-33 Comparison of effective and maximum crack width for specimen SH-30 immediately following prestress transfer.

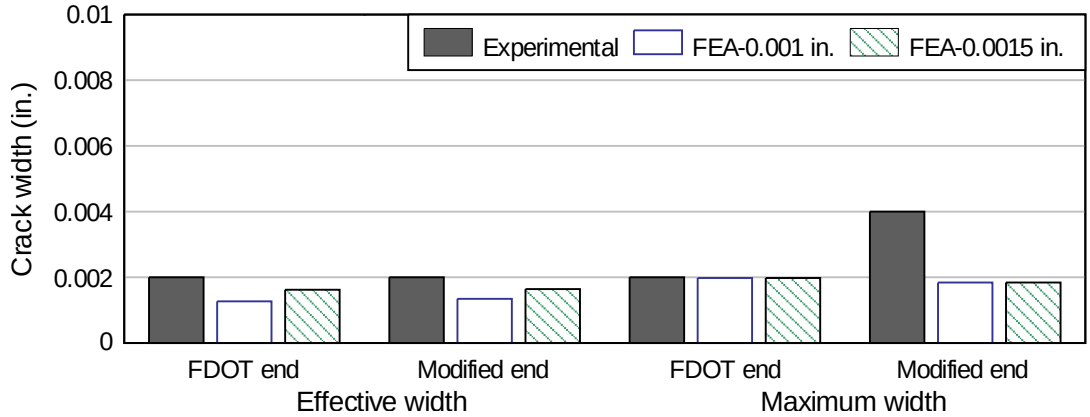

Figure 5-34 Comparison of effective and maximum crack width for specimen SH-70 immediately following prestress transfer.

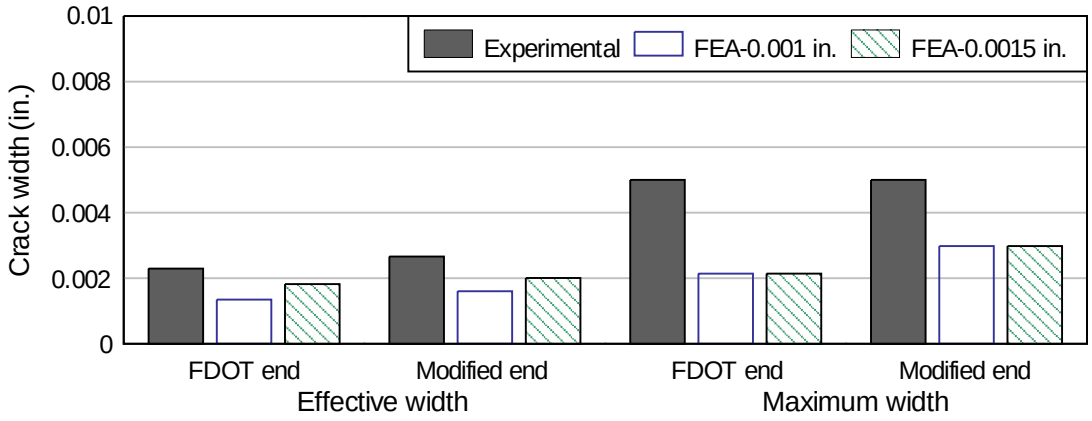

Figure 5-35 Comparison of effective and maximum crack width for specimen CR-70 immediately following prestress transfer.

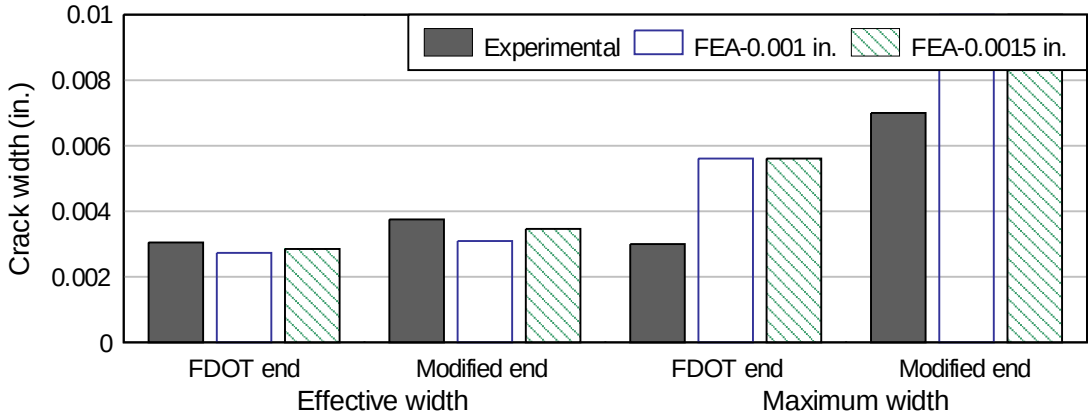

Figure 5-36 Comparison of effective and maximum crack width for specimen PP-50 immediately following prestress transfer.

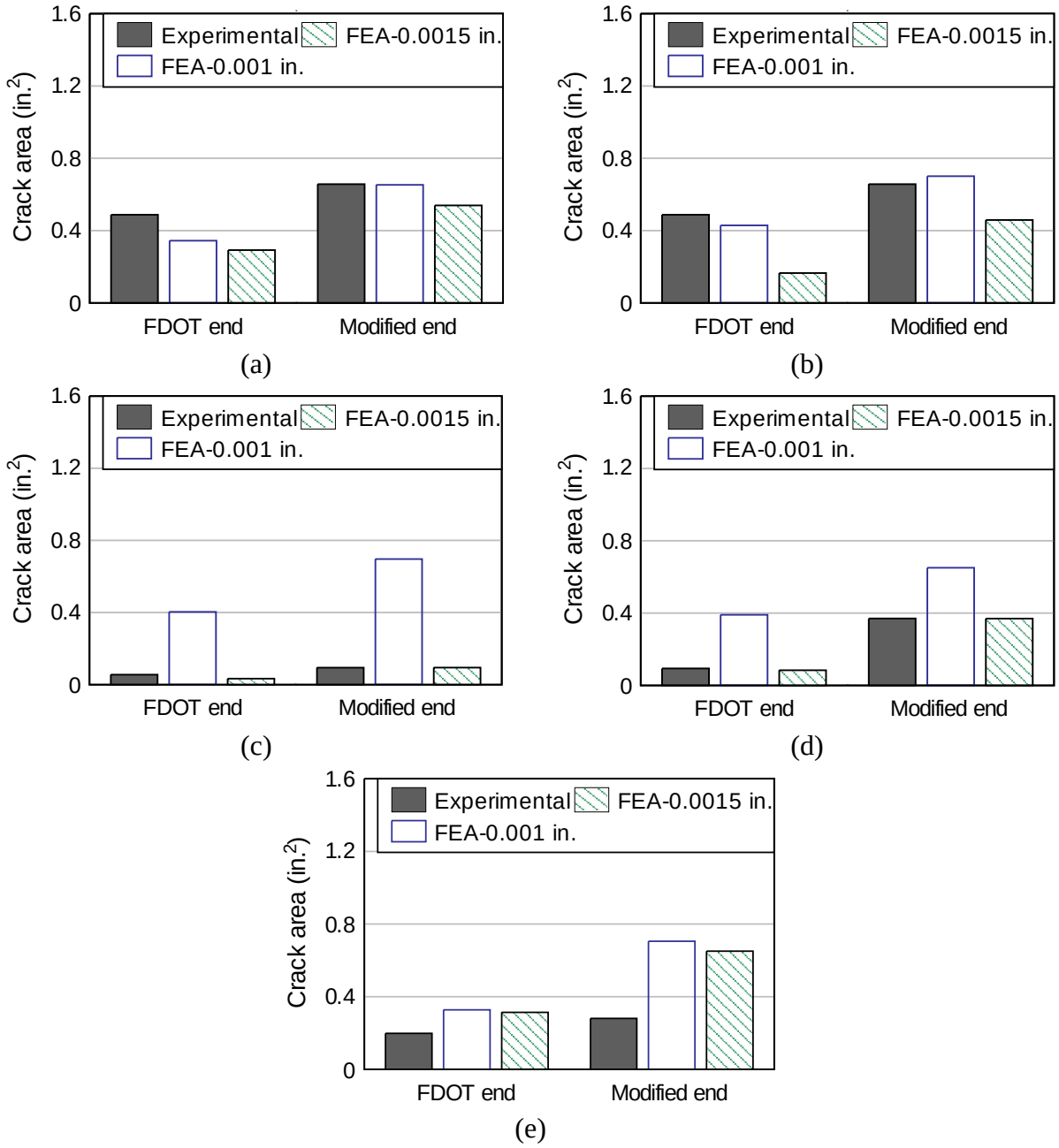

Figure 5-37 Comparison of crack area immediately following prestress transfer: (a) CT, (b) SH-30, (c) SH-70, (d) CR-70 and (e) PP-50

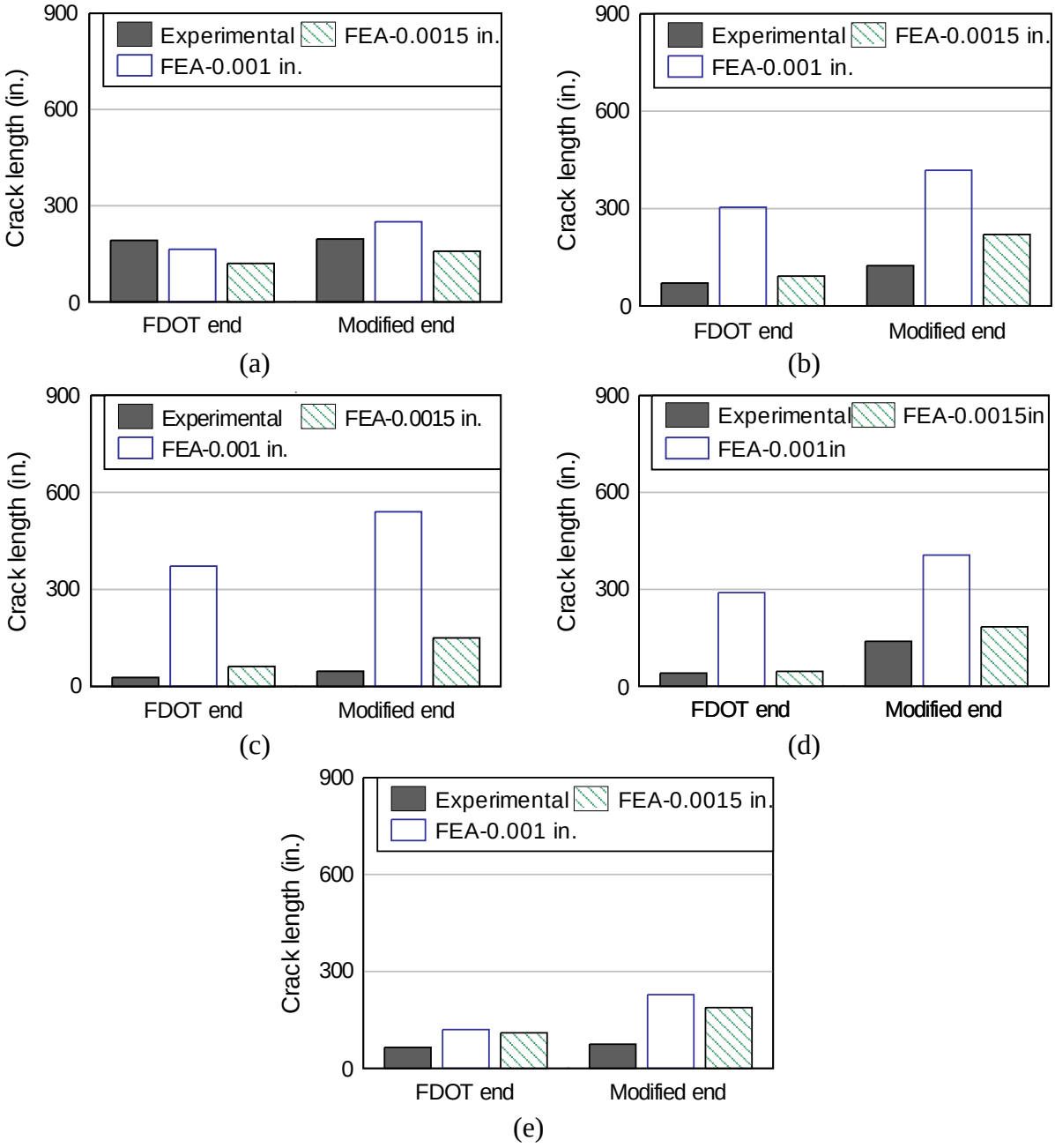

Figure 5-38 Comparison of crack length immediately following prestress transfer: (a) CT, (b) SH-30, (c) SH-70, (d) CR-70 and (e) PP-50

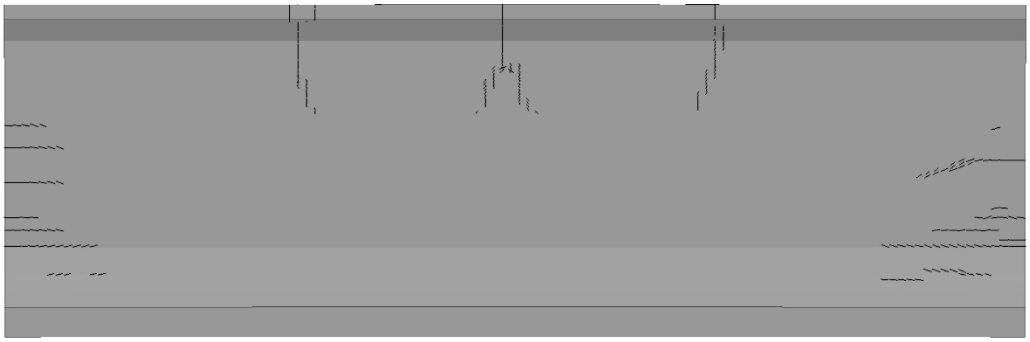

(a)

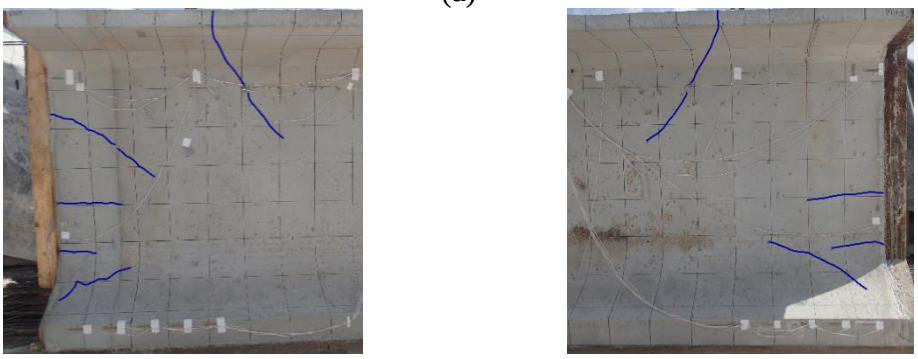

(b)

Figure 5-39 End region cracking after prestress transfer for CT specimen: (a) analytical and (b) experimental.

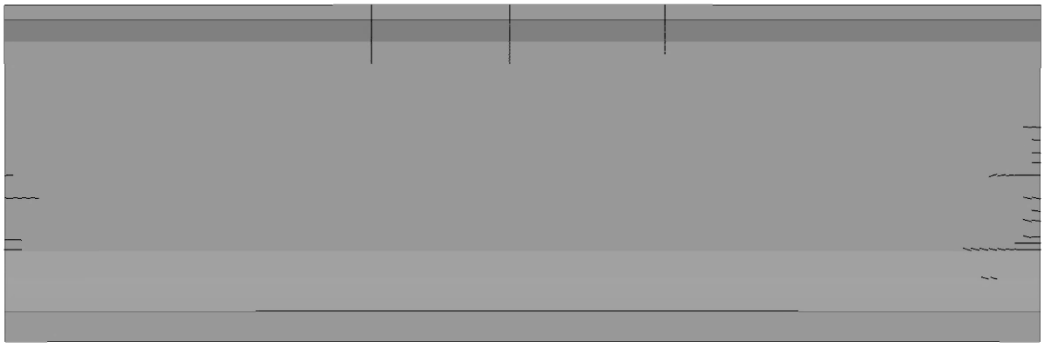

(a)

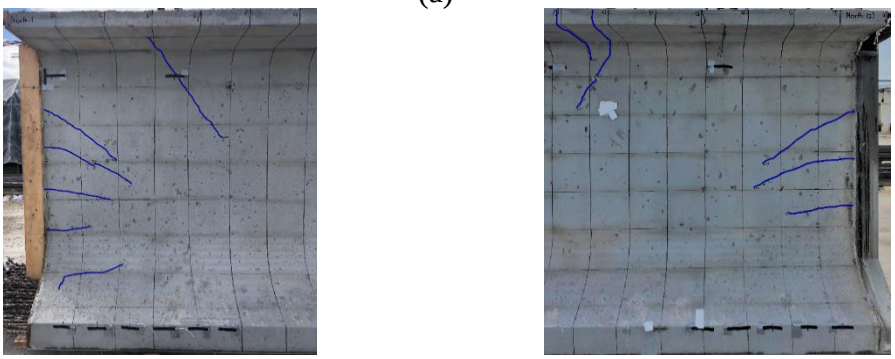

(b)

Figure 5-40 End region cracking after prestress transfer for SH-30 specimen: (a) analytical and (b) experimental.

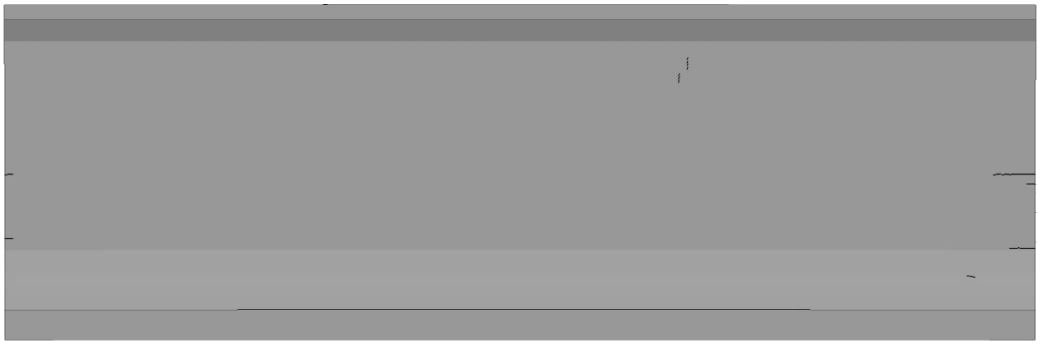

(a)

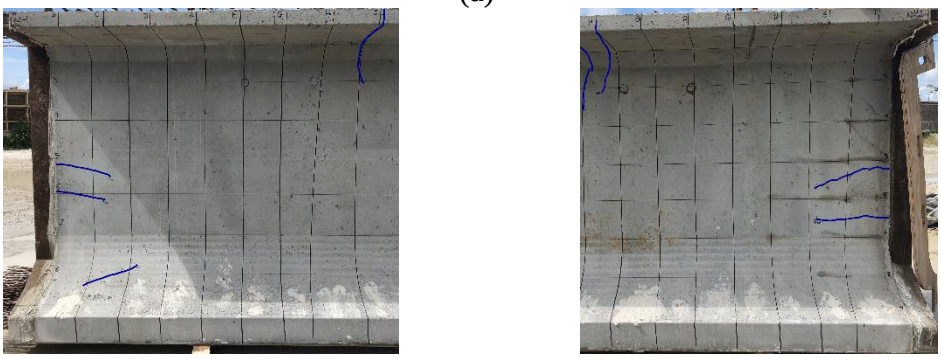

(b)

Figure 5-41 End region cracking after prestress transfer for SH-70 specimen: (a) analytical and (b) experimental.

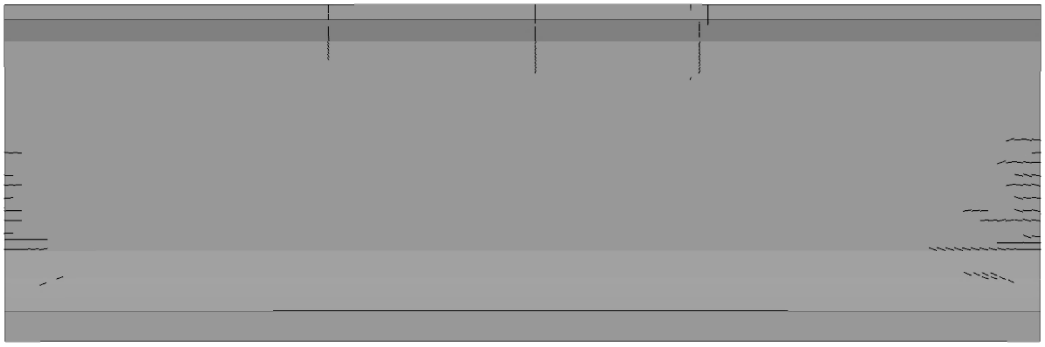

(a)

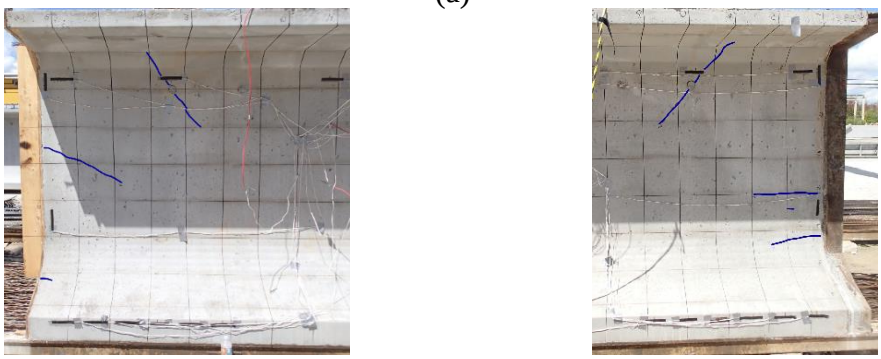

(b)

Figure 5-42 End region cracking after prestress transfer for CR-70 specimen: (a) analytical and (b) experimental.

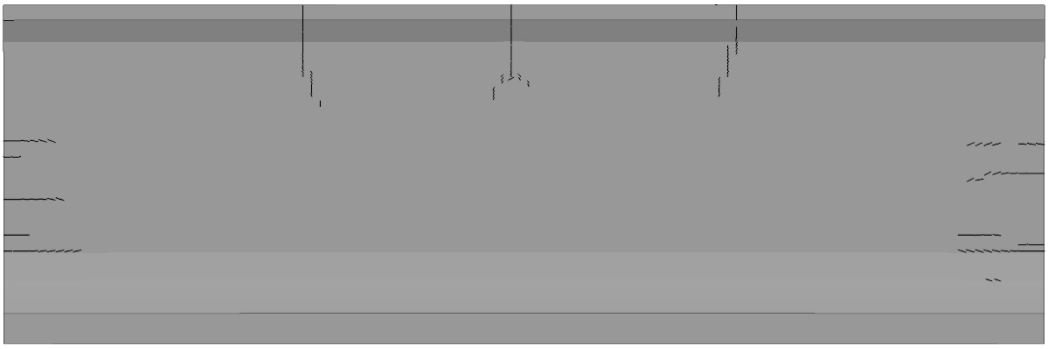

(a)

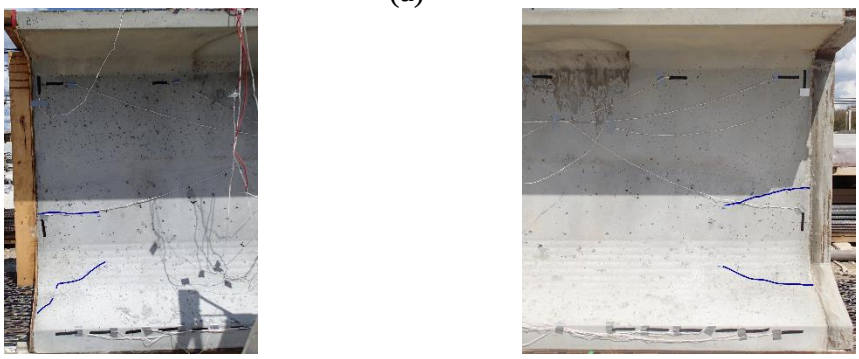

(b)

Figure 5-43 End region cracking after prestress transfer for PP-50 specimen: (a) analytical and (b) experimental.

Table 5-6 Strain gage location relative to girder end (y-direction)

Strain gage	Distance from girder end (in.)	
	Conventional	Modified
IS-1	3	6.5
IS-2	13.5	13.5
IS-3	24	20.5
IS-4	34.5	30.5
IS-5	45	40.5

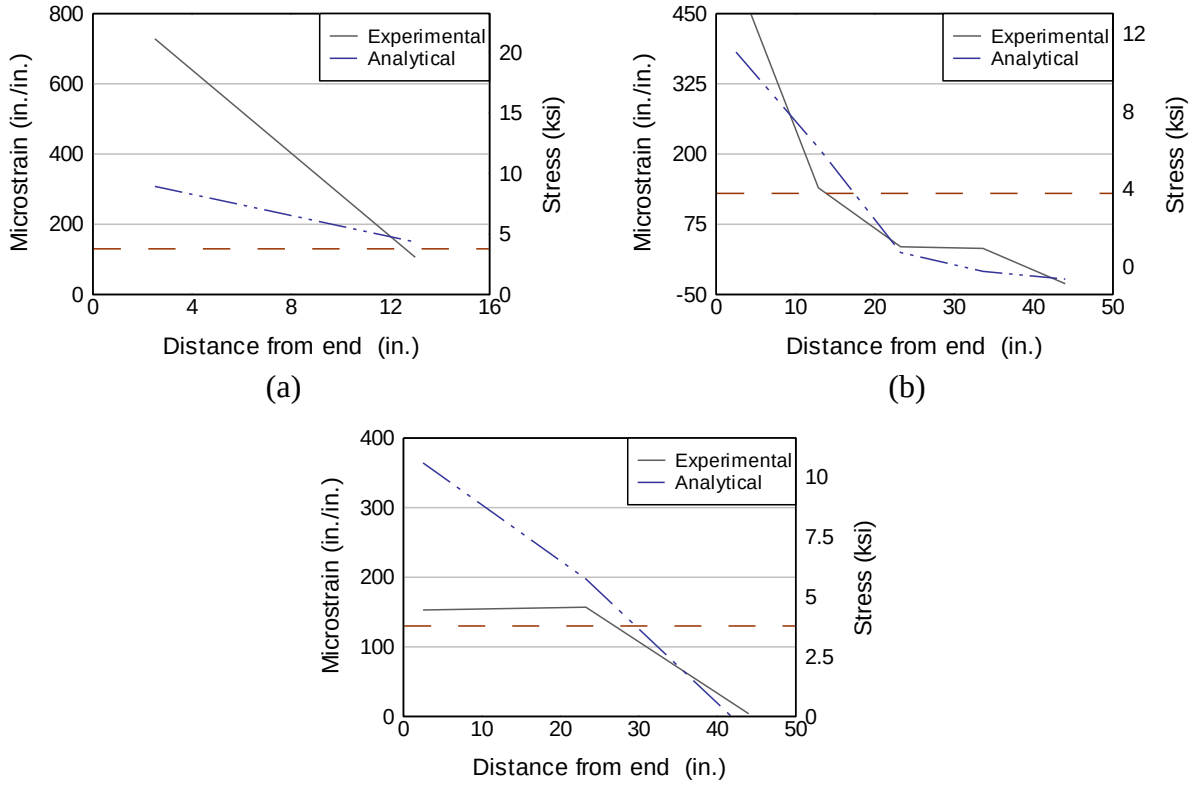

Figure 5-44 Comparison of strain in mild steel reinforcement in end with conventional end region detailing: (a) CT, (b) SH-30, and (c) CR-70

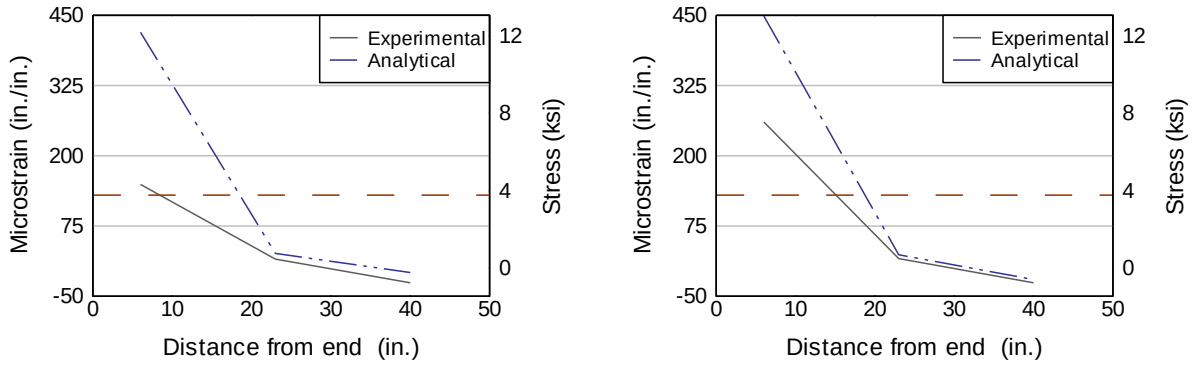

Figure 5-45 Comparison of strain in mild steel reinforcement in end with modified end region detailing: (a) CR-70 and (b) PP-50

5.8 Findings

Finite element modeling of end region cracking during and immediately following prestress transfer was conducted to better understand the behavior of the end region of prestressed FIB girders. The analytical work was divided into two stages: (1) FRC model

calibration using results from laboratory testing and (2) model validation using results from the experimental testing of end region cracking.

Key findings based on the analytical work conducted to calibrate the material models for FRC include:

- Procedures for EN-14651 offers the advantage over the ASTM C1399 that testing is not divided in stages, with continuous data collected through the entire duration of the testing. For this reason, using results from EN-14651 test makes the process of calibrating a material model less demanding.
- The smeared reinforcement technique can be used to accurately model the response of FRC at service level conditions.

Key findings based on the work conducted to validate the analytical model of full-scale prestressed girders during prestress transfer:

- Analytical model can predict end region maximum crack width and crack length immediately following prestress transfer, however, it overestimates total crack length.

6 Summary and conclusions

The objective of this study was to determine the effectiveness of macrosynthetic fibers to control end region cracking in prestressed precast concrete bridge girders. Five full-scale FIB78×20 ft. girder specimens were constructed using conventional SCC mixture as control and FRSCC mixtures formulated for this project. These new mixtures contained 0.5% macrosynthetic fibers and 0.3% and 0.7% steel fibers (on volume fraction basis) and were developed as part of this project.

The specimens were constructed in a precast yard concurrently with similar girders that were in production for a bridge project. Prestress force levels were selected at a sufficiently high level to cause bursting cracks to occur during prestress transfer. As planned, end region cracking developed in all specimens, which had characteristics similar to cracks typically observed on production girders. Cracks developed in all girders during prestress transfer and continued to lengthen and widen over the next few months.

Concrete and mild steel reinforcement strains were measured during prestress transfer. Crack widths and lengths were measured periodically over the 148 days following prestress transfer. Crack widths were measured with a portable microscope and lengths were measured and located using a grid system etched onto the girders before prestress transfer. Maximum tensile strain measured during prestress release occurred in the web within approximately 15 in. from the girder end. This confirmed other research and analytical work that emphasizes the importance of placing transverse reinforcement as close as possible to the end of the member for the most effective bursting crack control.

The following findings and conclusions can be made based on the results of the FRSCC mixture development:

- For mixing in a laboratory setting, fiber addition into the mixture after all ingredients were mixed and good SCC consistency was obtained provided better workability and fiber distribution than adding fibers along with aggregates at early stages of mixing.
- FRSCC mixtures were developed using fiber reinforcement at volumes ranging between 0.1-0.7% while still maintaining flow and passing ability properties of SCC.
- FRSCC mixtures with macrosynthetic fiber at volumes higher than 0.5% had issues with fiber clumping during mixing procedures and/or fiber nesting inside the J-Ring. This is a concern for placeability and passing ability of mixtures when incorporated into precast production.
- In general, higher fiber volumes and the use of stiffer fibers led to a higher residual strength.
- At volume fraction of 0.3%, hooked end steel fibers (SH) provided average residual strength 90% higher than basalt fibers (B) and 60% than macrosynthetic fibers (PP2).
- Hooked end steel fibers (SH) at volume of 0.3% provided similar average residual strength than the synthetic macrofiber (PP2) at a volume of 0.7%. However, under service stress, hooked end steel fibers provided residual strength up to 70% higher than the macrosynthetic fiber.
- Chemically enhanced macrofiber (PP) at a volume of 0.45% and synthetic macrofiber (PP2) had similar load-displacement response and residual strength, therefore the chemically enhanced bond did not provide significant increase in post cracking response. However, fiber PP was easier to handle and include during mixing procedures compared to PP2.

- Steel fibers (SH and CR) at volume of 0.7% provided higher residual strength than other fibers while still maintaining flowability and passing ability properties of SCC.

The following findings and conclusions can be made based on testing performed during full-scale girder production to assess concrete fresh properties and the monitoring of strains during prestress transfer include:

- Including fiber reinforcement reduced flowability and passing ability of SCC mixtures. However, during full-scale production of precast prestressed FIB girders, no issues with placement or consolidation were observed when using FRSCC mixtures with passing ability ranging between 2.5 in. and 3.25 in. Current provisions might be ineffective at assessing passing ability properties of FRSCC.
- Maximum tensile strain during prestress release occurred within first 15 in from girder end, reinforcement detailing at the end of the girder is critical to effectively controlling end region cracks.
- Maximum tensile strain in mild steel reinforcement was reduced by up to 30% when using hooked end steel fibers at 0.3%,

The following findings and conclusions can be made based on the results of the full-scale girder testing when comparing the specimens with FDOT end region reinforcement:

- The use of FRC resulted in maximum crack widths as much as 50% of those in the specimen with conventional concrete. Similarly, effective crack widths were as much as 40% of those in the specimen with conventional concrete.
- Hooked end steel fibers at volume fraction of 0.7% (SH-70) were the most effective at maintaining crack widths smaller than 0.006 in. Less than 2% of the cracks in SH-70 were larger than 0.006 in.

The following findings and conclusions can be made based on the results of the full-scale girder testing when comparing the specimens with reduced end region reinforcement:

- The use of FRC resulted in effective crack widths as much as 50% of those in the specimen with conventional concrete. Maximum crack widths in specimens with FRC, however, were of similar magnitude to those in the specimen with conventional concrete.
- Steel hooked end and steel crimped fibers at a volume of 0.7% were the most effective of the FRC mixtures at controlling end region crack widths. The number of cracks wider than 0.006 in. was reduced from 12% in control specimen to less than 7% in specimen's SH-70 and CR-70.

The following findings and conclusions can be made on the results of the full-scale girder testing when comparing the crack width distribution when using FDOT and modified end region detailing:

- FDOT end region reinforcement was effective at maintaining the majority of crack widths smaller than 0.006 in. Specimen with conventional concrete had 12% of measured crack widths larger than 0.006in, and of those only 2% were wider than 0.012 in.
- Fibers at volumes of 0.5% and 0.7% were more effective than FDOT end region reinforcement at maintaining crack widths smaller than 0.006 in. The percentage of measured cracks larger than 0.006 in. when using conventional concrete and FDOT end region reinforcement was 12%. Whereas, when end region reinforcement was reduced,

steel hooked end fibers and steel crimped fibers at volume of 0.7% had less than 7% of measured cracks larger than 0.006 in., while macrosynthetic fibers at volume of 0.5% (PP-50) had 9% of measured cracks larger than 0.006 in.

7 Implementation

End region cracking, if severe enough, can have an adverse impact on structural integrity and long-term durability of prestressed concrete bridge girders. Cracks located in critical areas may reduce ultimate strength or fatigue resistance of the element. FDOT Specifications require that crack treatment be determined based on the crack width, location, and environmental exposure to which the element will be subjected (Table 7-1). Further discussion of this is included in Section 2.1.2. This section compares crack treatment that would be required for the test girders.

Crack treatment for specimens with FDOT end region detailing:

Without the use of fibers, 13% of measured crack widths were wider than 0.006 in. and 2% of the cracks were wider than 0.012 in. Consequently, according to Table 7-1, this beam would require crack repair and engineering evaluation. The specimen with steel hooked end fibers at 0.7% had less than 2% of measured cracks wider than 0.006 in. and no cracks observed that were wider than 0.012 in. The specimen with macrosynthetic fibers at 0.5% had 7% of measured cracks wider than 0.006 in. and no cracks observed that were wider than 0.012 in. Consequently, according to Table 7-1, both of these FRC specimens would require crack repair, but not engineering evaluation. Figure 7-1a shows the total crack length that would require repair for cracks wider than 0.006 in. The specimen with hooked end steel fibers at 0.7% would require the least amount of repair and is about 10% of that required for the specimen without fibers. The specimen with 0.5% macrosynthetic fibers would require a repair length that is 60% of that required for the specimen without fibers.

Crack treatment for specimens with modified end region detailing:

Without the use of fibers, 19% of measured crack widths were wider than 0.006 in. and no cracks were wider than 0.012 in. It is not clear why cracks wider than 0.012 were observed on the specimen with FDOT detailing, but not on this specimen. In the end, however, a larger percentage of cracks wider than 0.006 were noted on this specimen rather than on the FDOT detailed specimen. According to Table 7-1, this beam would require crack repair but not engineering evaluation. Both steel fiber specimens at 0.7% fiber volume had less than 7% of measured cracks wider than 0.006 in. and no cracks observed that were wider than 0.012 in. Macrosynthetic fibers at 0.5% had 9% of measured cracks wider than 0.006 in. and no cracks observed that were wider than 0.012 in. Consequently, according to Table 7-1, both of these FRC specimens would require crack repair, but not engineering evaluation. Figure 7-1b shows the total length of crack that would require repair for all specimens. Even when crack repair is needed, FRC specimens require less repair than conventional concrete. The specimen with crimped steel fibers at 0.7% would require the least amount of repair, 30% of that required when conventional concrete is used. The specimen with macrosynthetic fibers at 0.5% would require a repair length that is 40% of that required without the use of fibers.

Table 7-1 Crack treatment per Standard Specifications for Road and Bridge Construction (FDOT, 2018)

Classification	Width (in.)	Location	Environment	Treatment
Cosmetic Crack	$w \leq 0.006$ in	Non-critical	Slight or moderate	Do not treat
			Extreme	Penetrant sealer
Minor Crack	$0.006 \leq w \leq 0.012$	Non-critical	Slight	Do not treat
			Moderate	Do not treat (elevation of more than 12 ft.) or penetrant sealer
			Extreme	Penetrant sealer (elevation of more than 12 ft.) or inject epoxy
Major Crack	$w > 0.012$	Non-critical	-	Engineering evaluation
	Any	Critical	-	Engineering evaluation

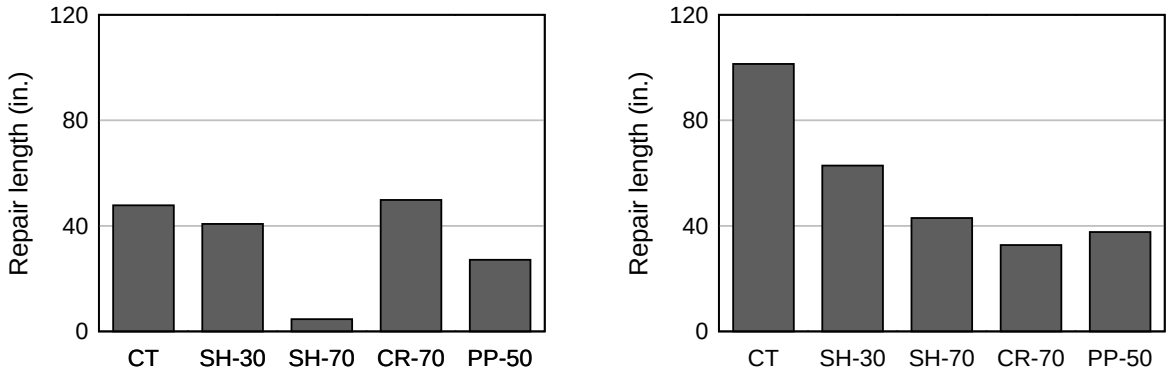

Figure 7-1 Repair length needed for cracks wider than 0.006 in. for: (a) FDOT and (b) modified end region detailing

The modified end region detailing utilized in the experimental investigation is not recommended in its current form. This detailing was designed to allow for cracks to freely propagate in order to quantify the fiber reinforcement contribution to end region crack control.

8 Future research

This study covered the evaluation of effectiveness of FRC mixtures at volumes ranging between 0.3% and 0.7%. It is recommended that the effect of using higher fiber volumes ranging between 0.7% and 1% be investigated. In combination with mild steel reinforcement, these volumes could potentially eliminate end region cracks wider than 0.006 in.

During the investigation, end region cracks were monitored for a period of 5 months after prestress transfer. Even when it is not expected that end region cracks continue to grow after this period, long-term exposure and monitoring of one or more of the specimens from this research is recommended to determine if durability of the steel fibers is a concern. Long-term monitoring of end region cracks, in addition to coring of specimen to evaluate if corrosion of the fibers or mild steel reinforcement near areas of cracks has occurred are recommended.

The implementation of fiber reinforced concrete in prestressed girders can provide, in addition to crack control, enhanced strength and ductility when compared to conventional concrete. The authors recommend that the contribution of fiber reinforcement to shear strength in prestressed girders be evaluated. Recommended mixture proportions, specimen design and test procedures to evaluate fiber contribution to shear strength are provided as part of Appendix G.

Including fiber reinforcement is expected to cause reduction in flowability and passing ability of SCC mixtures. However, during full-scale production of precast prestressed FIB girders, no issues with placement or consolidation were observed when using well-prepared FRSCC mixtures with passing ability ranging between 2.5 in. and 3.25 in. This is well above current FDOT limits for passing ability of SCC. The authors recommend that additional investigations are conducted focused on development of acceptance criteria for fresh properties of FRSCC.

This investigation covered synthetic, basalt, and steel fibers to evaluate contribution to residual strength. The extent to which concrete mechanical properties are improved is dependent on the fiber mechanical properties, geometry, and dosage. It is recommended that additional research be conducted with the focus on establishing minimum FRC characteristics for replacement of reinforcement in prestressed bridge girders, including but not limited to residual tensile strength and fiber ultimate tensile strength.

The present study focused on the effectiveness of FRC at controlling web cracking, however, is possible that fiber bridging action can provide resistance to bursting stresses generated in the bottom flange of prestressed girders, offering an alternative to conventional confinement reinforcement. Reduced cracking was qualitatively observed in the bulb during the present testing, and it is recommended that partial or complete replacement of conventional confinement reinforcement with fiber reinforced concrete be investigated.

References

ACI. (2008). Building Code Requirements for Structural Concrete and Commentary ACI 318-14. Farmington Hills, MI: American Concrete Institute (ACI).

ACI Committee 544. (1996). *544.1R-96: State-of-the-Art Report on Fiber Reinforced Concrete*. Farmington Hills, MI: American Concrete Institute (ACI).

ACI Committee 544. (2002). *544.4R-88: Design Considerations for Steel Fiber Reinforced*. Farmington Hills, MI: American Concrete Institute (ACI).

ACI Committee 544. (2008). *544.3R-08: Guide for Specifying, Proportioning, and Production of Fiber-Reinforced Concrete*. Farmington Hills, MI.

Altoubat, S., Yazdanbakhsh, A., & Rieder, K.-A. (2009). Shear Behavior of Macro-Synthetic Fiber-Reinforced Concrete Beams without Stirrup. *Aci Struct J*, *107*, 597–606.

American Association of State Highway and Transportation Officials. (2017). *AASHTO LRFD Bridge Design Specifications* (8th ed.). Washington, DC.

Amin, A., & Foster, S. J. (2016). Shear strength of steel fibre reinforced concrete beams with stirrups. *Engineering Structures*, *111*, 323–332.

Araújo, D. D. L., Nunes, F. G. T., Toledo Filho, R. D., & Andrade, M. A. S. de. (2014). Shear strength of steel fiber-reinforced concrete beams. *Acta Scientiarum. Technology*, *36*, 389.

Arslan, M. E. (2016). Effects of basalt and glass chopped fibers addition on fracture energy and mechanical properties of ordinary concrete: CMOD measurement. *Construction and Building Materials*, *114*, 383–391.

ASTM C1116. (2015). Standard specification for Fiber-Reinforced Concrete. ASTM International, West Conshohocken, PA.

ASTM C1399. (2010). Standard Test Method for Obtaining Average Residual-Strength of Fiber-Reinforced. ASTM International, West Conshohocken, PA.

ASTM C150. (2019). Standard Specifications for Portland Cement. ASTM International, West Conshohocken, PA.

ASTM C1550. (2012). Standard Test Method for Flexural Toughness of Fiber Reinforced Concrete (Using Centrally Loaded Round Panel). ASTM International, West Conshohocken, PA.

ASTM C1609. (2012). Standard Test Method for Flexural Performance of Fiber-Reinforced Concrete (Using Beam With Third-Point Loading). ASTM InternationalWest Conshohocken, PA.

ASTM C1610. (2014). Standard Test Method for Static Segregation of Self-Consolidating Concrete Using Column Technique. ASTM International, West Conshohocken, PA.

ASTM C1611. (2014). Standard Test Method for Slump Flow of Self-Consolidating Concrete. ASTM International, West Conshohocken, PA.

ASTM C1621. (2014). Standard Test Method for Passing Ability of Self-Consolidating Concrete by J-Ring. ASTM International, West Conshohocken, PA.

ASTM C1712. (2015). Standard Test Method for Rapid Assessment of Static Segregation Resistance of Self- Consolidating Concrete Using Penetration Test. ASTM International, West Conshohocken, PA.

ASTM C232. (2014). Standard Test Methods for Bleeding of Concrete. ASTM International, West Conshohocken, PA.

ASTM C260. (2010). Standard Specification for Air-Entraining Admixtures for Concrete. *American Society for Testing and Materials.* ASTM International, West Conshohocken, PA.

ASTM C39. (2015). Standard Test Method for Compressive Strength of Cylindrical Concrete

Specimens. ASTM International, West Conshohocken, PA.
ASTM C494. (2017). Standard Specification for Chemical Admixtures for Concrete. ASTM International, West Conshohocken, PA.
ASTM C618. (2019). Standard Specification for Coal Fly Ash and Raw or Calcined Natural Pozzolan for Use in Concrete. ASTM International, West Conshohocken, PA.
ASTM C995. (2001). Standard Test Method for Time of Flow of Fiber-Reinforced Concrete Through Inverted Slump Cone. ASTM International, West Conshohocken, PA.
ASTM STP 169D. (2006). *Significance of Tests and Properties of Concrete and Concrete-Making in: J.F. Lamond, J.H. Pielert (Eds.)*. ASTM International, West Conshohocken, PA.: ASTM, 2006.
Attiogbe, E., Schaef, S., Kerobo, C., Vojtko, D., & Nmai, C. (2014). A New Fiber for Enhanced Crack Control. *Concrete International*, *36*, 35–40.
Aydin, A. C. (2007). Self compactability of high volume hybrid fiber reinforced concrete. *Construction and Building Materials*, *21*, 1149–1154.
Ayub, T., Shafiq, N., & Nuruddin, M. F. (2014a). Effect of Chopped Basalt Fibers on the Mechanical Properties and Microstructure of High Performance Fiber Reinforced Concrete. *Advances in Materials Science and Engineering*, *2014*, 1–14.
Ayub, T., Shafiq, N., & Nuruddin, M. F. (2014b). Mechanical properties of high-performance concrete reinforced with basalt fibers. *Procedia Engineering*, *77*, 131–139.
Balaguru, P., & Ramakrishnan, V. (1988). Properties of Fiber Reinforced Concrete: Workability, Behavior Under Long-Term Loading, and Air-Void Characteristics. *ACI Materials Journal*, *85*, 189–196.
Banthia, N., Bindiganavile, V., Jones, J., & Novak, J. (2012). Fiber-reinforced concrete in precast concrete applications: Research leads to innovative products. *PCI Journal*, *7*, 33–46.
Bayasi, M. Z., & Soroushian, P. (1992). Effect of steel fiber reinforcement on fresh mix properties of concrete. *ACI Materials Journal*, *89*, 369–374.
Belytchko, T., & Bindeman, P. (1993). Assumed strain stabilization of the eight node hexahedral element Ted. *Computer Methods in Applied Mechanics and Engineering*, *105*, 225–260.
Bendtsen, B., & Sanjayan, J. G. (2015). Assessment of shear capacity methods of steel fiber reinforced concrete beams using full scale prestressed bridge beams. *Materials and Structures/Materiaux et Constructions*, *48*, 3473–3483.
Bernard, E. (2010a). Durability of cracked fibre reinforced shotcrete. *Shotcrete: More Engineering Developments*, 59–66.
Bernard, E. (2010b). Influence of fiber type on creep deformation of cracked fiber-reinforced shotcrete panels. *ACI Materials Journal*, *107*, 474–480.
Berrocal, C. G., Lundgren, K., & Löfgren, I. (2016). Corrosion of steel bars embedded in fibre reinforced concrete under chloride attack: State of the art. *Cement and Concrete Research*, *80*, 69–85.
Blanco, A. (2013). *Characterization and modelling of SFRC elements*. Universitat Politècnica de Catalunya.
Blunt, J., Jen, G., & Ostertag, C. P. (2015). Enhancing corrosion resistance of reinforced concrete structures with hybrid fiber reinforced concrete. *Corrosion Science*, *92*, 182–191.
Bolat, H., Şimşek, O., Çullu, M., Durmuş, G., & Can, Ö. (2014). The effects of macro synthetic fiber reinforcement use on physical and mechanical properties of concrete. *Composites Part B: Engineering*, *61*, 191–198.
Branston, J., Das, S., Kenno, S. Y., & Taylor, C. (2016). Influence of basalt fibres on free and

restrained plastic shrinkage. *Cement and Concrete Composites*, *74*, 182–190.
BS 1881-117: 1983. (1983). Method for determination of splitting tensile strength. BSI, London.
BS EN 12350-10. (2010). Testing fresh concrete Part 10: Self-compacting concrete - L box test. British Standards Institution (BSI).
BS EN 12350-9. (2010). Testing fresh concrete Part 9: Self-compacting concrete - V-funnel test. British Standards Institution (BSI).
BS EN 12350. (2009). Testing Fresh Concrete- Part 3: Vebe Test. British Standards Institution (BSI).
Chen, W. F. (1969). Double punch test for tensile strength of concrete, Sept (70-18) PB224770/AS (NTIS). *Fritz Laboratory Reports*, *356.7*.
Cook, R., Malkus, D., Plesha, M., & Witt, R. (2014). *Concepts and Applications of Finite Element Analysis* (4th ed.). John Wiley & Sons, Incorporated.
Cucchiara, C., La Mendola, L., & Papia, M. (2004). Effectiveness of stirrups and steel fibres as shear reinforcement. *Cement and Concrete Composites*, *26*, 777–786.
Dhonde, H. B., Mo, Y. L., & Hsu, T. T. C. (2005). *Fiber Reinforcement in Prestressed Concrete Beams*. Austin, TX.
Earney, T. P. (2002). *Girder-End Cracking in Prestressed I-Girders*. Columbia, MO.
EFNARC. (2002). Specification and Guidelines for Self-Compacting Concrete, English edition. Norfolk, UK: European Federation for Specialist Con- struction Chemicals and Concrete Systems.
EN 14651. (2005). Test method for metallic fibred concrete - Measuring the flexural tensile strength (limit of proportionality (LOP), residual). European Committee for Standardization (CEN), Brussels, Belgium.
Eren, Ö., & Marar, K. (2010). Effect of steel fibers on plastic shrinkage cracking of normal and high strength concretes. *Materials Research*, *13*, 135–141.
Ferrara, L., Park, Y. D., & Shah, S. P. (2007). A method for mix-design of fiber-reinforced self-compacting concrete. *Cement and Concrete Research*, *37*, 957–971.
Florida Department of Transportation (FDOT). (2015). Materials Manual. Florida Department of Transportation, Tallahassee, FL.
Florida Department of Transportation (FDOT). (2016). *Structures Design Guidelines* (Vol. 1). Florida Department of Transportation, Tallahassee, FL.
Florida Department of Transportation (FDOT). (2018). *Standard Specifications for Road and Bridge Construction*. *Concrete*. Florida Department of Transportation, Tallahassee, FL.
Folliard, K., Sutfin, D., Turner, R., & Whitney, D. P. (2006). Fiber in Continuously Reinforced Concrete Pavements, Report FHWA/TX-07/0-4392-2, *7*.
Forgeron, D., & Omer, A. (2010). Flow Characteristics of Macro-Synthetic Concrete.
Frazão, C., Camões, A., Barros, J., & Gonçalves, D. (2015). Durability of steel fiber reinforced self-compacting concrete. *Construction and Building Materials*, *80*, 155–166.
Furlan, S., & Hana, J. B. De. (1997). Shear Behaviour of Fiber Reinforced Concrete Beams. *Cement and Concrete Composites*, *19*, 359–366.
Gencel, O., Brostow, W., Datashvili, T., & Thedford, M. (2011). Workability and mechanical performance of steel fiber-reinforced self-compacting concrete with fly ash. *Composite Interfaces*, *18*, 169–184.
Groth, P. (2000). *Steel fiber reinforced SCC*.
Grünewald, S. (2004). *Performance-based design of self-compacting fibre reinforced concrete*. Delft University of Technology.

Grünewald, S., Ferrara, L., & Dehn, F. (2016). Flowable Fibre-Reinforced Concrete : Progress in Understanding and Development of Design Standards. *8th International RILEM Symposium on Self-Compacting Concrete - SCC 2016*, 467–477.

Gurjar, A. H. (2004). *Mix Design And Testing Of Self-Consolidating Concrete Using Florida Materials (Florida Department of Transportation Research Report BD 503)*. Daytona Beach, FL.

Hamilton, H., Consolazio, G., & Ross, B. (2013). *End region detailing of pretensioned concrete bridge girders (Florida Department of Transportation Research Report BDK75 977-05)*. Gainesville, FL.

Haroon, S. A., Yazdani, N., & Tawfiq, K. (2004). Feasibility of Steel Fiber Concrete in End Zones of Posttensioned Bridge Girders Results of Special Anchorage-Device Acceptance Test. *Transportation Research Record 1892*, 117–125.

Hognestad, E. (1951). *A Study of Combined Bending and Axial Load in Reinforced Concrete Members*. Bulletin Series No. 399, Engineering Experiment Station, Urbana, USA: University of Illinois.

Ideker, J., Banuelos, J. (2014). *The use of synthetic blended fibers to reduce cracking risk in high performance concrete*. Salem, OR.

Iyer, P., Kenno, S. Y., & Das, S. (2015). Mechanical Properties of Fiber-Reinforced Concrete Made with Basalt Filament Fibers. *Journal of Materials in Civil Engineering*, *27*, 04015015.

Jen, G., Trono, W., & Ostertag, C. P. (2016). Self-consolidating hybrid fiber reinforced concrete: Development, properties and composite behavior. *Construction and Building Materials*, *104*, 63–71.

Jiang, C., Fan, K., Wu, F., & Chen, D. (2014). Experimental study on the mechanical properties and microstructure of chopped basalt fibre reinforced concrete. *Materials and Design*, *58*, 187–193.

Khaloo, A., Raisi, E. M., Hosseini, P., & Tahsiri, H. (2014). Mechanical performance of self-compacting concrete reinforced with steel fibers. *Construction and Building Materials*, *51*, 179–186.

Kizilkanat, A. B., Kabay, N., Akyüncü, V., Chowdhury, S., & Akça, A. H. (2015). Mechanical properties and fracture behavior of basalt and glass fiber reinforced concrete: An experimental study. *Construction and Building Materials*, *100*, 218–224.

Kosa, K., & Naaman, A. (1990). Corrosion of Steel Fiber Reinforced Concrete. *ACI Materials Journal*, *87*, 27–37.

Krassowska, J., & Lapko, A. (2013). The Influence of Steel and Basalt Fibers on the Shear and Flexural Capacity of Reinforced Concrete Beams. *Journal of Civil Engineering and Architecture*, *7*, 789–795.

Kurtz, S., & Balaguru, P. (2000). Postcrack creep of polymeric fiber-reinforced concrete in flexure. *Cement and Concrete Research*, *30*, 183–190.

Kwak, Y., Eberhard, M. O., Kim, W., & Kim, J. (2002). Shear Strength of Steel Fiber-Reinforced Concrete Beams without Stirrups. *ACI Structural Journal*, *99*, 1–9.

Lawler, J. S., Zampini, D., & Shah, S. P. (2005). Microfiber and Macrofiber Hybrid Fiber-Reinforced Concrete. *Journal of Materials in Civil Engineering*, *17*, 595–604.

Livermore Software Technology Corporation (LSTC). (2014). *Keyword User ' S Manual* (Vol. II). Livermore, California: Livermore Software Technology Corporation.

Livermore Software Technology Corporation (LSTC). (2016). *Keyword User ' S Manual* (Vol.

I). Livermore, California: Livermore Software Technology Corporation.
Livermore Software Technology Corporation (LSTC). (2018a). *Keyword User's Manual (Vol. I)*. Livermore, California: Livermore Software Technology Corporation.
Livermore Software Technology Corporation (LSTC). (2018b). *Keyword User's Manual (Vol. II)*. Livermore, California: Livermore Software Technology Corporation.
Majdzadeh, F., Soleimani, S. M., & Banthia, N. (2006). Shear strength of reinforced concrete beams with a fiber concrete matrix. *Canadian Journal of Civil Engineering*, *33*, 726–734.
Mansur, M. ., Ong, K. C. ., & Paramasivam, P. (1986). Shear Strength of Fibrous Concrete beams without stirrups. *Journal of Structural*, *112*, 2066–2079.
Markovic, I. (2006). *High-Performance Hybrid-Fibre Concrete*. Delft University of Technology.
Mobasher, B. (2011). Mechanics of Fiber and Textile Reinforced Cement Composites, 1–8.
Mondo, E. (2011). *Shear Capacity of Steel Fibre Reinforced Concrete Beams without Conventional Shear Reinforcement*. Royal Institute of Technology (KTH), Stockholm, Sweden, 2011.
Murray, Y., Abu-Odeh, A., & Bligh, R. (2007). *Evaluation of LS-DYNA Concrete Material Model 159*. *Federal Highway Administration*.
Naaman, A. E., Wongtanakitcharoen, T., & Hauser, G. (2005). Influence of different fibers on plastic shrinkage cracking of concrete. *ACI Materials Journal*, *102*, 49–58.
Narayanan, R., & Darwish, I. Y. S. (1987). Use of Steel Fibers As Shear Reinforcement. *ACI Structural Journal*, *84*, 216–227.
Nehdi, M., & Ladanchuk, J. D. (2004). Fiber synergy in fiber-reinforced self-consolidating concrete. *ACI Materials Journal*, *101*, 508–517.
Ning, X., Ding, Y., Zhang, F., & Zhang, Y. (2015). Experimental study and prediction model for flexural behavior of reinforced SCC beam containing steel fibers. *Construction and Building Materials*, *93*, 644–653.
Noghabai, K. (2000). Beam of fibreous concrete in shear and bending: exoeriment and model. *Journal of Structural Engineering*, *126*, 243–251.
Okumus, P., & Oliva, M. G. (2014). Evaluation of crack control methods for end zone cracking in prestressed concrete bridge girders. *PCI Journal*, *58*, 91–105.
Oliva, M. G., & Okumus, P. (2011). *Finite element analysis of deep wide-flanged pre-stressed girders to understand and control end cracking*. Madison, WI.
Ozyurt, N., Mason, T. O., & Shah, S. P. (2007). Correlation of fiber dispersion, rheology and mechanical performance of FRCs. *Cement and Concrete Composites*, *29*, 70–79.
Patnaik, A. (2013). *Gen 3.1 MiniBar^{TM} Reinforced Concrete (MRC)*. Akron, OH.
Pauw, A. (1960). Static Modulus of Elasticity of Concrete as Affected by Density. *ACI Journal Proceedings*, *57*, 679–688.
PrUNE 83515. (2010). *Fibre reinforced concrete. Determination of cracking strength, ductility and residual tensile strength. Barcelona Test.* Asociación Española de Normalización y Certificación Madrid (AENOR), Madrid.
Qi, C., Weiss, J., & Olek, J. (2003). Characterization of plastic shrinkage cracking in fiber reinforced concrete using image analysis and a modified Weibull function. *Materials and Structures*, *36*, 386–395.
Qian, C. X., & Stroeven, P. (2000). Development of hybrid polypropylene-steel fibre-reinforced concrete. *Cement and Concrete Research*, *30*, 63–69.
Ramakrishnan, V., Brandshaug, T., Coyle, W. V, & Schrader, E. K. (1980). A Comparative Evaluation of Concrete Reinforced with Straight Steel Fibers and Fibers with Deformed

Ends Glued Together into Bundles. *ACI Journal Proceedings*, *77*, 135–143.
Sahmaran, M., & Yaman, I. O. (2007). Hybrid fiber reinforced self-compacting concrete with a high-volume coarse fly ash. *Construction and Building Materials*, *21*, 150–156.
Sanjuán, M. A., Andrade, C., & Bentur, A. (1997). Effect of crack control in mortars containing polypropylene fibers on the corrosion of steel in a cementitious matrix. *ACI Materials Journal*, *94*, 134–141.
Sanjuán, M. A., Andrade, C., & Bentur, A. (1998). Effect of polypropylene fibre reinforced mortars on steel reinforcement corrosion induced by carbonation. *Materials and Structures*, *31*, 343–349.
Schlaich, J., Schafer, K., & Jennewein, M. (1987). Toward a Consistent Design of Structural Concrete. *J. Prestressed Concrete Inst.*, *32*, 74–150.
Schwer, L. (2014). Modeling rebar: The forgotten sister in reinforced concrete modeling, 1–28.
Serna, P., Martí-Vargas, J. R., Bossio, M. E., & Zerbino, R. (2015). Creep and residual properties of cracked macro-synthetic fibre reinforced concretes. *Magazine of Concrete Research*, *68*, 197–207.
Sharma, A. K. (1986). Shear Strength of Steel Fiber Reinforced Concrete Beams. *ACI Journal Proceedings*, *83*, 624–628.
Siddique, R., Kaur, G., & Kunal. (2016). Strength and permeation properties of self-compacting concrete containing fly ash and hooked steel fibres. *Construction and Building Materials*, *103*, 15–22.
Sivakumar, A., & Santhanam, M. (2007). Mechanical properties of high strength concrete reinforced with metallic and non-metallic fibres. *Cement and Concrete Composites*, *29*, 603–608.
Solgaard, A. O. S., Carsana, M., Geiker, M. R., Küter, A., & Bertolini, L. (2013). Experimental observations of stray current effects on steel fibres embedded in mortar. *Corrosion Science*, *74*, 1–12.
Soliman, A. E. K. S., & Osman, M. A. M. (2012). Efficiency of using discrete fibers on the shear behavior of R.C. beams. *Ain Shams Engineering Journal*, *3*, 209–217.
Soroushian, P., Plasencia, J., & Ravanbakhsh, S. (2004). Assessment of Reinforcing Effects of Recycled Plastic and Paper in Concrete. *ACI Materials Journal*, *100*, 203–207.
Soutsos, M. N., Le, T. T., & Lampropoulos, A. P. (2012). Flexural performance of fibre reinforced concrete made with steel and synthetic fibres. *Construction and Building Materials*, *36*, 704–710.
Strauss, D. A., Silva, F. de A., & Toledo Filho, R. D. (2014). Mechanical behavior of hybrid steel-fiber self-consolidating concrete: Materials and structural aspects. *Materials and Design*, *54*, 32–42.
Suksawang, N., Mirmiran, A., Surti, V. H., Yohannes, D., & Yohannes, D. (2014). Use of Fiber Reinforced Concrete for Concrete Pavement Slab Replacement, 80.
Suksawang, N., Mirmiran, A., & Yohannes, D. (2014). *Use of Fiber Reinforced Concrete for Concrete Pavement Slab Replacement (Florida Department of Transportation Research Report BDK80 TWO 977-27)*.
Tadepalli, P. R., Mo, Y. L., Hsu, T. T. C., & Vogel, J. (2009). Mechanical Properties of Steel Fiber Reinforced Concrete Beams, 1–10.
Tadros, M. K., Badie, S. S., & Tuan, C. Y. (2010). *Evaluation and Repair Procedures for Precast/Prestressed Concrete Girders with Longitudinal Cracking in the Web*. *National Cooperative Highway Research Program, Report 654*. Washington, DC.

Uygunoglu, T. (2011). Effect of fiber type and content on bleeding of steel fiber reinforced concrete. *Construction and Building Materials*, *25*, 766–772.

Yao, W., Li, J., & Wu, K. (2003). Mechanical properties of hybrid fiber-reinforced concrete at low fiber volume fraction. *Cement and Concrete Research*, *33*, 27–30.

Yazdanbakhsh, A., Altoubat, S., & Rieder, K.-A. (2015). Analytical study on shear strength of macro synthetic fiber reinforced concrete beams. *Engineering Structures*, *100*, 622–632.

Yazdani, N., Spainhour, L., & Haroon, S. (2002). *Application of Fiber Reinforced Concrete in the End Zones of Precast Prestressed Bridge Girders (Florida Department of Transportation Research Report BC-386)*. Tallahassee, FL.

Yazici, Ş., Inan, G., & Tabak, V. (2006). Effect of aspect ratio and volume fraction of steel fiber on the mechanical properties of SFRC. *Construction and Building Materials*, *21*, 1250–1253.

Yin, S., Tuladhar, R., Shi, F., Combe, M., Collister, T., & Sivakugan, N. (2015). Use of macro plastic fibres in concrete: A review. *Construction and Building Materials*, *93*, 180–188. Retrieved from http://dx.doi.org/10.1016/j.conbuildmat.2015.05.105

Yurtseven, A. (2004). *Determination of mechanical properties of hybrid fiber reinforced concrete.* . Middle East Technical University.

Appendix A — Test methods for SCC fresh properties

A.1 Slump Flow (ASTM C1611)

ASTM C1611 provides the methodology to determine the flowability of SCC having coarse aggregates with nominal maximum size of up to 1 in. This test is used to measure the SCC consistency and its unconfined flow potential. It also provides a visual criterion to determine resistance to segregation.

The test is conducted by filling an inverted slump mold without consolidation. The mold is then gently lifted allowing the concrete to flow out onto the surface. The diameter of the concrete, once it stops flowing, is measured as the slump flow (Figure A-1). In addition, the time required for the diameter to reach 20 in. is measured and visual inspection of distribution of aggregates is performed to determine ability to resist segregation.

Figure A-1 Test setup for ASTM C1611-11

$$Slump\ flow = \frac{d_1 + d_2}{2} \qquad \text{Equation A-1}$$

Where d_1 is the largest diameter of the resulting circular spread, and d_2 is the diameter of the circular spread perpendicular to d_1.

A.2 J-Ring (ASTMC1621)

ASTM C1621, commonly known as the J-Ring test, provides a methodology to determine the passing ability of SCC with coarse aggregate of nominal maximum size up to 1 in. The test setup and J-Ring dimensions are shown in Figure A-2 and Figure A-3. The test procedure consists of placing the J-Ring on a flat surface and placing the inverted cone at the center of the J-ring. The inverted cone is then filled, without vibration or tamping, and is removed by raising it vertically, allowing the concrete to flow through the bottom of the cone. Once the concrete stops flowing, the largest diameter of the concrete spread and a second diameter perpendicular to the first are measured (if a difference among the two is greater than 2 in. then the test is considered invalid). J-Ring flow is computed as the average of the two measured spread diameters. Passing ability is determined as the difference between the J-Ring flow and the slump flow (ASTM C1611) and can be used to perform a blocking assessment (Table A-1).

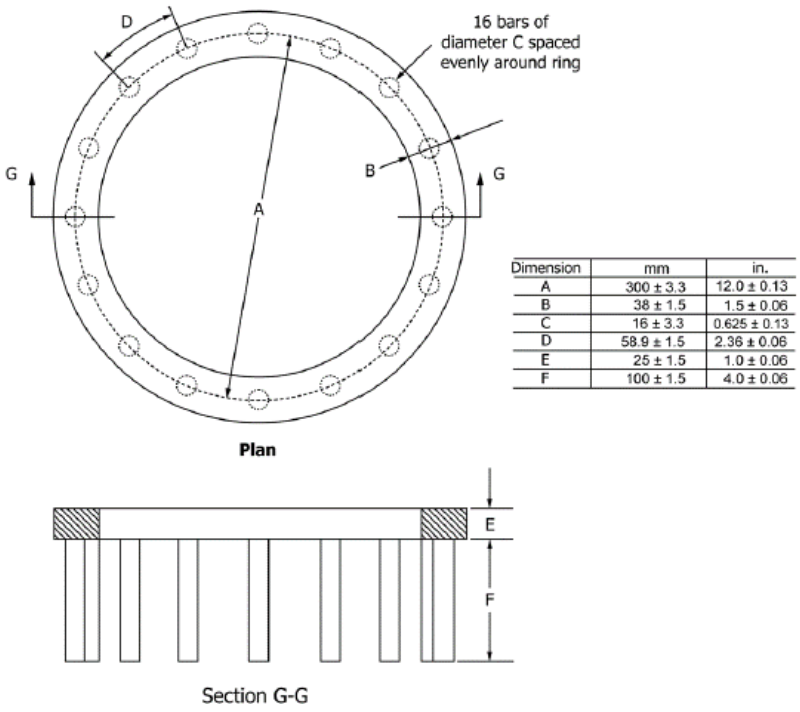

Dimension	mm	in.
A	300 ± 3.3	12.0 ± 0.13
B	38 ± 1.5	1.5 ± 0.06
C	16 ± 3.3	0.625 ± 0.13
D	58.9 ± 1.5	2.36 ± 0.06
E	25 ± 1.5	1.0 ± 0.06
F	100 ± 1.5	4.0 ± 0.06

Figure A-2 J-Ring dimensions (ASTM C1621-14)

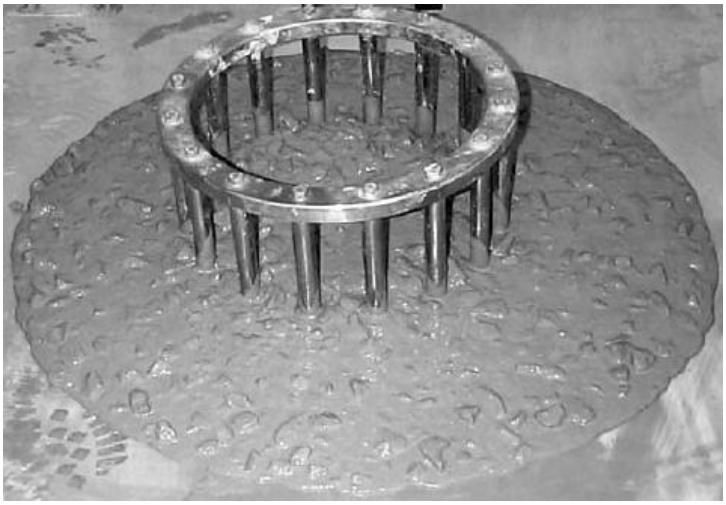

Figure A-3 Test setup: ASTM C1621 (ASTM C1621-14)

Table A-1 Blocking assessment (ASTM C1621-14)

Slump flow and J-Ring flow	Blocking assessment
0 to 1 in.	No visible blocking
>1 to 2 in.	Minimal to noticeable blocking
>2 in.	Noticeable to extreme blocking

A.3 Bleeding (ASTM C232)

ASTM C232 provides a methodology to determine the relative quantity of water that will bleed from a freshly mixed concrete with coarse aggregates of nominal maximum size up to 2 in.

Temperature is maintained at 65-75°F for the test duration. The procedure consists of filling a cylindrical container with concrete and drawing off accumulated water on the surface until bleeding stops. For the first 40 minutes, water is drawn off at intervals of 10 minutes and then at 30 minute intervals until bleeding stops. (The sample should be kept covered except when removing water). Volume of water removed at each interval and the total amount of water removed are recorded. Volume of bleed water per unit area and the bleeding percent are determined using Equation A-2 and Equation A-3.

$$V = V_1/A \qquad \text{Equation A-2}$$

where V is the volume of bleed water per unit area of surface, V_1 is volume of bleed water during the selected time interval, and A is the area of exposed concrete

$$Bleeding\% = \frac{D}{(\frac{w}{W}xS)}x100 \qquad \text{Equation A-3}$$

where D is the total accumulated mass of bleed water, w is the mass of net mixing water (total amount of water minus water absorbed by aggregates), W is the total mass of the batch and S is the mass of the specimen.

A.4 Static segregation (ASTM C1610)

ASTM C1610 provides methodology to determine the static segregation of SCC. The coarse aggregate content is measured at the top and bottom of a cylindrical column (Figure A-4) and used to determine the static segregation percent. The mold is filled without any tamping or vibration and allowed to stand undisturbed for 15 minutes. The concrete at the top and bottom of the column are washed using a No. 4 sieve. The coarse aggregate is brought to surface-dry condition and the mass of coarse aggregate in each section are determined.

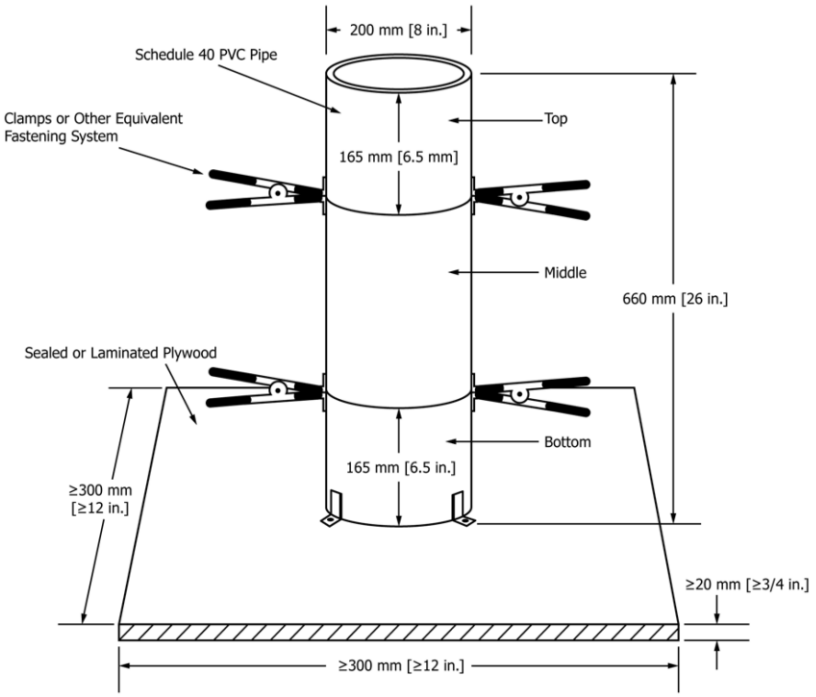

Figure A-4 Detail of column mold (ASTM C1610-14)

Percent of static segregation is determined using Equation A-4

$$S = 2\left[\frac{CA_B - CA_T}{CA_B + CA_T}\right] \times 100 \; if \; CA_B > CA_T$$

$$S = 0 \; if \; CA_B \leq CA_T$$

Equation A-4

where S is the static segregation percent, CA_T is the mass of coarse aggregate in the top section of the column, and CA_B is the mass of coarse aggregate in the bottom section of the column.

A.5 Rapid static segregation (ASTM C1712)

ASTM C1712 provides the methodology for rapid assessment of static segregation of normal weight SCC with coarse aggregate of nominal maximum size up to 1 in. The test setup is shown in Figure A-5. The test procedure consists of filling the inverted slump cone without applying external vibration and placing the penetration apparatus on top. The penetration apparatus is aligned in the center of the cone. The hollow cylinder is lowered onto the concrete surface and released, allowing free penetration of the fresh concrete.

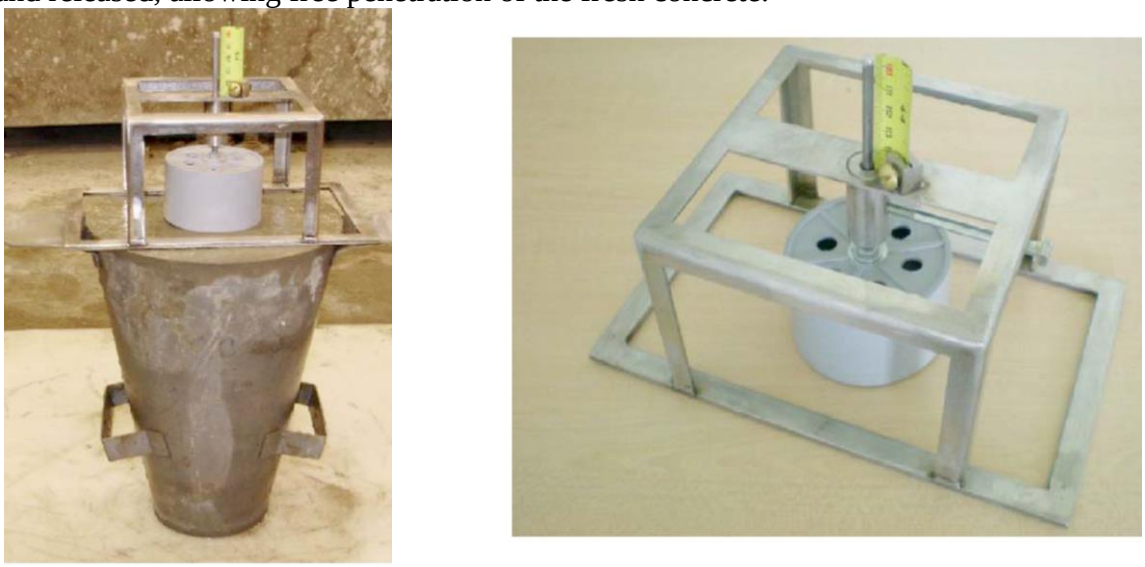

Figure A-5 Test setup and penetration apparatus (ASTM C1712-14)

The depth of penetration (P_d) is determined using Equation A-5 and is used to evaluate the static segregation resistance of the mixture (Table A-2)

$$P_d = d_2 - d_1$$

Equation A-5

where P_d is the penetration depth, d_1 is the initial reading (mm), and d_2 is the final reading (mm).

Table A-2 Degree of static resistance (ASTM C1712-14)

Penetration depth (Pd)	Degree of static segregation
Pd ≤ 0.4 in.	Resistant
0.4 in. < Pd < 1.0 in.	Moderately resistant
Pd ≥ 1.0 in.	Not resistant

A.6 V-funnel (EN 12350-9)

The V-funnel test (EN 12350-9) is a Euronorm test that measures the filling ability and segregation resistance of SCC (Figure A-6). The test procedure consists of filling the V-funnel without compaction while the gate located at the bottom of the funnel is closed. The concrete is allowed to rest for approximately 10 seconds and then the gate is opened. The time required for the funnel to empty is recorded as the V-funnel flow time. The flow of concrete should be continuous. If the flow stops before the funnel empties, then the mixture does not have the necessary viscosity and filling ability required to be considered SCC.

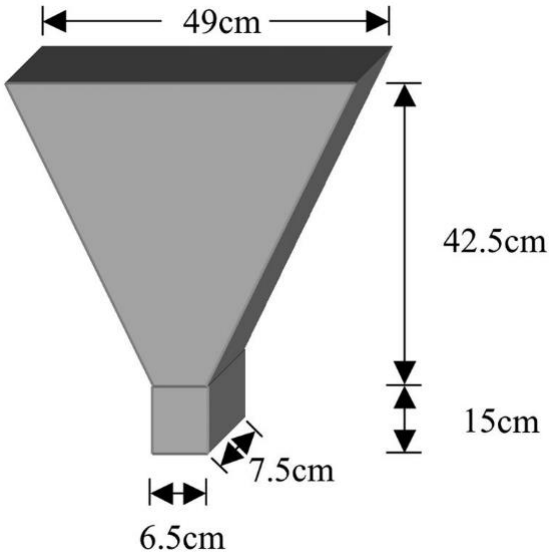

Figure A-6 V-Funnel test (ASTM STP 169D 2006)

A.7 L-Box (EN 12350-10)

L-Box test (BS EN 12350-10 2010) is a test that measures the passing ability of SCC between reinforcing bars and other obstructions without segregating or forming a blockage. The test setup consists of a box with vertical and horizontal components through which the concrete flows (Figure A-7). Bars are placed at the change in flow direction to test the passing ability of the concrete through reinforcement. The test procedure consists of filling the vertical portion of the box without vibration or compaction. After resting for one minute, the gate between the vertical and horizontal components is opened. When the flow stops, H_1 and H_2 are measured at three locations across the width of the box and averaged.

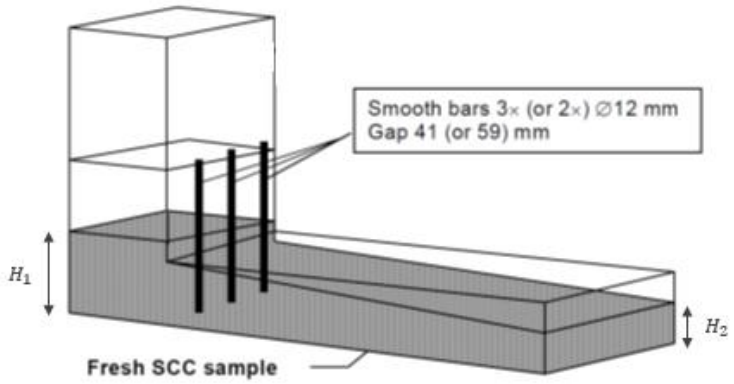

Figure A-7 Test Setup (BS EN 12350-10 2010)

Passing ability ratio is determined using Equation A-6.

$$PL = \frac{H_2}{H_1}$$ Equation A-6

where H_1 is the average difference between the height of the vertical section and the height of the level of concrete and H_2 the average difference between the height of the horizontal section and the height of the level of concrete.

Appendix B — Mixture development test results

EN 14651

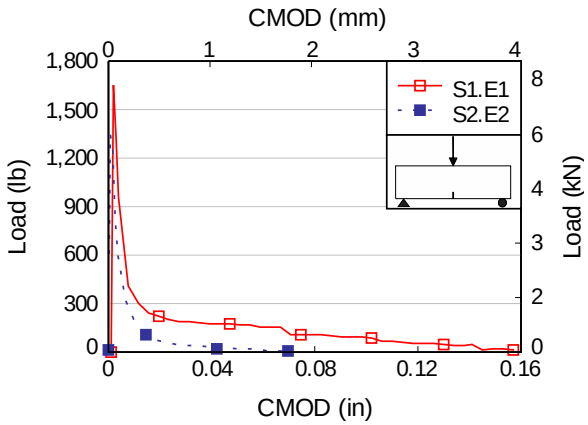

Figure B-1 Load-CMOD for SH-010-01-DM

ASTM C1399

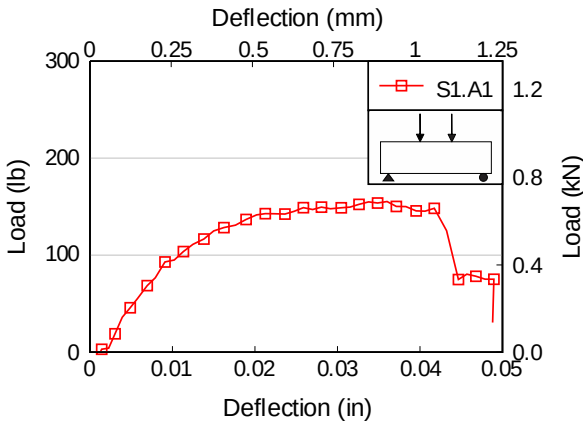

Figure B-2 Load-deflection for SH-010-01-DM

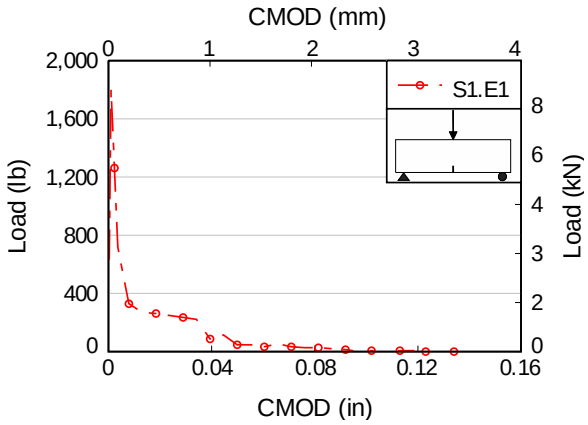

Figure B-3 Load-CMOD for SH-010-01-DG

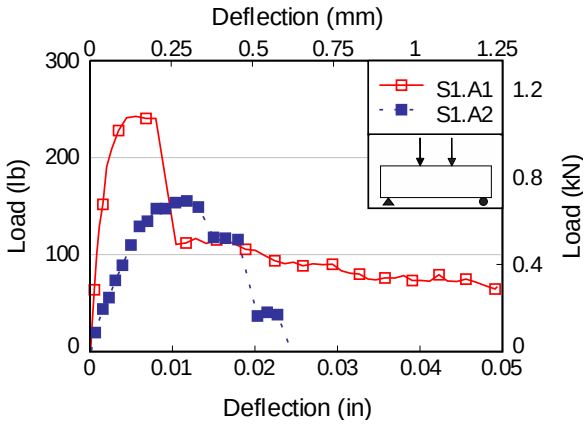

Figure B-4 Load-deflection for SH-010-01-DG

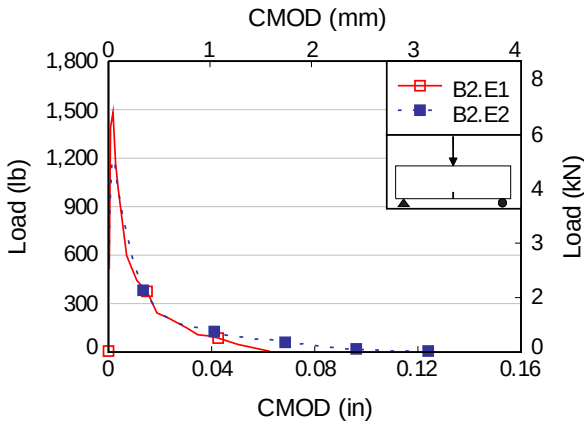

Figure B-5 Load-CMOD for B-030-04-DM

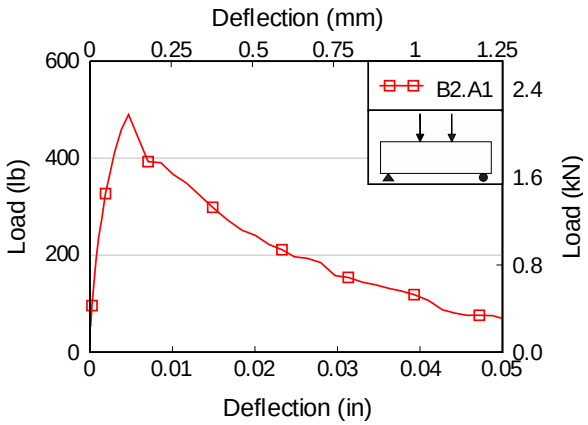

Figure B-6 Load-deflection for B-030-04-DM

EN 14651

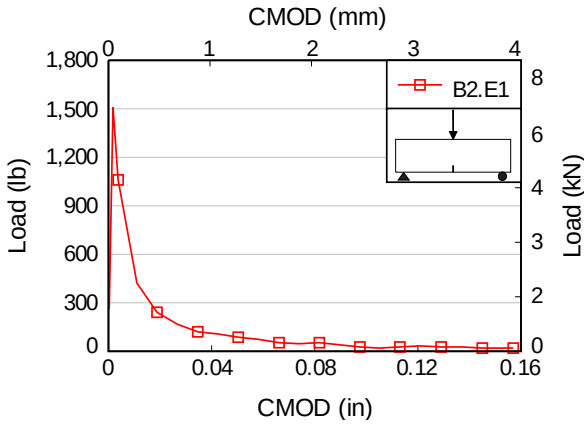

Figure B-7 Load-CMOD for B-030-04-DG

ASTM C1399

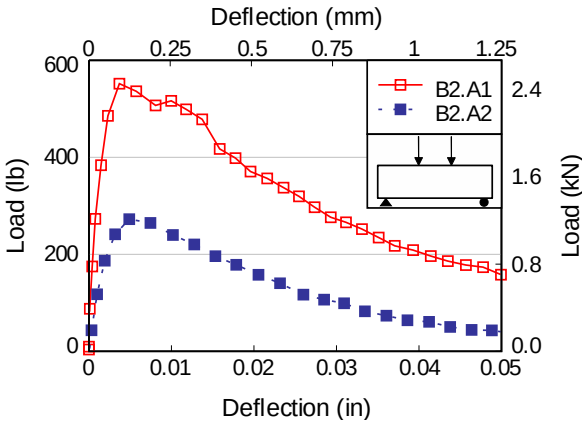

Figure B-8 Load- deflection for B-030-04-DG

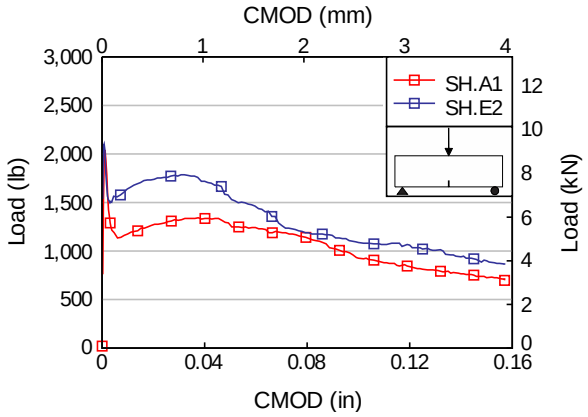

Figure B-9 Load-CMOD for SH-30-05-DM

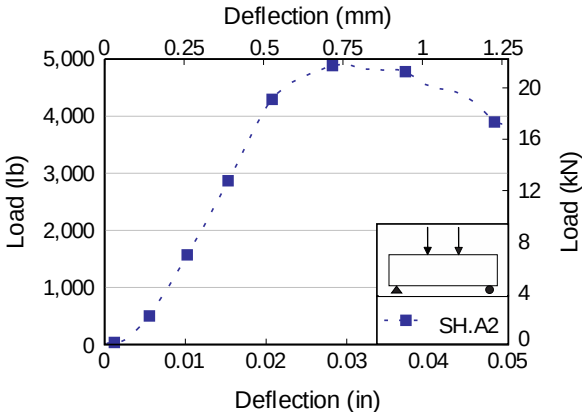

Figure B-10 Load-deflection for SH-30-05-DM

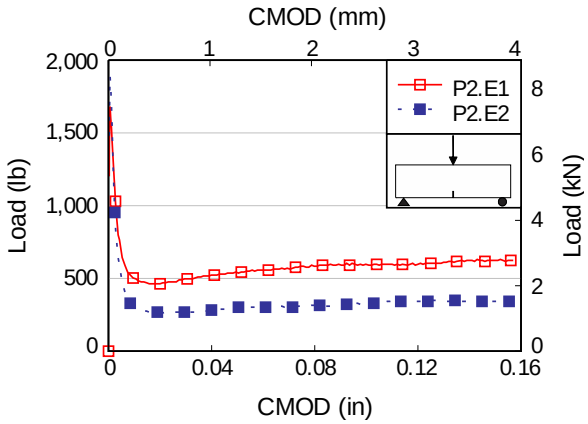

Figure B-11 Load-CMOD for PP2-30-06-DM

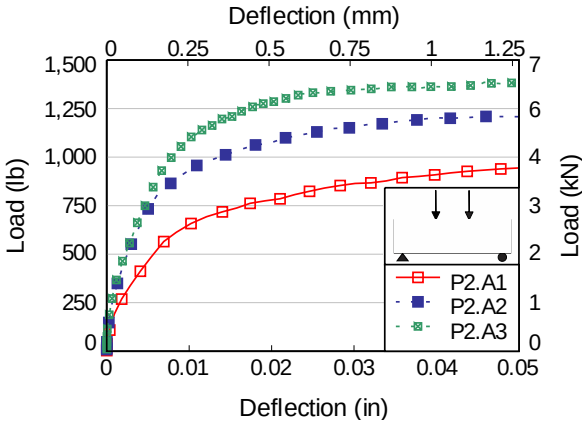

Figure B-12 Load-deflection for PP2-30-06-DM

EN 14651

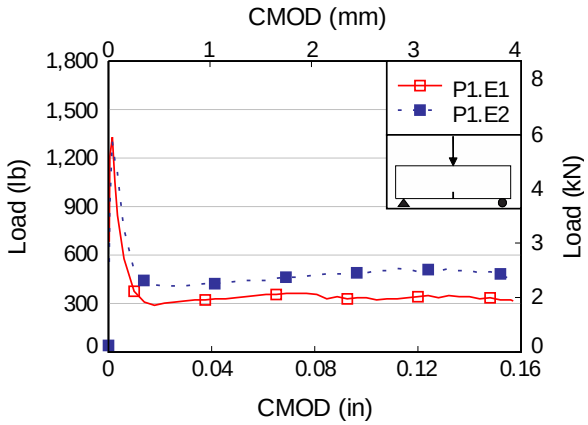

Figure B-13 Load-CMOD for P1-045-09-DM

ASTM C1399

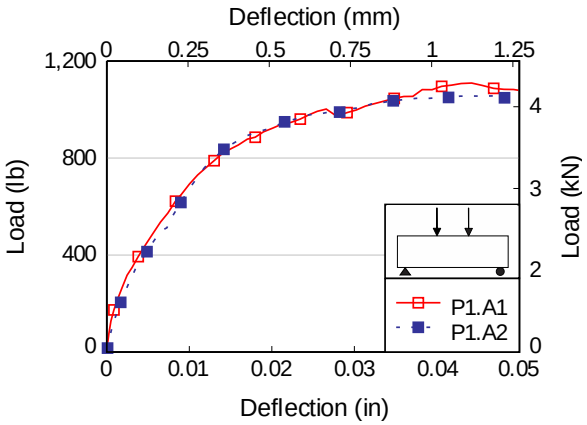

Figure B-14 Load-deflection for P1-045-09-DM

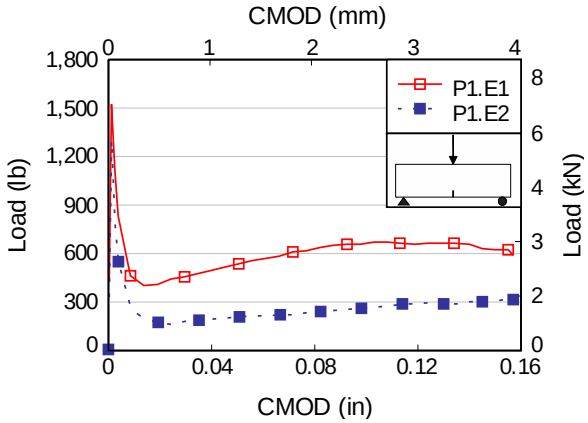

Figure B-15 Load-CMOD for P1-045-09-DG

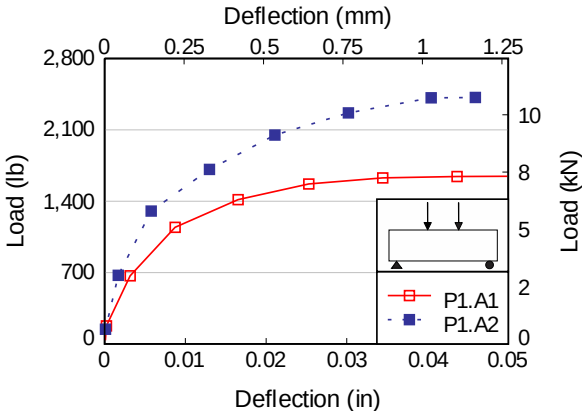

Figure B-16 Load-deflection for P1-045-09-DG

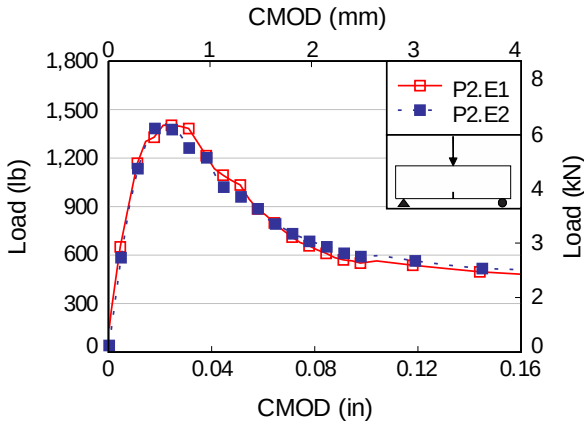

Figure B-17 Load-CMOD for PP2-70-12-DM

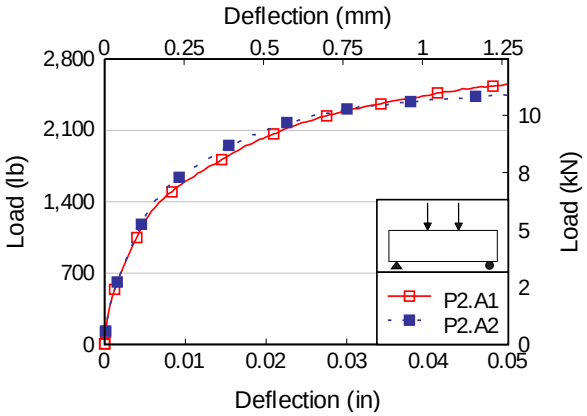

Figure B-18 Load-deflection for PP2-70-12-DM

EN 14651

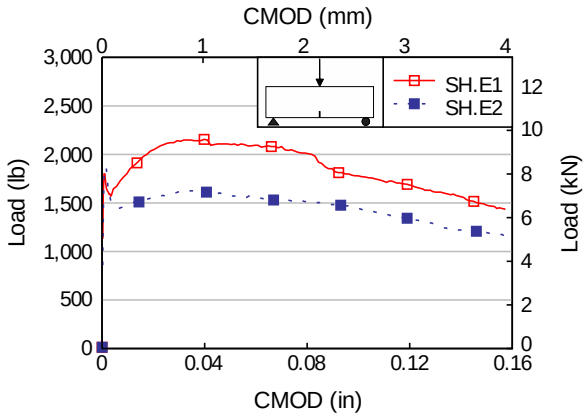

Figure B-19 Load-CMOD for SH-70-13-DM

ASTM C1399

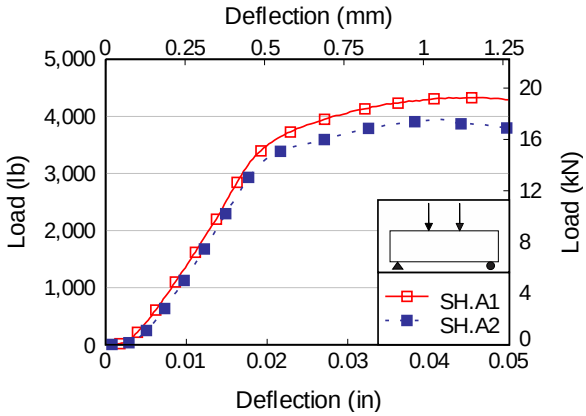

Figure B-20 Load-deflection for SH-70-13-DM

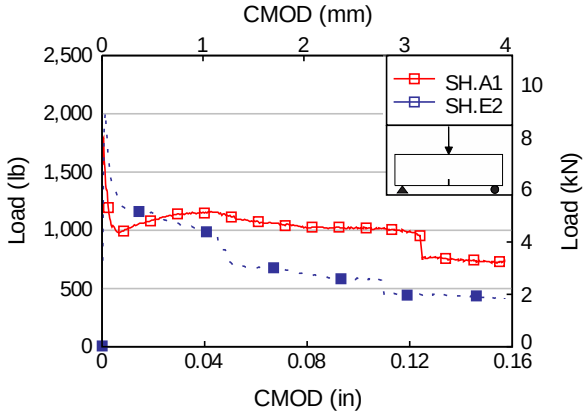

Figure B-21 Load-CMOD for CR-70-14-DM

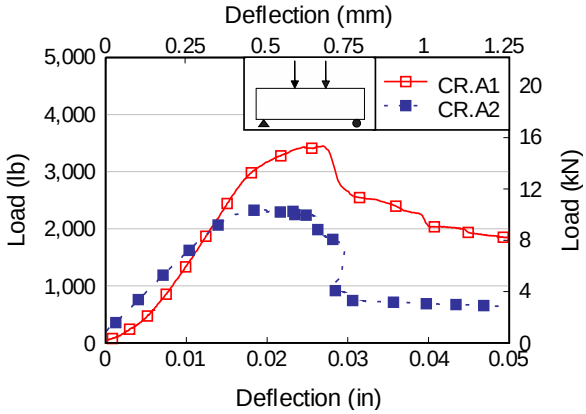

Figure B-22 Load-deflection for CR-70-14-DM

Appendix C — Mockup segregation test

C.1 Introduction

FIB mockups specimens were cast at the precast plant to evaluate procedures for implementing FRC in full-scale precast production and to test for issues regarding consolidation or fiber nesting. Four FIB-72 specimens were constructed. The first specimen was a control which was constructed using conventional Class VI concrete and three (3) FRC specimens. For each mixture prepared in the batch plant, a 3-ft span specimen was cast and prestressed at the precast plant and transferred to the FDOT Structures Research Center (SRC), Tallahassee for cutting and testing. The Modified Mujtaba and Buhler (FDOT 2015) test was used to evaluate issue of segregation or fiber nesting. In addition, each specimen was evaluated for signs of poor consolidation or fiber clumping by means of visual inspection.

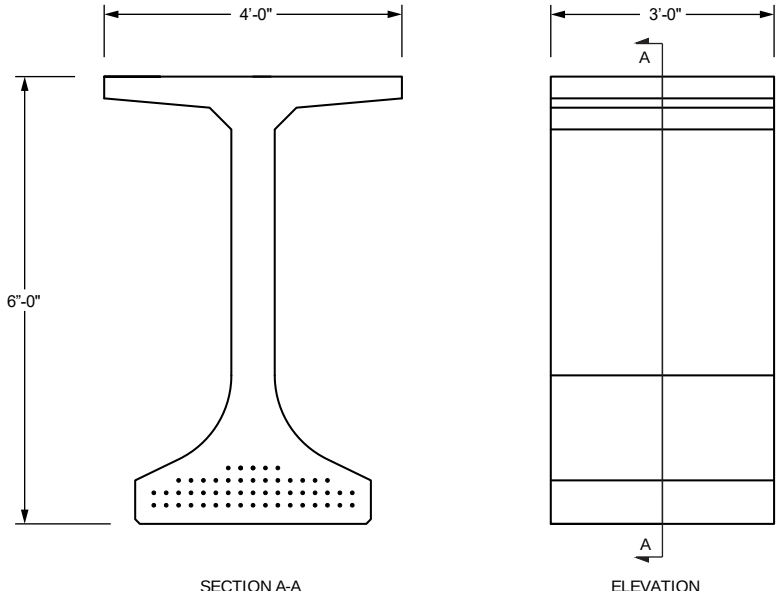

Figure C-1 Mockups elevation and cross-section of FIB-72

C.2 Test procedures

Mujtaba and Buhler test methodology consists of selecting five locations (8x8in.) along the height of each specimen's saw-cut face and sub diving it into eight sections. Locations were designated as A, B, C, D, and E, starting from the top flange. A was located in the top flange, B, C and D were located along the web and E was located in the bottom flange. Due to the size of the exposed surface, for some locations the use of smaller areas was necessary. For each section, a horizontal line was drawn and the width of each aggregate greater than 0.1 in. was measured. Total coarse aggregate content in each location was determined by averaging the total length of aggregates along each of the eight sections. Using weighted average of all locations, the average coarse aggregate content of the specimen was determined. FDOT (2015) states that segregation has occurred if the difference between the average coarse aggregate content and the content at any given location exceeds 15% and if the difference between the average coarse aggregate content of the mockup differs by more than 15% with the mixture design.

C.3 Mixture proportions

Four mockup specimens were constructed to verify evaluate procedures for implementing FRC in full-scale precast production and to test for issues regarding consolidation or fiber nesting. Three FRC mixtures developed in the laboratory were used for the construction of the mockup specimens, in addition a control specimen was constructed for reference. For the control specimen, a standard Class VI SCC mixture was used. Mixture proportions are provided in Table C-1, for this chapter mixtures will be denoted using a reference number as provided in Table C-2.

Table C-1 Mixture proportions (lb/cy)

Mixture	CT	B-30-04	PP-45-09	SH-10-01
Cement	735	790	790	790
Flyash	165	175	175	175
#67	1370	565	565	578
#89	0	776	774	774
FA	1265	1212	1212	1212
Water	279	279	279	279
B	-	11	-	-
PP	-	-	7	-
SH	-	-	-	7

Table C-2 Mixture reference number for mockup specimens

Mixture	Reference number
CT	0
B-30-04	5
PP-45-09	6
SH-10-01	7

C.4 Specimen construction

Molded beams for flexural testing were cast at the precast plant using individual 4 in.x4 in.x14 in. steel molds, where they were cured until transferred to UF for testing (Figure C-2). Cylinder specimens (4x8 in.) were cast, cured, and tested at the precast plant (Figure C-3). To test for segregation at full-scale, FIB-72 mockup specimens (3-ft length) were cast and prestressed at the precast plant (Figure C-4). Three cy mixtures were prepared for each mockup specimen in the nine cy mixer at the precast batch plant. Mixture proportions and procedures used in laboratory setting were not adjusted for mixing in batch plant.

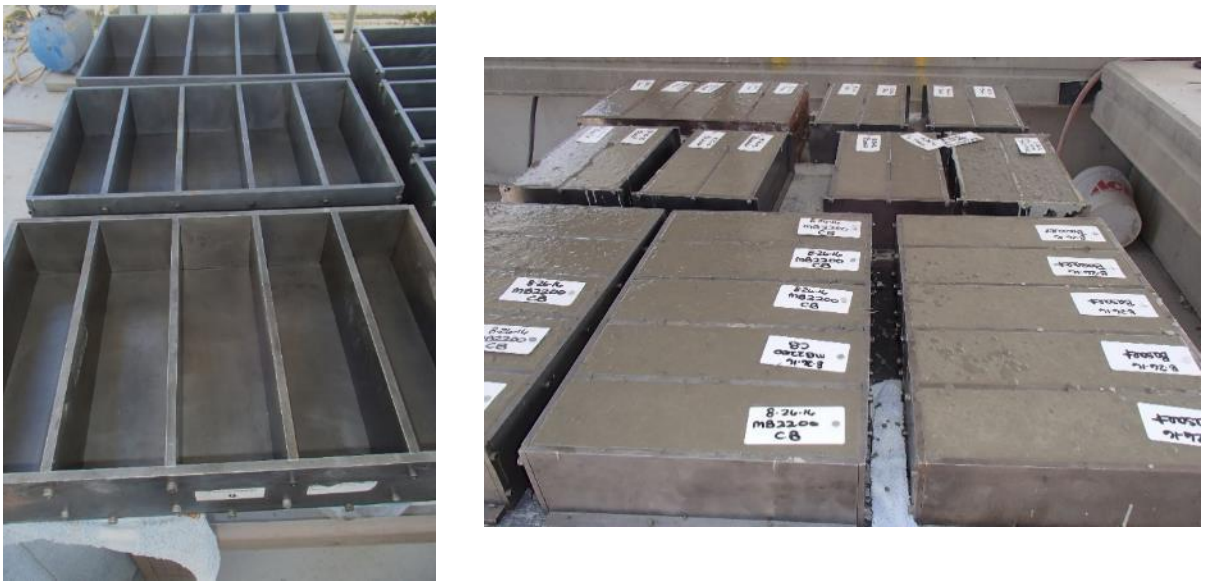

Figure C-2 Beam molds and cast specimens

Figure C-3 Cylinders for testing of compressive strength

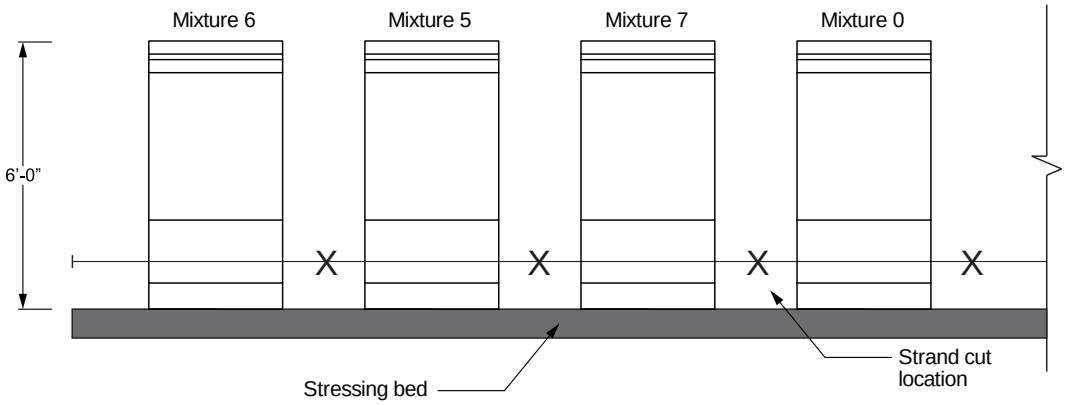

Figure C-4 Specimen orientation during casting

C.5 Fresh properties

Table C-3 shows results of fresh property tests obtained for mixtures prepared at the precast batch plant. All FRC mixtures exceeded the maximum allowed unrestricted flow of 27 inches by up to 30%. All FRC mixtures showed poor consistency, with evidence of mortar halo at the exterior, and had a VSI of two (Figure C-5b)). Compared with mixtures prepared in a laboratory setup concrete stability and quality was greatly decreased as shown in Figure C-6. This can be due to scaling issues when incorporating the same proportions in a mixer with higher capacity, for further work admixtures should be adjusted accordingly to avoid this issue.

Table C-3 Fresh properties for mixtures prepared in batch plat

Mixture	Slump flow (in.)	VSI	Air content (%)
0	24.75	0	3
5	34.5	2	0.08
6	33.5	2	0.08
7	35.5	2	0.07

(a) (b)

Figure C-5 Slump flow for mixtures prepared in (a) laboratory mixer and (b) batch plant

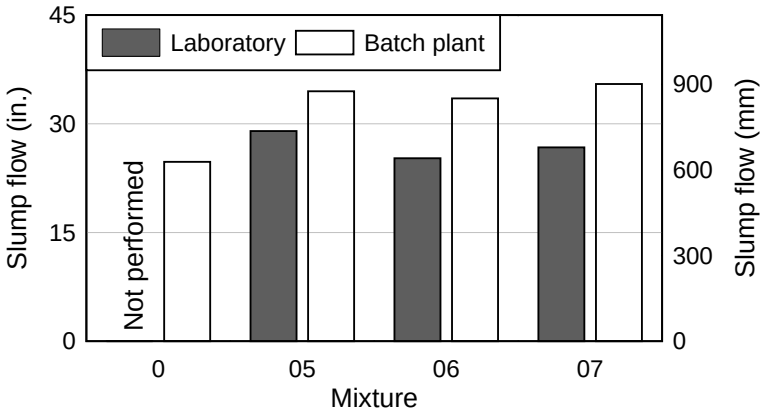

Figure C-6 Slump flow of mixtures prepared in laboratory mixer vs batch plant

C.6 Compressive strength (ASTMC39)

For each mixture prepared in the batch plant, nine specimens were prepared to determine the average compressive strength; two were tested at 24 hours, 7 days, and 14 days and three were tested at 28 days.

Compressive strength of cylinders exceeded the specified 28-day specified compressive strength of 8,500 psi (Table C-4). In general, early age strength (24 hours) was increased by as little as 5% to up to 65% when compared to control mixture; this was likely due to the confinement provided by the fiber reinforcement. The effect of fiber reinforcement on 28-day strength was found to be negligible (up to 12.5% difference).

Table C-4 Compressive strength (Batch plant mixtures)

Sample	24 hours (psi)	7 days (psi)	21 day (psi)	28 day (psi)
Control (0)	3,220	8,140	10,060	10,790
B2-030-05	4,310	8,890	10,300	10,862
P1-045-06	4,000	8,930	10,245	10,850
S1-010-07	4,670	9,220	-	11,680

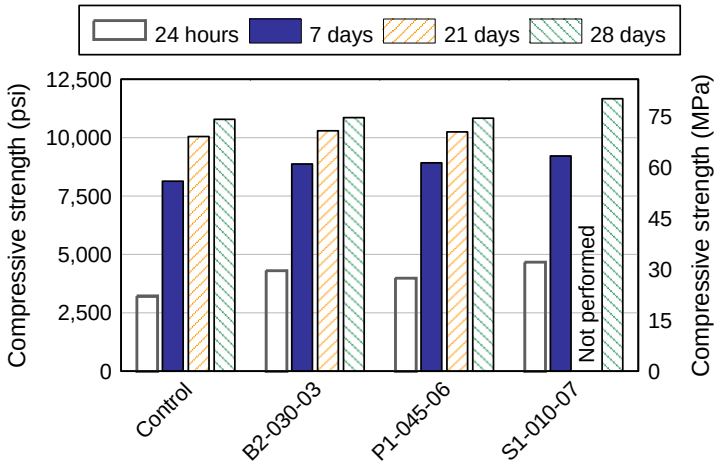

Figure C-7 Compressive strength (batch plant mixtures)

C.7 Average residual strength (ASTM C1399)

Figure C-8 show ARS results for molded specimens and those saw-cut from full-scale girders. Results showed a difference in ARS of over 50%. It is not clear at this point why such a difference occurred, but possible reasons include the effect of specimen size, sampling method used for casting of molded specimens and fiber distribution. Due to the low volume of fibers used, some samples showed relatively low ARS. P2-070-08 provided the maximum ARS, with S1-030-09 being the second highest ARS with a difference of 36% in ARS. Nonetheless, P2-070-08 required a volume 60% higher and almost twice the length of the fiber used for S1-030-09 to provide an increase of 36% ARS. At the same volume fraction of 0.30%, steel fibers (S1-030-09) provided a higher residual strength than both basalt (B2-030-05) and synthetic fiber (P2-030-11). P1-045-06 and P2-030-11 have similar load-deflection response and a difference of 2.3% in ARS.

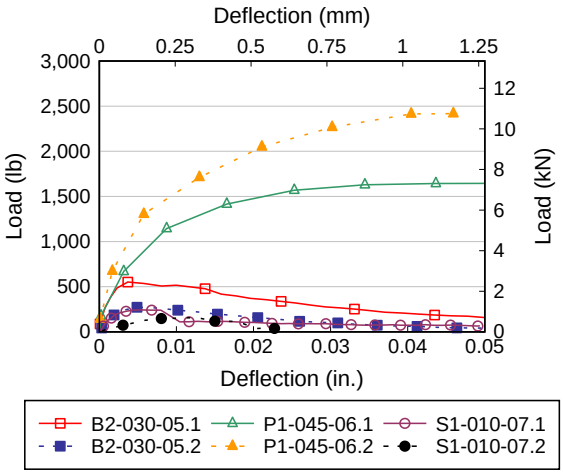

Figure C-8 Reloading curves for saw-cut specimens

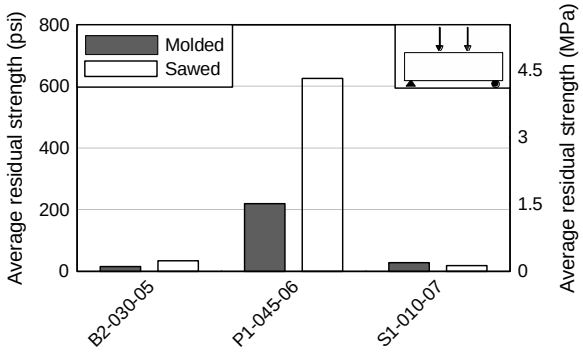

Figure C-9 ARS for molded and saw-cut specimens

C.8 Flexural tensile strength (EN 14651)

Flexural tensile residual strength testing was performed to evaluate the effect of the different fiber materials on the post cracking behavior of concrete at various stress levels. Typical behavior showed a sudden decrease in stiffness once cracking occurred with the exception of specimen's using higher fiber volume (0.7%) or stiffer fibers (S1). The residual strength was generally less than 30% of the limit of proportionality (LOP) after CMOD reached 0.04 in. (1 mm).

Figure C-10

Figure C-10 shows typical load-CMOD curves for sawn FRC specimens tested. Peak loads obtained ranged between 1.1-1.7 kip, after which most specimens showed a rapid loss in stiffness. B2-030-05 and S1-010-07 showed residual strength less than 5% of LOP after CMOD reached 1mm. This low strength is likely due to the low fiber dosage used for these mixtures. P2-030-11 and P1-045-06 showed similar LOP, P1-045-06 had residual strength almost 50% higher than P2-030-11 at all stress levels. Both synthetic macrofibers, however, showed a more ductile behavior than B2-030-05 and S1-010-07. Specimens exhibited modest strength well beyond cracking with a residual stress of up to 30% of LOP. S1 (0.30%) showed hardening behavior, with residual strength of up to 30% of cracking load. This behavior is attributed to the high stiffness and tensile strength of steel (S1) fibers. P2-070-08 showed a considerably lower peak load and stiffness when compared with all the specimens tested. After corroborating, this data set is deemed invalid and was not be considered for the analysis of results of this particular test method.

Figure C-11 shows residual flexural tensile strength for crack mouth opening displacement (CMOD) increments of 0.02, 0.06, 0.10, and 0.15 in. (0.5, 1.5, 2.5 and 3.5 mm). LOP of sawn specimens was up to 10% less than that of molded specimen. S1-010-07 and B2-030-05 sawn specimens showed 5% ($f_{R,1}$) to up to 100% ($f_{R,2}$) higher residual stress than that of molded specimens. Similarly as for results from ASTM 1399 testing, it is not clear at this point why such a difference occurred, but possible reasons include sampling method used for casting of molded specimens and fiber distribution. In contrast, when compared with the molded specimen, P1-045-06 sawn specimen showed a lower residual stress at CMOD of 0.5 and 1.5mm of 31% and 10% respectively. Higher capacity from molded specimens could be attributed to fiber preferential alignment and size effect.

For task 3, because end region cracking is a serviceability issue not an ultimate strength, the focus was on the post-cracking flexural strength between first cracking and $f_{R,1}$ (EN 14651), shown in Figure C-12 and Figure C-13.

At the same volume fraction of 0.30%, S1-030-09 showed higher residual stress at all stress levels when compared with B2-030-05 and P2-030-11 specimens, this can be attributed to steel fibers (S1) high tensile strength and stiffness. LOP of B2-030-05 and P2-030-11 was 21% and 22% less than that of S1 fibers specimens. Residual stress at CMOD of 0.5 mm ($f_{R,1}$) of B2-030-05 and P2-030-11 was 30% and 15% less than that of S1-030-09. Similarly as in results for ASTM 1399 testing, mixtures 03, 06, 80, 09, and 11 were selected based on fresh and hardened properties. However, due to limited availability of macro-configured basalt fibers, inclusion of these fibers is still to be confirmed for task 3 and 4.

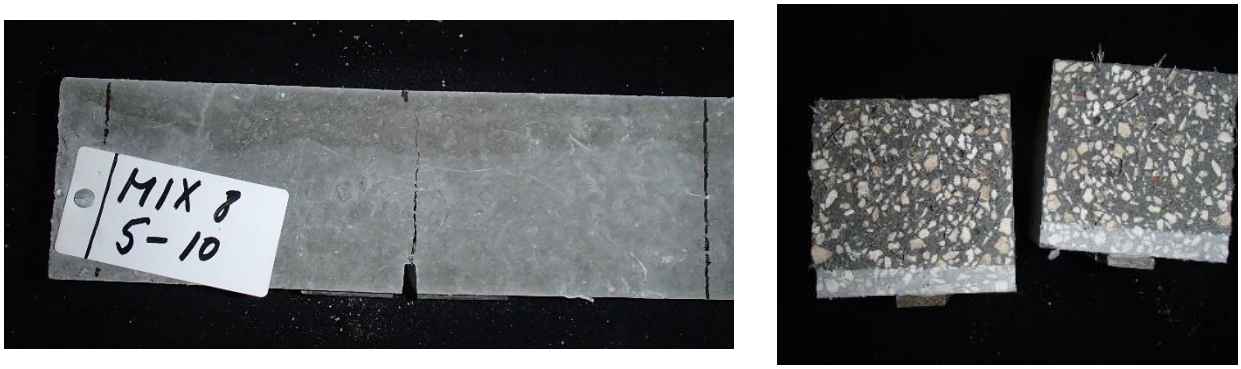

Figure C-10 Test specimens (after testing)

able C-5 Limit of proportionality and residual tensile strength results for molded specimens

Specimen	LOP (psi)	$f_{R,1}$ (psi)	$f_{R,2}$ (psi)	$f_{R,3}$ (psi)	$f_{R,4}$ (psi)
B2-030-05	635.4	112.6	22.9	3.0	0.0
P1-045-06	681.9	175.3	193.6	199.5	205.5
S1-010-07	776.8	69.9	39.9	22.3	11.1
P2-070-08	-	-	-	-	-
S1-030-09	807.9	238.2	171.8	170.6	164.2
P2-030-11	-623.3	-86.7	-99.0	-107.8	-114.5

*Invalid data (-)

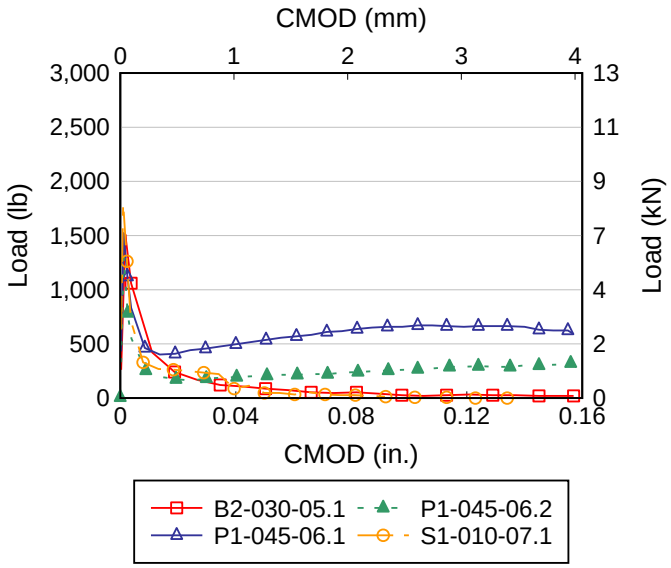

Figure C-10curves for sawn specimens

Table C-6 Limit of proportionality and residual tensile strength results for sawed specimens

Specimen	LOP (psi)	$f_{R,1}$ (psi)	$f_{R,2}$ (psi)	$f_{R,3}$ (psi)	$f_{R,4}$ (psi)
B2-030-05	703.4	118.6	35.9	10.1	6.4
P1-045-06	739.5	133.8	176.8	208.4	217.7
S1-010-07	804.1	124.7	81.8	39.1	22.3

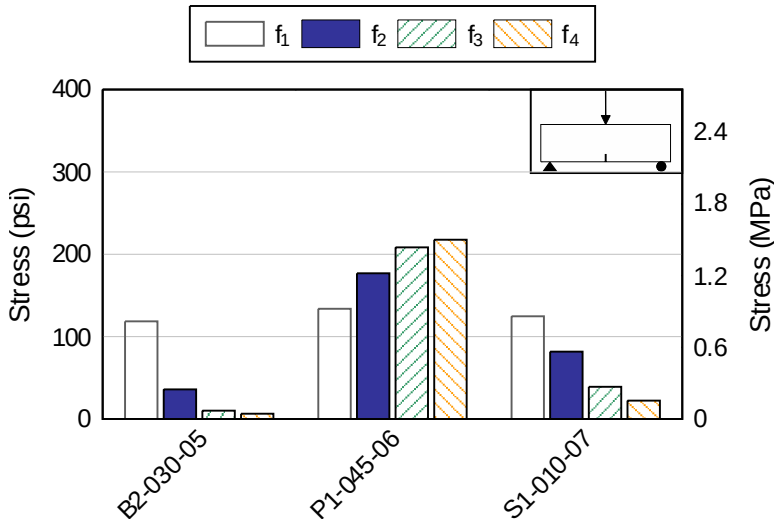

Figure C-11 Residual flexural tensile strength for sawn specimens

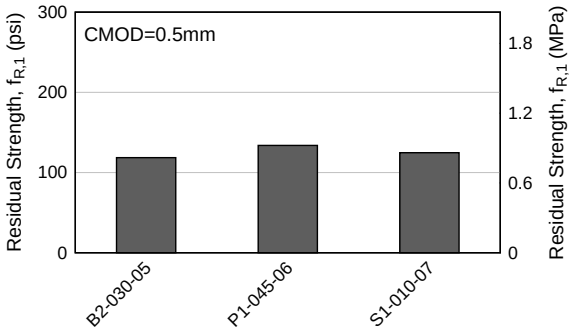

Figure C-12 Residual stress ($f_{R,1}$) for sawn specimens

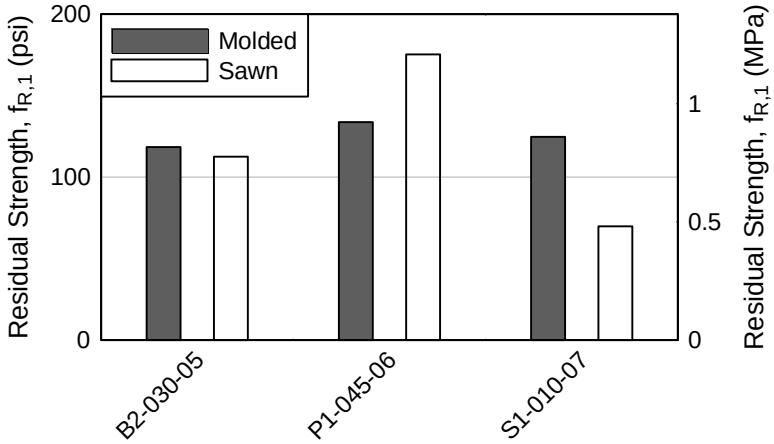

Figure C-13 Residual stress ($f_{R,1}$) for molded and sawn specimens

C.9 Segregation test

This section describes the results of the strand detensioning, saw-cutting, and evaluation of segregation using the procedures from the Mujtaba and Buhler test method (FDOT 2015). Initially, the strands were cut and the sections were lifted from the prestressing bed to prepare them for transporting to the FDOT structures laboratory by truck. Once the mockups were delivered, they were saw cut and inspected to quantify the aggregate segregation.

Figure C-14 shows mockups after cutting of prestressing strands and removal from the prestressing bed. Immediately following removal, it was apparent that the FRC specimens had less visible damage due to prestress transfer than the control specimen, which showed extensive damage in the web and bottom flange. In fact, when lifting and placement into the truck was attempted, the bottom flange completely detached from the web. Among the FRC specimens, steel fibers (Figure C-14d) showed fewer and narrower cracks in the bottom flange.

Results of the Mujtaba and Buhler test are shown qualitatively in Figure C-15 and quantitatively in Figure C-16. B2 (0.30%) and S1 (0.10%) showed a difference between the weighted average and section average of less than 15%. P1 (0.45%), however, showed up to 20% difference in locations E and D. P1 fibers are almost twice as long as S1 and B2 and used at higher volume dosage. These factors could account for P1 fibers showing a larger difference between the weighted average and section average. Visual inspection of full-depth specimens, however, showed that despite batch plant mixtures failing conventional fresh properties tests

intended to quantify passing ability (ASTM C1611) and laboratory mixtures showing signs of nesting inside the J-Ring (ASTM 1621), mixtures 5, 6, and 7 flowed and consolidated properly, showing no signs of fiber nesting between the prestressing strands (Figure C-17). This indicates that conventional methods might be ineffective at assessing passing ability of FRC. Similar conclusions were found in the literature by Dhonde et al (2005), where specimens were cast using acrylic sheet formwork to evaluate consolidation and flowability of FRSCC.

After completion of the Mujtaba and Buhler test, web sections of the FIB-72 were cut using a hand-held saw. Sections were transported to FDOT State Materials Office (SMO) for final cutting of beams.

(a)

(b)

(c)

(d)

Figure C-14 Prestressed mockup specimens using mixture (a) 0 (control), (b) 05, (c) 06, and (d) 07

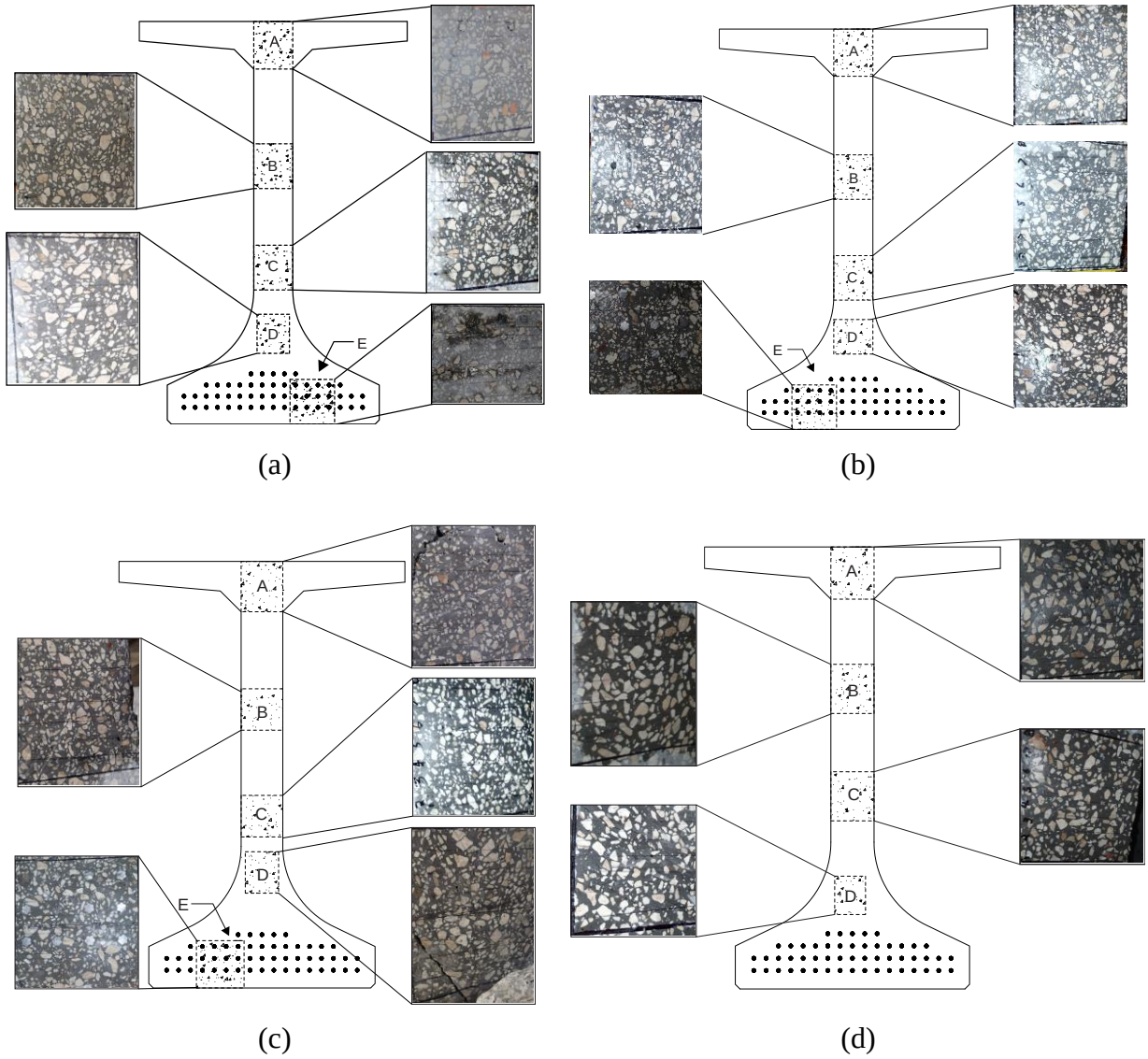

Figure C-15 Test location for Mujtaba and Buhler testing: (a) 05, (b) 06, (c) 07, (d) 0 (control)

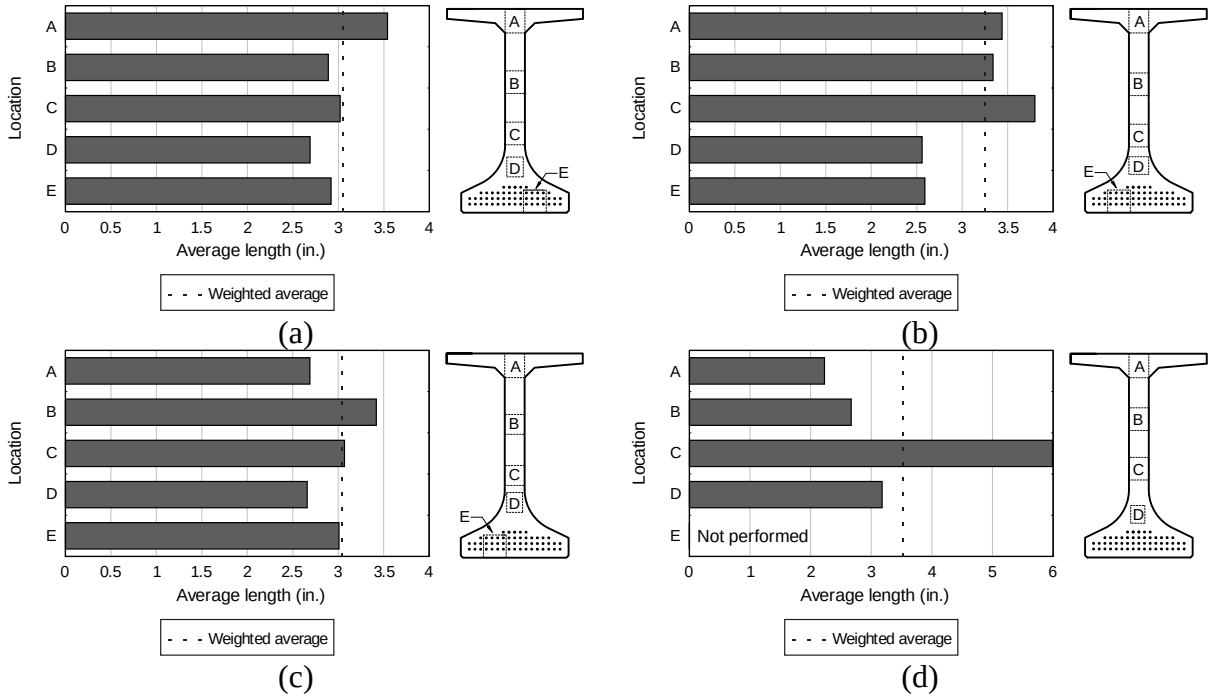

Figure C-16 Average aggregate length for specimen cast using mixture (a) 05, (b) 06, (c) 07, and (d) 0 (control)

Figure C-17 Bottom flange sectional elevation (Mixture 06)

C.10 Findings

FIB-72 mockups were constructed to evaluate procedures for implementing FRC in full-scale precast production and to test for issues regarding consolidation or fiber nesting. Key findings include:

- Casting of full-depth specimens showed that conventional methods to assess passing ability might be ineffective at assessing fresh properties of FRC,
- Casting of mockups showed that FRC reduced width and length of cracking occurring at prestress transfer.

Appendix D — End region specimen construction

D.1 Construction schedule

A timeline of specimen casting is provided in Table D-1. Table D-2 contains a summary of activities for each girder. Table D-3 through Table D-7 contains a detailed timeline for each girder, including dates for each activity performed during construction.

Table D-1 Casting schedule

Girder	Date
CT	August 2, 2018
SH-30	August 15, 2018
SH-70	August 21, 2018
CR-70	August 31, 2018
PP-50	September 14, 2018

Table D-2 Fabrication stages

Activity
Bulkhead placed
Strands tensioned
Placement of mild reinforcement
Install and test internal instrumentation
Concrete pour
Concrete cure
Form removal
Install external instrumentation
Setup data acquisition
Strand cutting
Inspect specimens
Transport for storage
Monitor cracking

Table D-3 Specimen CT construction schedule

Date	Activity	Concrete age (days)
Tuesday, July 31, 2018	Layout prestressing strands	-
Tuesday, July 31, 2018	Place reinforcement	-
Thursday, August 2, 2018	Concrete pour	-
Friday, August 3, 2018	Forms removed	1
Monday, August 6, 2018	Install external gages and setup	4
Thursday, August 9, 2018	Strand cut down	7
Friday, August 10, 2018	Beam lifted of bed	8
Saturday, August 11, 2018	Beam lifted for storage	9
Thursday, August 23, 2018	Beam move to storage	21
Thursday, September 13, 2018	Beam move to storage	42

Table D-4 Specimen SH-30 construction schedule

Date	Activity	Concrete age (days)
Friday, August 10, 2018	Layout prestressing strands	-
Monday, August 13, 2018	Place reinforcement	-
Tuesday, August 14, 2018	Concrete pour - discarded	-
Wednesday, August 15, 2018	Concrete pour	-
Monday, August 20, 2018	Forms removed	5
	Install external gages and setup	
Tuesday, August 21, 2018	Strand cut down	6
Tuesday, August 21, 2018	Beam lifted of bed	6
Thursday, August 23, 2018	Beam moved to second storage	8

Table D-5 Specimen SH-70 construction schedule

Date	Activity	Concrete age (days)
Thursday, August 16, 2018	Layout prestressing strands	-
Friday, August 17, 2018	Place reinforcement	-
Tuesday, August 21, 2018	Concrete pour	0
Monday, August 27, 2018	Forms removed	6
	Install external gages and setup	
Monday, August 27, 2018	Strand cut down	6
Monday, August 27, 2018	Beam lifted of bed	6

Table D-6 Specimen CR-70 construction schedule

Date	Activity	Concrete age (days)
Tuesday, August 28, 2018	Layout prestressing strands	-
Wednesday, August 29, 2018	Place reinforcement	-
Friday, August 31, 2018	Concrete pour	-
Tuesday, September 4, 2018	Forms removed	4
Wednesday, September 5, 2018	Install external gages and setup	5
Friday, September 7, 2018	Strand cut down	7
Friday, September 7, 2018	Beam lifted of bed	7

Table D-7 Specimen PP-50 construction schedule

Date	Activity	Concrete age (days)
Tuesday, September 11, 2018	Layout prestressing strands	-
Wednesday, September 12, 2018	Place reinforcement	-
Friday, September 14, 2018	Concrete pour	-
Wednesday, September 19, 2018	Forms removed	5
Wednesday, September 19, 2018	Install external gages and setup	5
Wednesday, September 19, 2018	Strand cut down	5
Thursday, September 20, 2018	Beam lifted of bed	6
Thursday, November 15, 2018	Beam moved to second storage	62

D.2 Strand stress report specimen CT

DURA-STRESS INC.
STRAND STRESS REPORT

78 FIB

DATE:	7/31/2018	ITEM NO'S:	MARK #
PROJECT NO.	B1767, B1788		1767-3@B347, 1788-1@G1
PRODUCT	78 FIB		
BED NO.	19N		
NO. OF CABLE:	61		JACK CAL DATES: 10-27-17 / 10-27-18
TECHNICIAN.	NBrooks	Ambient temperature(at): 82	AMBIENT TEMP:
DATE:	7-31-18		JACK # : T-14
		CABLE TYPE:	.600 7W 270 LR ASTM A416

CHUCK SLIPPAGE			
LIVE		DEAD	
1/4 1/4 1/4 1/2 1/2 3/8 5/8		0 1/8 1/16 1/16 1/8 1/16 1/8	
AVERAGE:		AVERAGE:	
TOTAL:			

FINAL TENSION	44534
	44550
FINAL ELONGATION	38 7/8
+2.5%	39 7/8
- 2.5%	37 15/16

AASHTO MAX = 46872

IF TARGET = AASHTO ELONGATION MAY NOT WORK

	GAUGE	ELO		GAUGE	ELO		GAUGE	ELO		GAUGE	ELO		GAUGE	ELO		GAUGE	ELO		GAUGE	ELO
1	44550	38 1/2	12	44550	39	23	44550	38 1/2	34	44550	38 1/2	45	44550	38 1/2	56	44600	38 1/2	67		
2	44550	38	13	44550	39	24	44550	39	35	44550	38 3/8	46	44550	38 1/2	57	44550	38 1/4	68		
3	44550	38 1/2	14	44550	39	25	44550	38 3/4	36	44550	38 1/4	47	44550	39	58	44550	38 1/4	69		
4	44550	38 1/2	15	44600	38 3/8	26	44550	38 1/2	37	44550	38 1/2	48	44550	38 1/2	59	44550	38 1/4	70		
5	44550	38 1/4	16	44550	39	27	44550	39	38	44550	38 3/8	49	44550	38 1/2	60	44550	38 1/4	71		
6	44550	38 3/4	17	44550	38 1/2	28	44550	39	39	44550	38 1/2	50	44550	38 3/8	61	44550	38 1/4	72		
7	44550	38 1/2	18	44550	38 1/4	29	44550	38 1/2	40	44550	38 1/2	51	44600	38 1/2	62			73		
8	44550	39	19	44550	38 1/2	30	44550	38 3/4	41	44550	38 1/2	52	44550	38 1/2	63			74		
9	44550	39	20	44550	38 1/2	31	44550	39	42	44550	38 1/2	53	44550	38 3/4	64			75		
10	44550	38 3/4	21	44550	38 3/8	32	44550	38 1/2	43	44550	38	54	44550	38 1/2	65			76		
11	44550	39	22	44550	39	33	44550	38 1/2	44	44550	38	55	44550	38 1/2	66			77		

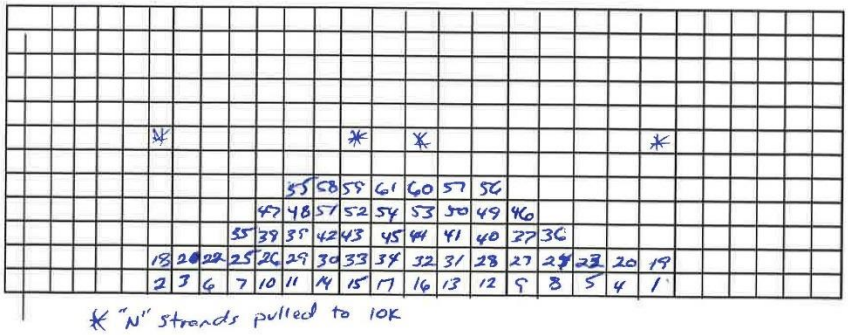

19N

7/31/2018 10:04

PRODUCT
78 FIB

JOB#:	B1767, B1788		MARK #
DATE:	7/31/2018		
BED #:	19N		1767-3@B347, 1788-1@G1
JACK #			
STRAND SIZE	.600 7W 270 LR ASTM A416		
COIL/PACK/REEL #	002675006-0	002669001-0	
0	002675007-0	002690007-0	
0	002668001-0	002689001-0	
	002675005-0	002668004-0	
BED LENGTH (L):	6174.125	0	
STRAND SIZE: (A)	0.2170	0	
FINAL TEN. (P)	43940	0	
PRE TEN. : (Pi)	5000	0	
M.O.E. (E):	28.78	0	
		0	
		0	

CORRECTION INFO.	
Number of cable #	61
Exp. Conc temp @ Placement:	85
Ambient temperature(at):	82
Abutment rotation (ar): N/A	0
Live end seating (les):	0.2969
Dead end slippage (des):	0.0938
anchorage movement:	0.5625

ELONGATION

delta.a.t (Ptxdb/Pb)=	0
delt.(Pi x L)/(A x E) =	4.9439
delta'b.(PxL)/(AxE)=	38.5032
delta'bed shortning (bs/2)+(bs/#strand)=	0.2905

GROSS ELONG. 39.184

NET ELONG.	38 7/8

RANGE + 2.5%	39 7/8
RANGE - 2.5%	37 15/16

FORCE ADJUSTMENTS

Pb (P - Pi) =	38940
Pt(=	0
Par (arxAxE)/(L)=	0
Pies(lesxAxE)/(L)=	300.2685
Pdes no adj. required	0
Pbs (dbsxAXE)/(L)=	293.7959
TOTAL FORCE ADJ.	594.0644
ADJUSTED FORCE =	39534.0644

JACKING FORCE = 44534

TOTAL ADJ. FORCE	44534

AASHTO MAX = 46872

RANGE +2.5% =	45647
RANGE -2.5% =	43421

19N

D.3 Strand stress report specimen SH-30

DURA-STRESS INC.
STRAND STRESS REPORT

78 FIB

DATE:	8/13/2018	ITEM NO'S:	MARK #
PROJECT NO.	B1767, B1788		1767-3@B347, 1788-1@G3
PRODUCT	78 FIB		
BED NO.	19N		
NO. OF CABLE:	61		JACK CAL DATES: 10-27-17
TECHNICIAN.	SB	Ambient temperature(at): 80	AMBIENT TEMP: 80
DATE:	8-13-18		JACK # : 114
			CABLE TYPE: .600 7W 270 LR ASTM A416

CHUCK SLIPPAGE	
LIVE	DEAD
3/8 3/8 3/8 1/4 1/4 7/16 3/8	1/8 0 1/8 1/8 1/16 1/8 1/8
AVERAGE:	AVERAGE:
TOTAL:	

FINAL TENSION	44533
FINAL ELONGATION	39
+2.5%	39 15/16
- 2.5%	38

AASHTO MAX = 46872

IF TARGET = AASHTO ELONGATION MAY NOT WORK

	GAUGE	ELO		GAUGE	ELO		GAUGE	ELO		GAUGE	ELO		GAUGE	ELO		GAUGE	ELO		GAUGE	ELO
1	44650	38 3/4	12	44600	38 1/2	23	44650	39	34	44650	39	45	44650	38 3/4	56	44650	38 1/2	67		
2	44650	39 1/2	13	44600	38 3/4	24	44650	38 1/2	35	44600	38 1/2	46	44650	39	57	44650	39	68		
3	44650	39	14	44650	39 1/2	25	44650	39 1/2	36	44650	39 1/2	47	44650	39	58	44650	38 1/2	69		
4	44650	39	15	44650	38 1/2	26	44600	38 1/2	37	44650	38 1/2	48	44650	38 1/2	59	44600	38 1/2	70		
5	44650	38 1/2	16	44650	38 1/2	27	44600	38 1/2	38	44650	38 3/4	49	44650	38 3/4	60	44600	38 1/2	71		
6	44650	38 1/2	17	44650	39	28	44650	39	39	44650	38 1/2	50	44650	39	61	44600	39	72		
7	44650	39	18	44600	38 3/4	29	44650	38 3/4	40	44650	38 3/4	51	44650	39	62			73		
8	44650	38 1/2	19	44650	39	30	44600	39	41	44600	38 1/2	52	44650	39	63			74		
9	44650	39	20	44650	39	31	44650	38 1/2	42	44650	39	53	44650	39	64			75		
10	44650	39	21	44650	39	32	44650	39	43	44650	38 1/2	54	44650	39	65			76		
11	44650	39	22	44650	39 1/4	33	44650	39 1/4	44	44650	38 1/4	55	44650	38 1/2	66			77		

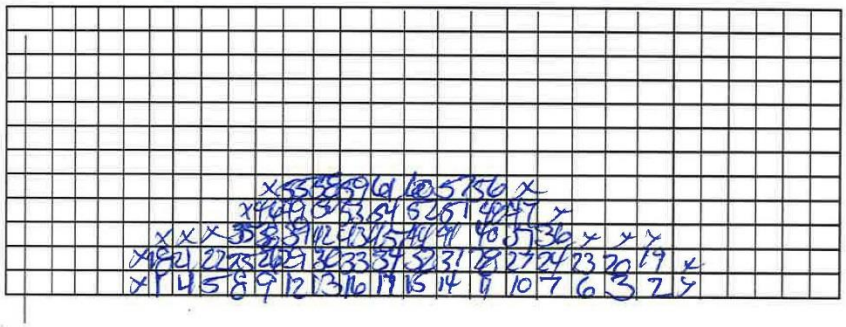

19N

8/13/2018 7:23

PRODUCT
78 FIB

JOB#:	B1767, B1788	
DATE:	8/13/2018	
BED #:	19N	
JACK #		
STRAND SIZE	.600 7W 270 LR ASTM A416	
COIL/PACK/REEL #	002692006-0	002692005-0
0	002807003-0	002808006-0
0	002807007-0	002782004-0
	002664002-0	002782002-0
BED LENGTH (L):	6174.125	0
STRAND SIZE: (A)	0.2170	0
FINAL TEN. (P)	43940	0
PRE TEN. : (Pi)	5000	0
M.O.E. (E):	28.71	0
		0
		0

MARK #
1767-3@B347, 1788-1@G3

CORRECTION INFO.	
Number of cable #	61
Exp. Conc temp @ Placement:	85
Ambient temperature(at):	80
Abutment rotation (ar): N/A	0
Live end seating (les):	0.2969
Dead end slippage (des):	0.0938
anchorage movement:	0.5625

ELONGATION

delta.a.t (Ptxdb/Pb)=	0
delt.(Pi x L)/(A x E) =	4.9547
delta'b.(PxL)/(AxE)=	38.587
delta'bed shortning (bs/2)+(bs/#strand)=	0.2905

GROSS ELONG. 39.268

NET ELONG.	39

RANGE + 2.5%	39 15/16
RANGE - 2.5%	38

FORCE ADJUSTMENTS

Pb (P - Pi) =	38940
Pt(=	0
Par (arxAxE)/(L)=	0
Ples(lesxAxE)/(L)=	299.6164
Pdes no adj. required	0
Pbs (dbsxAXE)/(L)=	293.1578
TOTAL FORCE ADJ.	592.7742
ADJUSTED FORCE =	39532.7742

JACKING FORCE = 44533

TOTAL ADJ. FORCE	44533

AASHTO MAX = 46872

RANGE +2.5% =	45646
RANGE -2.5% =	43420

19N

D.4 Strand stress report specimen SH-70

DURA-STRESS INC.
STRAND STRESS REPORT

~~12:00 AM~~ 78 FIB

DATE:	8/17/2018
PROJECT NO.	B1775
PRODUCT	~~12:00 AM~~ 78 FIB
BED NO.	19S
NO. OF CABLE:	61
TECHNICIAN.	JB
DATE:	8-17-18
Ambient temperature(at):	79

ITEM NO'S: MARK #

B1767 3@B344
B178 1@G4

JACK CAL DATES: 10-17-17
AMBIENT TEMP: 79
JACK # : T-14
CABLE TYPE: .600 7W 270 LR ASTM A416

CHUCK SLIPPAGE	
LIVE	DEAD
7/16 3/8 3/8 1/4 1/4 3/8 3/8	1/8 1/8 4/16 4/16 1/8 1/8
AVERAGE:	AVERAGE:
TOTAL:	

FINAL TENSION	44530
FINAL ELONGATION	37 1/2
+2.5%	38 7/16
- 2.5%	36 9/16

AASHTO MAX = 46872
IF TARGET = AASHTO ELONGATION MAY NOT WORK

GAUGE	ELO	GAUGE	ELO	GAUGE	ELO	GAUGE	ELO	GAUGE	ELO	GAUGE	ELO	GAUGE	ELO
1	44650 37 1/2	12	44650 37	23	44650 37 1/2	34	44650 37 1/2	45	44650 37 3/4	56	44650 37 1/2	67	
2	44650 37	13	44650 37	24	44650 37 1/4	35	44650 37 1/4	46	44650 37 1/4	57	44650 37 3/4	68	
3	44650 37 1/4	14	44650 37 1/2	25	44650 37 1/2	36	44650 37 3/4	47	44650 37	58	44650 37 1/4	69	
4	44650 37	15	44650 37 1/2	26	44650 37 3/4	37	44650 37 1/2	48	44650 37 1/4	59	44650 37 3/4	70	
5	44650 37 1/4	16	44650 37	27	44650 37 1/2	38	44650 37 3/4	49	44650 37 3/4	60	44650 37 1/2	71	
6	44650 37	17	44650 37 1/2	28	44650 37 1/4	39	44650 37 1/2	50	44650 37 1/2	61	44650 37 1/2	72	
7	44650 37	18	44650 37 3/4	29	44650 37 1/4	40	44650 37 1/2	51	44650 37 3/4	62		73	
8	44650 37 1/2	19	44650 37 1/2	30	44650 39	41	44650 37 3/4	52	44650 37 3/4	63		74	
9	44650 37 1/4	20	44650 37 1/4	31	44650 37 3/4	42	44650 37 3/4	53	44650 39	64		75	
10	44650 37 1/2	21	44650 37 1/4	32	44650 38 1/4	43	44650 37 1/2	54	44650 37 1/2	65		76	
11	44650 37 1/2	22	44650 37 1/2	33	44650 37 1/4	44	44650 37 1/2	55	44650 37 1/2	66		77	

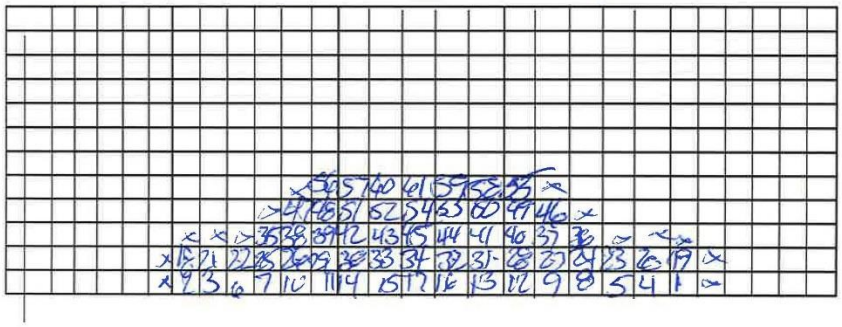

19S

8/17/2018 3:58

PRODUCT
12:00 AM
MARK #
0

JOB#:	B1775	
DATE:	8/17/2018	
BED #:	19S	
JACK #		
STRAND SIZE	.600 7W 270 LR ASTM A416	
COIL/PACK/REEL #	002807002-0	002807004-0
0	002692007-0	002782002-0
0	002807001-0	002782004-0
	002777006-0	002432006-0
BED LENGTH (L):	6170.75	002808004-0
STRAND SIZE: (A)	0.2170	0
FINAL TEN. (P)	43940	0
PRE TEN. : (Pi)	6500	0
M.O.E. (E):	28.70	0
		0
		0

CORRECTION INFO.	
Number of cable #	61
Exp. Conc temp @ Placement:	85
Ambient temperature(at):	79
Abutment rotation (ar): N/A	0
Live end seating (les):	0.2813
Dead end slippage (des):	0.0781
anchorage movement:	0.5875

ELONGATION

delta.a.t (Ptxdb/Pb)=	0
delt.(Pi x L)/(A x E) =	6.4404
delta'b.(PxL)/(AxE)=	37.0964
delta'bed shortning (bs/2)+(bs/#strand)=	0.3034

GROSS ELONG. 37.759

NET ELONG.	37 1/2

RANGE + 2.5%	38 7/16
RANGE - 2.5%	36 9/16

FORCE ADJUSTMENTS

Pb (P - Pi) =	37440
Pt(=	0
Par (arxAxE)/(L)=	0
Ples(lesxAxE)/(L)=	283.9052
Pdes no adj. required	0
Pbs (dbsxAXE)/(L)=	306.2099
TOTAL FORCE ADJ.	590.1151
ADJUSTED FORCE =	38030.1151

JACKING FORCE = 44530

TOTAL ADJ. FORCE	44530

AASHTO MAX = 46872

RANGE +2.5% =	45643
RANGE -2.5% =	43417

19S

D.5 Strand stress report specimen CR-70

DURA-STRESS INC.
STRAND STRESS REPORT

78 FIB

		ITEM NO'S:	MARK #
DATE:	8/29/2018		
PROJECT NO.	B1767, B1788		3-B341, 1-G5
PRODUCT	78 FIB		
BED NO.	19S		
NO. OF CABLE:	61		JACK CAL DATES: 8-18-16
TECHNICIAN.	SB	Ambient temperature(at):	AMBIENT TEMP: 77
DATE:	8-29-18	80	JACK # : T14

CABLE TYPE: .600 7W 270 LR ASTM A416

CHUCK SLIPPAGE	
LIVE	DEAD
1/4 2/16 3/16 3/16 3/16 4/16 5/16	1/16
	Production moved after 6 grommets
AVERAGE:	AVERAGE:
TOTAL:	

FINAL TENSION	44532
FINAL ELONGATION	38 13/16
+2.5%	39 13/16
- 2.5%	37 7/8

AASHTO MAX = 46872

IF TARGET = AASHTO ELONGATION MAY NOT WORK

	GAUGE	ELO		GAUGE	ELO		GAUGE	ELO		GAUGE	ELO		GAUGE	ELO		GAUGE	ELO		GAUGE	ELO
1	44550	37 1/8	12	44550	39	23	44600	38	34	44550	38 1/4	45	44600	38 1/4	56	44600	38 3/8	67		
2	44550	37 7/8	13	44550	38 1/4	24	44550	38 1/4	35	44600	38 1/2	46	44550	38	57	44550	38	68		
3	44600	38	14	44550	38 1/4	25	44600	38 1/2	36	44550	39	47	44600	38 3/8	58	44550	38 1/4	69		
4	44550	37 1/4	15	44550	38	26	44550	38 3/8	37	44550	39	48	44550	39	59	44550	38 1/8	70		
5	44600	38 1/8	16	44550	39	27	44550	38 1/2	38	44550	38 1/4	49	44550	38 1/2	60	44550	38 1/4	71		
6	44550	38 1/4	17	44550	38 1/2	28	44550	38 3/4	39	44550	38 3/8	50	44550	38 3/8	61	44600	38 1/2	72		
7	44550	38 1/4	18	44550	38 1/2	29	44550	38 1/2	40	44550	38 1/4	51	44550	38 1/4	62			73		
8	44550	38 1/4	19	44550	37	30	44550	38	41	44550	39	52	44600	39	63			74		
9	44550	37 7/8	20	44600	38 1/4	31	44550	39	42	44550	38 1/2	53	44600	38 1/4	64			75		
10	44550	38 1/4	21	44550	38 1/4	32	44550	38 1/2	43	44550	38 1/4	54	44600	38 1/2	65			76		
11	44550	38 1/4	22	44550	38 1/2	33	44550	38 3/8	44	44600	38 1/4	55	44550	38 1/2	66			77		

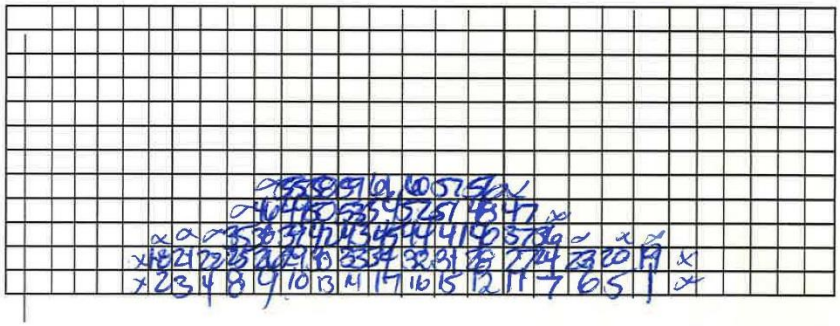

19S

8/29/2018 5:14

PRODUCT
78 FIB

JOB#:	B1767, B1788	
DATE:	8/29/2018	
BED #:	19S	
JACK #		
STRAND SIZE	.600 7W 270 LR ASTM A416	
COIL/PACK/REEL #	002808001-0	002868001-0
0	002875003-0	002429007-0
0	002875004-0	002869006-0
	002875007-0	002817003-0
BED LENGTH (L):	6170.75	002692003-0
STRAND SIZE: (A)	0.2170	0
FINAL TEN. (P)	43940	0
PRE TEN. : (Pi)	5000	0
M.O.E. (E):	28.79	0
		0
		0

MARK #
3-B341, 1-G5

CORRECTION INFO.	
Number of cable #	61
Exp. Conc temp @ Placement:	85
Ambient temperature(at):	80
Abutment rotation (ar): N/A	0
Live end seating (les):	0.2813
Dead end slippage (des):	0.0781
anchorage movement:	0.5875

ELONGATION

delta.a.t (Ptxdb/Pb)=	0
delt.(Pi x L)/(A x E) =	4.9388
delta'b.(PxL)/(AxE)=	38.4635
delta'bed shortning (bs/2)+(bs/#strand)=	0.3034

GROSS ELONG. 39.126

NET ELONG.	38 13/16

RANGE + 2.5%	39 13/16
RANGE - 2.5%	37 7/8

FORCE ADJUSTMENTS

Pb (P - Pi) =	38940
Pt(=	0
Par (arxAxE)/(L)=	0
Ples(lesxAxE)/(L)=	284.7845
Pdes no adj. required	0
Pbs (dbsxAXE)/(L)=	307.1583
TOTAL FORCE ADJ.	591.9428
ADJUSTED FORCE =	39531.9428

JACKING FORCE = 44532

TOTAL ADJ. FORCE	44532

AASHTO MAX = 46872

RANGE +2.5% =	45645
RANGE -2.5% =	43419

19S

D.6 Strand stress report specimen PP-50

DURA-STRESS INC.
STRAND STRESS REPORT

78 FIB

		ITEM NO'S:	MARK #
DATE:	9/11/2018		
PROJECT NO.	B1767, B1788		1767 - 1-B343, 1-B345, 1-B346, 1788 - 1-G2
PRODUCT	78 FIB		
BED NO.	19S		
NO. OF CABLE:	61		JACK CAL DATES: 8-18-18
TECHNICIAN.	SB	Ambient temperature(at):	AMBIENT TEMP: 82
DATE:	9-11-18	84	JACK # : T14

CABLE TYPE: .600 7W 270 LR ASTM A416

CHUCK SLIPPAGE				FINAL TENSION	44531
LIVE		DEAD			
3/16 1/4 3/16 5/16 3/16 3/16 1/4		1/16 1/8 1/16 1/16 1/16 1/16 1/8		FINAL ELONGATION	38 7/8
				+2.5%	39 13/16
				- 2.5%	37 7/8
AVERAGE:		AVERAGE:			
TOTAL:				AASHTO MAX =	46872

IF TARGET = AASHTO ELONGATION MAY NOT WORK

GAUGE	ELO	GAUGE	ELO	GAUGE	ELO	GAUGE	ELO	GAUGE	ELO	GAUGE	ELO	GAUGE	ELO
1	38 5/8	12	39	23	39	34	39	45	38 1/2	56	39	67	
2	39	13	38 1/2	24	38 3/4	35	39	46	38 1/2	57	38 1/2	68	
3	39 1/2	14	38 3/4	25	39	36	38 3/4	47	38 3/4	58	38 3/4	69	
4	39 3/4	15	38 3/4	26	39	37	38 1/2	48	38 3/4	59	38 3/4	70	
5	39 3/4	16	39	27	39	38	38 1/2	49	39	60	39	71	
6	39 1/4	17	38 1/2	28	39	39	39	50	38 3/4	61	38 3/4	72	
7	39	18	38 1/2	29	38 3/4	40	39	51	38 1/2	62		73	
8	39 1/4	19	39	30	39 1/4	41	38 1/2	52	38 1/2	63		74	
9	39	20	39	31	39	42	39	53	39	64		75	
10	38 1/2	21	39	32	38 1/2	43	39	54	39	65		76	
11	38 1/2	22	39 1/2	33	38 1/2	44	38 3/4	55	38 3/4	66		77	

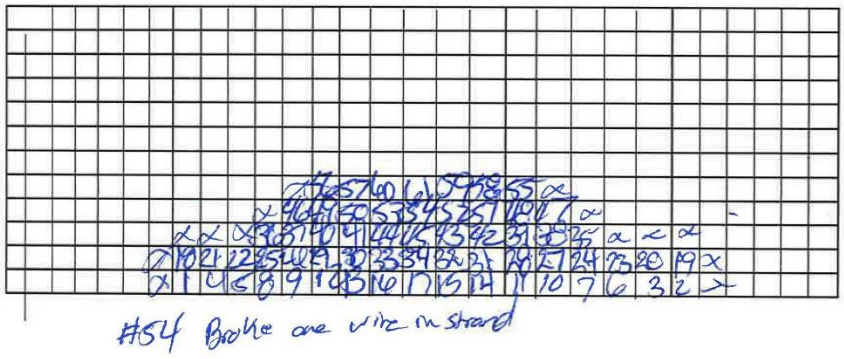

#54 Broke one wire in strand

19S

9/11/2018 9:57

PRODUCT
78 FIB

MARK #
1767 - 1-B343, 1-B345, 1-B346, 1788 - 1-G2

JOB#:	B1767, B1788	
DATE:	9/11/2018	
BED #:	19S	
JACK #		
STRAND SIZE	.600 7W 270 LR ASTM A416	
COIL/PACK/REEL #	002817007-0	002868002-0
0	002943006-0	002872001-0
0	002875006-0	002869001-0
	002944005-0	002811005-0
BED LENGTH (L):	6170.75	002817006-0
STRAND SIZE: (A)	0.2170	0
FINAL TEN. (P)	43940	0
PRE TEN. : (Pi)	5000	0
M.O.E. (E):	28.77	0
		0
		0

CORRECTION INFO.	
Number of cable #	61
Exp. Conc temp @ Placement:	85
Ambient temperature(at):	84
Abutment rotation (ar): N/A	0
Live end seating (les):	0.2813
Dead end slippage (des):	0.0781
anchorage movement:	0.5875

ELONGATION

delta.a.t (Ptxdb/Pb)=	0
delt.(Pi x L)/(A x E) =	4.9426
delta'b.(PxL)/(AxE)=	38.4933
delta'bed shortning (bs/2)+(bs/#strand)=	0.3034

GROSS ELONG. 39.156

NET ELONG.	38 7/8

RANGE + 2.5%	39 13/16
RANGE - 2.5%	37 7/8

FORCE ADJUSTMENTS

Pb (P - Pi) =	38940
Pt(=	0
Par (arxAxE)/(L)=	0
Ples(lesxAxE)/(L)=	284.5647
Pdes no adj. required	0
Pbs (dbsxAXE)/(L)=	306.9212
TOTAL FORCE ADJ.	591.4859
ADJUSTED FORCE =	39531.4859

JACKING FORCE = 44531

TOTAL ADJ. FORCE	44531

AASHTO MAX = 46872

RANGE +2.5% =	45644
RANGE -2.5% =	43418

19S

Appendix E — Residual strength of concrete mixtures for FIB construction

ASTM C1399

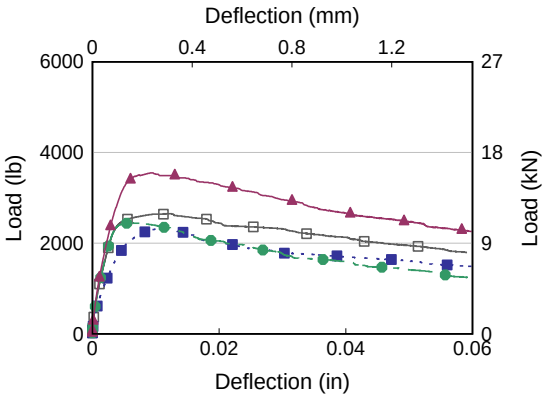

Figure E-1 Load-deflection for SH-30

EN 14651

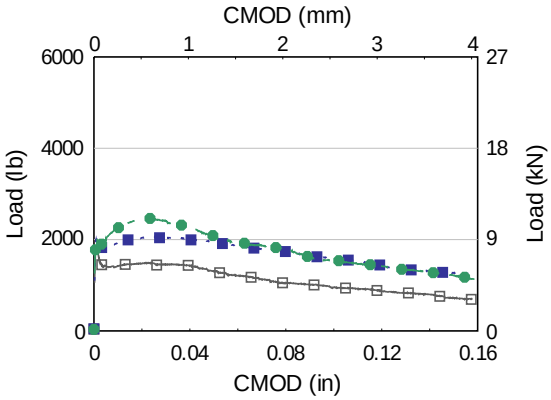

Figure E-2 Load-CMOD for SH-30

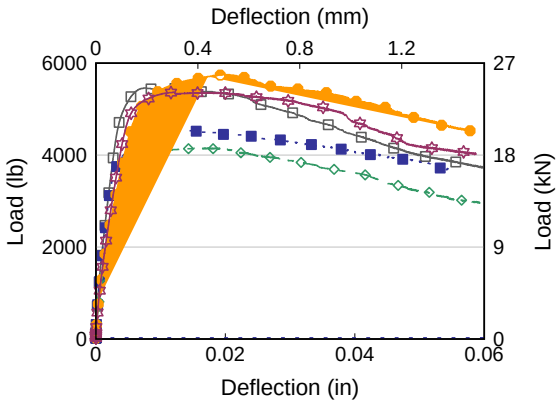

Figure E-3 Load-deflection for SH-70

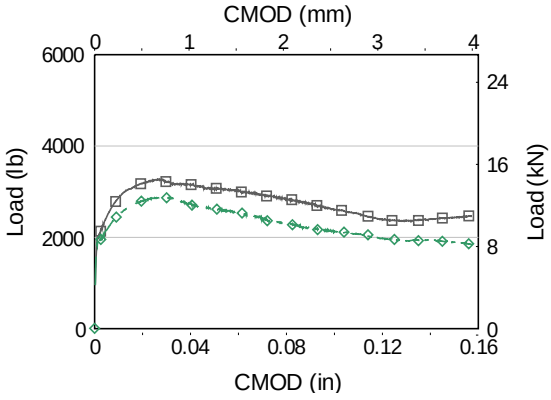

Figure E-4 Load-CMOD for SH-70

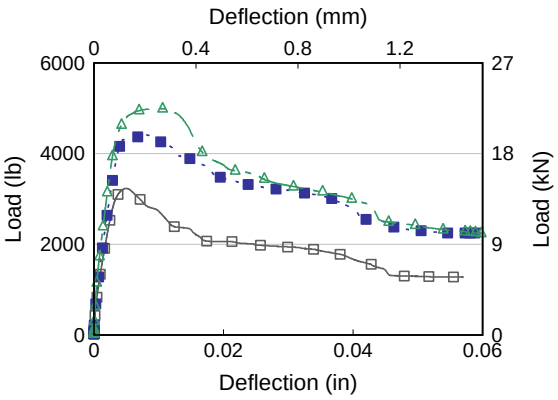

Figure E-5 Load-deflection for CR-70

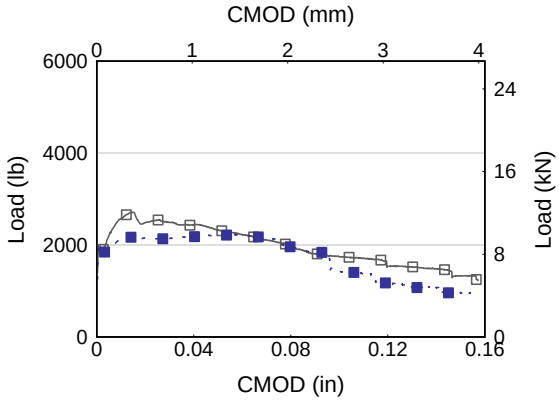

Figure E-6 Load-CMOD for CR-70

ASTM C1399

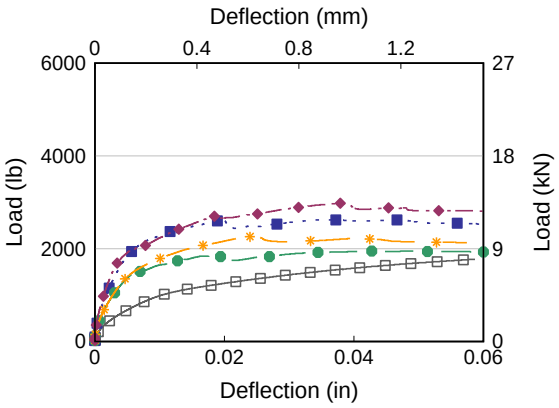

Figure E-7 Load-deflection for PP-50

EN 14651

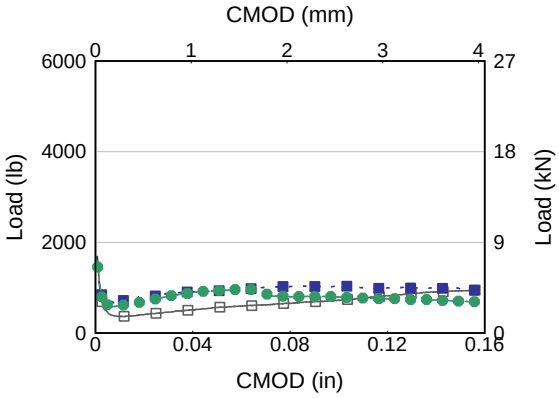

Figure E-8 Load-CMOD for PP-50

Appendix F — End region crack monitoring

F.1 Instrumentation for strain monitoring during prestress transfer

Figure F-1 shows the coordinate system used. Table F-3 through Table F-1contain coordinates of strain gages used to monitor concrete and mild steel reinforcement strains during prestress transfer. Strain measurements for gages XS, IS and ES were taken continuously during the prestress transfer using a computerized data acquisition system powered by a portable generator (Figure F-2). Data was collected at a sample rate of 12 Hz.

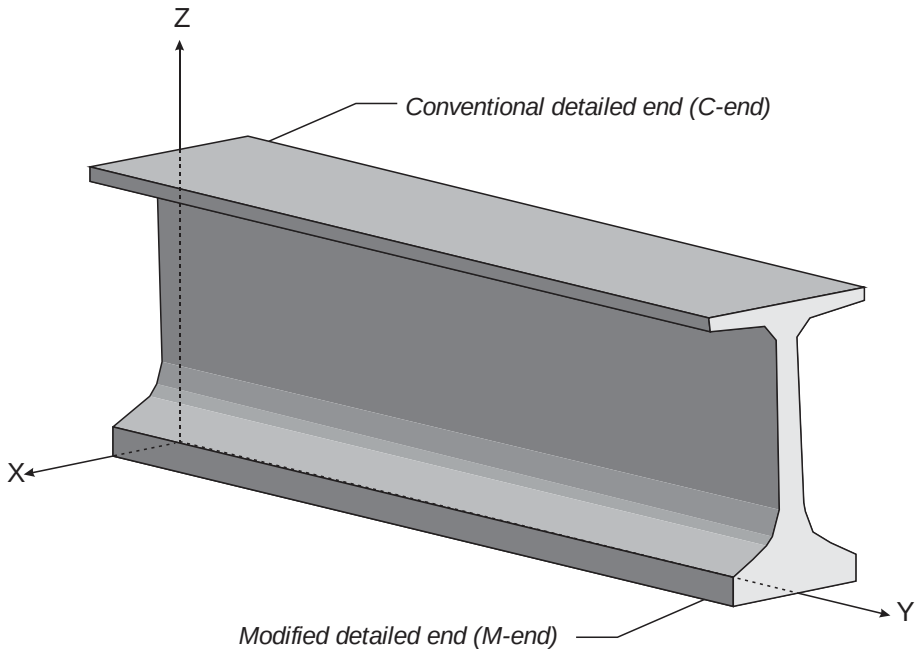

Figure F-1 Coordinate system

Table F-1 Internal foil gages coordinates.

Instrument	X (in.)	Y (in.)	Z (in.)	Orientation
IS-1-DC	1	2.25	46.25	Z
IS-2-DC	-1	5.75	46.25	Z
IS-3-DC	1	9.25	46.25	Z
IS-4-DC	-1	12.75	46.25	Z
IS-5-DC	1	16.25	46.25	Z
IS-1-DM	1	234.25	46.25	Z
IS-2-DM	-1	227.25	46.25	Z
IS-3-DM	1	220.25	46.25	Z
IS-4-DM	-1	210.75	46.25	Z
IS-5-DM	-1	200.75	46.25	Z

Table F-2 Internal embedded gages coordinates.

Instrument	X (in.)	Y (in.)	Z (in.)	Orientation
ES-1-DC	1	2.25	66.25	Z
ES-2-DC	1	2.25	23.25	Z
ES-1-DM	1	234.25	66.25	Z
ES-2-DM	1	234.25	23.25	Z

Table F-3 Bonded strain gages coordinates.

Instrument	X (in.)	Y (in.)	Z (in.)	Strain measurement direction
XS-1-DC	7	0	75.5	X
XS-2-DC	3.5	6	67	Y
XS-3-DC	3.5	35.5	67	Y
XS-4-DC	3.5	78	67	Y
XS-5-DC	3.5	1	67	Z
XS-6-DC	3.5	1	30	Z
XS-7-DC	19	8	6.25	Y
XS-8-DC	19	16	6.25	Y
XS-9-DC	19	24	6.25	Y
XS-10-DC	19	32	6.25	Y
XS-11-DC	19	40	6.25	Y
XS-12-DC	19	48	6.25	Y
XS-1-DM	7	240	75.5	X
XS-2-DM	3.5	3	67	Y
XS-3-DM	3.5	35.5	67	Y
XS-4-DM	3.5	78	67	Y
XS-5-DM	3.5	239	67	Z
XS-6-DM	3.5	239	30	Z
XS-7-DM	19	232	6.25	Y
XS-8-DM	19	224	6.25	Y
XS-9-DM	19	216	6.25	Y
XS-10-DM	19	208	6.25	Y
XS-11-DM	19	200	6.25	Y
XS-12-DM	19	192	6.25	Y

Figure F-2 Data acquisition setup

F.2 Crack measurement test procedures

Crack width, length, and location were measured and recorded periodically following prestress transfer. Crack measurement procedures were developed such that the crack measurements were taken consistently over time at the same location to allow for direct comparison between readings. Measurement procedures were as follows:

- Cracks were traced using a marker to highlight their location visually. Ends of the crack were labelled using date, to monitor length over time.
- Crack widths were measured using a crack microscope, at each gridline-crack intersection on the side closest to the girder end (Figure F-3). For instance, the width of the crack at location 1 in the figure would be measured. Its location would be denoted as L1 from the nearest horizontal line above. A similar approach would be used for cracks crossing horizontal gridlines. The crack microscope had magnification of 100X and was equipped with divisions allowing measurement to the nearest 0.001 in.
- The gridlines were used to monitor crack length and determine the location of each crack width measurement. The nearest gridline to the crack width measurement was used as reference to record the location of the measurement:
  - For cracks crossing horizontal gridlines, the distance to the vertical gridline within that quadrant closest to the top of the girder was used to determine the location along the Y-axis.
  - For cracks crossing vertical gridlines, the distance to horizontal gridline within that quadrant closest to the girder end was used to determine the location along the Z-axis.

Crack measurements were taken within the end region and at mid-length on both faces of each girder. Girder faces were labeled based on their orientation in the forms during fabrication.

The forms were aligned approximately on an east-west line. The North face of the girder is side of the girder facing north and the South face is the opposite side of the girder (Figure F-4 and Figure F-5).

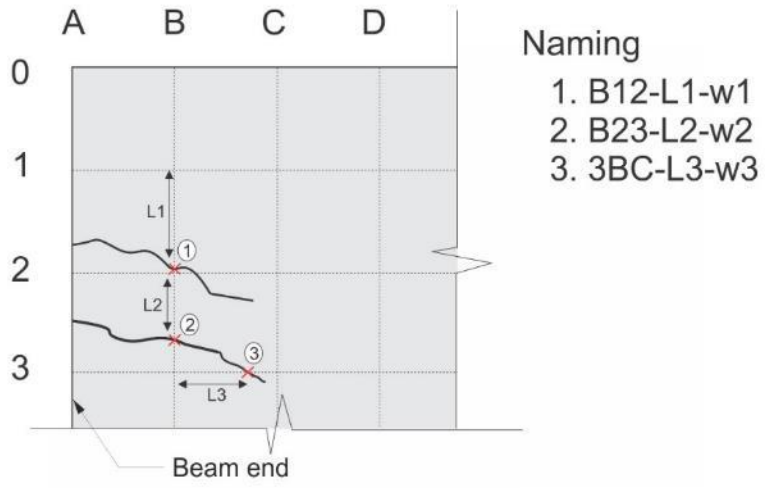

Figure F-3 Illustration of crack labeling and measurements taken

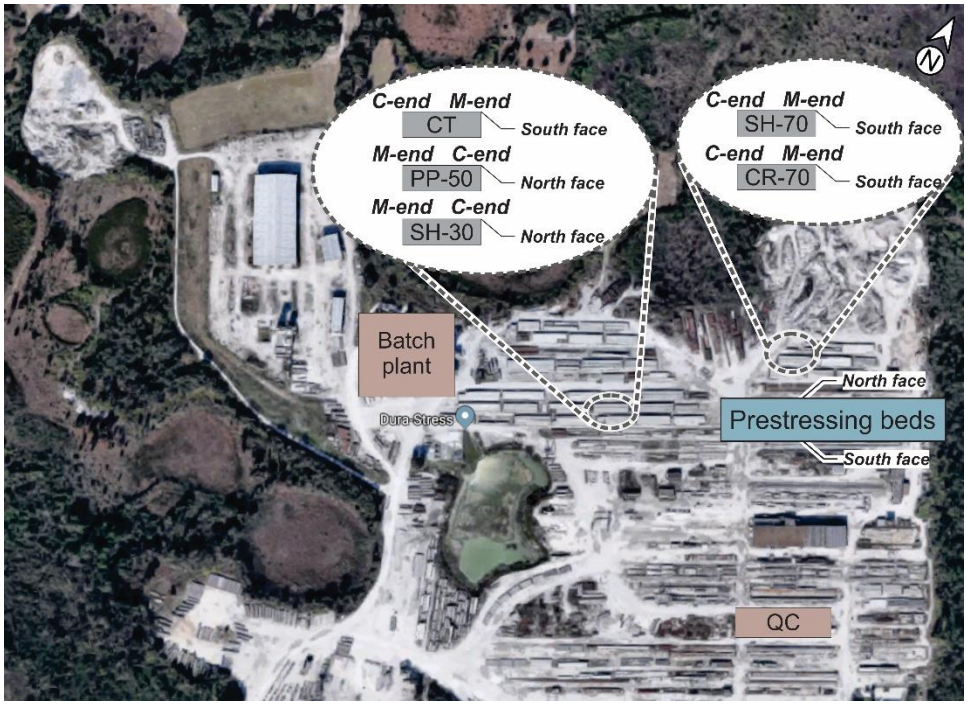

Figure F-4 Girder orientation during end region crack monitoring

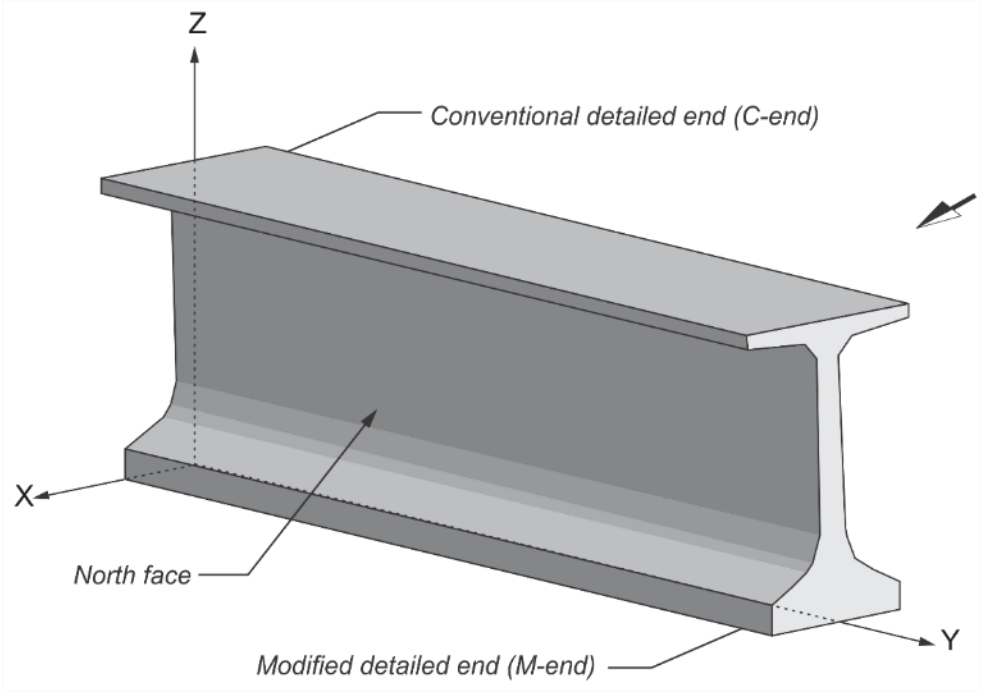

Figure F-5 Girder coordinate system and orientation

F.3 End region crack distribution

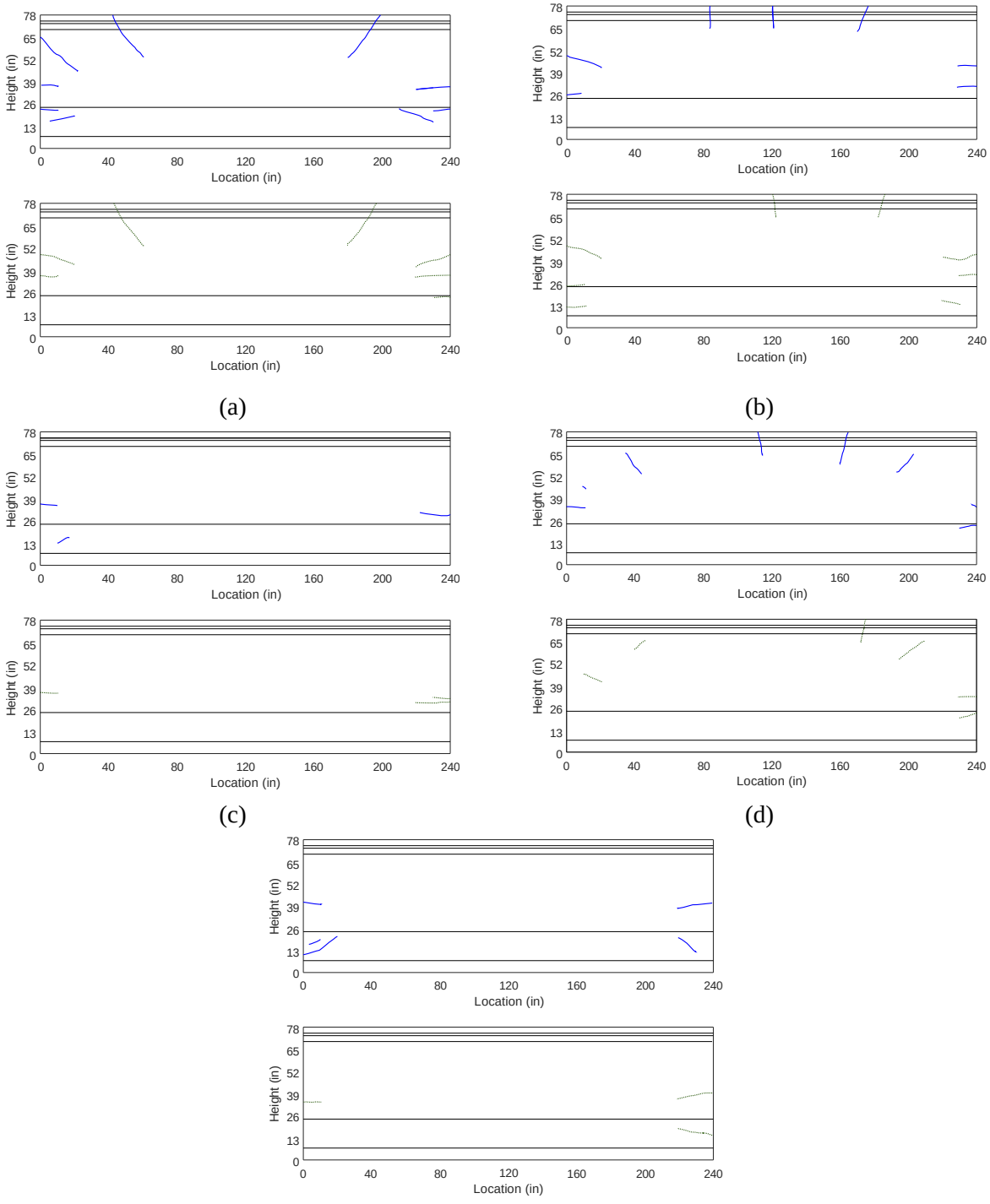

Figure F-6 End region cracking after prestress transfer shown on north elevations of specimen: (a) CT, (b) SH-30, (c) SH-70, (d) CR-70 and (e) PP-50. Solid blue lines depict cracks visible on the North face and dashed green lines depict cracks visible on the South face. Origin at conventional detailing.

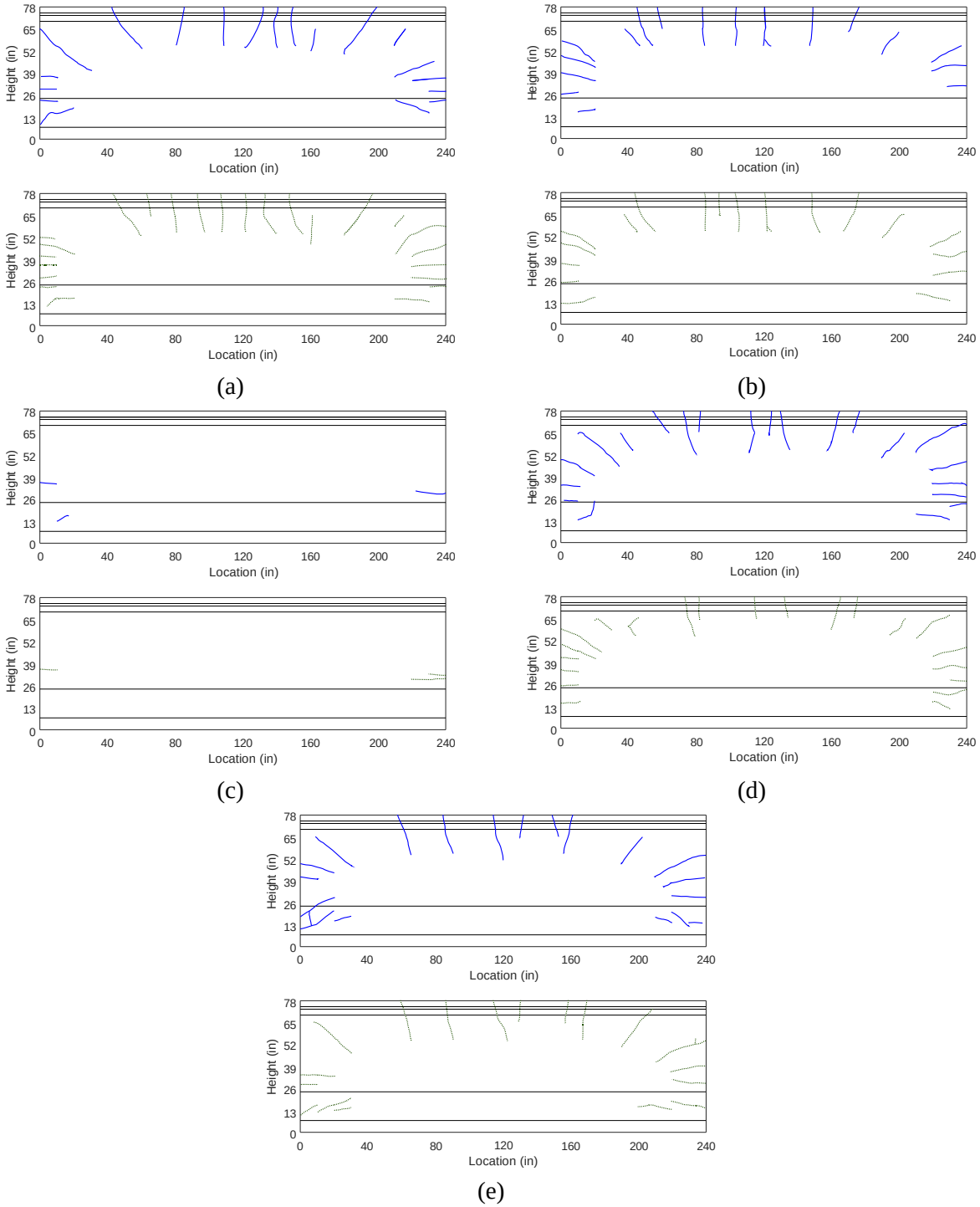

Figure F-7 End region cracking at 14 days shown on north elevations of specimen: (a) CT, (b) SH-30, (c) SH-70, (d) CR-70 and (e) PP-50. Solid blue lines depict cracks visible on the North face and dashed green lines depict cracks visible on the South face. Origin at conventional detailing.

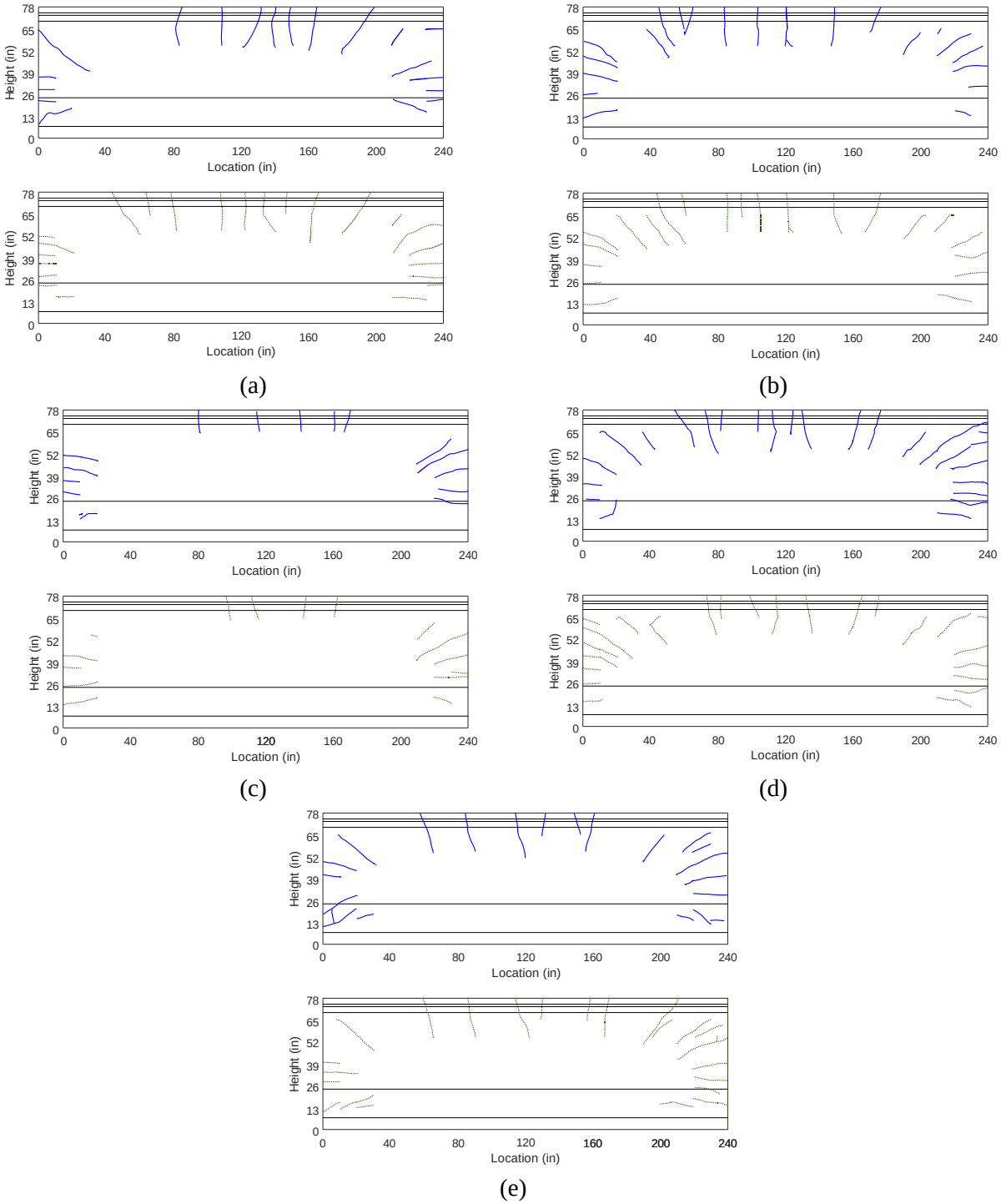

Figure F-8 End region cracking at 28 days shown on north elevations of specimen: (a) CT, (b) SH-30, (c) SH-70, (d) CR-70 and (e) PP-50. Solid blue lines depict cracks visible on the North face and dashed green lines depict cracks visible on the South face. Origin at conventional detailing.

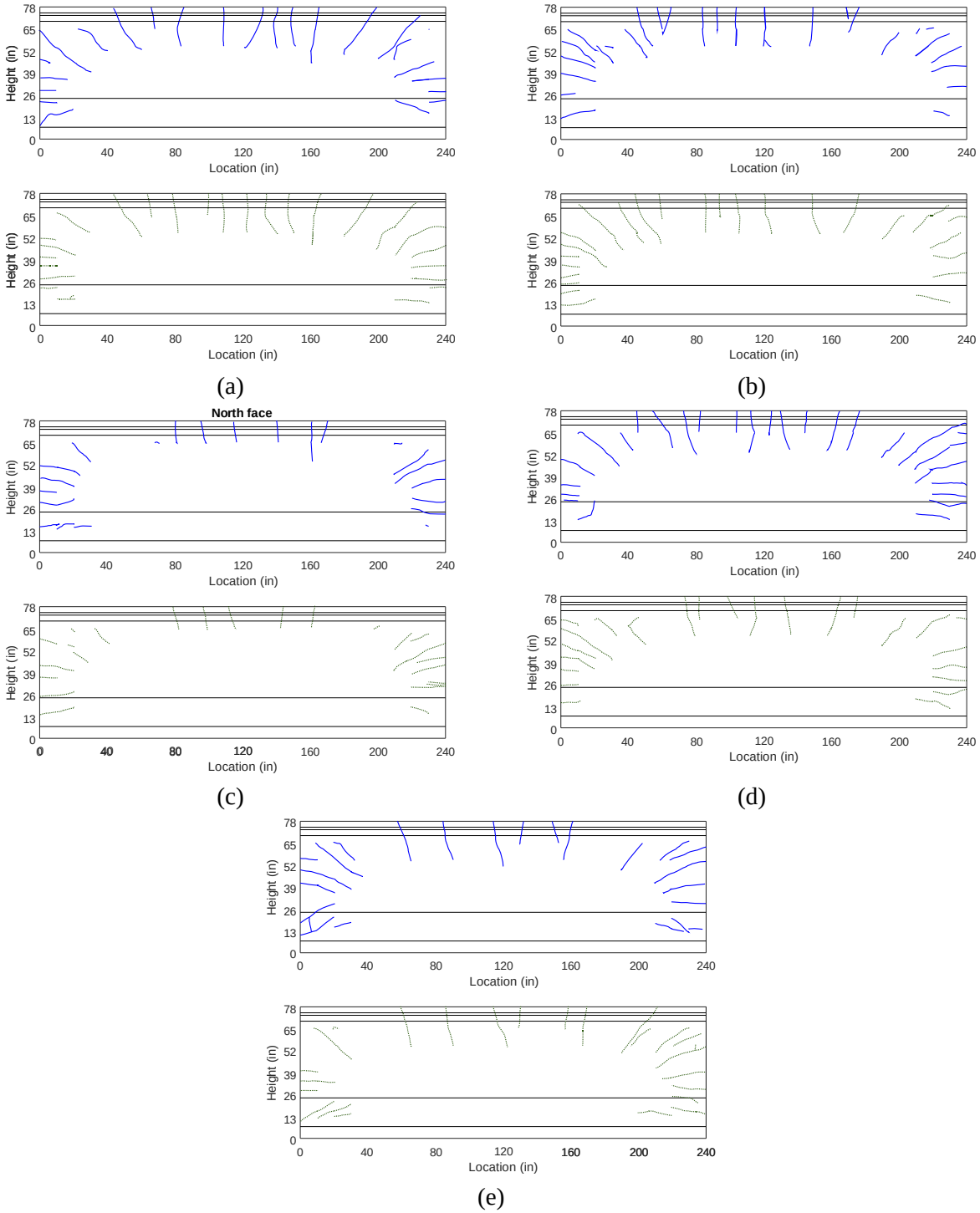

Figure F-9 End region cracking at 148 days shown on north elevations of specimen: (a) CT, (b) SH-30, (c) SH-70, (d) CR-70 and (e) PP-50. Solid blue lines depict cracks visible on the North face and dashed green lines depict cracks visible on the South face. Origin at conventional detailing.

F.4 Effective crack width over time

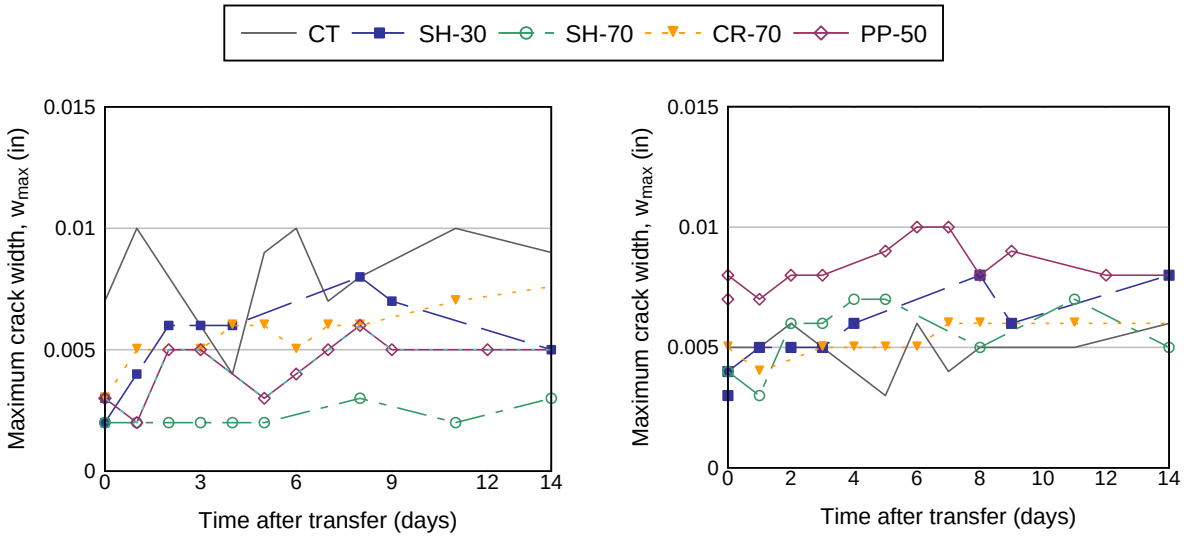

Figure F-10 Maximum web crack width within first 14 days of measurements: (a) Conventional and (b) modified detailing (North face)

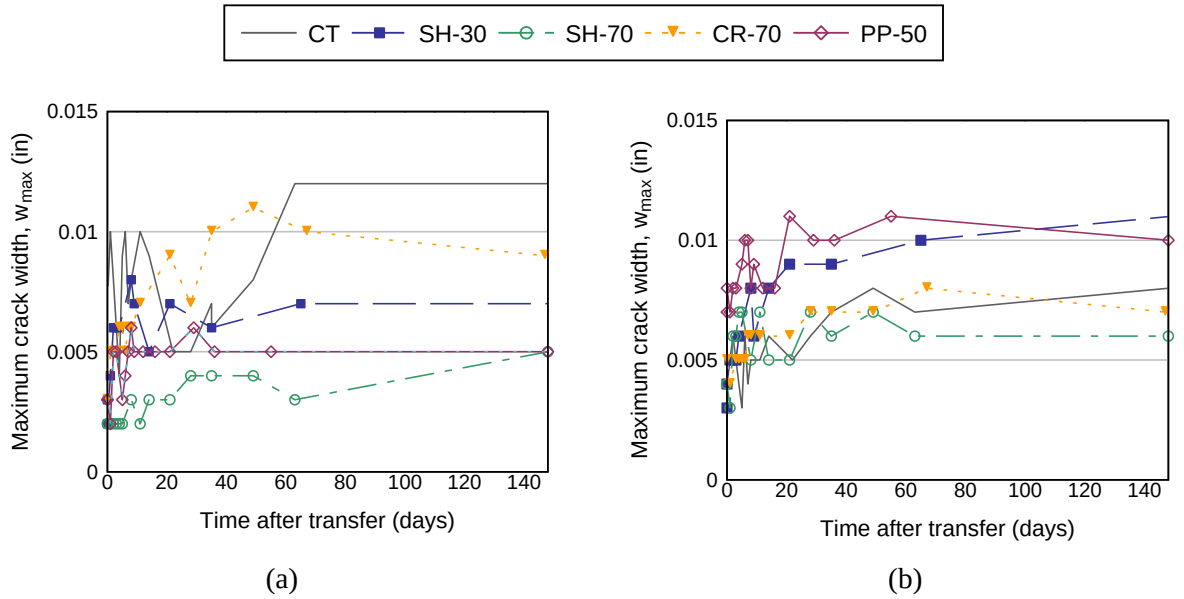

Figure F-11 Maximum web crack width: (a) Conventional and (b) modified detailing (North face)

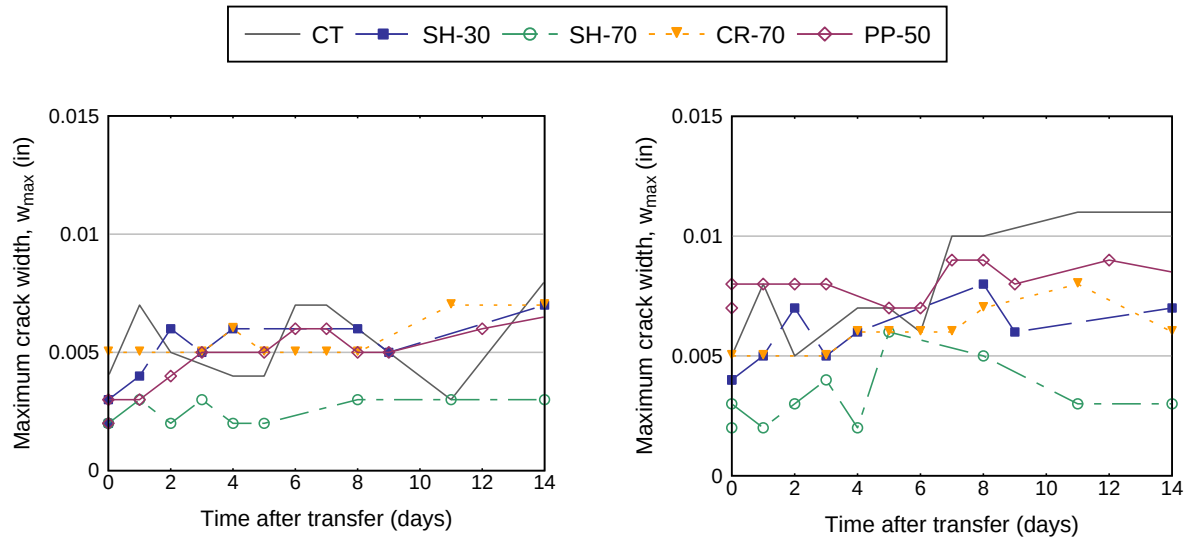

(a) (b)

Figure F-12 Maximum crack width within first 14 days of measurements: (a) Conventional and (b) modified detailing (South face)

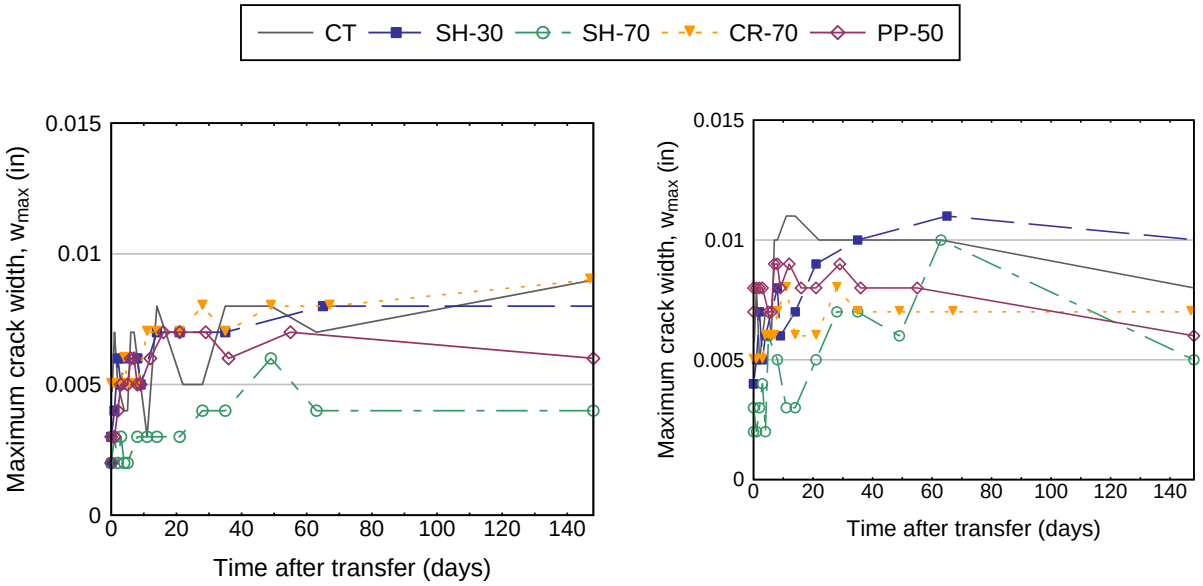

(a) (b)

Figure F-13 Maximum crack width along web: (a) Conventional and (b) modified detailing (South face)

F.5 Maximum crack width over time

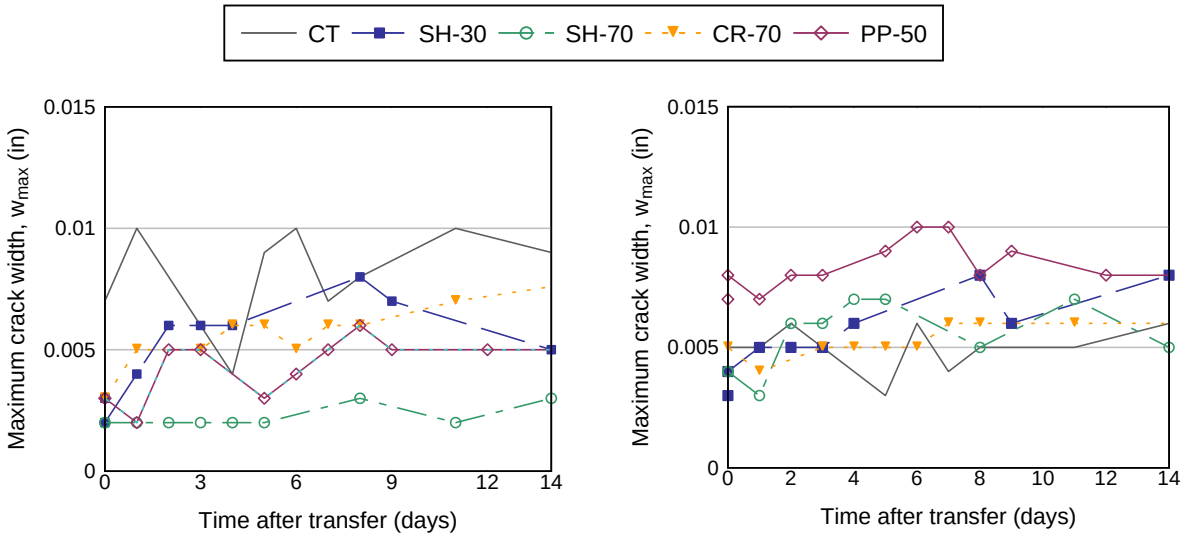

Figure F-14 Maximum web crack width within first 14 days of measurements: (a) Conventional and (b) modified detailing (North face)

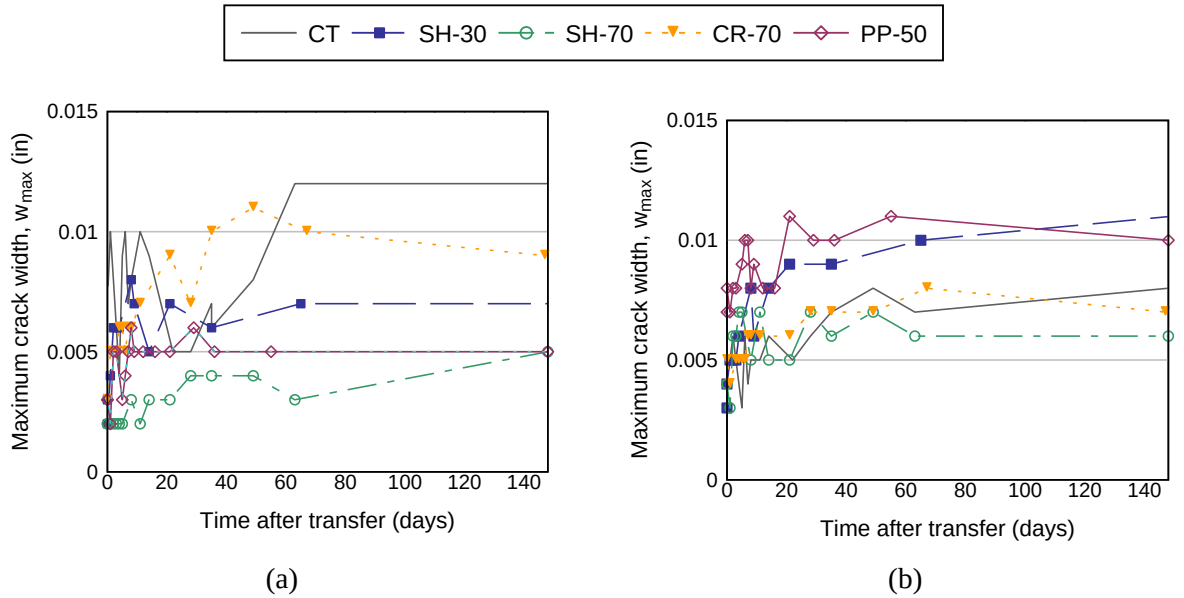

Figure F-15 Maximum web crack width: (a) Conventional and (b) modified detailing (North face)

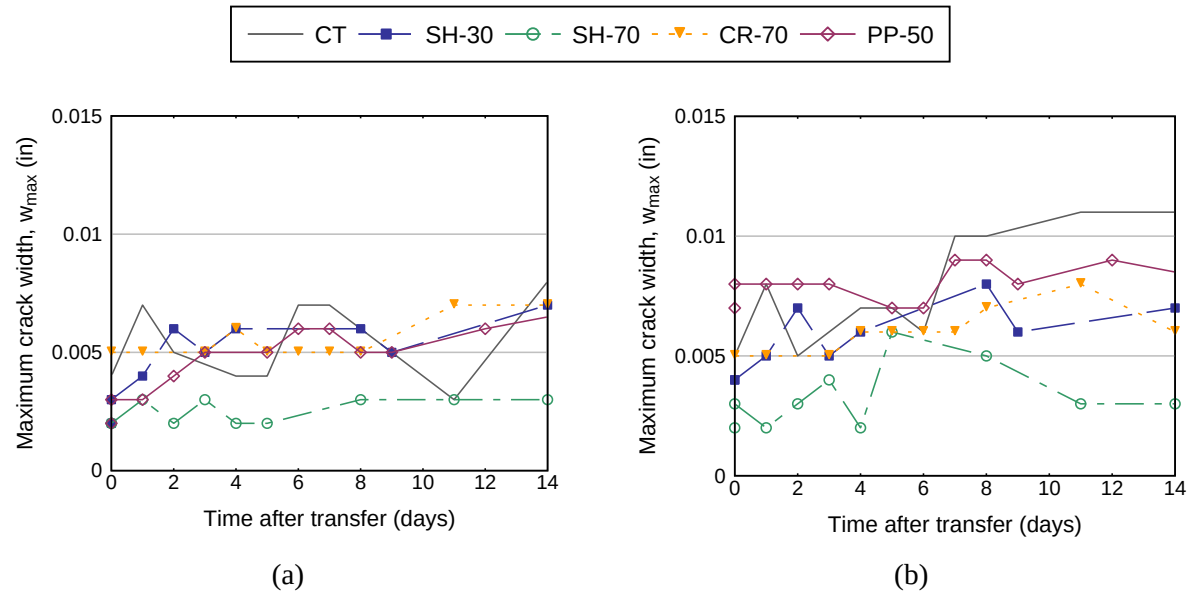

Figure F-16 Maximum crack width within first 14 days of measurements: (a) Conventional and (b) modified detailing (South face)

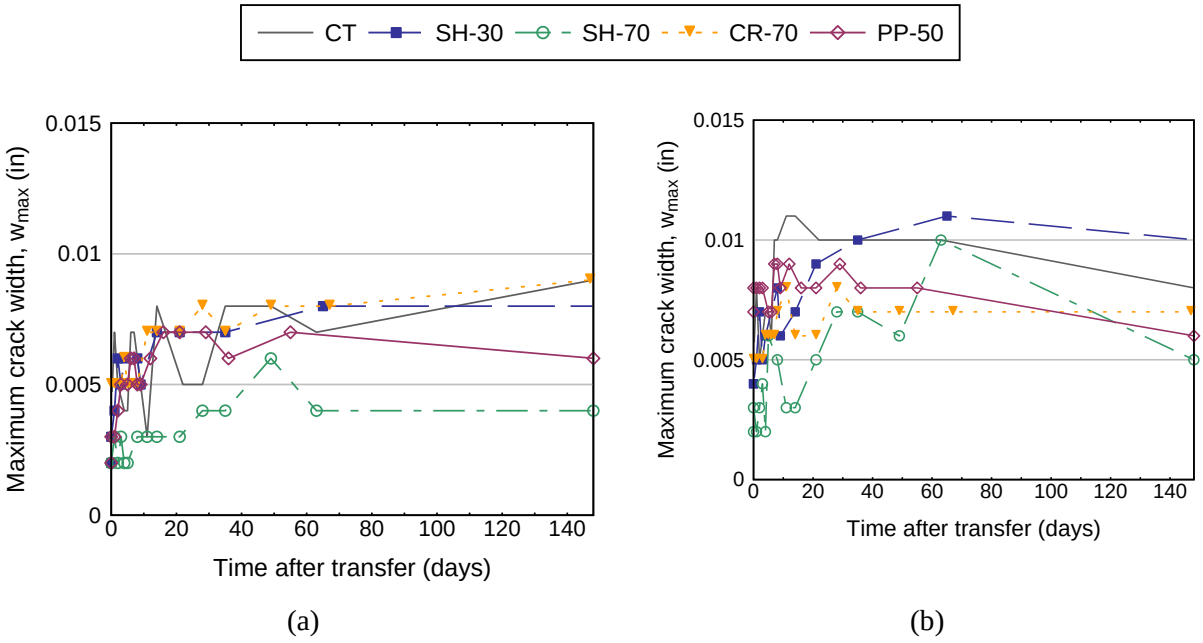

Figure F-17 Maximum crack width along web: (a) Conventional and (b) modified detailing (South face)

F.6 Total crack length over time

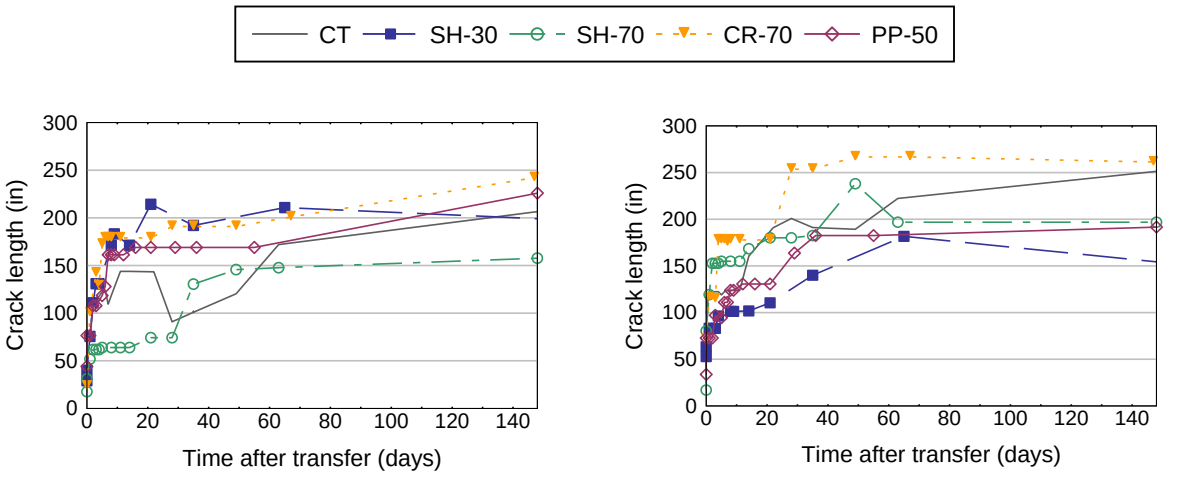

Figure F-18 Total crack length: (a) Conventional and (b) modified detailing (North face)

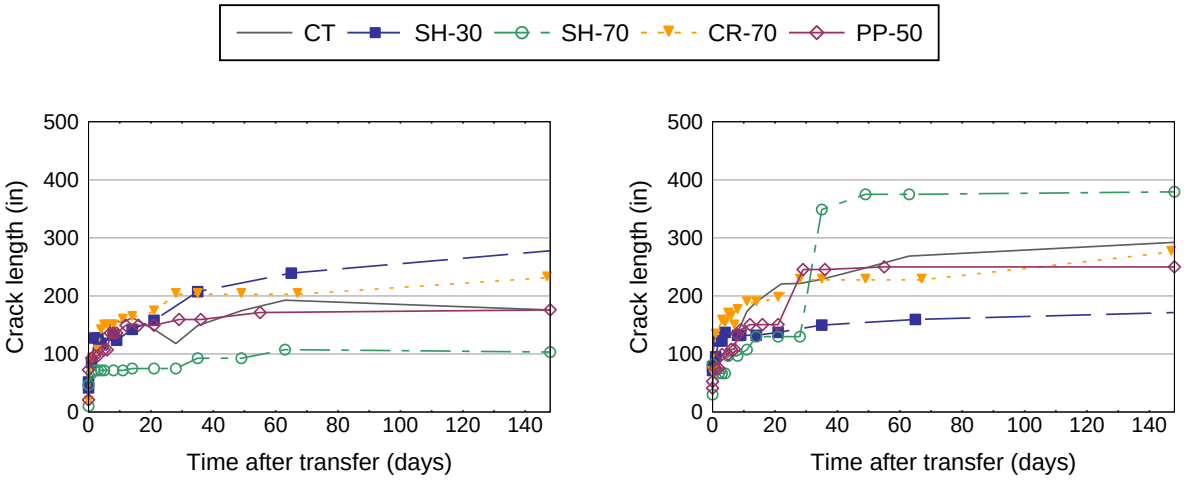

(a) (b)

Figure F-19 Total crack length: (a) Conventional and (b) modified detailing (South face)

F.7 Total crack area over time

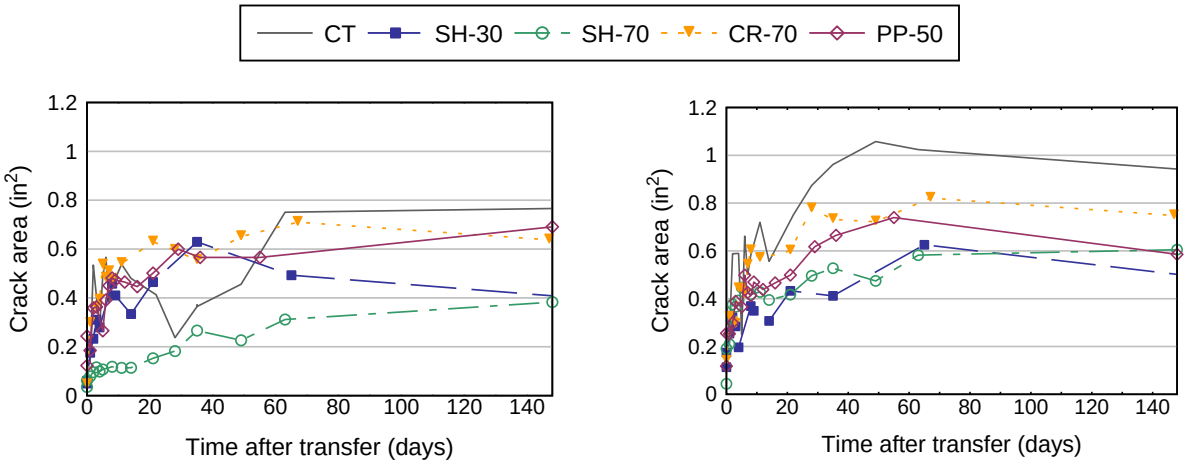

(a) (b)

Figure F-20 Total crack area: (a) Conventional and (b) modified detailing (North face)

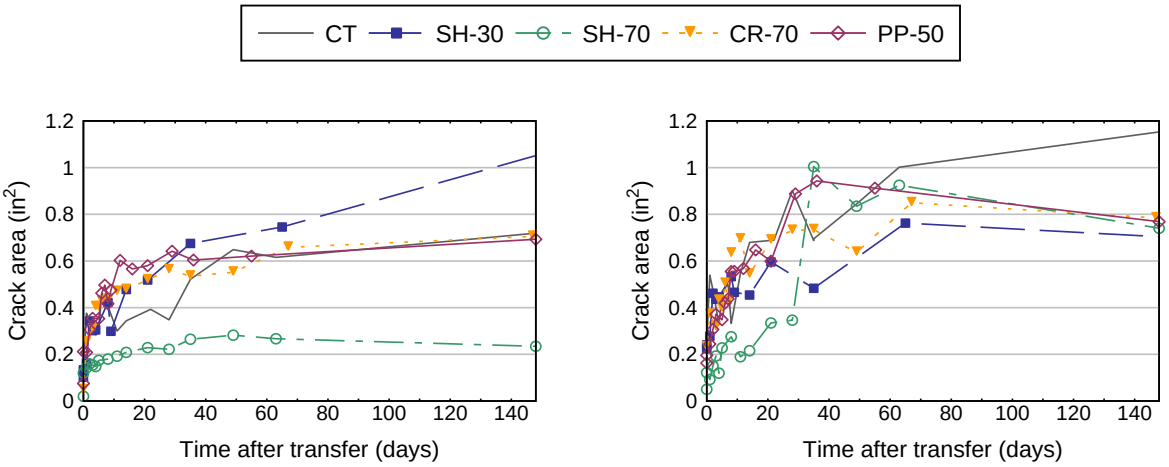

(a) (b)

Figure F-21 Total crack area: (a) Conventional and (b) modified detailing (South face)

Appendix G — Shear testing

G.1 Introduction

Considerable work has been conducted on the improvement in shear strength provided by steel fiber reinforced concrete (SFRC) (ACI 544.4R-88). Steel fibers have been shown to have the potential to either entirely replace or supplement traditional bar stirrups. Compared with samples containing minimum conventional shear reinforcement, however, beams with only fiber reinforcement showed similar capacities but post peak behavior of specimens containing only fiber was more brittle (Amin et al. 2016, Cucchiara and Osman 2004). Some of SFRC advantages include:

- The large number of random distributed fibers provide a much more closely spaced grid of reinforcement than is possible with traditional bars;
- Residual tensile strength of concrete is greatly improved; and
- Crack widths are reduced, which improves shear-friction strength.

In general, steel fibers have been found to increase shear strength by 30-100+% compared to conventional concrete (Amin et al. 2016, Araújo et al. 2014, Majdzadeh et al. 2006, Kwak et al. 2002, Furlan and Bento 1997, Mansur et al. 1986, Williamson 1978). Issues with steel fibers include corrosion when exposed to alkaline environments. Corrosion will cause a volumetric change in the fibers, leading to reduced mechanical bond and capacity of the fiber. In addition, due to its high specific gravity compared to that of concrete, fiber segregation is possible. This will affect fiber distribution and can reduce tensile residual strength.

The development of new generation of macrosynthetic fibers in recent years, particularly with higher modulus of elasticity and tensile strength along with enhanced mechanical and chemical bond has opened the possibility of extending the use of synthetic fibers for structural applications (Altoubat et al. 2009). The focus in this literature review was to cover relatively recent research conducted on macrosynthetic fiber reinforced concrete (SNFRC), new fiber materials and available methods for predicting shear strength.

This chapter focuses on the development of fiber-reinforced concrete mixtures and the evaluation of fresh and hardened properties to evaluate FRC contribution to shear strength complying with FDOT requirements. To quantify the contribution of FRC to shear strength, the load testing of four precast concrete girders is recommended. This chapter describes mixture selection, specimen design, construction and testing recommendations to evaluate FRC contribution to shear strength.

G.2 Effect of fiber addition on shear strength

Shear increase due to fiber addition has been attributed to the post-cracking strength at the inclined shear crack and the contribution of concrete to shear strength by improving aggregate interlock and dowel action of flexural reinforcement due to improve crack control provided by the fibers (Altoubat et al. 2009). In general, shear strength increases of more than 50% using steel fibers, 30% with glass, 40% with synthetic fibers, and 40% with basalt fibers are possible (Krassowska and Lapko2013, Majdzadeh et al. 2006).

Polymeric fibers (40 mm length) composed mainly of polypropylene and polyethylene at volumes 0-1.0% showed an increase in ultimate shear strength of 12 to 25% (Table G-1) depending on the volume fraction (Yazdanbakhsh et al. 2015, Altoubat et al. 2009). Used at 1.5% volume fraction, basalt fibers (50 mm) provided an increase of 36% in comparison to theoretical shear capacity of conventional concrete (Krassowska and Lapko et at. 2013) and glass fibers (15 mm) showed a 15% increase (Soliman et al. 2012).

Table G-1 Increase in shear using polymeric fibers. (Altoubat et al. 2009)

V_f, %	a/d	Increase in first crack load, %	Increase in maximum load, %
0.50	3.5	10	14
0.75	3.5	18	23
1.00	3.5	12	30
0.50	2.3	7	>20
0.75	2.3	14	>28

SNFRC behaves similarly to SFRC at different stages of cracking (Altoubat et al. 2009), but due to the difference in tensile capacity (at similar length and volume fraction) in general SFRC provided more strength than SNFRC. Majdzadeh et al. (2006) reported an increase in shear strength of up to 95% when using steel fibers (60 mm), and 30% for synthetic fibers (54 and 50mm) (Figure G-1). However, synthetic fibers did not provide significant increase in shear capacity after increasing volume fraction beyond 1%. In a study conducted by Noghabai (2000) with macrosynthetic and steel fibers, polyolefin fibers (25 mm) at 1% volume fraction behaved similarly to steel fibers (30 mm) at 0.5% volume, both providing 12% and 11% increase in shear strength respectively. While longer fibers provided a higher increase when compared with reference specimen, steel fibers (60 mm) at 0.7% increased shear capacity by 19% and macrosynthetic fibers (50 mm) at 1% increase by 34%.

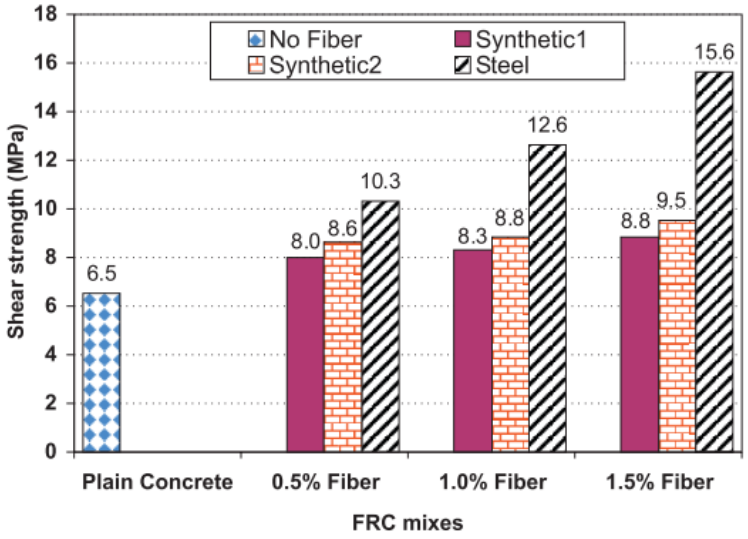

Figure G-1 Shear strength of FRC samples (direct shear test) (Majdzadeh et al. 2006)

Furlan et al. (1999) performed work to evaluate the effect of fiber reinforcement on prestressed I-sections (300 mm depth) with reduced shear reinforcement ratios. Steel (1%

volume and 25.4 mm length) and polypropylene (0.5% volume and 42 mm length) fibers were used, and shear reinforcement ratios varied from 0-0.225%. Both fibers provided an increase in ultimate shear strength of about 15% when compared to control sample.

G.3 Methods for predicting shear strength of FRC

Numerous methods to predict shear behavior of FRC are available in the literature (Table G-2 and Table G-3). Some methods consider the independent contribution of fiber reinforcement to shear capacity, while others consider the combined contribution of the concrete matrix and fiber reinforcement.

Extensive work is available on comparison of the accuracy of available methods to predict shear capacity (Kwak et al. 2002 and Araújo et al. 2014). Each performed statistical analysis of available data and their own experimental results on FRC beams with and without stirrups. They agreed that the equation developed by Narayanan and Darwish (1987) most accurately predicted shear capacity. The method by Narayanan and Darwish, however, can overestimate shear strength in short beams.

The method developed by Sharma (1986) can overestimate capacity at low volume dosages (Yazdanbakhsh et al. 2015).

Mondo (2011) performed a comprehensive study to evaluate the effectiveness of equations by Narayanan and Darwish's formula, the German, the RILEM and the Fib-Model Code to predict shear capacity of SFRC. From the equations that rely on post cracking behavior to estimate shear capacity, model by fib was determined to be the most reliable.

Table G-2 Statistical evaluation of several methods to predict shear strength (Kwak et al. 2002)

Test series	No. of tests	Mean value of $v_{u,exp}/v_{u,calc}$ (coefficient of variation)				
		Sharma	Narayanan	Ashour		Imam
		Eq. (1)	Eq. (2)	Eq. (5)	Eq. (6)	Eq. (7)
Ashour, Hasanain, and Wafa[3]	11	1.25 (0.40)	1.03 (0.15)	1.17 (0.12)	1.09 (0.10)	0.63 (0.32)
Batson, Jenkins, and Spatney[4]	42	0.96 (0.46)	1.10 (0.10)	1.14 (0.11)	1.29 (0.18)	—
Casanova and Rossi[19]	2	1.45 (0.00)	1.53 (0.00)	1.80 (0.00)	1.44 (0.00)	0.98 (0.00)
Imam, Vandewalle, and Mortelmans[5]	5	0.79 (0.37)	1.20 (0.14)	1.53 (0.12)	1.23 (0.16)	0.97 (0.11)
Kaushik, Gupta, and Tarafdar[7]	9	1.17 (0.05)	1.11 (0.12)	1.25 (0.11)	0.89 (0.16)	0.76 (0.14)
Li, Ward, and Hamza[9]	6	1.26 (0.24)	1.47 (0.15)	1.61 (0.10)	1.20 (0.12)	—
Lim, Paramasivam, and Lee[10]	7	1.01 (0.36)	0.97 (0.05)	1.08 (0.11)	0.85 (0.10)	0.67 (0.23)
Mansur, Ong, and Paramasivam[11]	9	1.50 (0.15)	1.19 (0.12)	1.29 (0.12)	0.94 (0.13)	0.88 (0.12)
Murty and Venkatacharyulu[12]	4	1.30 (0.14)	1.07 (0.09)	1.11 (0.13)	0.82 (0.10)	—
Narayanan and Darwish[13]	29	1.54 (0.27)	1.09 (0.15)	1.23 (0.16)	1.00 (0.15)	—
Noghabai[21]	11	1.71 (0.17)	1.33 (0.16)	1.52 (0.16)	1.23 (0.16)	1.13 (0.17)

Table G-3 Statistical evaluation of several methods to predict shear strength (Yazdanbakhsh et al. 2015).

Model	Mean value of $v_{fc,THEO}/v_{fc,EXP}$	Standard deviation of $v_{fc,THEO}/v_{fc,EXP}$	Coefficient of variation
Sharma	1.01	0.13	0.13
Mansur et al.	0.71	0.05	0.07
Narayanan and Darwish	0.97	0.15	0.15
Ashour et al. (ACI)	1.15	0.16	0.14
Ashour et al. (Zsutty's)	0.90	0.11	0.12
Li et al.	1.71	0.36	0.21
Swamy et al.	0.73	0.05	0.07
Imam et al.	1.47	0.29	0.20
Kwak et al.	1.14	0.22	0.19
RILEM	0.80	0.09	0.11
fib-MC2010	0.89	0.09	0.10

Bendtsen et al. (2015) performed work using full-scale prestressed bridge beams to compare the fib Model Code and plastic design method (Table G-4), it was found that plastic design method is more accurate to predict shear capacity.

Table G-4 Comparison of test result with Fib Model and Plastic method. (Bendtsen et al. 2015)

Beam	Type	Shear capacities (kN)		
		Test results	*Fib* Model Code	Plastic method
Plain 1	No steel fibers added	250	208	214
Plain 2		172		
SFRC 1	Steel fibers added at 60 kg/m^3	466	264	429
SFRC 2		432		

The approach developed by Narayanan and Darwish (Narayanan et al. 1987), as well as recommended methods by ACI (based on Sharma 1986), RILEM, and fib model (Fib Model Code 2010) are discussed in the following chapters.

G.4 Sharma (1986)

Sharma's model developed in 1986 for predicting the average shear stress in beams with conventional reinforcement and steel fibers as defined by Equation 7. This method considers the combined contribution of steel fibers and concrete which is then added to the individual contribution of conventional shear reinforcement as defined by ACI 318-14 (22.5).

$$v_{cf} = \frac{2}{3} f'_t \left(\frac{d}{a}\right)^{0.25} \quad \text{Equation 7}$$

Where f'_t is the splitting tensile strength of the SFRC mixture, $\frac{d}{a}$ is the effective depth-to-shear-span ratio.

G.5 Narayanan and Darwish (1987)

Narayanan and Darwish (1987) developed an empirical approach to predict ultimate shear strength of FRC. The approach developed is described next:

$$V_u = e\left[0.24 f_{spfc} + 80\rho d/a\right] + v_b \quad \text{Equation 8}$$

Where ρ is the reinforcement ratio, f_{spfc} is the ultimate split cylinder strength of FRC (MPa), $\frac{d}{a}$ is the effective depth-to-shear-span ratio, v_b is the fiber pullout force, e as is a factor to account for the effect of arch action , this factors are defined in the following equations.

$$e = 1.0 \; for \frac{a}{d} > 2.8$$
$$= 2.8 \frac{d}{a} for \; a/d \leq 2.8 \quad \text{Equation 9}$$

$$v_b = 0.41 \tau F \quad \text{Equation 10}$$

Where τ is the average fiber matrix interfacial bond stress taken as 4.15 MPa and F is the fiber factor.

G.6 RILEM TC 162-TDF

The RILEM Committee TC 162-TDF, Test and Design Methods for Steel Fiber Reinforced Concrete developed recommendations for shear design of elements with conventional and fiber reinforcement. This method considers the individual contributions of concrete, shear reinforcement and fiber reinforcement to the shear capacity as shown in Equation 11.

$$V = V_{cd} + V_{fd} + V_{wd} \quad \text{Equation 11}$$

Where V_{cd} is concrete contribution to shear strength V_{wd} is the contribution of the shear reinforcement and V_{fd} (Newton) is the fiber contribution as given by Equation 12.

$$V_{fd} = 0.7 k_f k_l \tau_{fd} b_w d \quad \text{Equation 12}$$

Where b_w is the web width (mm), d is the beam depth (mm), and k_f, k_l , τ_{fd} are factors to take into account contribution of flanges in T-section and increase in shear strength due to steel fibers as defined by Equation 13-Equation 15.

$$k_f = 1 + n(h_f/b_w)(b_f/d) \leq 1.5$$
$$n = (b_f - b_w)/\, h_f \leq 3 \leq 3b_w/h_f \quad \text{Equation 13}$$

$$k_l = 1 + \left(\frac{200}{d}\right)^{1/2} \leq 2 \quad \text{Equation 28}$$

$$\tau_{fd} = 0.12 f_{R,k,4} \quad \text{Equation 15}$$

Where h_f is the flange height (mm), $f_{R,k,4}$is the measure of the residual strength in bending (MPa) and shall be greater than 1 MPa.

G.7 fib-Model Code (2010)

Fib-Model Code (2010) developed recommendations for shear design of elements with conventional and fiber reinforcement. This method considers the contribution to shear capacity as a combination of fiber and concrete and develops approach to determine shear capacity as defined on Equation 30.

$$V_{Rdf} = \left\{ \frac{0.18}{\gamma_c} k \left[100 \rho_1 \left(1 + \frac{7.5 f_{Ftuk}}{f_{ctk}} \right) f_{ck} \right]^{\frac{1}{3}} + 0.15 \sigma_{cp} \right\} b_w d \quad \text{Equation 30}$$

Where γ_c is the partial safety factor for concrete without fibers, b_w is the smallest width of the cross-section in the tensile area (mm), d is the effective depth of the section, ρ_1 is the longitudinal reinforcement ratio, f_{Ftuk} is the ultimate residual strength for FRC with crack width of 1.5 mm, f_{ctk} is the tensile strength for concrete without fibers, f_{ck} is the compressive strength, k is a factor that takes into account size effect ($k \leq 2$), σ_{cp} is the average stress acting in the cross-section (N/mm^2) and are defined by the Equation 31-Equation 32.

$$k = 1 + \sqrt{200/d} \quad \text{Equation 31}$$

$$\sigma_{cp} = N_{Sd}/A_c \quad \text{Equation 32}$$

Where N_{Sd} is the longitudinal force due to loading or prestressing (with compression positive), A_c is the cross-sectional area and d is the effective depth (mm).

G.8Mixture requirements and proportions

Due to the high congestion of reinforcement in prestressed bridge girders and the loss of workability when fibers are incorporated, all mixtures developed will be self-consolidating concrete (SCC). All SCC mixtures prepared for this study were designed to meet requirements for FDOT Class VI concrete and fresh properties requirements for SCC, as described in section 3.3.

SCC mixtures incorporating fibers were prepared using an FDOT approved mixture as a starting point; this mixture will be referred to as the control (CT). The control mixture was modified to incorporate fibers while still complying with FDOT requirements for proportioning, as well as hardened properties. Fiber dosage was adjusted based on recommended dosages provided by each of the fibers manufacturers. Table 3-5 contains a summary of mixture proportions used for the investigation, including the mixture designations used through the report. Fiber volumes ranging between 0.5-1% were used. Volume of coarse aggregate was reduced to accommodate the respective fiber volume. The mixture naming format was selected to include details regarding fibers and volume used. Figure G-2 and Table G-7 provide naming details used to label laboratory specimens and for referencing in this report. The first two characters refer back to the fiber designation (Table G-6), these where assigned considering the different fiber material and fiber shape. The second set of characters refers to the volume of fibers used multiplied by a factor of 100.

All mixtures were prepared and tested for fresh properties at a local precast facility in Florida. Commonly available materials were used to develop the mixtures to maintain realistic conditions for concrete mixing when casting real girders for bridge construction. Mixture constituents are as described in section 3.2.

Table G-5 Mixture proportions (lb/cy)

	Proportions (lb/cy)							Properties tested	
Mixture	Cement	Flyash	#67	#89	FA	Water	Fiber	Fresh	Hardened
CT	735	165	1370	0	1265	279	-	-	-
PP-50	790	175	565	774	1212	279	7	X	X
PP-70	790	175	0	1320	1063	279	11	-	X
PP2-70	790	175	565	774	1212	279	11	-	X
SH-70	790	175	0	1320	1063	279	93	X	X
CR-70	790	175	0	1320	1063	279	93	X	X
PP-100	790	175	0	1310	1060	279	15	X	X

*Not performed (-)

* Performed (X)

Table G-6 Fiber properties

Fiber designation	PP	PP2	SH	CR
Material	Polypropylene	Polypropylene	Steel	Steel
Length (in.)	2.1	2.1	1.4	1.5
Length (mm)	54	54	35	38
Tensile strength (ksi)	85	83-96	160	140
SG	0.91	0.91	7.85	7.85

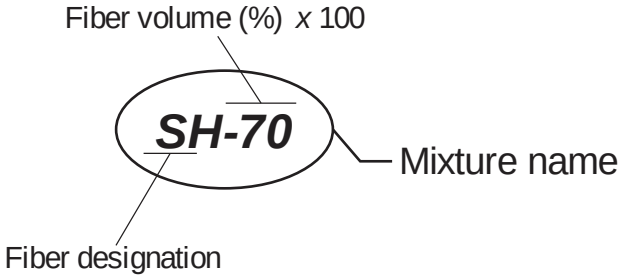

Figure G-2 Specimen naming format

Table G-7 Summary of specimen name and description

Mixture	Fiber description	Fiber designation	Volume (%)
CT	-	-	-
PP-50	Polypropylene chemically enhanced	PP	0.50
PP-70	Polypropylene chemically enhanced	PP	0.70
PP2-70	Polypropylene	PP2	0.70
SH-70	Hooked end	SH	0.70
CR-70	Crimped steel	CR	0.70
PP-100	Polypropylene chemically enhanced	PP	1.0

G.9 Laboratory specimens-fresh properties testing and results

Typically self-consolidating concrete (SCC) is used in construction of bridge girders in Florida. For this reason the goal was to integrate the fiber reinforcement into the mixture while still satisfying passing ability and flowability requirements for SCC. Slump flow, T50, VSI, air content, density, passing ability testing was conducted for each mixture. Testing was conducted by the precaster following respective ASTM procedures shown in Table 4-6.

Table G-8 Test for fresh properties

Test	ASTM	Limits
Slump flow	C1611	Shall be less or equal to 27.0 inches (±2.5inches)
Visual Stability Index (VSI)	C1611	Shall be less or equal to 1
T-50	C1611	Recommended 2-7 seconds
Passing ability	C1621	Shall not exceed 2.0 inches
Air content	C231	0-6%
Unit weight	C138	-

Most mixtures exceeded the limit for unrestricted flow of 27 inches (Figure 4-20a). Mixtures with steel fibers, however, showed good consistency, no bleeding, and good resistance to segregation. Mixtures with steel fibers had VSI (Visual Stability Index) equal to zero and T-50 varied between 2 and 6 seconds (Figure 4-20c), which were well within the required values for SCC (Figure G-3a). However, macrosynthetic fibers at volumes higher than 0.70% showed concentration of coarse aggregate and fibers in the center of the slump (Figure G-3b). In addition, PP2 showed fiber clumping during mixing procedures. Requirements for passing ability less than 2 inches was exceeded except for mixture containing steel crimped fibers (CR-70). However, no issue with fiber clumping was observed in mixtures containing hooked end or crimped steel fibers. Fiber nesting was apparent, inside the J-Ring when synthetic fibers were used (mixture PP-100), as shown in Figure G-4b.

Figure G-3 Slump flow for (a) CR-70 and (b) PP-100

(a)

(b)

(a)

(b)

(c)

Figure G-4 J-Ring for (a) SH-70, (b) PP-100 and (c) PP2-70

Figure G-5 Fiber clumping during mixing procedures (PP2-70)

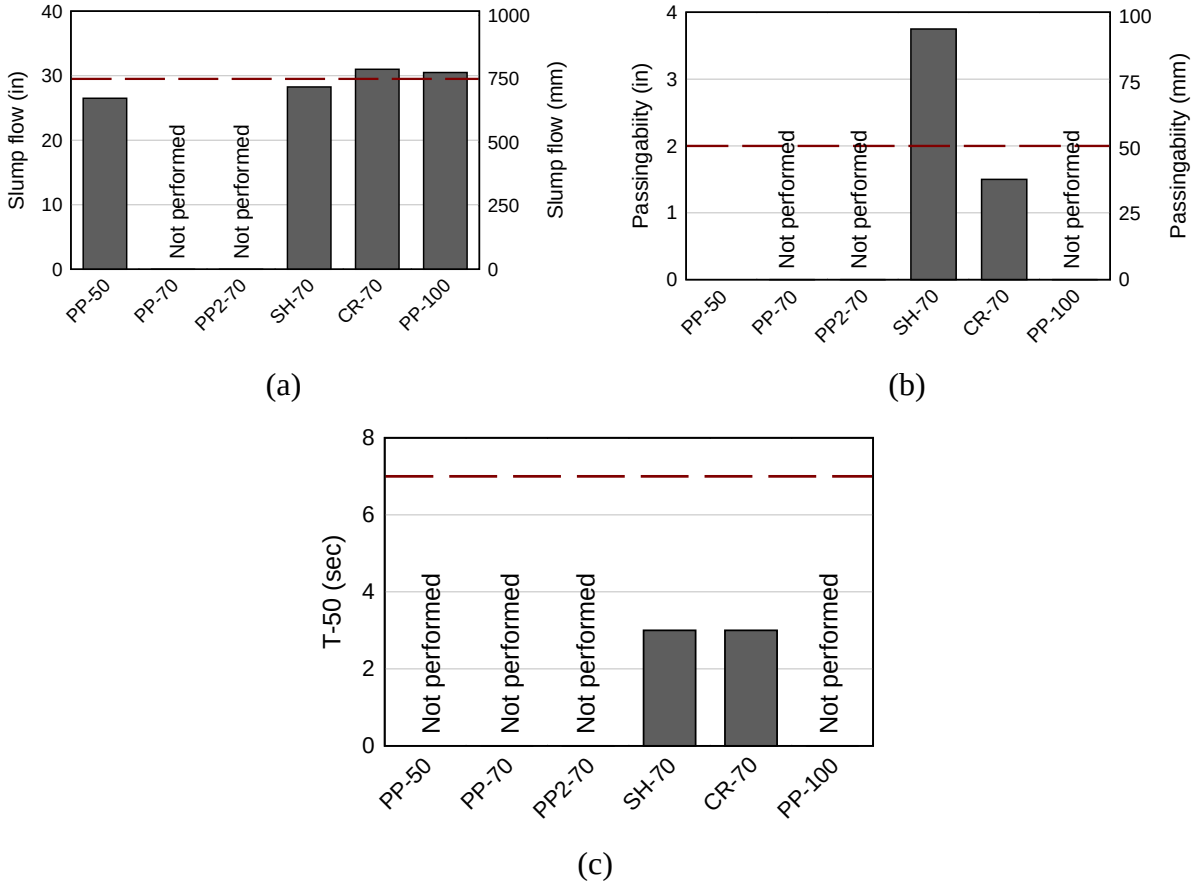

Figure G-6 SCC properties: (a) slump flow, (b) passing ability, and (c) T-50

G.10 Average residual strength (ASTM C1399)

ASTM 1399 provides procedures to determine average residual strength of fiber-reinforced concrete; average residual strength is computed as the average load carrying capacity at four specified deflections. During the test, load, deflection, and closed-loop control

displacement were recorded using National Instruments hardware controlled by LabVIEW software. An aluminum frame was used to mount an LVDT on each side of the specimen to measure midspan deflection (Figure G-7a). At midspan, a steel plate was clamped to the top of the beam for use as reference points for deflection measurements (Figure G-7b). This setup minimized extraneous contributions due to rotation or seating of the specimen.

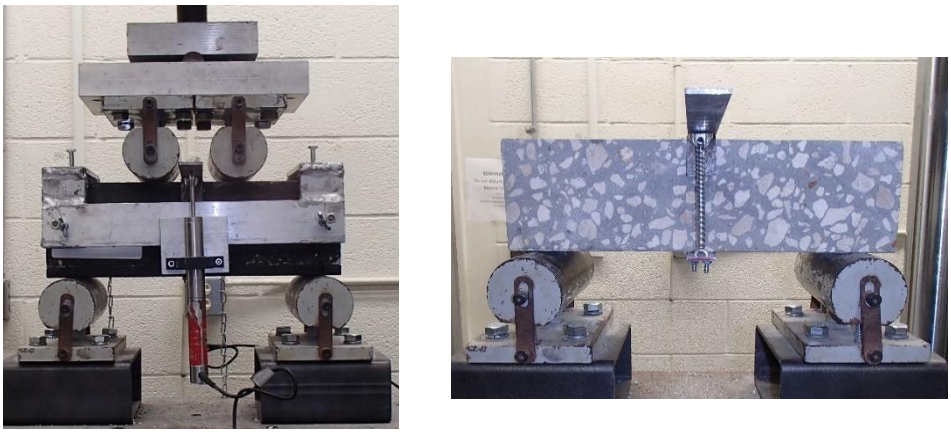

(a) (b)

Figure G-7 ASTM C1399 (a) test setup and (b) LVDT steel plate clamped

Figure G-8 shows average load-displacement curves for each of the mixtures tested. Because of bridging action across the cracked surface provided by the fiber reinforcement, load carrying capacity continued even after deflection of 0.05 in. when the test was terminated. In general, higher fiber volumes and the use of stiffer fibers led to a higher residual strength at all loading stages.

Figure G-9 shows the residual strength at the four key displacements and Figure G-10 shows the average residual strength for each of the mixtures tested. It is apparent that synthetic fibers at a volume of 1.0% provided the highest average residual strength among all fibers tested, followed by hooked end steel fibers (SH) at 0.70% volume dosage. These fibers provided up to 50% higher average residual strength than any other fiber. When compared with the crimped steel fibers (SC) at the same volume dosage of 0.70%, SH provided about 40% higher average residual strength than CR. At the same dosage of 0.70%, PP and PP2 showed similar average residual strength, the enhanced mechanical bond did not provide significant increase in average residual strength. At a volume of 0.50%, synthetic macrofibers did not provide significant residual strength, compared to the remaining mixtures.

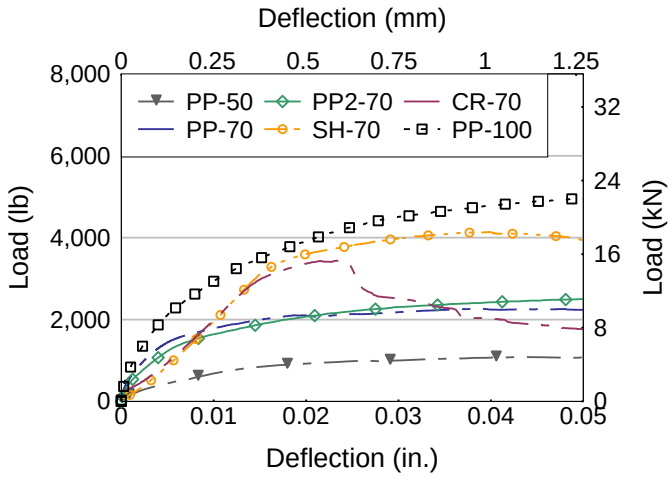

Figure G-8 ASTM C1399 Load-displacement curve (average of all specimens tested)

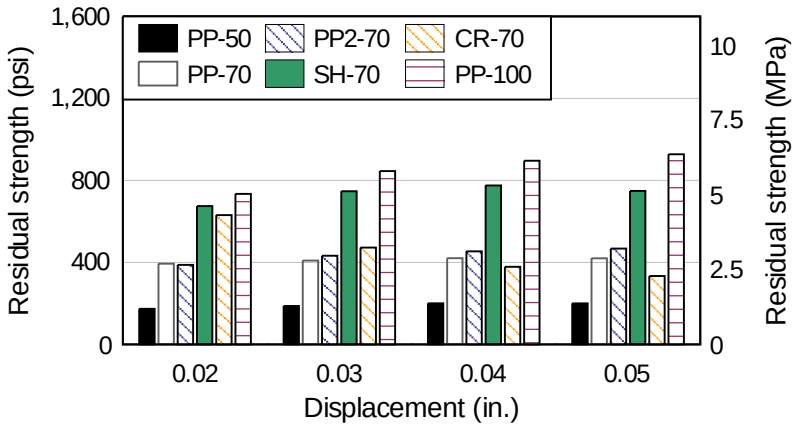

Figure G-9 Residual strength residual strength at specified displacements

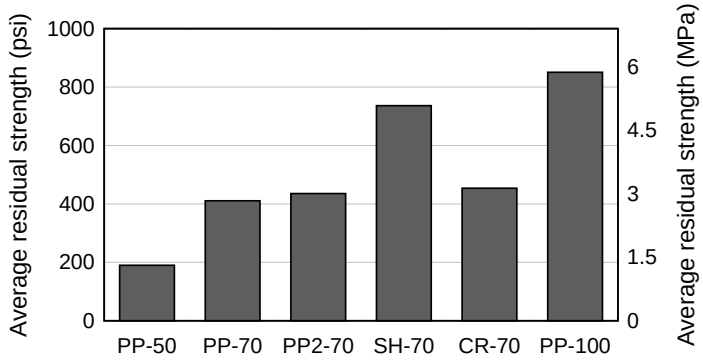

Figure G-10 Average residual strength when tested in accordance with ASTM C1399

G.11 Flexural tensile strength (EN 14651)

EN 14651 provides procedures to determine residual strength of a notched beam at various stages of displacement. This test is controlled by the crack mouth opening displacement (CMOD) of the notch. Load and deflection data were collected externally using a LabVIEW program prepared at the University of Florida. Figure 4-24 shows the test setup used during testing.

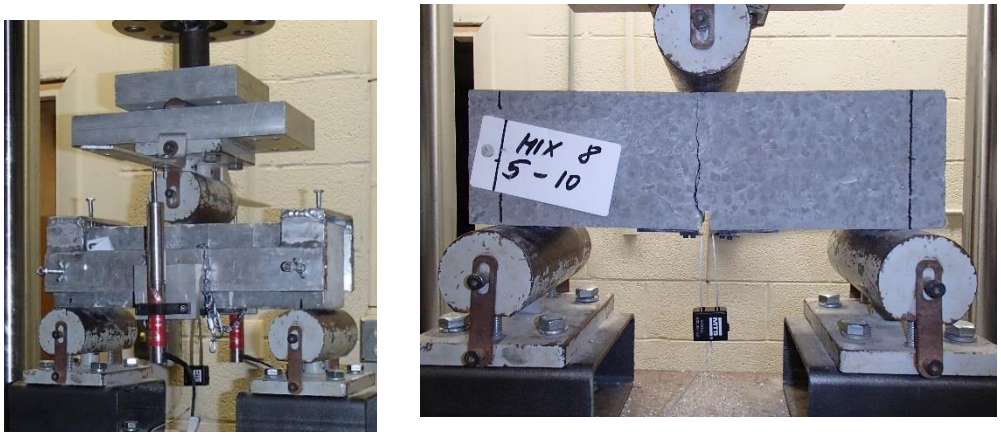

Figure G-11 EN 14651 test setup

Figure 4-25 shows average load-CMOD curves for each of the mixtures tested. Cracking loads obtained ranged between 1.6 and 2.0 kip, after which specimens containing steel fibers showed hardening behavior followed by a gradual loss in stiffness. Synthetic fibers showed a rapid loss in stiffness immediately after cracking (Figure 4-25b). To evaluate contribution to ultimate strength, post-cracking flexural strength between first cracking and $f_{R,2}$ (CMOD of 3.5 mm) was evaluated. Residual strength varied with fiber material and fiber volume used. In general, higher fiber volumes and the use of stiffer fibers led to a larger residual strength.

Figure 4-26 shows residual strength at specified CMOD increments of 0.02, 0.06, 0.10, and 0.15 in. (0.5, 1.5, 2.5 and 3.5 mm). Crimped end steel fibers (CR) at 0.70% volume dosage provided the highest residual strength among all fibers tested. This fiber provided higher load carrying capacity than any other by up to 40%. When compared with the hooked end steel fibers (SH) at the same volume dosage, CR showed higher residual strength by over 30% at ultimate stress (CMOD of 3.5mm). At the same dosage of 0.70%, at CMOD less than 2.5 mm macrosynthetic fiber (PP) showed significantly lower residual strength than steel fibers. At ultimate stress, similar contribution to residual strength was achieve using synthetic fibers and hooked end steel fibers, however, PP had length of almost twice of that of SH fibers. At a volume of 0.50%, synthetic macrofibers did not provide significant residual strength, compared to the remaining mixtures.

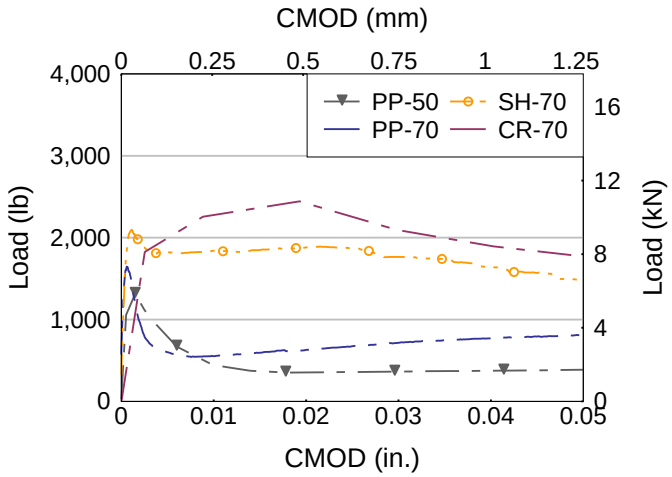

Figure G-12 EN 14651 Load-CMOD curve

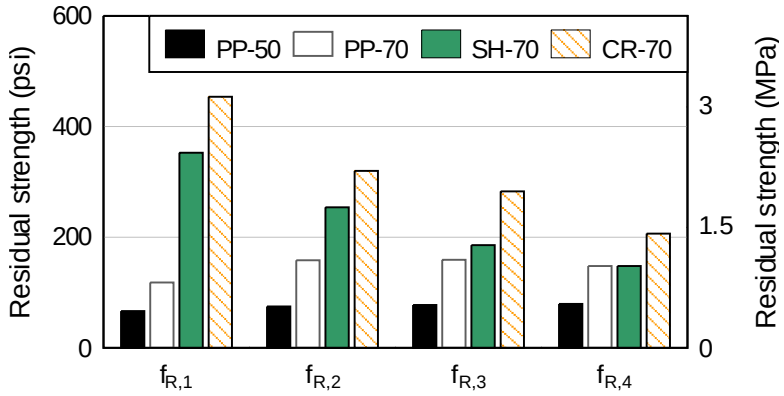

Figure G-13 Residual strength results when tested in accordance with EN 14651

G.12 Recommended shear test

To quantify the contribution of FRC to shear strength, the load testing of four precast concrete girders is recommended. This chapter describes recommendation for specimen design, construction and testing to evaluate FRC contribution to shear strength.

G.13 Recommended FRC mixtures

Workability, and residual strength were considered while making the final selection for fiber type and volume to be tested in full-scale production of precast prestressed girders. Ease of mixing, passing ability results, and fiber clumping/nesting were also considered. Table G-9 shows a summary of the details for the recommended mixtures, it also recommended that a control specimen be tested.

Table G-9 Recommended mixtures for full-scale testing

Specimen	Fiber	Length (in.)	Length (mm)	Volume (%)
1	Control (no fibers)			
2	PP	2.1	54	0.7
3	SH	1.4	35	0.7
4	CR	1.5	38	0.7

PP – polypropylene macrofiber chemically enhanced
SH – hooked-end steel fiber
CR – crimped steel fiber

G.14 Recommended specimen design

Specimen and prestressing pattern, along with testing procedures has been selected to develop either web-shear cracking or flexure shear cracking. The influence of fiber reinforcement on shear capacity is uncertain, based on the literature review shear strength can be increased anywhere between 10-60%. For this reason modified AASHTO Type II cross section is recommended (Figure G-14) with a span of 35-ft. The proposed section has wider top and bottom flanges, while maintaining conventional web thickness. Specimens can be constructed by using conventional AASHTO Type II formwork, and mounting it on an AASHTO TYPE III pallet. This section maximizes the flexural capacity of the specimen, and allow the desired shear failure mode to occur.

Specimens have (25) 0.6-in. diameter fully bonded prestressing strands in the bottom flange and (2) 3/8-in. diameter strands in the top flange (Figure G-15). The only variable considered in the test program are the different fiber reinforcement. Strand pattern and transverse reinforcement is kept constant in all specimens. Transverse reinforcement was designed to ensure that shear failure occurs. As shown in Figure G-16, within the area where shear failure is expected, vertical end zone reinforcement consisted of 10 #5 bars placed within 7-ft. from the girder end. Five of the ten #5 bars were placed within 2 ft. of the girder end. Reinforcement layout is consistent on both girder ends. Expected capacity of specimens was determined following LRFD Bridge Design Specification (2014) and ACI 318-14. A summary of the expected capacity for the specimens is shown in Table G-11.

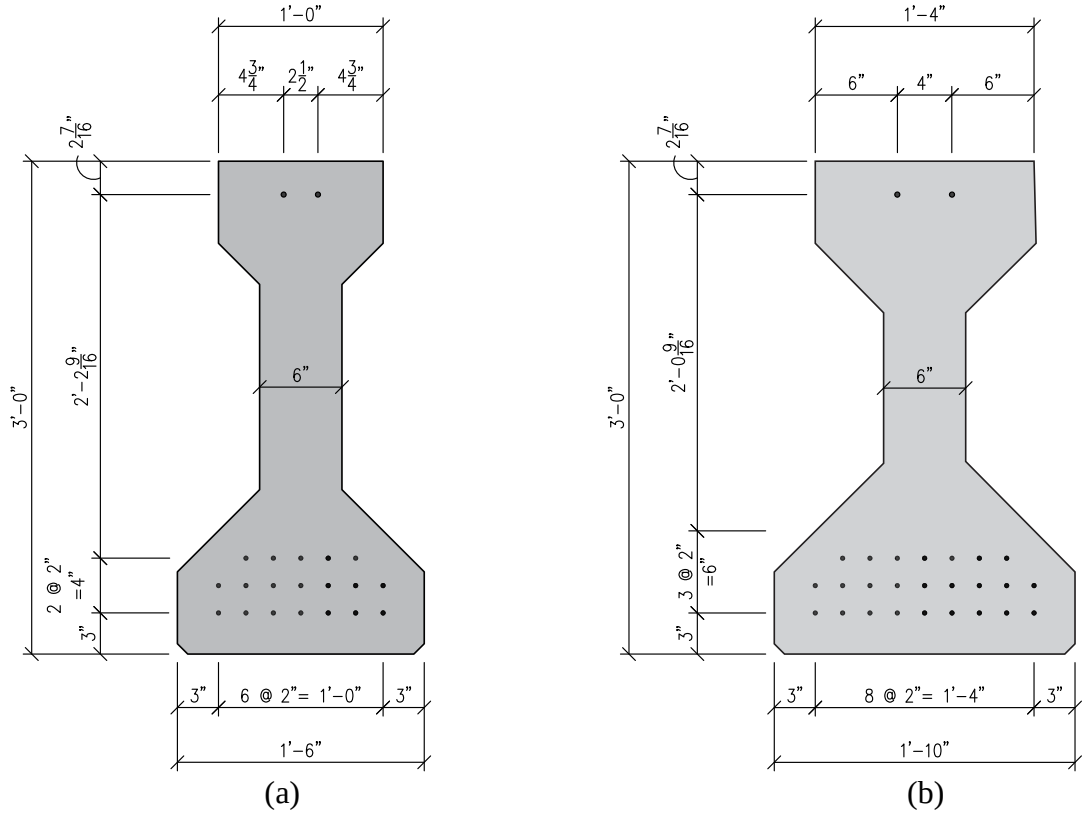

Figure G-14 Typical AASHTO Type II (a) and Modified section (b)

Table G-10 Recommended test setup

Length	35 ft.
Cross-section	Modified AASHTO Type II
a/d	2.75
No.test/beam	2

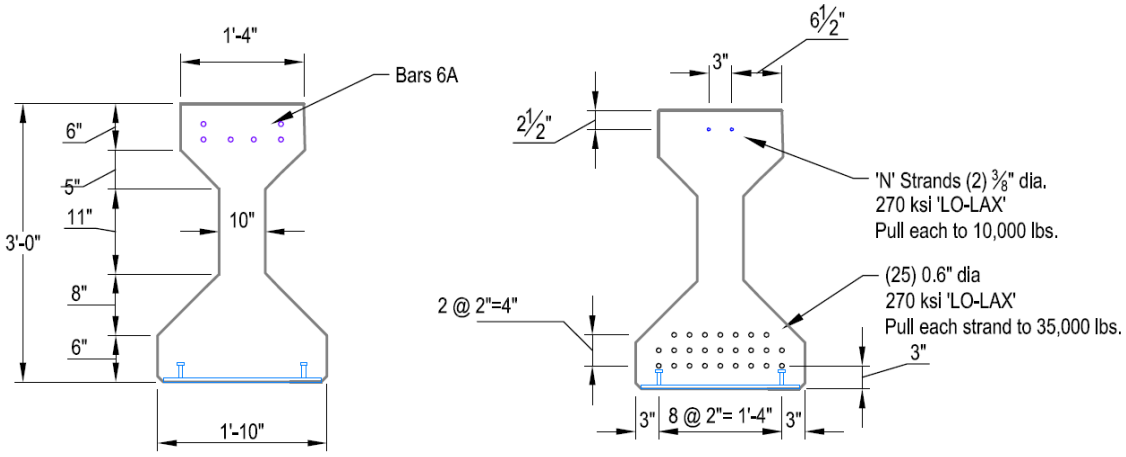

Figure G-15 Longitudinal reinforcement and prestressing strand layout

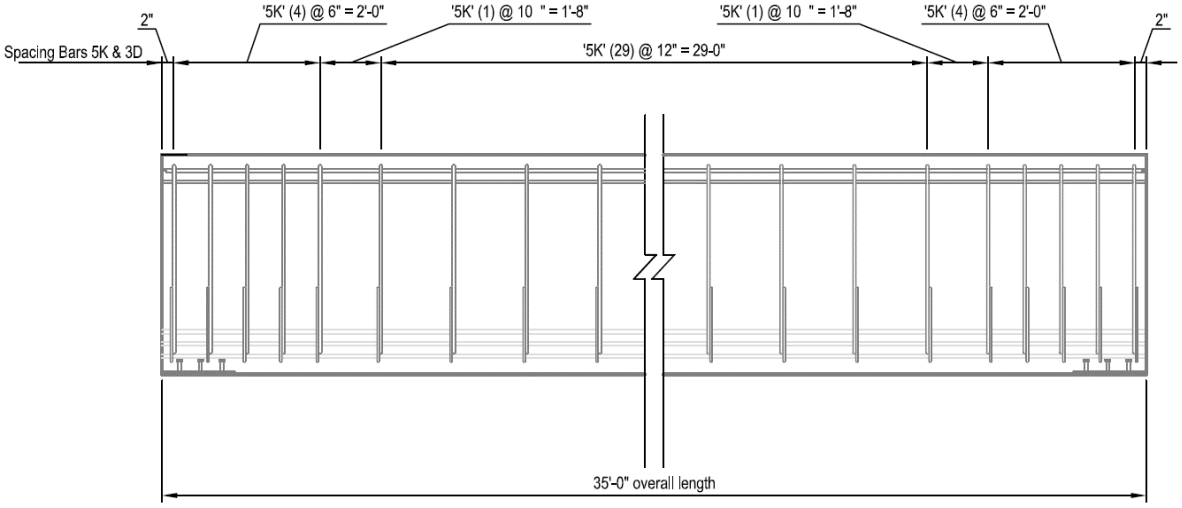

Figure G-16 Transverse reinforcement

Table G-11 Expected capacity

	Shear	Flexure
Capacity per LRFD	190 kip	2950 kip ft
Capacity per ACI	200 kip	3030 kip ft
Maximum applied load	200 kip	390 kip

G.15 Recommended test setup and procedures

Shear test are design to load the specimens under a three-point-loading scheme at a shear span-to-depth (a/d) ratio of 2.75 to ensure the likelihood of a shear failure. Each girder end is to be tested independently following the setup shown in Figure G-17 and Figure G-18. After the first end is tested (Figure G-17), the load point and supports are to be moved has shown in Figure G-18 to test the second end. Load, displacement, and strain will be measured continuously during load testing as described in section G.16. The contribution of the fiber reinforcement will be determined by comparing the behavior of control and FRC specimens. The procedure for load testing is as follows:

1. Inspect specimens for cracking prior to starting load testing, mark and label all cracks.
2. Record prestress losses prior to beginning of load testing
3. Setup load and supports for load configuration of the near end
4. Load the specimen at a loading rate of 0.2kip/sec until cracking load is reached. At this point the test is to be stopped to inspect, and label cracks.
5. Continue load testing at a loading at rate of 0.2kip/sec until failure, but stop every 20 kip to monitor cracking.
6. Document cracking at end of the test
7. Move load and supports following load configuration of the far end
8. Repeat procedures for testing of the far end

For each specimen (if needed) test material properties including concrete compressive strength at time of shear test (ASTM C39), residual tensile strength (ASTM C1399), reinforcement yield strength and elongation, and prestressing strands strength. During construction attention should be given to fresh properties of the concrete to ensure good fiber distribution, it is recommended that at least flowability and passing ability properties are assessed for all mixtures used (ASTM C1611 and ASTM C1621).

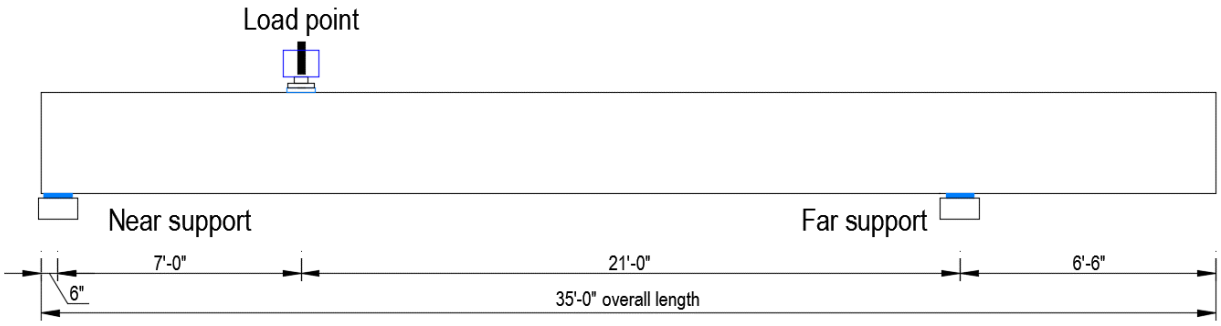

Figure G-17 Test setup for load testing of near end

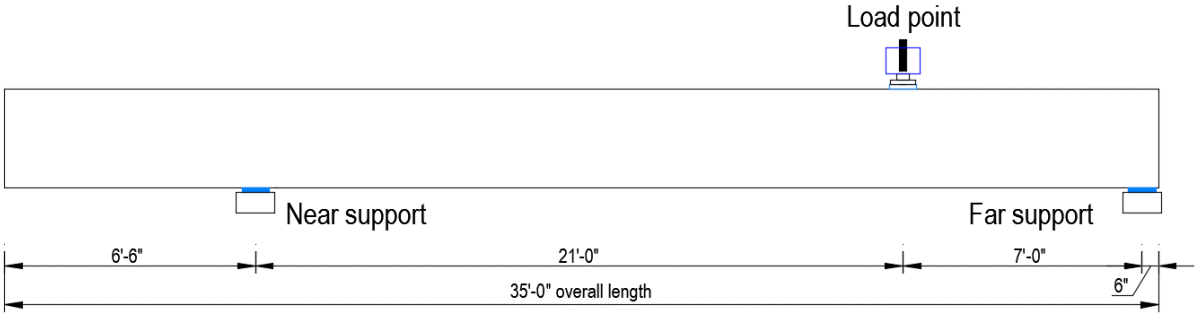

Figure G-18 Test setup for load testing of far end

G.16 Recommended instrumentation

During load testing of the specimens, data should be collected using load cells, LVDTs, and strain gages. Table 4-9 list the different instrumentation, along with labelling associated and general description. A consistent coordinate system is used throughout this report to define instrumentation location and direction of strains, stresses and forces. The origin of the coordinate system is located at the bottom of the near end of each girder. The x-axis is horizontal across the width of the girder, the y-direction runs longitudinally along the beam and z-axis is vertical, as shown in Figure G-19. Figure G-20 and Figure G-21 show location of external and internal instrumentation, Table G-13 through Table G-16 contain coordinates for each type of instrumentation to be used. For the case of LVDTs used to measure vertical displacement, difference is made regarding coordinates during the first and second test.
Instrumentation recommended prior to and during load testing:

- SG strain gages are to be used to measure concrete strain during load testing. These gages are 60 mm gage length and are attached to the concrete surface. A total of four external gages are included in each girder end to be tested.

- RS strain gages have 5 mm gage length and are installed on the mild steel reinforcement to monitor rebar strain during load testing. A total of six internal gages are included.
- Vibrating wire gages have 152 mm gage length and are embedded in the test girders. These are to be used in monitoring prestress losses over time. A total of two vibrating wire gages are included in each girder end to be tested.
- LVDTs are used to measure vertical displacement and strand slip during load testing. A total of four LVDTs are included to monitor vertical displacement at the supports and the load point and two for strand slip. LVDTs used to monitor strand slip could be replaced by variable resistant potentiometers.
- Load cells used to measure applied force during load testing.

Table G-12 Instrumentation type and placement

Label	Type	Placement
SG	Foil strain gage	Concrete surface
RS	Foil strain gage	Reinforcement
VW	Vibrating wire strain gage	Concrete interior
L	LVDT	Strands
D	LVDT	Load point, supports
-	Load cell	Load point

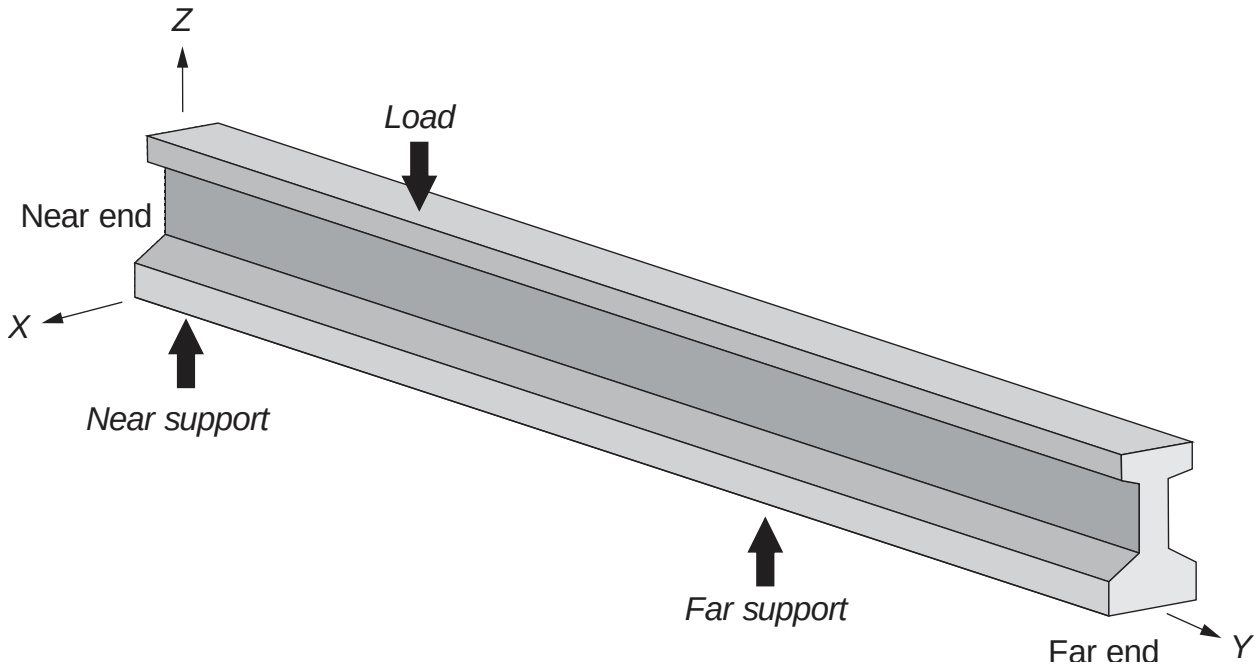

Figure G-19 Coordinates system (near end first end tested)

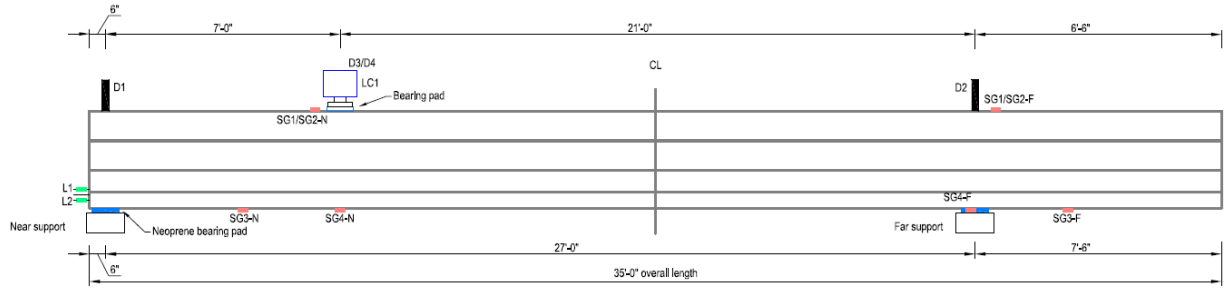

(a)

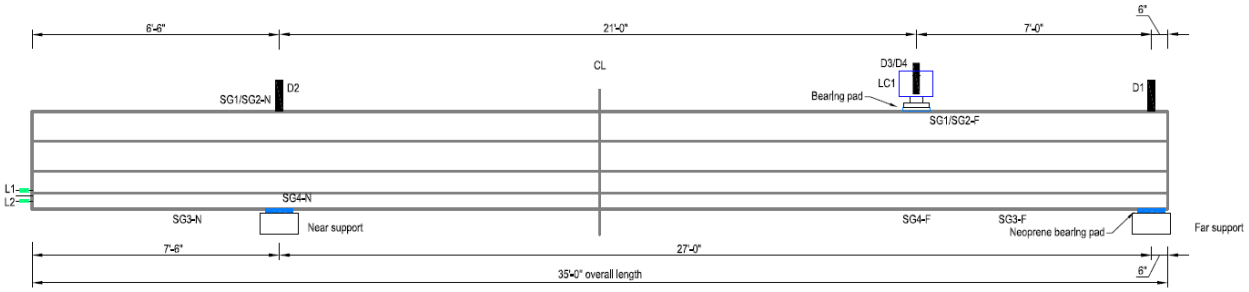

(b)

Figure G-20 Load setup and external instrumentation: (a) near end tested, (b) far end tested

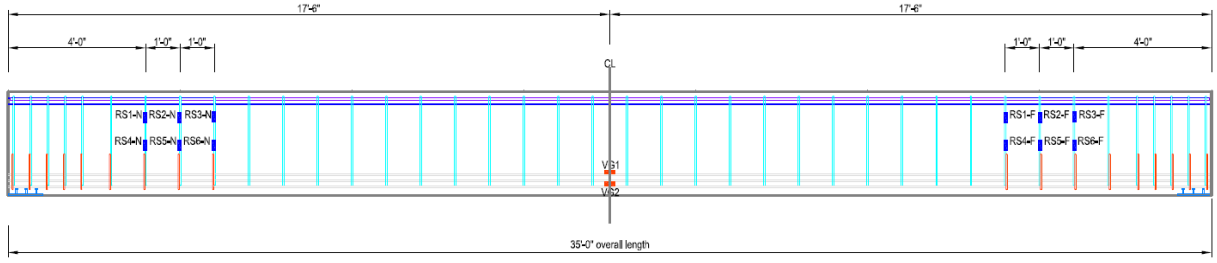

Figure G-21 Internal instrumentation for shear testing

Table G-13 Coordinates of external foil strain gages (SG)

Instrument	X (in.)	Y (in.)	Z (in.)	Orientation
SG1-N	0	84	36	Y
SG2-N	0	84	36	Y
SG3-N	0	57	0	Y
SG4-N	0	93	0	Y
SG1-F	0	336	36	Y
SG2-F	0	336	36	Y
SG3-F	0	363	0	Y
SG4-F	0	327	0	Y

Table G-14 Coordinates of internal foil strain gages (RS)

Instrument	X (in.)	Y (in.)	Z (in.)	Orientation
RS1-N	1	84	27	Y
RS2-N	1	96	27	Y
RS3-N	1	108	27	Y
RS4-N	1	84	17.5	Y
RS5-N	1	96	17.5	Y
RS6-N	1	108	17.5	Y
RS1-F	1	336	27	Y
RS2-F	1	324	27	Y
RS3-F	1	312	27	Y
RS4-F	1	336	17.5	Y
RS5-F	1	324	17.5	Y
RS6-F	1	312	17.5	Y

Table G-15 Coordinates of vibrating wire strain gages (VW)

Instrument	X (in.)	Y (in.)	Z (in.)	Orientation
VG1	0	210	5	Y
VG2	0	210	3	Y

Table G-16 Coordinates of LVDTs (L and D)

Instrument	X (in.)	Y (in.)	Z (in.)	Orientation	End tested
L1	0	0	5	Y	All
L2	0	0	3	Y	All
D1	0	6	36	Y	Near
D2	0	342	36	Y	Near
D3	0	78	36	Y	Near
D4	0	78	36	Y	Near
D1	0	414	36	Y	Far
D2	0	78	36	Y	Far
D3	0	342	36	Y	Far
D4	0	342	36	Y	Far

G.17 Shear test specimen detailed drawings

This section contains detailed drawings of specimens to be used for shear testing, including longitudinal and transverse reinforcement and general notes for construction.

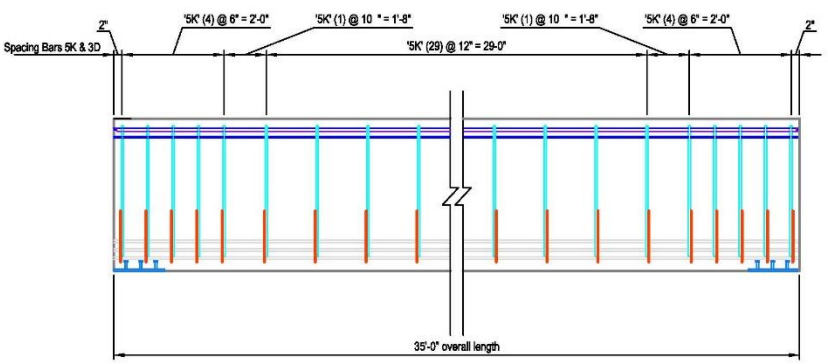

Elevation:
Flanges not shown for clarity

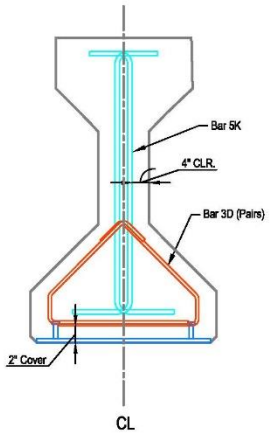

End Cross Section
Strands not shown for clarity

All reinforcement sizes and locations and quantities are typical each end unless noted otherwise

See sheet 3 for information on prestressing, shielding, & detensioning

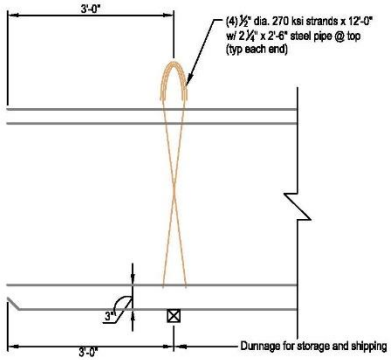

Handling & Dunnage

Bending Diagrams

NOTE: ALL DIMENSIONS ARE OUT-TO-OUT
#4 BARS BENT AROUND A 2" DIA. PIN
#3 BARS BENT AROUND A 1½" DIA. PIN

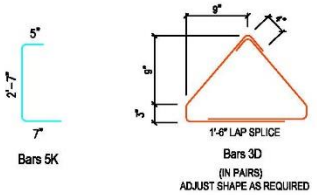

FDOT Research
FRC Shear strength

University of Florida
Dept. of Civil and Coastal Engineering
352.392.9537

General Notes
Sheet 1 of 2
07/09/2019

1

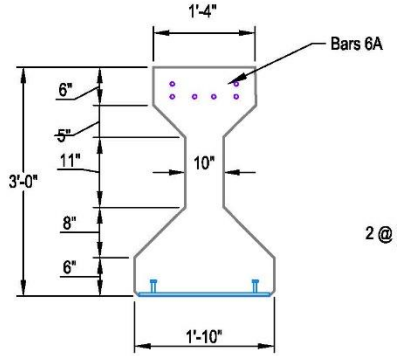

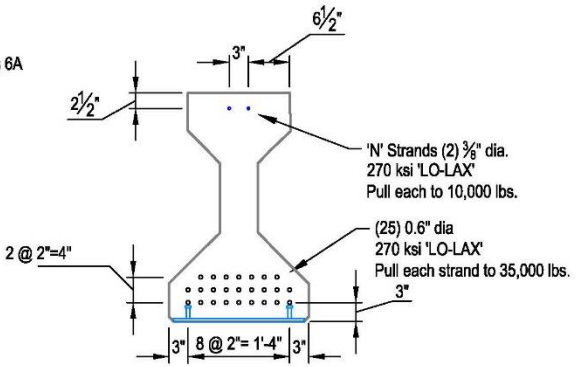

Strand Patten & Pretensioning
Typical each girder

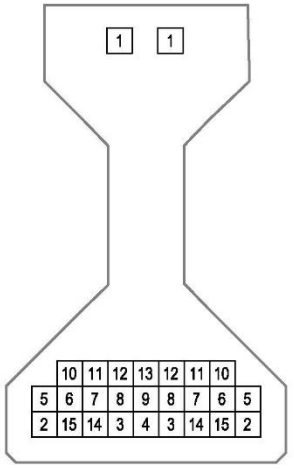

Detensioning Sequence
Typical each girder

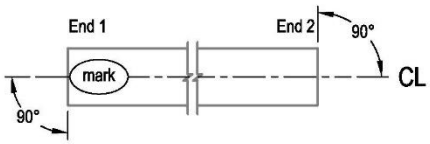

Plan View

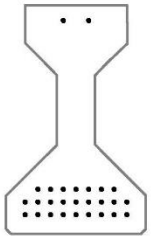

Shielding
Typical each end each girder

Shielding Legend
• – Fully Bonded

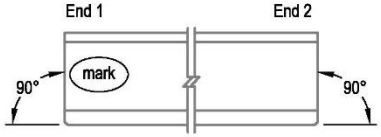

Elevation

Bill of material:				
Piece	Size	Qty.	Length	Notes
6A	#6	2	31'-0"	
3D	#3	42	6'-0⅜"	
5K	#4	42	7'-2"	

FDOT Research
FRC Shear strength

University of Florida
Dept. of Civil and Coastal Engineering
352.392.9537

General Notes
Sheet 2 of 2
07/09/2019

2

G.18 Instrumentation details for shear testing

This section contains drawings of setup and instrumentation recommended for shear testing, including internal and external instrumentation for individual testing of each girder.

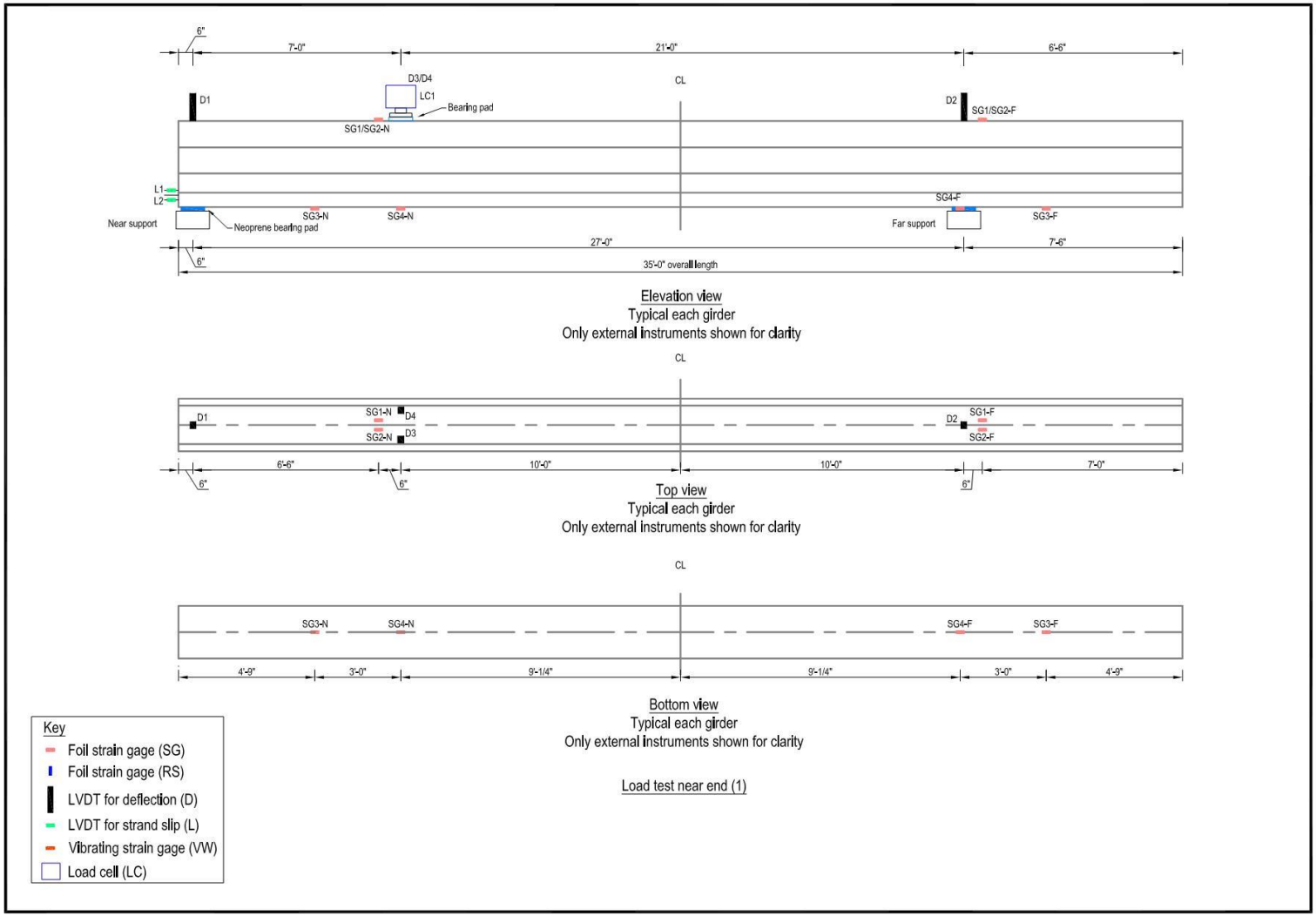
6"
7'-0"
21'-0"
6'-6"
D3/D4
LC1
Bearing pad
CL
D1
D2
SG1/SG2-N
SG1/SG2-F
L1
L2
SG3-N
SG4-N
SG4-F
SG3-F
Near support
Neoprene bearing pad
Far support
27'-0"
7'-6"
6"
35'-0" overall length
Elevation view
Typical each girder
Only external instruments shown for clarity
CL
D1
SG1-N
D4
SG2-N
D3
D2
SG1-F
SG2-F
6'-6"
10'-0"
10'-0"
7'-0"
6"
6"
6"
Top view
Typical each girder
Only external instruments shown for clarity
CL
SG3-N
SG4-N
SG4-F
SG3-F
4'-9"
3'-0"
9'-1/4"
9'-1/4"
3'-0"
4'-9"
Bottom view
Typical each girder
Only external instruments shown for clarity
Load test near end (1)
Key
Foil strain gage (SG)
Foil strain gage (RS)
LVDT for deflection (D)
LVDT for strand slip (L)
Vibrating strain gage (VW)
Load cell (LC)
Macro Synthetic Fiber Reinforcement for Improved Structural Performance of Concrete Bridge Girders
University of Florida
Dept of Civil and Coastal Engineering
352.392.9537
Specimen test setup 1 and instrumentation plan
BDV31-977-41
07/09/2019
1

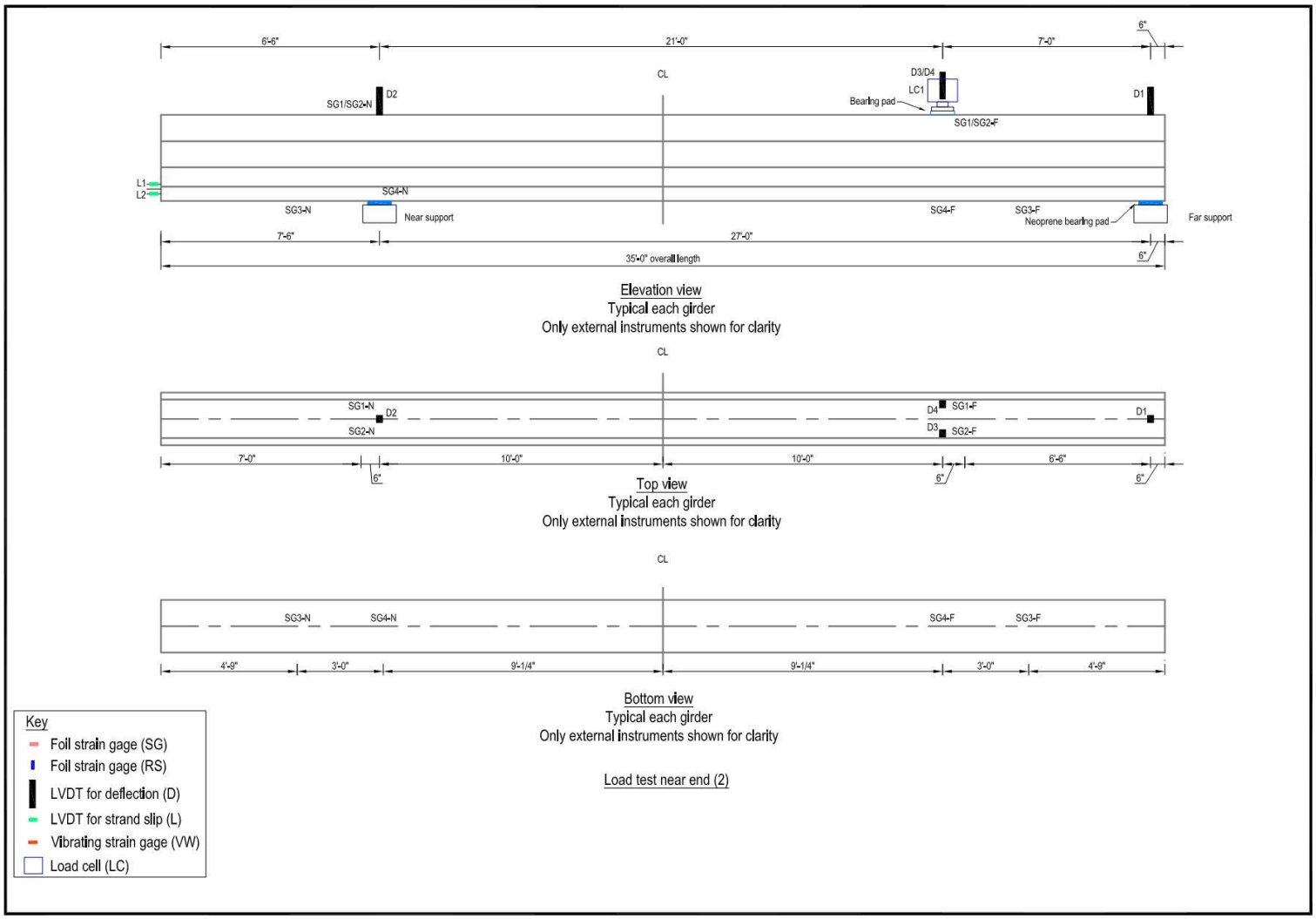
6'-6"
21'-0"
7'-0"
6"
CL
D3/D4
LC1
SG1/SG2-N
D2
Bearing pad
D1
SG1/SG2-F
L1
L2
SG4-N
SG3-N
Near support
SG4-F
SG3-F
Neoprene bearing pad
Far support
7'-6"
27'-0"
35'-0" overall length
6"
Elevation view
Typical each girder
Only external instruments shown for clarity
CL
SG1-N
D2
SG2-N
D4
SG1-F
D3
SG2-F
D1
7'-0"
10'-0"
10'-0"
6'-6"
6"
6"
6"
Top view
Typical each girder
Only external instruments shown for clarity
CL
SG3-N
SG4-N
SG4-F
SG3-F
4'-9"
3'-0"
9'-1/4"
9'-1/4"
3'-0"
4'-9"
Bottom view
Typical each girder
Only external instruments shown for clarity
Load test near end (2)
Key
Foil strain gage (SG)
Foil strain gage (RS)
LVDT for deflection (D)
LVDT for strand slip (L)
Vibrating strain gage (VW)
Load cell (LC)
Macro Synthetic Fiber Reinforcement for Improved Structural Performance of Concrete Bridge Girders
University of Florida
Dept of Civil and Coastal Engineering
352.392.9537
Specimen test setup 2 and Instrumentation plan
BDV31-977-41
07/09/2019
2

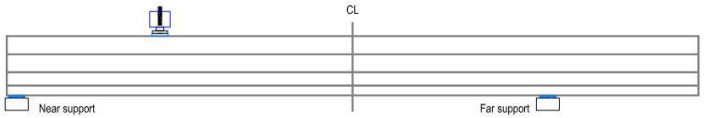

Load test 1
Loading applied at near end

Instrument	X (in.)	Y (in.)	Z (in.)	Orientation
D1	0	6	36	Y
D2	0	342	36	Y
D3	0	78	36	Y
D4	0	78	36	Y

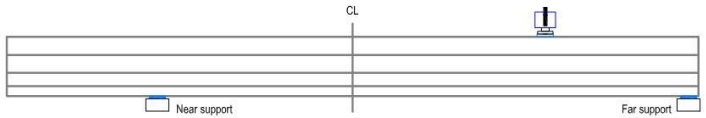

Load test 2
Loading applied at far end

Instrument	X (in.)	Y (in.)	Z (in.)	Orientation
D1	0	414	36	Y
D2	0	78	36	Y
D3	0	342	36	Y
D4	0	342	36	Y

Key
- Foil strain gage (SG)
- Foil strain gage (RS)
- LVDT for deflection (D)
- LVDT for strand slip (L)
- Vibrating strain gage (VW)
- Load cell (LC)

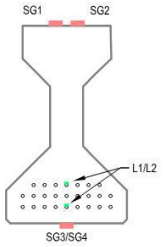

Cross Section
Typical each girder
Only external instruments
shown for clarity

Instrument	X (in.)	Y (in.)	Z (in.)	Orientation
SG1-N	0	84	36	Y
SG2-N	0	84	36	Y
SG3-N	0	57	0	Y
SG4-N	0	93	0	Y
SG1-F	0	336	36	Y
SG2-F	0	336	36	Y
SG3-F	0	363	0	Y
SG4-F	0	327	0	Y

Instrument	X (in.)	Y (in.)	Z (in.)	Orientation
L1	0	0	5	Y
L2	0	0	3	Y

Macro Synthetic Fiber Reinforcement for Improved Structural Performance of Concrete Bridge Girders

University of Florida
Department of Civil and Coastal Engineering
352.392.9537

External Instrumentation coordinates
BDV31-977-41
07/09/2019

3

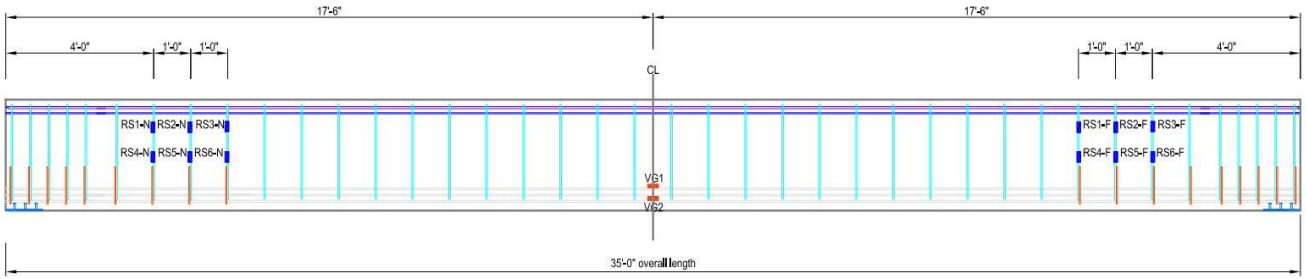

Elevation view:
Typical each girder
Flanges not shown for clarity
Only internal instruments
shown for clarity

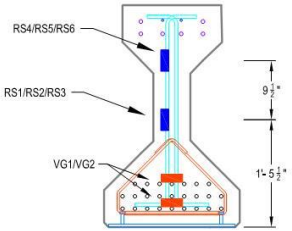

Cross Section
Typical each girder
Only internal instruments shown for clarity

Instrument	X (in.)	Y (in.)	Z (in.)	Orientation
RS1-N	1	84	27	Y
RS2-N	1	96	27	Y
RS3-N	1	108	27	Y
RS4-N	1	84	17.5	Y
RS5-N	1	96	17.5	Y
RS6-N	1	108	17.5	Y
RS1-F	1	336	27	Y
RS2-F	1	324	27	Y
RS3-F	1	312	27	Y
RS4-F	1	336	17.5	Y
RS5-F	1	324	17.5	Y
RS6-F	1	312	17.5	Y

Instrument	X (in.)	Y (in.)	Z (in.)	Orientation
VG1	0	210	5	Y
VG2	0	210	3	Y

Key
- Foil strain gage (SG)
- Foil strain gage (RS)
- LVDT for deflection (D)
- LVDT for strand slip (L)
- Vibrating strain gage (VW)

Macro Synthetic Fiber Reinforcement for Improved Structural Performance of Concrete Bridge Girders

University of Florida
Department of Civil and Coastal Engineering
352.392.9537

Internal Instrumentation coordinates
BDV31-977-41
07/09/2019

4